



# **Liquid Crystalline Organic Semiconductors for Application in Opto-electronic Devices**

---

being a Thesis submitted for the Degree of  
Doctor of Philosophy (PhD)

in the University of Hull

by

Muralidhar Reddy Billa

March 2015

## **Acknowledgements**

I would like to thank my supervisor Professor Stephen M. Kelly for my introduction to the world of liquid crystals and organic light emitting diodes and for his continued support, guidance, encouragement, patience and advice throughout the course of this work. I would also like to thank my second supervisor Dr. Mike Hird for his guidance in the preparation of this thesis.

Special thanks to Dr. Stuart P. Kitney for his great support, useful discussions, suggestions and evaluation of the compounds throughout my time spent in the lab. I would also like to thank Dr. Fei Cheng and Dr. Songjie Yang for their support and guidance in the laboratory. I thank my friends Srinivas Reddy, Viswanath Reddy, Anupam Das and Andrew J. Johnson for providing support and friendship when it was most needed. A huge thank to Michael J. Kelly for his time and great help throughout the preparation of this thesis.

I also wish to thank Professor Mary O'Neill and other members (Brian Lambert, William Harrison and Steve Meyers) of the Physics Department for useful discussions and physical evaluation of the compounds synthesised in this thesis. I would like to thank the University of Hull and Polar OLED for funding this research.

Thanks must also go to the technical staff for the analysis of intermediates and final products synthesised during the period of research, especially Dr. Kevin Welham (Mass Spectroscopy) and Mrs Carol Kennedy (elemental analysis).

Above all, I wish to thank my family, who have been a constant source of love and encouragement throughout my life.

Muralidhar Reddy Billa

March-2015

## Abstract

The synthesis and evaluation of novel photo-reactive liquid crystalline materials that exhibit light emitting, charge transporting and photovoltaic properties is described. Low-molar-mass liquid crystalline monomers, based on a series of substituted thiophenes, thieno[3,2-b]thiophenes, benzo[1,2-b:4,5-b']dithiophene, 4,7-dibromobenzo-1,2,5-thiadiazole, fluorenes and carbazoles have been synthesised. Most of the materials synthesised incorporate two 9-octyl carbazole end groups at 3 positions. Some of the materials synthesised incorporate methacrylate end groups attached to the peripheries of the molecule at the end of flexible aliphatic chains. Polymerisation of these end groups allows the production of multilayer OLEDs with a very small pixel size due to the insoluble cross-linked network obtained after photo-polymerisation. The creation and analysis of novel multi-layer OLEDs with exceptionally small pixel size was possible by the incorporation of photo-polymerizable group into the liquid crystalline compounds.

The molecular core incorporates either a 9-octyl carbazole end groups at the two ends of a fluorene moiety or an *N*-alkyl-substituted carbazole in the centre of the molecule. The presence of these two new types of liquid crystalline monomers for use as polymer networks in OLEDs should lead to higher electrochemical stability towards oxidation and thereby give rise to longer life-times in OLEDs containing them.

Exceptinally, several of these novel OLED materials exhibit blue photoluminescence and electroluminescence, enabling their incorporation into multicolour OLEDs. This thesis details the synthesis of two different types of molecular central moieties, i.e., fluorene and carbazole with photopolymerisable end groups or 9-octyl carbazole end groups for implementation as initiators in multilayer organic devices. The photo reactive end groups are based on the acrylate moieties.

## Contents

1. Introduction .....	1
1.1. Luminescence.....	1
1.1.1. Historical development .....	1
1.1.2. Fluorescence.....	1
1.1.3. Phosphorescence .....	3
1.1.4. Photoluminescence.....	4
1.1.5. Electroluminescence .....	4
1.2. Conductors, semiconductors and insulators.....	6
1.3. Organic Light-Emitting Diodes (OLEDs) .....	7
1.3.1. Historical development .....	7
1.3.2. OLED device structure.....	9
1.3.2.1. Single layer OLEDs .....	9
1.3.2.2. Multiple-Layer OLEDs .....	10
1.3.2.3. Electron transport materials.. .....	12
1.3.2.4. Hole transport materials .....	13
1.3.2.5. Dopants... .....	13
1.3.2.6. Deposition technique.....	14
1.4. Phosphorescent OLEDs: Singlet and triplet harvesting.....	15
1.5. Recent developments in OLED technology.....	16
1.6. Stability and Reliability of OLEDs and PhOLEDs .....	18
1.7. Organic Photovoltaics (OPVs).....	19
1.7.1. OPV mode of operation .....	20
1.7.2. Materials for Organic Solar Cells .....	22

1.8. Liquid crystals .....	23
1.8.1. Morphology of liquid crystals .....	24
1.8.1.1. Calamitic Liquid Crystals .....	25
1.8.1.2. Nematic Phase .....	26
1.8.1.3. Smectic Phase .....	27
1.9. Cross coupling reactions .....	28
1.9.1. Direct arylation .....	29
1.10. References .....	31
2. Aims of the Research .....	36
2.1. References .....	44
3. Experimental .....	46
3.1. Evaluation of the Materials .....	46
3.2. Experimental Discussion.....	52
3.3. Reaction Schemes .....	66
3.4. Synthesis of the Materials .....	94
3.5. References .....	163
4. Results and Discussion.....	165
4.1. Derivatives incorporating 3-substituted carbazole rings .....	165
4.1.1. Fused rings/carbazoles .....	165
4.1.2. Benzothiadiazole/carbazoles .....	172
4.1.3. Oligothiophene/carbazoles .....	179
4.2. 2,7-Disubstituted-9-alkylcarbazoles .....	186
4.3. 2,7-Disubstituted-9,9-dialkylfluorenes .....	190
4.4. Oxadiazoles .....	195

4.5. Dithienopyrroles.....	203
4.6. Fused phenylenes .....	210
4.7. Isoindigo.....	218
4.8. Derivatives incorporating 2-substituted carbazole rings .....	225
4.8.1. Oxadiazole/carbazoles .....	225
4.8.2. Thiophene/carbazoles.....	245
4.8.3. Tercarbazoles .....	249
4.8.4. Biphenyl/carbazoles .....	259
4.8.5. Fluorene/carbazoles .....	262
4.8.6. Triphenylamine/carbazoles .....	268
4.9. References .....	271
5. Conclusions .....	272

## Appendix- Publication

## **1. Introduction**

### **1.1 Luminescence**

#### **1.1.1 Historical development**

The emission of light from any substance is defined as luminescence. The first recorded scientific reports of luminescence appeared in the middle of the 18<sup>th</sup> century, e.g., Sir J. F. W Herschel reported in 1845 an experiment that he had carried out twenty years earlier, but was unable to repeat because of the lack of “a specimen of the wood”. Herschel observed that a colourless solution of quinine in water emitted a blue colour under certain circumstances. Herschel concluded that “specie” in the solution, “exerts its peculiar power on the incident light” and disperses the blue light.<sup>1</sup> The experiment can be repeated simply by observing a glass of tonic water exposed to sunlight. Often a blue glow is visible at the surfaces. Sir G. G. Stokes studied the same compound and found that the emitted light has a longer wavelength than the ultra-violet light absorbed. This phenomenon is now referred to as the Stokes’ shift.<sup>2</sup> Luminescence is formally divided in to two sub-categories, i.e., fluorescence and phosphorescence.

#### **1.1.2 Fluorescence**

The processes that occur between the absorption and emission of light are often illustrated by the Jablonski diagram, Figure 1 shows a typical Jablonski diagram in which the ground, first and second electronic states are depicted by  $S_0$ ,  $S_1$  and  $S_2$ , respectively. The fluorophores can exist in a number of vibrational energy levels, depicted by 0, 1, 2, etc, in each of these quantised electronic energy levels. The transitions between states are depicted as vertical lines to illustrate the instantaneous nature of light absorption. The Franck-Condon principle states that such electronic transitions occur too quickly ( $\sim 10^{-15}$  s) for significant displacement of nuclei to occur.

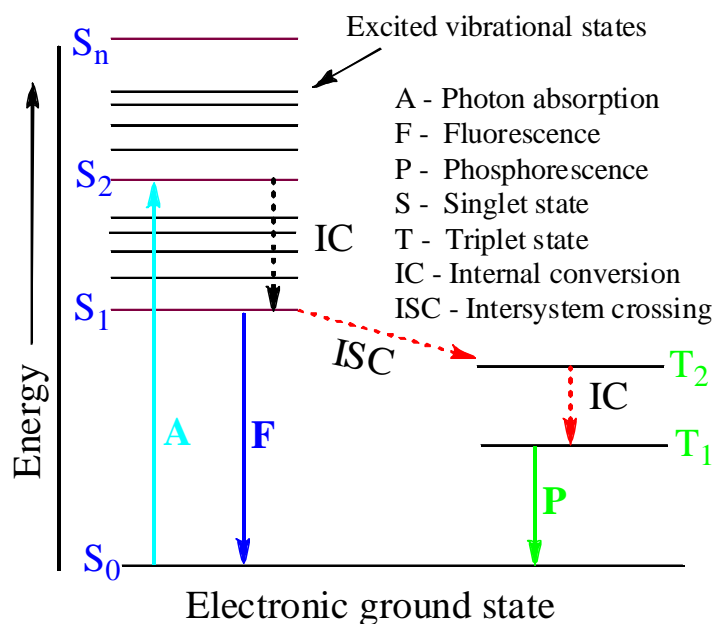


Figure 1: A typical Jablonski diagram.

The energy spacing between the various vibrational energy levels is illustrated by the emission spectrum of the highly conjugated aromatic compound perylene, Figure 2. The individual emission maxima and vibrational energy levels are separated by about  $1500\text{ cm}^{-1}$ . At room temperature there is insufficient thermal energy to significantly populate the excited vibrational states and absorption and emission usually occur from molecules with the lowest vibrational energy. The difference in energy (band gap) between the  $S_0$  and  $S_1$  excited states is too large for thermal population of  $S_1$  and consequently light (photoluminescence, PL) and electricity (electroluminescence, EL) but notably not heat-induce fluorescence. A fluorophore is usually excited to some higher vibrational level of either  $S_1$  or  $S_2$  following light absorption in photoluminescence. Molecules in condensed phases usually then relax rapidly to the lowest vibrational level of  $S_1$  in an internal conversion process ( $< 10^{-12}\text{ s}$ ) and, since fluorescence lifetime are typically about  $10^{-8}\text{ s}$ , internal conversion is generally complete prior to emission of light. Therefore, fluorescence emission generally occurs from a thermally-equilibrated excited state, that is the lowest energy vibrational state of  $S_1$ , to a higher excited vibrational level of the ground state, which itself then reaches thermal equilibrium ( $10^{-12}\text{ s}$ ), Figure 1.<sup>3</sup> This process is the reason for the vibrational structure in the emission spectrum of organic compounds, e.g., perylene, Figure 2.

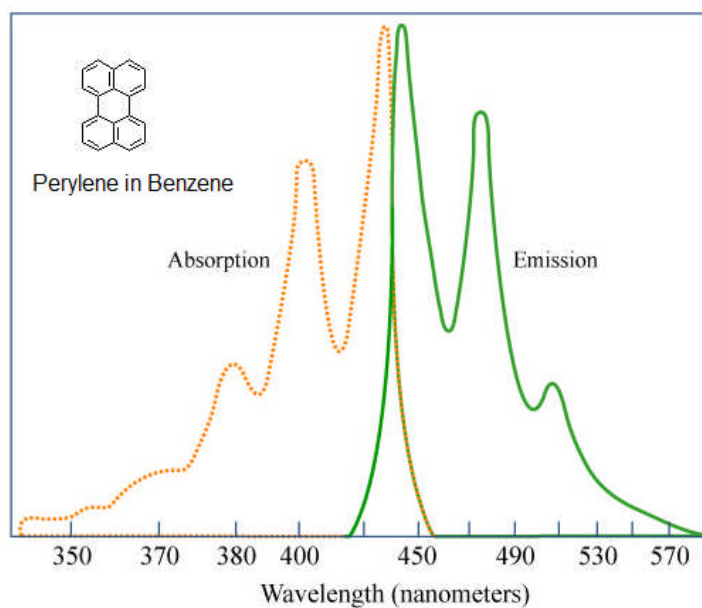


Figure 2: Absorption and fluorescence emission spectra of perylene.

### 1.1.3 Phosphorescence

Although population of triplet states by direct absorption from the ground state is usually insignificant, a more efficient process exists for population of triplet states from the lowest excited singlet state in many molecules i.e., electrons in the  $S_1$  state can undergo a spin conversion to the first triplet state  $T_1$ , Figure 3, in a process called intersystem crossing and is a spin-dependent internal conversion process. Relaxation from the triplet to the ground state by the emission of light is termed phosphorescence. In the production of excited states by promotion of an electron into a higher orbital, the direction of the spin of the electron is usually preserved. However, quantum theory predicts that an electron in an excited state can exist in three forms of very slightly different energy and the molecule is said to exist in a triplet state. A direct transition from the ground state to an excited triplet state is theoretically forbidden, which means that the reverse transition from the triplet state to the ground state is also slow ( $10^{-4}$ - $10^2$  s).

Once intersystem crossing has occurred the molecule undergoes the usual internal conversion process ( $10^{-13}$  to  $10^{-11}$  s) and falls to the zeroth vibrational level of the triplet state. There are two factors that tend to enhance a radiationless transition between the lowest triplet state and the ground state. First the energy difference between the triplet state and the ground state is smaller than the difference between the lowest singlet state

and the ground state. This tends to enhance vibrational coupling between these two states and therefore to enhance internal conversion. Second, the life time of a triplet state is much longer than that of an excited singlet state (about  $10^{-4}$  to  $10$  s) and therefore loss of excitation energy by collisional transfer is generally enhanced.

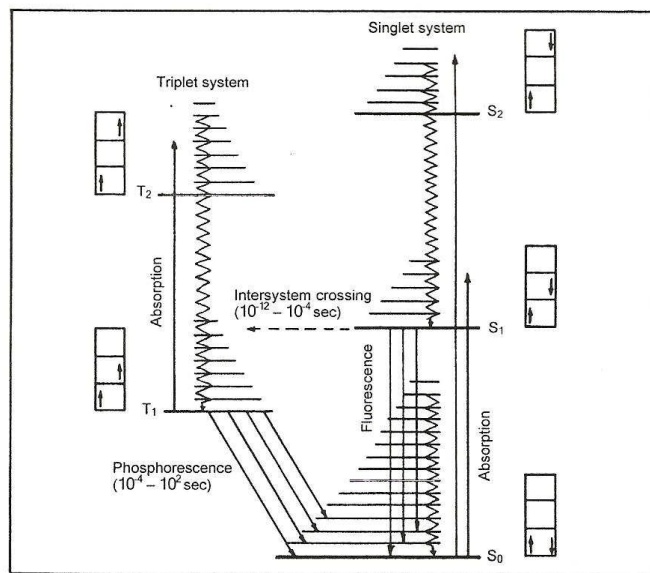


Figure 3: Transition from the excited singlet state ( $S_1$ ) to the triplet state (intersystem crossing).<sup>3</sup>

### 1.1.4 Photoluminescence

Photoluminescence (PL) is the process whereby light energy is absorbed by a molecule which promotes an electron into the excited state. The electron will subsequently relax to the ground state by re-emitting the energy with a red shift due to the Stokes shift. In an organic molecule the adsorption of light promotes an electron from the HOMO to the LUMO state, to give rise to a  $\pi$ - $\pi^*$  transition, which is followed by relaxation and a photon emission.

### 1.1.5 Electroluminescence

Electroluminescence is the direct conversion of electrical energy into light. Light emitting diodes (LEDs) are flat-panel displays, which emit light under the action of an electrical current passing through a thin layer of electroluminescent material. In the early 1960s the first commercial monochrome LEDs using inorganic semiconductors such as GaAsP were manufactured as low-information-content displays.<sup>4</sup> However,

inorganic LEDs are expensive and impractical as high-information-content, full-colour (RGB) displays due to the requirement for individual dedicated pixel electrodes.

The first observation of electroluminescence from organic material was from a very thick (~5 mm) single crystal of anthracene at high voltage ranging from 400-2000 V using liquid electrolytic electrodes for charge injection.<sup>5-7</sup> Much lower threshold voltages were observed when thin wafers of cleaved anthracene crystal or thin films were used with solid electrodes.<sup>8</sup> Unfortunately, the efficiency of these devices was low.

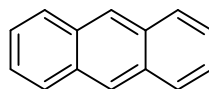


Figure 4: Chemical structure of anthracene.

However, the introduction of vapour deposited thin films made it possible for prototype Organic Light-Emitting Diodes (OLEDs) to be made.<sup>9</sup> A major break-through came in 1987 when Tang and van Slyke<sup>10-11</sup> demonstrated efficient EL from an organometallic compound, Figure 5, using a bilayer-configuration.

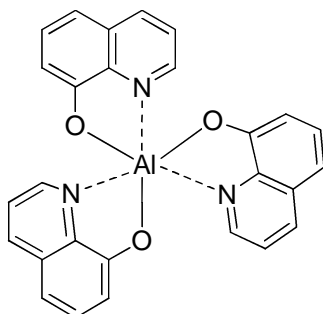


Figure 5: Chemical structure of *tris*(8-hydroxyquinolate)aluminium (III) ( $\text{Alq}_3$ ).

In 1989 Richard Friend and co-workers observed that conjugated organic main chain polymers could also exhibit EL efficiently,<sup>12</sup> i.e., poly(*para*-phenylenevinylene) (PPV), which exhibits yellow/green EL, Figure 6. An advantage of using organic electroluminescent materials is the ability to control the wavelength of emission by chemically altering the chromophore. It is the HOMO-LUMO gap, more commonly referred as the band gap, which determines the colour of emission. Main chain polymers, such as PPV and related derivatives, have been shown to emit light at wavelength covering the entire visible spectrum.<sup>13</sup> The photoluminescence and electroluminescence emission spectra of an organic molecule are usually almost identical.<sup>14</sup>

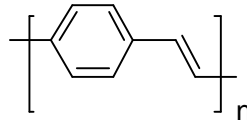


Figure 6: Chemical structure of poly(*para*-phenylenevinylene) (PPV).

## 1.2 Conductors, Semiconductors and Insulators

Materials can be categorised as conductors, semiconductors and insulators (dielectrics) by their ability -or not- to conduct an electric current. Metals conduct electricity readily because the energy levels between the conduction bands (CB) and valence bands (VB) are closely spaced, or there are more energy levels available than there are electrons to fill them, so very little energy is required to promote electrons into new energy levels, Figure 7. For example, the valence band is partly filled in copper or the valence band is completely filled but overlapping with the conduction band in magnesium. This means that there are vacant energy states adjacent to the highest filled energy levels. Therefore very little energy is required to promote sufficient electrons into the low-lying empty states. The free electrons are able to allow an electrical current to flow when a potential difference is applied to the conductor.

Semiconductors are characterised by a band gap ( $E_g$ ), i.e., a forbidden energy gap between the highest energy states of the VB and the lowest energy states of the CB. The band gap is often several eV in semiconductors. Therefore, the VB is filled and the CB is empty in semiconductors, at low temperatures, i.e., at absolute zero (0 K) semiconductors are insulators and no electrons are present in the CB. For an electron to become free, it must be excited or promoted, by an amount of energy greater than that of the band gap, into one of the empty and available energy state, i.e., at room temperature, for example, the thermal energy is high enough to raise sufficient electrons into the CB to generate an electrical current.

It is commonly believed that insulators (dielectrics) do not conduct electricity because their valence electrons are not free to move throughout the material. In fact they are free to move within the bulk of the material. Moreover, in an insulator there are as many electrons as there are energy levels for them to occupy. However, the band gap in insulators is so wide that it cannot be overcome by electrons, even those with a very high energy. Therefore, no technically-relevant conductivity is observed.<sup>15</sup>

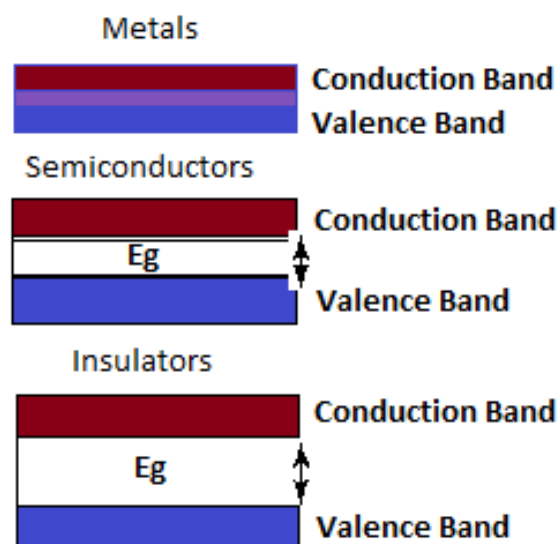


Figure 7: Schematic representation of energy levels and the band gap between the valence and conduction bands.

### 1.3 Organic Light-Emitting Diodes (OLEDs)

Organic light-emitting diodes (OLEDs) based on organic electroluminescence are emissive and have the potential to be very efficient sources of lighting and as well as high-information-content, full-colour, flat-panel displays. OLEDs are self-luminous and do not require backlighting, diffusers, polarizers like by LCDs and are therefore intrinsically more efficient than LCDs or LEDs EL from inorganic compounds.<sup>16</sup> OLEDs are light-weight, they can operate with low DC voltages and they have very wide viewing angles, high brightness, video-rate addressing and low power consumption. OLEDs use significantly less power than comparable backlit LCDs.<sup>17</sup>

#### 1.3.1 Historical development

In 1977 Chiang et al developed the idea of high electrical conductivity in doped polyacetylene.<sup>18</sup> This initial idea has since prompted mass research areas in academia and industry involving the synthesis of new organic semiconductors and to give understanding of their properties for optoelectronics and electronic devices. Organic semiconductors are now enabling the emergent and disruptive plastic electronics industry based on their charge transport and light emitting properties in OLEDs, photovoltaic (PV) cells and Organic Field-Effect transistors, for example. In the early 1960s, the first low-information-content LEDs utilized GaAsP as an inorganic

semiconducting material. However, EL was reported as early as 1936 by Destriau and co-workers who observed EL from ZnS phosphor powder.<sup>19</sup> The first OLED was built by Pope and co-workers in 1963 using an anthracene, see above.<sup>5</sup> The first OLED device with a high efficiency was developed by Van Slyke in 1987 (Eastman Kodak Company).<sup>10-11</sup> They combined a hole transport layer (HTL) and an emission layer (Alq<sub>3</sub>) to fabricate a bilayer OLED with a green emission and low driving voltage (10 V).

Friend and co-workers in 1990 overcame the drawback of expensive and technologically inconvenient vapour deposition of fluorescent dyes and inorganic semiconductors by depositing PPV, Figure 8 from solution as the active material in the single layer Polymer Light-Emitting Diode (PLED).<sup>12</sup> It is believed that the luminescent and charge-transporting properties of liquid crystalline polymer networks could be used to create LC-OLEDs as a low-cost alternative to small molecule OLEDs and PLEDs. LC-OLEDs have the advantage of being photolithographically patternable.<sup>20</sup>

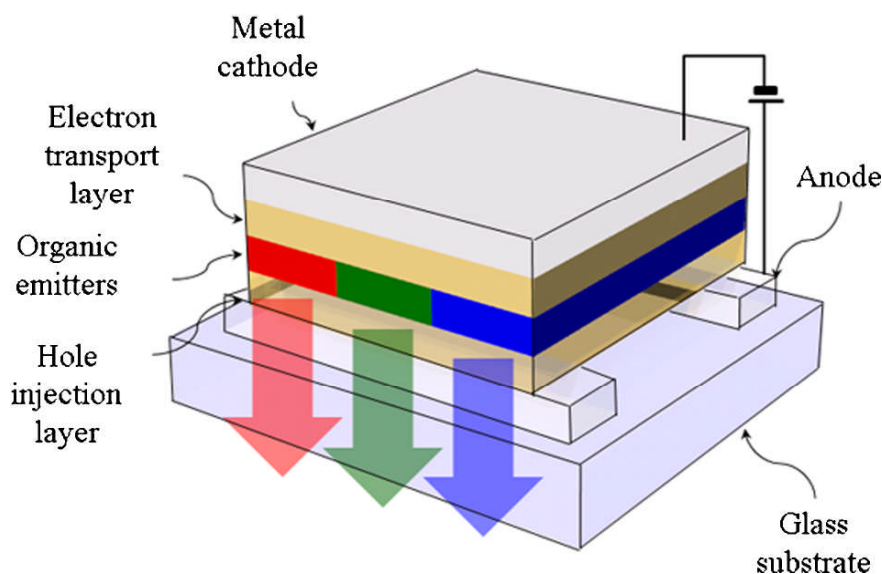


Figure 8: The physical structure of an OLED cell.<sup>21</sup>

To enter the emitting layer the holes and electrons have to overcome an energy barrier on each side of the electrodes. This makes it necessary to adjust the energy levels of the electrodes to the HOMO/LUMO levels of the emitter layer to obtain high external quantum efficiency. After the electrons and holes enter the emitting layer they are allowed to recombine by emitting photons.

## 1.3.2 OLED Device structure

### 1.3.2.1 Single layer OLEDs

A schematic diagram of the simplest type of OLED is shown in below Figure 9. Figure 9 shows that the organic light-absorbing layer (100 nm thick) is sandwiched between two different electrodes. The substrate is made from glass or plastic. One electrode (anode-high work function) is transparent, often indium-tin-oxide<sup>22</sup> (ITO) and the other electrode (cathode-low work function) is metallic, typically aluminium<sup>17</sup> (calcium, magnesium, gold and others can be used). Because ITO is non-stoichiometric the way in which it is prepared is critical to the efficiency of the device.<sup>16</sup> In OLEDs an electron is introduced at the cathode electrode and to keep a charge balance, holes are introduced at the anode electrode. For the metal cathode to be effective it must possess a low work function, this assists electron injection into the lowest unoccupied molecular orbital (LUMO). The anode is responsible for hole injection by extracting electrons from the highest unoccupied molecular orbital (HOMO) of the adjacent layer of the organic material. Anion radicals (electrons) and cation radicals (holes) travel through the active organic layer and recombine to form either a singlet or triplet excited state. The singlet state can decay radioactively with the emission of visible light passing to the ground state. This physical effect is known as electroluminescence. Below Figure 9 shown a single layer OLED.

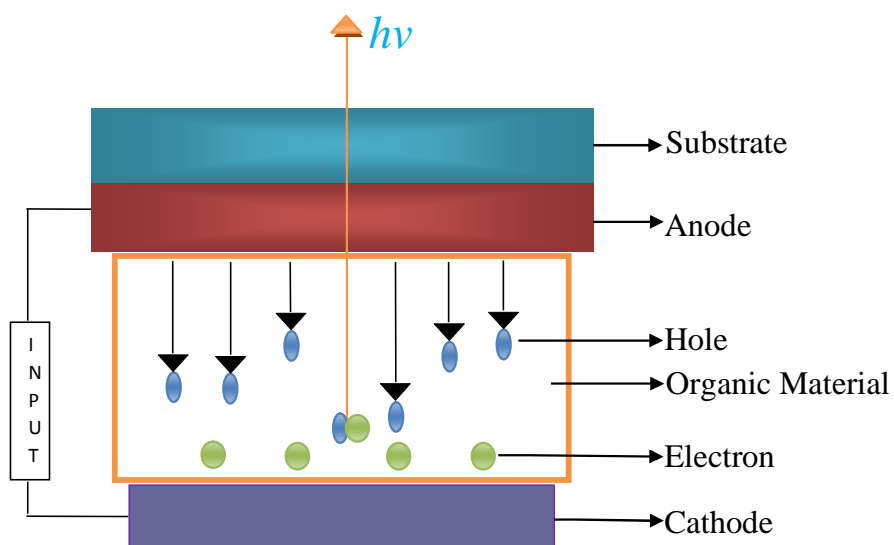


Figure 9: Schematic representation of a single layer OLED.

In many inorganic semiconductors, photon absorption produces free electrons and holes directly.<sup>17</sup> However, in molecular semiconductors, at some point the electrons and the holes meet (a chromophore site) and recombine to form an excited state.<sup>12</sup> This leads to light emission and luminescence. Imbalances in the hole injection/transport and electron injection/transport within these devices are problematic and result in non-radiative (heat) processes. This imbalance also results in lower external quantum efficiency and less light emission.

Figure 10 illustrates that the work function of the anode material should match the ionisation potential (IP) of the organic material whilst the work function of the cathode material should match its electron affinity.<sup>23</sup> Single layer devices are actually inefficient due to mismatching of the work function of the electrodes and of the active organic layers.

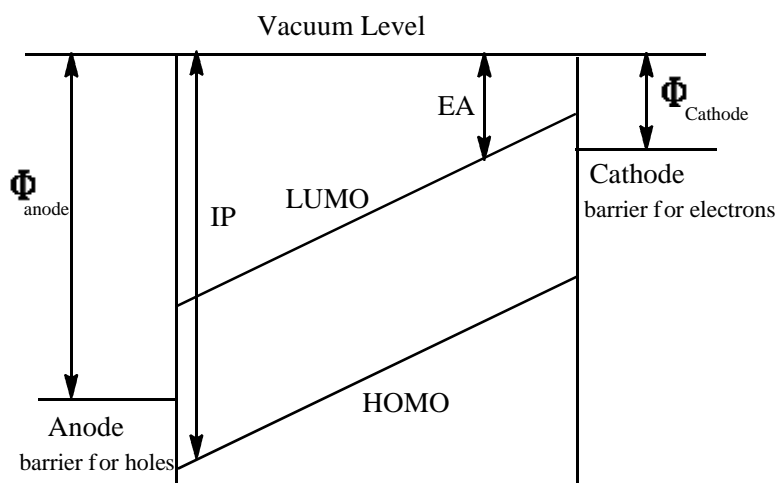


Figure 10: Energy scheme of a single layer OLED.<sup>24-25</sup>

### 1.3.2.2 Multiple-Layer OLEDs

The OLED depicted in Figure 11 is based on a single layer organic semiconductor, however for a more sophisticated approach there would be multiple layers sandwiched together between hole and electron-injection/transport layers. As previously mentioned, for best results it is beneficial to have matching energy levels as to minimize the barriers for carrier injection and to hold electrons and hole in the luminescent region. These multi-layer OLEDs have proven to be the most successful and the best performance so far is a power efficiency of 60 lm/W and an external quantum efficiency of 19%.<sup>26</sup>

In 1987 Tang and Van Slyke reported the first multiple layer devices consisting of an ITO (coated glass) substrate with a hole-transporting, aromatic diamine on top of the substrate.<sup>10</sup> Alq<sub>3</sub> was used for both emission and electron transport. The cell was made by vacuum deposition with the top electrode being an alloy of magnesium and silver (10:1). The advantages of this device were high EL emission efficiencies, a fast response, low-voltage operation and the simplicity of fabrication.

In 1992 Friend *et al* reported a bi-layer PLED using PPV for hole-transporting an emissive material and an electron-transporting/hole-blocking layer of 2-(biphenyl-4-yl)-5-(tert-butylphenyl)-1, 3, 4-oxadiazole (PBD).<sup>27</sup> This device gave an eight-fold increase in efficiency in comparison to the PPV single layer device. The benefits of a bi-layer device include improved transport mobilities of the charge carriers, which lower the potential energy barrier for charge injection and prevent charge recombination close to the electrode-emissive layer interface where defects may cause non radiate decay.

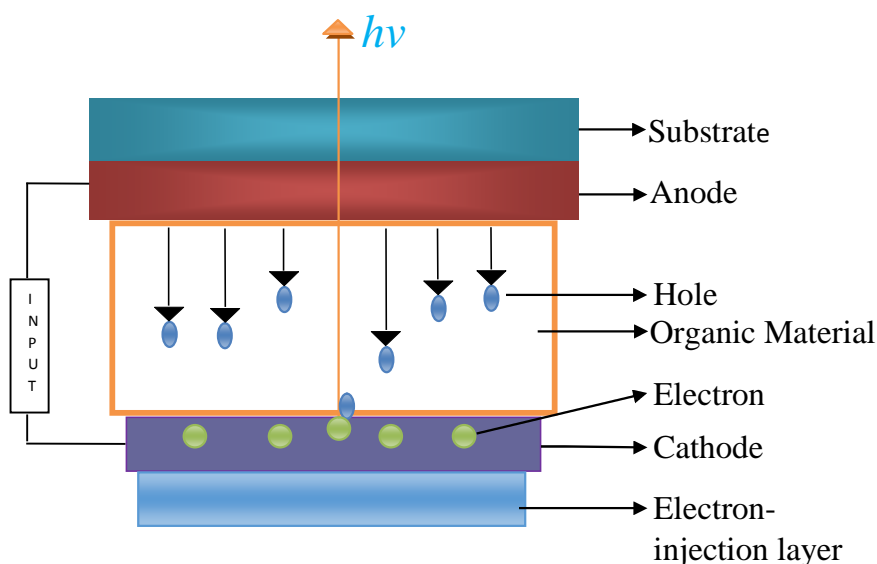


Figure 11: Schematic representation of a bilayer OLED.

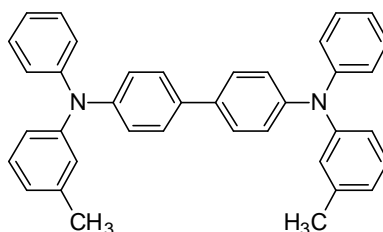


Figure 12: Chemical structure of *N,N*-diphenyl-*N,N*-di-(*m*-tolyl)-*p*-benzidine (TPD).

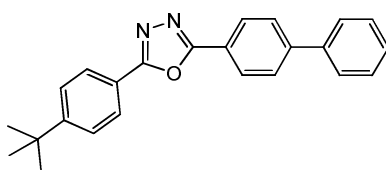
The compound *N,N*-diphenyl-*N,N*-di-(*m*-tolyl)-*p*-benzidine (TPD), Figure 12, has been used very often as a molecular hole transport layer in the construct of OLEDs. It is used for molecular hole transport layers with high-hole drift mobility and is used in xerography.<sup>28-29</sup>

The use of multilayer OLEDs is very beneficial and ongoing research may consequently eliminate problematic areas. For example Adachi and co-workers devised a configuration of very thin EL layers (<100 Å), which causes confinement of charge recombination to a small area, where electrons and holes recombine efficiently to result in very bright light emission.<sup>30</sup>

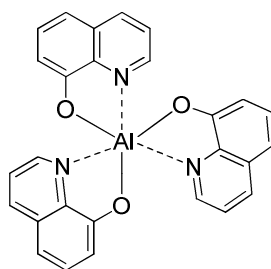
### 1.3.2.3 Electron transport materials

Electron transport materials should have good thermal stability, appropriate energy levels and good charge carrier mobility to enhance the OLED device performance. They should also possess the following characteristics.

- 1) High reduction potential: this facilitates the charge transport in the organic thin film.
- 2) Appropriate EA and IP values to minimize electron injection barrier.
- 3) Capable of hole-blocking.
- 4) High electron mobility to improve the exciton creation rate.
- 5) Generally these materials should have the HOMO energy levels approximately >6eV
- 6) High glass transition temperatures (T<sub>g</sub>).
- 7) Easy processability to form an uniform thin film.<sup>31</sup>



2-(4-biphenyl)-5-(4-tert-butylphenyl)-1,3,4-oxadiazole (PBD)

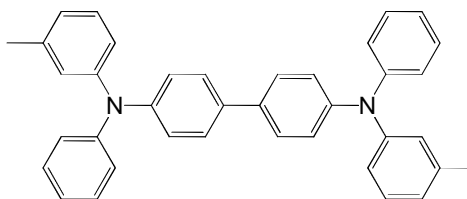


*tris*-(8-hydroxyquinoline)aluminium (Alq3)

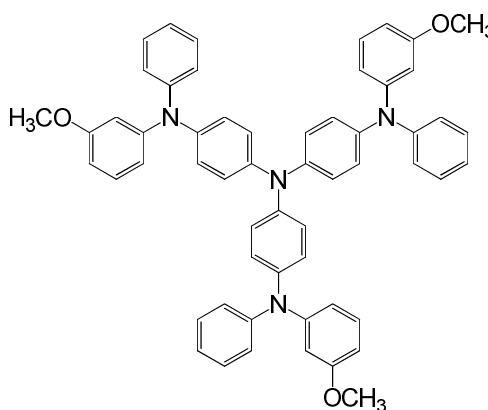
Figure 13: Typical examples of electron transport materials.

### 1.3.2.4 Hole transport materials

An important strategy in constructing an OLED device is to carefully select electron- and hole-transport layers for optimal performance. Materials with low ionisation potentials would act as potential hole-transport layers. They must have high hole-mobility and should be able to act as an electron blocking layer to block the electrons coming from cathode. Generally materials with electron donating properties serve as hole-transport materials in OLEDs.<sup>32-33</sup>



*N,N*-bis(3-methylphenyl)-*N,N*-diphenylbenzidine (TPD)



4,4',4''-tris(*N*-3-methylphenyl-*N*-phenyl-amino)triphenylamine (MTDTA)

Figure 14: Typical examples of hole-transport materials.

### 1.3.2.5 Dopants

To achieve higher efficiency phosphorescent emission both the dopant and the host material should satisfy certain properties such as suitable HOMO and LUMO energy levels, variable dopants concentration and low charge trapping and exciton quenching. An ideal host material should be ambipolar in nature, this means it has similar hole and electron transport properties, for the balanced charge transfer. Most importantly for a triplet dopant, the host materials triplet energy has to be high enough for the efficient transfer of exciton energy to that of dopants triplet energy, Figure 15.<sup>34</sup> It is also important for the dopant to have an even distribution within the host material and have a

stable morphology that is subjected to the minimum possible morphology change over time.<sup>35</sup>

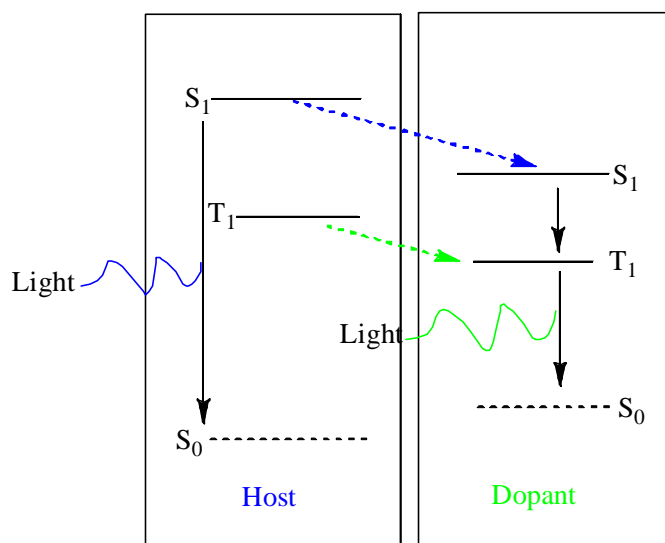


Figure 15: Energy transfer between the host and dopant in an OLED.<sup>34</sup>

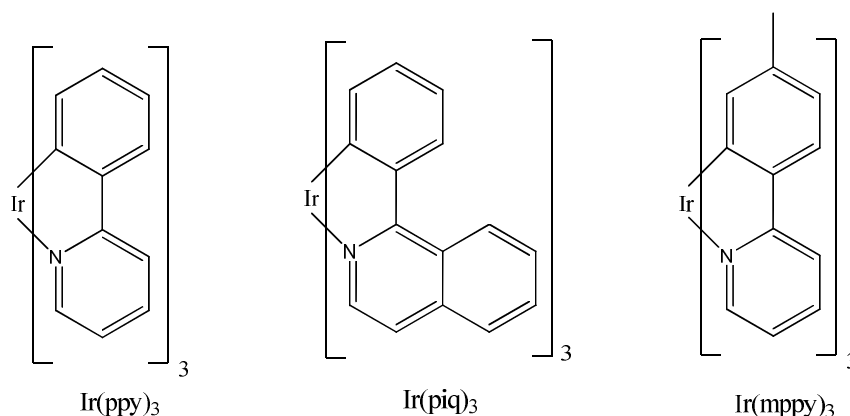


Figure 16: Examples of dopants used in this thesis.

### 1.3.2.6 Deposition technique

In this technique organic semiconducting materials are dissolved in a suitable solvent and this fluid is deposited onto a substrate. This substrate is spun at high velocity of 10,000 rpm to uniformly spread the liquid over the substrate and subsequently evaporate the solvent. The thickness of the thin film depends on the solution concentration, spinning speed, viscosity and acceleration. The disadvantage of this method is not easily scalable to large scale production.<sup>36</sup>

## 1.4 Phosphorescent OLEDs: Singlet and triplet harvesting

For the production of an effective OLED, negatively charged electrons and positively charged holes should recombine to form excited states that are capable of undergoing continuous radiative recombination without any energy loss. The electron and hole attract each other to form an exciton in an OLED. Quantum statistics plays a vital role in the ultimate output of the device. Considering, both electron and hole possess spins, potentially four different spin combinations are viable according to the quantum theory. One is antisymmetric spin with singlet state in which total spin quantum number  $S=0$ . This quantum mechanically allowed relaxation transition to the lowest energy state results in fluorescence within nanoseconds. Next are three symmetrical combinations with a triplet state in which total spin quantum number  $S=1$ . This quantum mechanically forbidden transition gives rise to phosphorescence, with a significantly longer relaxation process to a lower energy state with a life time of microseconds to one second. Statistically 25% of the excitons are of the singlet character, where as 75% of excitons possess triplet character. So fluorescent OLEDs can only produce singlet excitons leading to the internal quantum efficiency of 25%, where as in phosphorescent OLEDs, which generate the light from both singlet and triplet excitons, result in significant conversation of internal quantum efficiency to reach nearly 100%. Since the phosphorescence process is very slow in organic molecules due to the week spin-orbit coupling, this leads to fluorescence. In order to overcome this delayed transition, organo-transition metal dopants are used to accelerate the intersystem crossing rate. In organo-metal complexes the central metal atom induces significant spin-orbit coupling resulting in the significant harvesting of the singlet as well as triplet excitons. So by using the metal complexes as dopants in an OLED we can successfully achieve higher efficiency with triplet phosphorescent emitters than the singlet fluorescent emitters.<sup>37-40</sup>

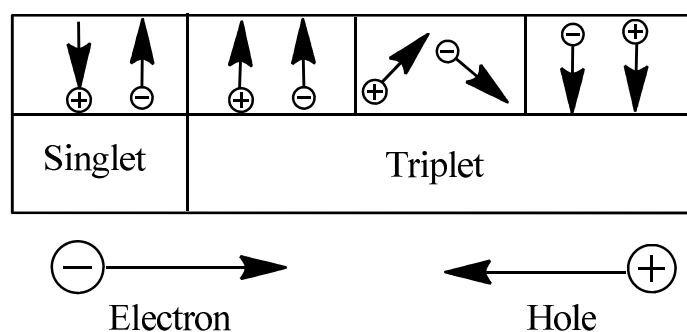


Figure 17: Spin combinations of one singlet and three triplet states.<sup>37</sup>

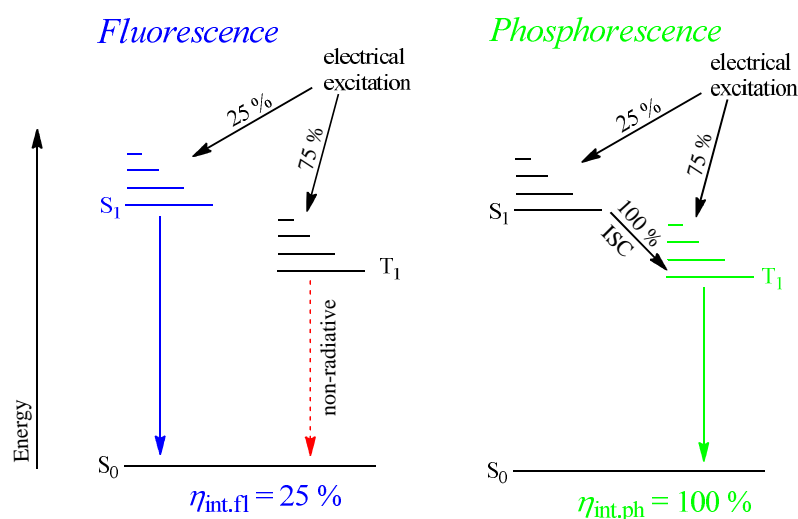


Figure 18: Singlet and triplet excitation of organic molecules.<sup>40</sup>

## 1.5 Recent developments in OLED technology

OLED technology is emerging as an alternative and future display technology to LCDs. Both fluorescent and phosphorescent OLEDs have fuelled active research, because the use of pure organic materials can result in flat panel displays with higher brightness and lower power consumption than existing LCD technology.

In 1993, Kido and co-workers reported a metal-doped organic layer device with Li/Ag, which showed higher performance as compared to those with a conventional cathode Mg:Ag.<sup>72-74</sup>

In 1997, Mason and co-workers reported an (NPD)/(Alq) device with LiF. Compared to the conventional Mg:Ag based device, the LiF/Al based device showed a significant reduction in the operating voltage to 7 V at 100 mA cm<sup>-2</sup>. This was followed by the subsequent investigation by Wakimoto and co-workers describing the use of inorganic salts, such as sodium chloride (NaCl) and lithium oxide (Li<sub>2</sub>O).<sup>75-76</sup>

In 1998, Kido and co-workers reported a device with a Li-doped Alq/Al layer which had a higher luminance of over 30,000 cd cm<sup>-2</sup> at 10.5 V, when compared to a device without the metal-doped Alq layer that exhibited a luminance of only 3400 cd cm<sup>-2</sup> at 14 V.<sup>77</sup>

In 1998, Mark Thompson and Stephen Forrest reported the first phosphorescent OLEDs using a platinum (II) emissive layer. Subsequently they developed an iridium based PhOLEDs.<sup>78</sup>

In 2002, Huang and Leo reported a Li-doped Alq device with a 4,7-diphenyl-1,10-phenanthroline (Bphen)/Al layer, which showed luminescence over 1000 cd cm<sup>-2</sup> at 2.9 V. In the same year, Leo and co-workers reported an Ir(ppy)<sub>3</sub>-based device with a Cs-doped Bphen/Al layer, which showed a luminance of 1000 cd cm<sup>-2</sup> at 3.0 V. The major drawback with using these highly reactive alkaline metals (i.e, Li) is that they are difficult to handle, as they can easily oxidize in the presence of oxygen.<sup>79-80</sup>

White light-emitting phosphorescent OLEDs have emerged as commercially important for lighting applications. In 2005, a white OLED panel was made using a multilayer device, which had a peak efficiency of 64 lm/W. Later on, a white OLED panel was introduced by Novaled/Philips with power efficiency of 90 lm/W and brightness of 1000 cd/m<sup>2</sup>.<sup>81-83</sup>

In July 2010, a breakthrough in white OLED efficiency was made by GE-Konica Minolta, which demonstrated a device efficiency of 56 lm/W that proves that flexible, white OLED devices can be made at low cost by using solution-coatable organic materials.<sup>84</sup>

In 2010, Osram opto-semiconductors introduced the first example of OLED lighting for commercial applications i.e home and business. The ORBEOS OLED emits diffused white light at 2800 K, and only consumes the fraction of the power consumed by the commercial light bulbs. The brightness is approximately 1,000 cd/m<sup>2</sup> and has a lifespan of about 5,000 hours.<sup>85</sup>

One of the major problems associated with OLED technology is the high cost of manufacturing and many research groups are seeking routes to low cost deposition of organic compounds onto flat surfaces. In April 2011, Mitsubishi and Verbatim introduced a deposition technique in the place of conventional vapour deposition, which allowed the mass production of devices with lower costs and enabled the creation of larger displays.<sup>86</sup>

In 2012, an OLED panel was reported with a graphene anode, which had a high work function and low resistance. It produced luminous efficiencies of 37.2 lm/W in fluorescent OLEDs and 102.7 lm/W in phosphorescent OLEDs.<sup>87</sup>

In 2012, a white OLED panel was independently introduced by Toshiba and Panasonic with an efficiency of 90 lm/W and a brightness of 1000 cd/m<sup>2</sup>. LG chemicals plan to develop a white OLED panel with an efficiency of 135 lm/W and higher brightness of 3000 cd/m<sup>2</sup> by 2015.<sup>41, 88-90</sup>

In April 2013, LG introduced the first curved 54.6 inch OLED TV into the market, which has a thickness of just 4.3 mm and a weight of only 17 kg. According to the company researchers, it took nearly 5 years to get optimum curvature so that complete screen surface is equal distance from the eyes.<sup>90</sup>

In March 2014, the most efficient OLED panel was reported that had a peak efficiency of 131 lm/W, which was developed by Konica Minolta. The Japan-based company has claimed that this is the world's most efficient OLED panel. It measures 15 square centimetres and has a life time of 55,000 hours when run at a constant current density from an initial brightness of 1,000 cd/m<sup>2</sup>.<sup>42</sup>

Blue phosphorescent OLEDs have a shorter life-span compared to red and green phosphorescent OLEDs. This is in large part due to the large band-gap of the blue materials used, which tends to make them relatively unstable, with identification and evaluation of suitable host materials being complicated. Research has been carried out to improve the life-time of blue OLEDs. In September 2014, Prof. Stephen Forrest and his group at Michigan State University successfully extended the lifetime of a blue OLED by a factor of 10, increasing their efficiency from 5% to 20%.<sup>43</sup>

## **1.6 Stability and reliability of OLEDs and PhOLEDs**

The lifetime of an OLED or a PhOLED is one of the most important issues in characterising its performance. An operating lifetime of at least 10,000 hours is required combined with 5 years storage lifetime. The lifetime of current OLEDs remain inferior to those of comparable inorganic LEDs. One of the most important factors, which effects OLED stability and lifetime, is the purity of the organic semiconductors used in the devices. It has been shown that ionic impurities can have a dramatic effect on device

life time, as they act as a traps for excitons formed during the recombination process. The ionic impurities also promote electrochemical degradation of the electrodes *via* redox reactions. These ionic impurities seem to have more of an effect than organic impurities resulting from the organic synthesis. Column chromatography and HPLC can be used to remove organic impurities to produce product purity above 99.9%. However, these chromatographic techniques often fail to remove ionic impurities that may be introduced by the organic solvents and/or during the synthetic procedures. Techniques to remove these ionic impurities include using ion-exchange resins and metal trapping agents. Other factors that can affect device stability and reliability include the following.<sup>44</sup>

Photochemical degradation: often caused by photo-oxidation, when the organic semiconductors react with any traces of residual oxygen in the device.

Electrochemical degradation: often caused by ionic impurities or water, which can cause redox reactions at the device electrodes.

Structural degradation: often caused by molecular-reorganisation and relaxation or recrystallisation of glassy phases or mesophases. This is often attributed to the damaging effects of a constant voltage bias.

Electrode degradation: the electrodes can react with the materials. This has been regarded as a form of ITO-diffusion into the organic layers.

Colour purity: often red and blue pixels are the first to fail, which leaves a predominantly green display.

## **1.7 Organic Photovoltaics (OPVs)**

Photovoltaic (PV) technology converts incident solar energy into electric current. Most photovoltaic cells utilise doped silicon or other inorganic semiconductors absorb light, generate the excited state, separate the electron/hole pair and then transport holes and electrons in opposite directions to the electrodes during the photovoltaic process to generate an electric current and a photovoltage. Solar panels based on a wide range of inorganic semiconductors are a very important commercial product in terms of green energy production.

Organic Photovoltaic (OPV) devices use organic semiconductors as the active layers, rather than inorganic ones, in a very similar photovoltaic process to generate electricity. OPV devices offer many potential advantages over current commercial PVs including possibility of inexpensive processing of lightweight, flexible solar cells. OPVs are complicated to make due to their requirement of having multiple materials and layers that must be incorporated to enable the device to function. The commercial of very large scale OPVs is feasible due to the use of roll-to-roll, wet-chemistry deposition techniques, such as inkjet printing on very large plastic substrates.

The general structure used for organic solar cells is similar to OLEDs. At its simplest, terms it consists of one or more layers of organic semiconducting material sandwiched between two conducting electrodes, which are deposited on glass or plastic substrates. The active layer consists, depending on the device configuration, of an electron-donor (ED) and an electron acceptor (EA). The electron-donor should have a low Ionisation Potential (IP) and the electron acceptor should have a high electron affinity (EA). These properties are defined by values of the highest occupied molecular orbital (HOMO) and the lowest unoccupied molecular orbital (LUMO) energy levels and by the energy/band gap ( $E_g$ ) between them. One or both of these layers can act as the light absorption layer. A transparent material, such as glass covered with Indium Tin Oxide (ITO), is used to allow light to pass through the surface of the OPV and enter the active layer of organic semiconductor, which then absorbs the incident light. The general photovoltaic process is then very similar to that described above for PVs, see below for a more detailed description of OPVs.<sup>45</sup>

### **1.7.1 OPV Mode of Operation**

The bulk heterojunction (BHJ) solar cell has become one of the most successful OPV prototype device structures developed so far. In this device configuration, Figure 19, the electron donor is an electron-rich organic semiconductor and the electron acceptor is an electron-deficient organic semiconductor. The ED and EA materials are blended together to form a bi-continuous interpenetrating network as a thin, planar layer on the device substrate. This device configuration provides a very interfacial area donor-acceptor (D-A) available for the exciton dissociation.

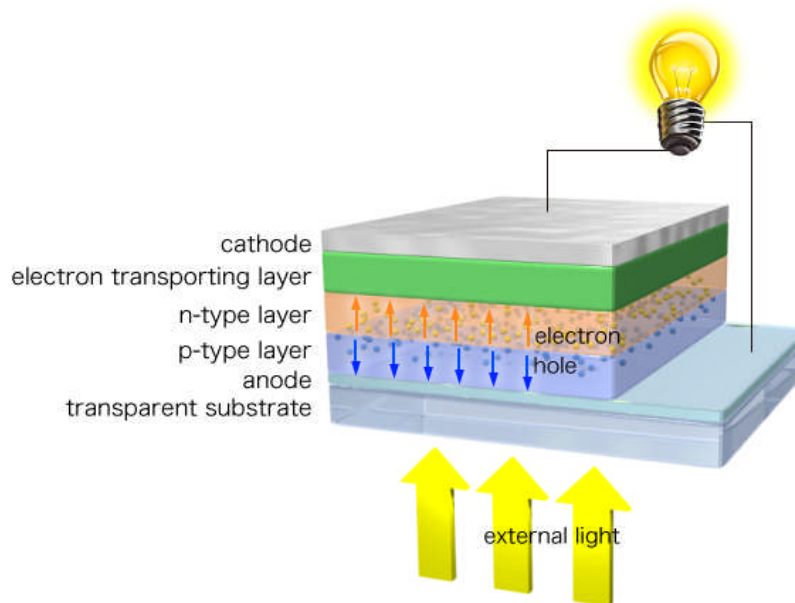


Figure 19: Diagram illustrates the general photovoltaic process.<sup>46</sup>

Sunlight falls on the OPV and the incident photons are absorbed by the organic material making up the active layer, if the photon energy is higher than that of the active layer's band-gap. When the energy from the photon is absorbed, a bound electron/hole pair is generated (an exciton). Charge separation occurs at the interface between the electron acceptor (EA) and electron donor (ED) semiconductors (active layer), where the electron migrates to one electrode and the hole migrates to the other electrode, thereby producing direct current (DC) and generating a photovoltage. The donor-acceptor heterojunction (interfacial area) is a critical component of OPVs because it controls the charge dynamics in the devices.

The performance of an OPV cell is usually measured by its energy conversion efficiency ( $\eta$ ), which measures the amount of solar energy converted to electricity relative to the total energy incident upon the solar cell.  $\eta$  is primarily influenced by three main factors:

**Absorption:** the percentage of light that is absorbed by the active layer, is primarily determined by the band-gap and thickness of the absorption layer.

**Charge Separation:** when excitons are created, the pairs of electrons and holes (excitons) must be separated from each other so that they can flow in opposite directions to be collected at the electrodes and so generate a photocurrent and a photovoltage. It is also important that the hole and electrons do not recombine whereby

their energy is lost as heat rather than being used to create electric current. Charge separation generally occurs at the ED/EA organic semiconductor interface and the differences in IA and EA should be large enough to overcome the exciton binding energy and so separate the exciton to form an unbound hole and electron, Figure 20. Since excitons can only diffuse a short distance (10-20 nm), the morphology of the active layer should be such that the individual paths for the holes and electrons to the electrodes, i.e., the cathode and the anode, respectively, are different and they should be as short as possible in order to minimise electron/hole recombination.

**Charge Transport:** the mobility of the holes and electrons through the organic semiconductor active layer should be as high as possible so that the charge flows as quickly as possible to the appropriate electrodes, i.e., the anode for electrons and the cathode for holes, in order to generate a high electric current and to minimise charge recombination. Interaction with atoms, other charges, or crystal grain boundaries, i.e., defects, may reduce the charge transport.<sup>47-49</sup>

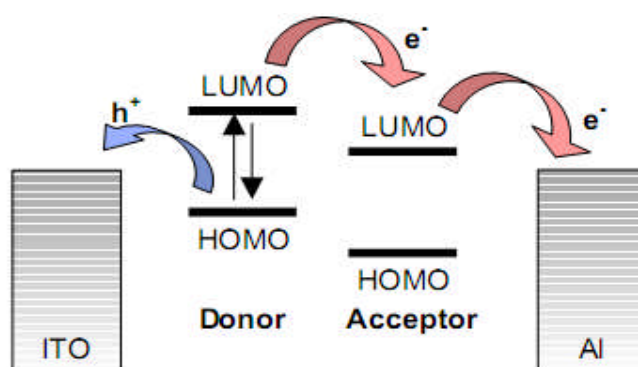


Figure 20: Diagram illustrates the exciton dissociation taking place at the acceptor/donor interface.<sup>50</sup>

### 1.7.2 Materials for Organic Solar Cells

The most common electron acceptor material in organic solar cells is [6,6]-phenyl-C61-butyric acid methyl ester (PCBM), Figure 21. One of the most common electron donors is the main-chain, highly conjugated polymer P3HT, Figure 22.

Highly conjugated organic compounds with a Donor-Acceptor-Donor (D-A-D) molecular structure, Figure 23, have recently attracted great attention due to their outstanding photovoltaic performance in OPVs. The D-A-D molecules possess

extended  $\pi$ -conjugation and good (HOMO and LUMO) energy levels. A relatively high degree of crystallization is also for stable OPV devices. The combination of donor (D) and acceptor (A) groups leads to very efficient internal charge transfer (ICT), which produces a red shift extension of the absorption spectrum and a decrease of the HOMO level, which results in higher photon absorption and an increase of the open-circuit voltage of an OPV cell, respectively.<sup>51-54</sup>

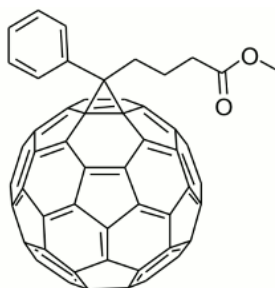


Figure 21: Chemical structure of [6,6]-phenyl-C61-butyric acid methyl ester (PCBM).

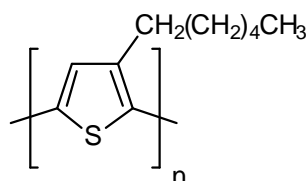


Figure 22: Chemical structure of poly(3-hexylthiophene) (P3HT).

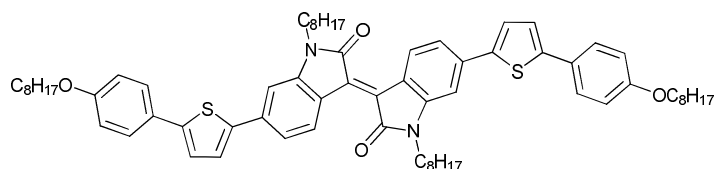


Figure 23: Typical structure of a D-A-D molecule.

## 1.8 Liquid crystals

Liquid crystals are a state of matter in between that of a disordered, isotropic liquid and that of an amorphous or crystalline solid. Compounds that form the liquid crystalline state possess an anisotropic structure; see later for details of different types of liquid crystal. However, thermotropic calamitic liquid crystals, that often form nematic and smectic liquid phases, have lathe-like, rigid-rod molecular structures. Thermotropic liquid crystals are formed by the action of heat and lyotropic liquid crystals are formed by the addition of a solvent, see below. Lyotropic liquid crystalline mesophases are also

usually thermotropic, i.e., change with temperature. Calamitic molecules in a crystalline solid maintain their orientation and stay in the same position with respect to one another, but may rotate around their long molecular axis, Figure 24. When the molecules are heated the interactions between the molecules begin to break down. If all interactions break down simultaneously then an isotropic liquid is formed. However, if the interactions break down in stages, e.g., side-to-side or end-to-end, then intermediate states of matter are formed between the solid state and liquid state. These intermediate phases are characteristic of liquid crystals and are called mesophases. Mesophases are characterised by partial ordering of the molecules within domains. The molecules have the same orientation, but no positional ordering, in the nematic phase or the smectic A phase, for example, mesophases. However, due to the high orientational ordering the liquid crystals show a strong anisotropy in many of their physical and chemical properties.<sup>16</sup>

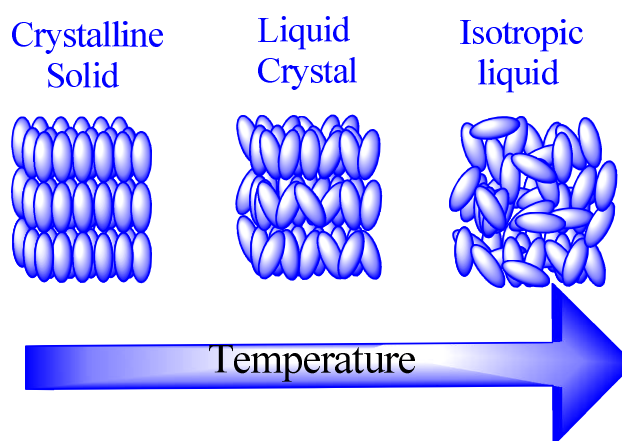


Figure 24: Schematic representation of the formation of a nematic phase from a crystalline solid on heating and the formation of the disordered, isotropic liquid state on further heating to a higher temperature.

### 1.8.1 Morphology of liquid crystals

Liquid crystals can be divided into two main categories, lyotropic and thermotropic liquid crystals, Figure 25. Thermotropic liquid crystals are formed by a change in temperature, whereas lyotropic liquid crystals are formed by the addition of solvent. Thermotropic liquid crystals are the most common type of synthetic liquid crystals due to the use nematic liquid crystalline mixtures in commercial Liquid Crystal Displays (LCDs). Thermotropic liquid crystals can be subdivided into calamitic, discotic and polymeric types. Calamitic liquid crystals possess a lathe-like or rigid-rod-like shape,

where one molecular axis is much longer than the other two axes. There are three main types of calamitic liquid crystalline phases referred as the nematic phase, smectic phase and the chiral nematic phase.<sup>55</sup>

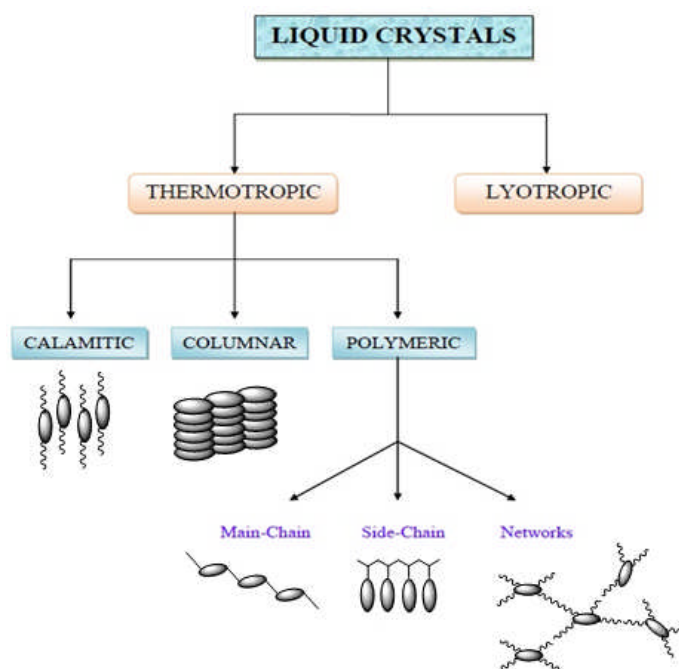


Figure 25: A schematic representation of the main types of thermotropic liquid crystalline mesophases.

### 1.8.1.1 Calamitic Liquid Crystals

Calamitic liquid crystals (Greek “calami”: long and thin) are usually long rod-like molecules containing a molecular core usually made up of two or more six membered rings, either aromatic or alicyclic, with at least one flexible end group and a polar end group, such as a halogen or a cyano group. They can be subdivided into two categories: nematic and smectic mesophases. When a calamitic liquid crystal is heated in the solid state (Cr) the molecules begin to vibrate. At the point when the vibration energy overcomes the attractive forces between the molecules the solid starts to melt and an isotropic liquid (I) is formed, Figure 26. This is known as the melting point (Cr-I). In the case of smectic mesophases (Sm) the attractive forces between the ends of the molecules are overcome while interactions between their long molecular axes are still maintained. This gives rise to a layered structure, where the molecules are still parallel to each other. This temperature is known as a crystal to smectic transition (Cr-Sm). In a nematic mesophase (N) both the attractive forces between the ends of the molecules and

the interaction between their molecular axes are overcome, this gives rise to a non-layered structure where the molecules are orientated mostly in the same direction. This temperature is known as crystalline to nematic transition (Cr-N). If a smectic liquid crystal is heated further it can form a nematic phase by overcoming the attractive forces between the molecular axes. This is called the smectic to nematic transition (Sm-N). If all the remaining forces are overcome, whether in the smectic or in the nematic phase, then the molecules are free to move in a random order giving an isotropic liquid (I). These transitions are called Sm-I or N-I and are all known as the clearing point.

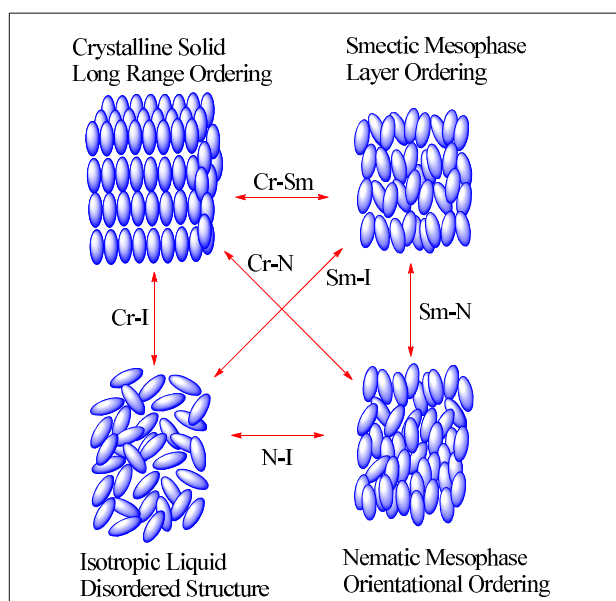


Figure 26: Typical transitions in liquid crystal.

### 1.8.1.2 Nematic Phase

The molecules in a nematic phase have no positional order, but have orientational order. That is, the mesogens all point in roughly the same direction, essentially expressing the molecular anisotropy as a phase anisotropy, Figure 27. A given molecule's orientation is not constant and all the mesogens do not point in exactly the same direction. For an isotropic liquid, averaging molecular orientations gives no result, since there are as many molecules lying along one axis as another. In the nematic phase, averaging molecular orientations gives a definite preferred direction, which is referred to as the director. It is important to remember that liquid crystals are *liquids*, meaning that although there is an average order, molecules are constantly flowing and moving, changing position and orientation.

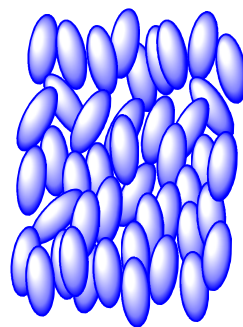


Figure 27: Schematic diagram of a nematic liquid crystal.

### 1.8.1.3 Smectic Phase

Molecules in the smectic phase are more ordered than those in the nematic phase and so smectic phases appear at lower temperatures beneath a nematic phase if one is present. In the smectic phase the molecules are arranged in layers. The molecular long axes are oriented parallel to each other and can be orthogonal or tilted with respect to the layer plane. Twelve smectic phases have been identified so far.<sup>32</sup> In order to illustrate the different smectic phases two have been picked out (smectic A, smectic C). The smectic A phase (SmA) exhibits a layer structure like a density wave and the molecules are free to rotate about their molecular long axis, which is perpendicular to the layer plane. The molecules do not exhibit positional order within the layers and the layers may slide over each other so there is no positional correlation between the layers. Molecules may also move from one layer to another so the smectic A phase is the least ordered of the smectic phase and is relatively fluid, although the viscosity is much higher than that of the nematic phase. The smectic C phase (SmC) is simply the tilted version of the SmA phase, where the molecules are arranged as in the SmA mesophase, but they are tilted with respect to the layer plane, Figure 28.

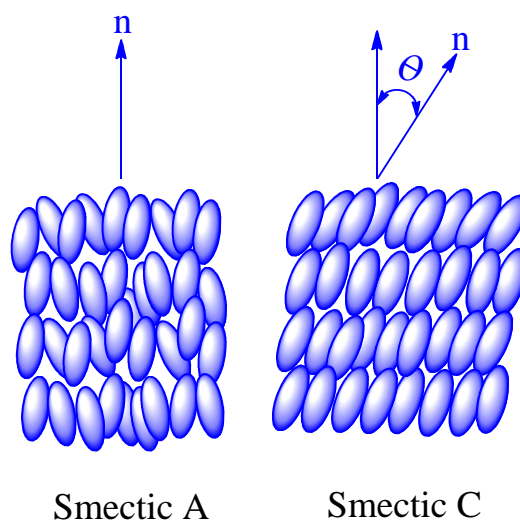
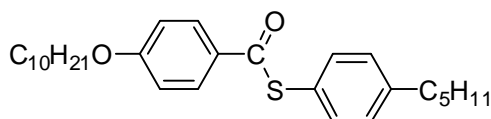


Figure 28: Schematic representation of the smectic A and smectic C mesophase.

Smectic phases are often observed for compounds with an aromatic core composed of two or more aromatic rings, connected by a conjugated linking group or direct carbon-carbon bonds and two long aliphatic chains attached to each end of the molecular core. The chemical structure shown below is for a typical smectic liquid crystal.



## 1.9 Cross coupling reactions

Organometallic chemistry had provided various metal-catalysed cross coupling reactions including Pd, Ni and Cu. Consequently, there are a number of methods available for the synthesis of the required organic compounds, which are useful in wide variety of applications. Three most important and widely using cross coupling reaction methods for synthesis of new C-C bond formation are Suzuki, Stille and Negishi. Suzuki, Stille and direct arylation cross coupling methods are employed to synthesis a wide range of organic compounds in this thesis.<sup>64-71</sup>

A typical palladium based catalytic cycle involves the oxidative addition-transmetalation-reductive elimination sequences as shown below in Figure 29. Various palladium catalysts are used in organic reactions, among those Pd(PPh<sub>3</sub>)<sub>4</sub> is the most widely used catalyst, other examples, Pd(OAc)<sub>2</sub> and Pd(PPh<sub>3</sub>)<sub>2</sub>Cl<sub>2</sub> are also useful in palladium catalyst reactions.

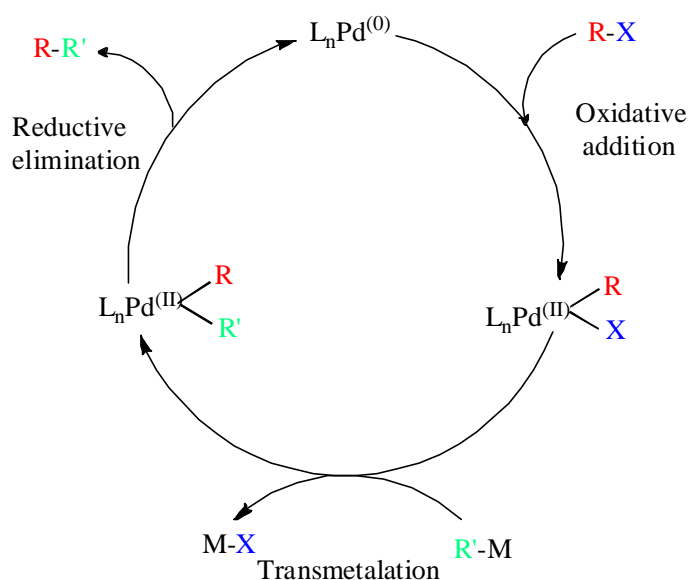


Figure 29: General mechanism of cross coupling.

### 1.9.1 Direct arylation

Pd-catalysed direct arylation is a rapid and an efficient method for the formation of C-C aryl bonds, which is an economically attractive alternative to the conventional metal catalysed cross coupling reactions such as Stille and Suzuki. These traditional methods demand the preparation of organometallic reagents as one of the starting precursor, which generates a quantitative amount of toxic by-products such as organo-tin compounds, which can be difficult to remove from purified intermediates and products. These reactions also require the prior preparation of organo-metallic reactants and are expensive.<sup>56-57</sup>

To overcome these disadvantages, the direct arylation method is a powerful alternative for the construction of heteroatom-containing bi-aryls. In recent years, direct arylation synthetic method has garnered considerable attention due to its ecologically friendly nature. The investigation into direct arylation was first begun in early 1980s for the preparation of hetero atom bi-aryls. In 2006 Fagnou et al. developed a successful synthetic method for the direct arylation of phenyls which followed by subsequent improvements, was adapted for the wide variety of hetero aromatic compounds in different applications such as OLEDs, OPVs and organic field effect transistors.<sup>58-61</sup>

The reactivity of this synthetic tool completely depended on the acidity of C-H but not on aryl halide nucleophilicity. The C-H bonds are common in most organic compounds and are typically unreactive. Consequently, activation of C-H bond is a key challenge.

In 2006 the Fagnou group reported palladium-pivalic acid co-catalyst system and found that pivalic acid plays a vital role in C-H bond cleavage. Experimental evidence reveals that the pivalate anion lowers the energy of C-H bond cleavage by acting as a catalytic proton shuttle.<sup>62-63</sup>

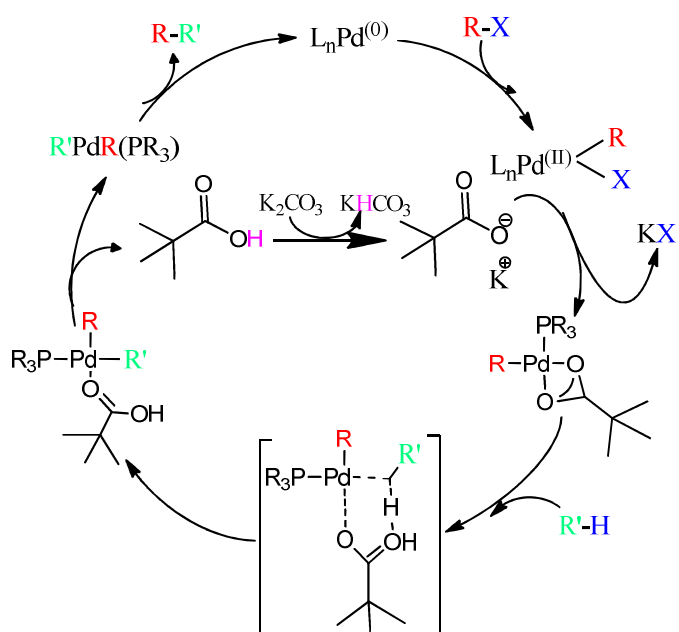


Figure 30: Depicted mechanism of C-H direct arylation.<sup>62</sup>

## 1.10 References

1. J. F. W. Herschel, *Phil. Trans. R. Soc. Lond.*, 1982, **135**, 143.
2. G.G. Stokes, *Phil. Trans. R. Soc. Lond.*, 1852, **142**, 463.
3. J.R. Lakowicz, Kluwer, “*Principles of Fluorescence Spectroscopy*”, Sec. Ed, Academic/Plenum Publishers, New York: 1999.
4. N. Holonyak and S. F. Bevacqua, *Appl. Phys. Lett.*, 1962, **1**, 82.
5. M. Pope, H. P. Kallmann and P. Magnante, *J. Chem. Phys.*, 1963, **38**, 2042.
6. W. Helfrich and W. G. Schneider, *Phys. Rev. Lett.*, 1965, **14**, 229.
7. R. E. Kellogg, *J. Chem. Phys.*, 1966, **44**, 411.
8. P. S. Vincent, W. A. Barlow, R. A. Hann and G. G. Roberts, *Thin Solid Films.*, 1982, **94**, 171.
9. F. J. Campas and M. Goutermann, *Chem. Phys. Lett.*, 1977, **48**, 233.
10. C. W. Tang and S. A. Van Slyke, *Appl. Phys. Lett.*, 1987, **51**, 913.
11. C. W. Tang, S. A. Van Slyke and C. H. Chen, *Appl. Phys. Lett.*, 1989, **65**, 3610.
12. J. H. Burroughes, D. D. C. Bradley, A. R. Brown, R. N. Marks, R. H. Friend, P. L. Burn and A. B. Holmes, *Nature.*, 1990, **347**, 539.
13. C. H. Chem, J. Shi and C. W. Tang, *Macromol. Symp.*, 1997, **125**, 1.
14. P. Vlachos, PhD Thesis, University of Hull, 2003.
15. W. D. Callister, “*Fundamentals of Material Science and Engineering*”, Wiley, New York, 2001.
16. M. P. Aldred, Ph.D. Thesis, University of Hull, 2004.
17. U. Mitschke and P. Bauerle, *J. Mater. Chem.*, 2000, **10**, 1471.
18. C. K. Chiang, C. R. Fincher, H. Shirakawa, E. J. Louis, S. C. Gau and A. G. Macdiamid, *Phys. Rev. Lett.*, 1977, **39**, 1098.
19. G. Destriau, *J. Chem. Phys.*, 1936, **33**, 587.
20. S. R. Farrar, A. E. A. Contoret, M. O’Neill, J. E. Nicholls, G. J. Richards and S. M. Kelly, *Phys. Rev. B.*, 2002, **66**, 125107.

21. Y. Kim, J. Kim, Y. Kim, H. Choi, J. H. Jung, and B. Lee, *Applied. Optics.*, 2008, **47**, 4927.
22. A. E. Becquerel, *Compt. Rend. Acad. Sci.*, 1839, **9**, 145, 565.
23. A. C. Arias, N. Corcoran, M. Banach, R. H. Friend, J. D. MacKenzie and W. T. S. Huck, *Appl. Phys. Lett.*, 2001, **80**, 1695.
24. L. Schmidt-Mende, A. Fechtenkötter, K. Müllen, E. Moons, R. H. Friend and J. D. MacKenzie, *Science.*, 2001, **293**, 1119.
25. J. Salbeck and B. Bunsenges, *Phys. Chem.*, 1996, **100**, 1667.
26. C. Adachi, M. A. Baldo, M. E. Thompson and S. R. Forrest, *J. Appl. Phys.*, 2001, **90**, 5048.
27. A. R. Brown, D. D. C. Bradley, P. L. Burn, J. H. Burroughes, R. H. Friend, N. Greenham, A. B. Holmes and A. Kraft, *Appl. Phys. Lett.*, 1992, **61**, 2793.
28. P. M. Brosenberger and D. S. Weiss, “*Organic Photoreceptors for Xerography*”, Marcel Dekker Inc., New York, 1998.
29. F. Santerre, I. Bedja, J. P. Dodelet, Y. Sun, J. Lu, A. S. Hay and M. D'Iorio, *Chem. Mater.*, 2001, **13**, 1739.
30. C. Adachi, T. Tsutsui and S. Saito, *Appl. Phys., Lett.*, 1990, **57**, 531.
31. A. P. Kulkarni, C. J. Tonzola, A. Babel, and S. A. Jenekhe, *Chem. Mater.*, 2004, **23**, 4556.
32. S. M. Kelly “*Flat panel displays: Advanced organic materials*” RSC, 2000.
33. K. Müllen and U. Scherf “*Organic light emitting devices: Synthesis, properties and application*”, Wiley, 2006.
34. B. Diouf, W. S. Jeon, R. Pode and J. H. Kwon, *Adv. Mat Sci & Eng.*, 2012.
35. M. A. Baldo, S. Lamansky, P. E. Burrows, M. E. Thompson and S. R. Forrest, *App. Phy. Lett.*, 1999, **75**, 4.
36. Y. Diao, L. Shaw, Z. Bao and S. C. B. Mannsfeld, *Energy. Environ. Sci.*, 2014, **7**, 2145.
37. H. Yersin, *Top. Curr. Chem.*, 2004, **241**, 1.
38. S. Kappaun, C. Slugovc and E. J. W. List, *Int. J. Mol. Sci.*, 2008, **9**, 1527.

39. H. Yersin, A. F. Rausch, R. Czerwieniec, T. Hofbeck and T. Fischer, *Coordination Chemistry Reviews.*, 2011, **255**, 2622.
40. S. Reineke, M. Thomschke, B. Lüsse and K. Leo, *Rev. Mod. Phys.*, 2013, **85**, 1245.
41. H. Sasabe and J. Kido, *J. Mater. Chem.*, 2013, **1**, 1699.
42. <http://www.electronics-eetimes.com>, (accessed January 2014).
43. <http://www.eecs.umich.edu>, (accessed September 2014).
44. S. P. Kitney, Ph.D. Thesis, University of Hull, 2008.
45. E. J. Lubber and J. M. Buriak, *ACS Nano.*, 2013, **7**, 4708.
46. <http://www.cstf.kyushu-u.ac.jp>, (accessed September 2014).
47. C. W. Tang, *Appl. Phys. Lett.*, 1986, **48**, 183.
48. H. Hoppe and N.S. Sariciftci, *Materials. Research*, **19**, 1924.
49. T. J. Savenije, “*Organic Solar Cells*”, Wiley, 2010.
50. H. Spanggaard and F. C. Krebs, *Solar. Ener. Mate & Solar Cells.*, 2004, **83**, 125.
51. A. Yassin, P. Leriche, M. Allain and J. Roncali, *New. J. Chem.*, 2013, **37**, 502.
52. C. Li, Y. Chen, Y. Zhao, H. Wang, W. Zhang, Y. Li, X. Yang, C. Ma, L. Chen, X. Zhua and Y. Tu, *Nanoscale.*, 2013, **5**, 9536.
53. S. Jin, K. Furukawa, M. Addicoat, L.Chen, S. Takahashi, S. Irle, T. Nakamura and D. Jiang, *Chem. Sci.*, 2013, **4**, 4505.
54. R. S. Kularatne, H. D. Magurudeniya, P. Sista, M. C. Biewer and M. C. Stefan, *Polymer chemistry.*, 2013, **51**, 743.
55. P. J. Collings and M. Hird, “*Introduction to Liquid Crystals*”, Taylor and Francis, London, UK, 1997.
56. A. Facchetti, L. Vaccaro and A. Marrocchi, *Angew, Chem. Int. Ed.*, 2012, **51**, 3520.
57. B. Liegault, D. Lapointe, L. Caron, A. Vlassova and K. Fagnou, *J. Org. Chem.*, 2009, **74**, 1826.
58. M. Baghbanzadeh, C. Pilger and C. O. Kappe., *J. Org. Chem.*, 2011, **76**, 8138.
59. D. J. Schipper and K. Fagnou, *Chem. Mater.*, 2011, **23**, 1594.

60. Y. Fujinami, J. Kuwabara, W. Lu, H. Hayashi and T. Kanbara, *Acs Macro Lett.*, 2012, **1**, 67.
61. A. E. Rudenko and B. C. Thompson, *Pol. Chem.*, 2015, **53**, 135.
62. M. Lafrance and K. Fagnou, *J. Am. Chem. Soc.*, 2006, **128**, 16496.
63. J.Q. Yu and Z. Shi, “*Topics in Current Chemistry*”, C-H activation, Springer, 2010.
64. T. J. Colacot, *Platinum Metals Rev.*, 2011, **55**, 84.
65. N. Miyaura and A. Suzuki, *Chem. Rev.*, 1995, **95**, 2457.
66. N. Miyaura, K. Yamada and A. Suzuki, *Tetrahedron Lett.*, 1979, **20**, 3437.
67. N. Miyaura and A. Suzuki, *J. Chem. Soc. Chem. Commun.*, 1979, 866.
68. M. Kosugi, K. Sasazawa, Y. Shimizu and T. Migita, *Chem. Lett.*, 1977, 301.
69. D. Milstein and J. K. Stille, *J. Org.Chem.*, 1979, **44**, 1613.
70. J. K. Stille, *Pure Appl. Chem.*, 1985, **57**, 1771.
71. V. Uchil, B. Seo and V. Nair, *J. Org. Chem.*, 2007, **72**, 8577.
72. J. Kido, K. Nagai and Y. Okamoto, *IEEE Trans. Electron Device.*, 1993, **40**, 1342
73. K. Walzer, B. Maennig, M. Pfeiffer and K. Leo, *Chem Rev.*, 2007, **107**, 1233.
74. C. W. Tang and S. A. VanSlyke, *Appl. Phys. Lett.*, 1987, **51**, 913.
75. L. S. Hung, C. W. Tang and M. G. Mason, *Appl. Phys. Lett.*, 1997, **70**, 152.
76. T. Wakimoto, Y. Fukuda, K. Nagayama, A. Yokoi, H. Nakada and M. Tsuchida, *IEEE Trans. Electron Device.*, 1997, **44**, 1245.
77. J. Kido and T. Matsumoto, *Appl. Phys. Lett.*, 1998, **73**, 2866.
78. A. Buckley, “*Organic Light-Emitting Diodes: Materials, Devices and Applications*” Woodhead Publishing, 2013.
79. J. Huang, M. Pfeiffer, A. Werner, J. Blochwitz, K. Leo and S. Liu, *Appl. Phys. Lett.*, 2002, **80**, 139.
80. M. Pfeiffer, S. R. Forrest, K. Leo and M. E. Thompson, *Adv. Mater.*, 2002, **14**, 1633.
81. R. J. Bushby, S. M. Kelly and M. O'Neill, “*Liquid crystalline semiconductors: Materials, properties and applications*”, Springer, 2013.

82. Nakayama, T. Hiyama, K. Furukawa and K. Ohtani, *Society for Information display International*, Symposium, 2007, **38**, 1018.
83. <https://www.novaled.com>, (accessed January 2014).
84. <https://www.photonics.com>, (accessed January 2014).
85. <https://www.ledlight.osram-os.com>, (accessed January 2014).
86. <https://www.displays.mitsubishielectric.eu>, (accessed January 2014).
87. T. H. Han, Y. Lee, M. R. Choi, S. H. Woo, S. H. Bae, B. H. Hong, J. H. Ahn and T. W. Lee, *Nature Photonics.*, 2012, **6**, 105.
88. T. Komoda, K. Yamae, V. Kittichungchit, H. Tsuji and N. Ide, *SID 12 Digest.*, 2012, 610.
89. S. T. Ono, D. Kato, T. Yonehara, T. Sawabe, S. Enomoto and I. Amemiya, *SID 12 Digest.*, 2012, 1548.
90. <https://www.lgchem.com>, (accessed January 2014).

## 2. Aims of the Research

One main aim of this thesis was to synthesise light-emitting and/or charge transporting liquid crystalline semiconductors more efficiently *via* simple synthetic pathways, such as direct arylation of thiophene with aryl halides *via* C-H bond activation using palladium catalysts. Liquid crystalline organic semiconductors are promising materials for plastic electronic devices, such as light emitting diodes<sup>1</sup>, organic photovoltaics<sup>2</sup> and field-effect transistors due to their high charge carrier mobility and the ability to emit plane or circularly polarised light. The conventional method to synthesise most organic semiconductors uses traditional metal catalysed, aryl-aryl, cross-coupling reactions such as Suzuki-Miyaura, Stille, Kumada and Negishi coupling.<sup>27-30</sup> However, these conventional methods have drawbacks including the use of organometallic reagents, which generates a stoichiometric amount of -often toxic- metal waste, which is difficult to handle. These reactions also require the prior preparation of organo-metallic reactants.<sup>3-5</sup> In order to avoid the need to prepare and/or use organo-metallic reagents, it was decided to synthesise the target compounds using direct arylation reactions, which have been shown, for example, to be a viable, alternative to traditional aryl-aryl cross-coupling reactions in the synthesis of high-molecular-weight conjugated mainchain polymers. Such highly conjugated liquid crystalline organic semiconductors, such as that shown in Figure 2.01, have previously synthesised in six to eight steps by using traditional aryl-aryl cross-coupling reactions, such as Suzuki and Stille reactions. Most of the intermediate steps required heating over 16-20 hours. The new direct-arylation synthetic procedure, to be used in the work for this thesis, in the synthesis of known liquid crystalline organic semiconductors allows compounds, such as that shown in Figure 2.01, to be synthesised in just three steps using only two reaction intermediates. All the intermediate steps can be carried out in just 2-3 hours using similar reagents, catalysts and solvents, but with lower catalyst loadings.

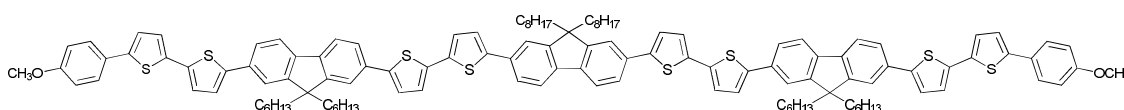


**Figure 2.01** Typical structure of a liquid crystalline organic semiconductor.

Many conjugated mainchain polymers, oligomers and reactive mesogens incorporating the 2,7-disubstituted-9,9-dialkyl-fluorene moiety have been synthesised for use in OLEDs, PLEDs and organic photovoltaic devices. Many of these fluorenes exhibit efficient blue photoluminescence and electroluminescence in thin films<sup>6-8</sup> and also exhibit good hole-transporting properties.<sup>9-10</sup> The length of the alkyl chain at the bridging benzylic position (9-position) of the fluorene aromatic core influences the transition temperatures, such as the melting point and the glass transition temperature of such compounds. The presence of the two long alkyl chains at the 9-position of the fluorene aromatic core also give rises to soluble compounds with a relatively low melting point and a high glass transition temperature that allows these fluorene derivatives to be quenched to form a glass at room temperature in which any liquid crystalline order is preserved. A common problem with many conjugated mainchain polymers, oligomers and reactive mesogens incorporating the 2,7-disubstituted-9,9-dialkyl-fluorene moiety is the appearance of a tail of green emission, colour instability and lower efficiency. This phenomenon has been attributed to the formation of aggregates or excimers as well as the formation of keto defects to form fluorenone derivatives *via* oxidative degradation of the 9,9-dialkyl fluorene moieties.

Therefore, the second main aim of this thesis was to synthesise novel liquid crystalline organic semiconductors, where the central 2,7-disubstituted-9,9-dialkyl-fluorene moiety will be replaced by the 2,7-disubstituted-9-*N*-alkyl-carbazole moiety shown in Figure 2.02.

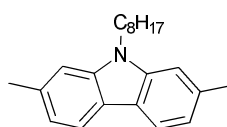


**Figure 2.02** Structure of 2,7-disubstituted *N*-alkyl carbazole building block.

Furthermore, the 3-substituted *N*-octyl carbazole end-group was chosen as another important building block for new liquid crystalline organic semiconductors because of its desirable electronic and charge-transport properties, as well as their high thermal stability.<sup>11</sup> It has a similar shape to the fluorene moiety, but oxidative degradation of this group should occur much less readily. In the case of analogous 2,7-carbazole-based polymers the nitrogen atom is in the *meta*-position in the highly conjugated polymer backbone. The electron-donating nature of the 3,6-disubstituted carbazole ring bound to an electron-deficient ring in such polymers is stronger than that of the 2,7-carbazole

ring because the alkyl-substituted nitrogen atom is in the *para*-position with respect to the polymer backbone in the 3,6-disubstituted carbazoles. The presence of the 3,6-disubstituted carbazole ring with one alkyl chain attached to the nitrogen atom should produce a planar aromatic core with the alkyl substituent in the same plane as the rest of the aromatic molecular core. This configuration should also reduce the intermolecular distance between adjacent molecules and so facilitate charge transport by a hopping mechanism. This should produce liquid crystalline materials with improved charge transport properties. Furthermore, stronger intra-molecular charge transfer due to a more planar conjugated backbone is expected to improve the hole mobility.<sup>12-14</sup>

Liquid crystalline, small-molecule carbazole derivatives with columnar phases have been reported.<sup>15-18</sup> Carbazole oligomers and side-chain polymers with carbazole side-chains have also been reported to exhibit nematic and smectic phases.<sup>19-22</sup> However, no small molecule carbazole-based liquid crystals with a nematic phase have been prepared to the author's knowledge. Chromophores incorporating the 2,7-disubstituted-9-*N*-alkyl-carbazole group have been reported to exhibit efficient blue photoluminescence and electroluminescence and function as efficient hole-transporting layers in thin films.<sup>23</sup> Therefore, it appears well worthwhile to attempt to synthesise the first liquid crystalline, light-emitting and hole-transporting reactive mesogens for use in LC-OLEDs.

A subsidiary aim of the work for this thesis was to synthesise a new class of liquid crystalline organic semiconductor materials, such as those shown in Figure 2.03 with *N*-alkyl carbazole end groups and a 2,7-disubstituted-9,9-dialkyl-fluorene moiety in the centre of the molecular core, which should form stable glasses above room temperature and ideally exhibit liquid crystalline behaviour.

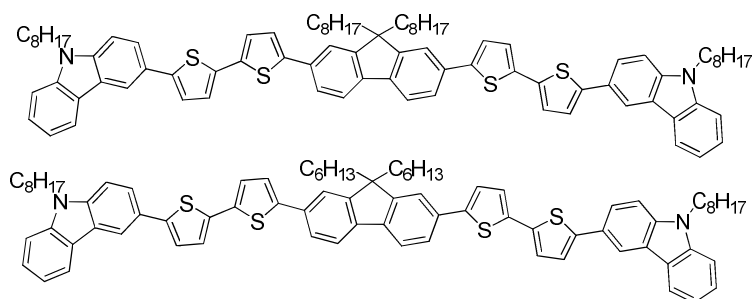


**Figure 2.03** Typical structure of new materials with *N*-alkyl carbazole end-groups.

Furthermore, the Organophotonics Research Group at the University of Hull, along with other groups, such as E. Merck, had previously synthesised polymerisable liquid

crystalline organic semiconductors (reactive mesogens) with either an acrylate, methacrylate, oxetane or diene groups at the end of an aliphatic chain attached to each end of the aromatic core. Therefore, it was decided to synthesise the kind of compound shown in Figure 2.03, but with a polymerisable group attached to the end of the flexible alkyl chain in the *N*-alkyl carbazole position in order to see whether this would produce new polymerisable liquid crystalline organic semiconductors with an improved property spectrum. These reactive mesogens would then be deposited from solution onto a substrate and photochemically polymerised to form an insoluble, intractable layer, i.e., as a polymer network, in an electronic device, such as an OLED, OPV or OFET, for the first time.

Incorporating aromatic heterocyclic organic rings, such as 2,5-disubstituted thiophene rings, or *N*-alkyl-2,7-disubstituted carbazole rings, into such structures, e.g., such as those shown in Figures 2.03 and 2.04, should produce liquid crystalline organic semiconductors with the desired physical properties and appropriate transition temperatures, such as a low melting point and a high clearing point with glass transition above room temperature. The synthesis of materials, such as those shown above in Figures 2.03 and 2.04, would also allow a direct comparison of the liquid crystal transition temperatures of mesogens differing in the nature of the dialkyl substituents and *N*-octyl carbazole end chains to be made.

A number of oligomeric compounds with a number ( $n = 1-5$ ) of 2,5-disubstituted thiophene rings in the centre of the molecular core with a 3-substituted carbazole moieties at each end of the molecular core, as shown in Figure 2.04, will be synthesised as organic semiconducting materials. The combination of the presence of the 2,5-disubstituted thiophene and 3-substituted carbazole rings should lead to a low band gap ( $E_g$ ) and high HOMO levels. The magnitude of both of these properties is expected to decrease with increasing number of thiophene rings ( $n$ ). A low electron affinity is also expected for this type of compound.

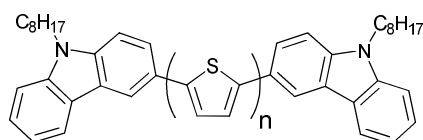


**Figure 2.04** Oligomeric 2,5-disubstituted thiophenes with 3-substituted carbazole moieties at the end of the aromatic molecular core.

An important additional aim of this research was to synthesise a wide range of novel liquid crystalline organic semiconductors with different aromatic cores in order to study their structure-property relationships, such as the type of mesophases, their the liquid crystalline transition temperatures, charge-transport, HOMO, LUMO energy levels, ionisation potential and electron affinity. The correlation between molecular structure and charge-transporting properties was to be achieved by synthesising a series of related compounds with different central moieties, such as those shown in Figure 2.05, in order to facilitate clear comparisons of the efficiency of each of the chromophores to be established.

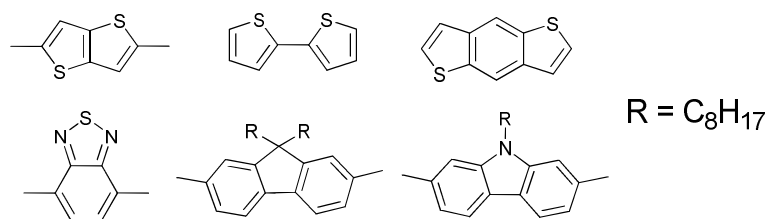


**Figure 2.05** The main aromatic rings used as part of the central reactive mesogens prepared in this research.

A further aim of this research was to synthesise a new class of liquid crystalline organic semiconductors, incorporating a 2,5-disubstituted 1,3,4-oxadiazole ring in the molecular core, with bipolar transport properties for use in OLEDs, OPVs and OFETs. The 1,3,4-oxadiazole ring is an attractive building block for this purpose, because it is a good electron-withdrawing group and known organic semiconductors containing it possess high thermal and oxidative stability and good film forming ability, high electron injection and charge-carrier mobility, and act as hole-blocking layers, which can potentially lead to OLEDs with low operating voltages.<sup>8</sup> Carbazole derivatives have been widely used as host layers for phosphorescent organo-metallic emitters in OLEDs due to their hole transporting ability. Therefore, compounds incorporating a combination of 3-substituted *N*-alkyl carbazole and 2,5-disubstituted 1,3,4-oxadiazole rings in the molecular core are expected to act as bipolar host layer for phosphorescent organo-metallic dopants in PhOLEDs.<sup>24</sup> Therefore, in a new approach, we intend to combine sterically hindered 3-substituted *N*-octyl carbazole end-groups with 2,5-disubstituted 1,3,4-oxadiazole rings in a central position in the aromatic core of new organic semiconductors where the carbazole groups will be linked to a 2,5-disubstituted 1,3,4-oxadiazole ring by 1,4-disubstituted phenyl and/or 2,5-disubstituted thiophene rings in order to prepare liquid crystalline materials with good processability from

solution, e.g., using spin coating, suitable HOMO-LUMO energy levels, high thermal and electrochemical stability and, potentially, blue light-emitting properties.<sup>9</sup>

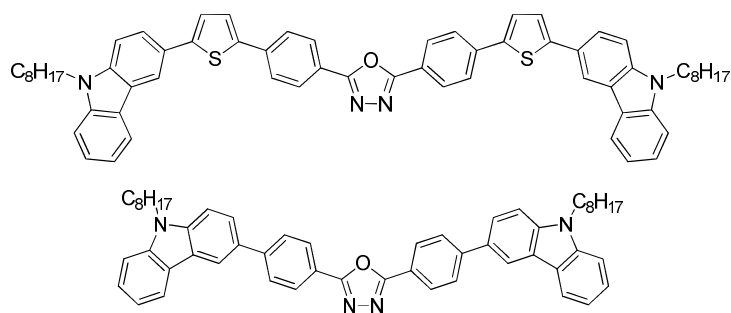


**Figure 2.06** Proposed structures of oxadiazole and carbazoles.

In order to make use of colour rendering and colour tunability over the whole visible spectrum in OPVs and OFETs, materials that emit other than in the red-green-blue primary regions of the spectrum are also required. Therefore, the synthesis of a compound incorporating a 4,7-disubstituted benzothiadiazole moiety, such as that shown in Figure 2.07, that emits in the yellow region of the electromagnetic spectrum will be synthesised in an attempt to create yellow-emitting materials. Such highly conjugated aromatic Donor-Acceptor-Donor (D-A-D) compounds are very useful materials for OPVs due to a high degree of intra-molecular charge transfer. The carbazole moiety is suitable for such D-A-D materials due to its strong electron-donating nature, which should produce a low band gap and high HOMO energy levels, when combined with electron-accepting rings, such as the 4,7-disubstituted benzothiadiazole moiety, in the molecular core. Therefore, a number of liquid crystalline D-A-D compounds, such as that shown in Figure 2.07, will be synthesised.

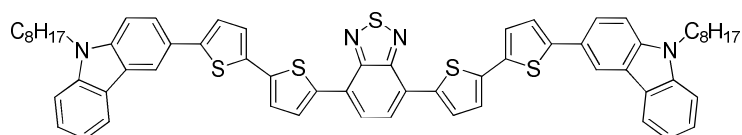


**Figure 2.07** Proposed structure of benzothiadiazole.

Another aim of this thesis was to synthesise compounds with fused aromatic rings, such as naphthalene and anthracene, in the molecular core with carbazole as the end-groups in order to produce liquid crystalline semiconductors, such as that shown in Figure 2.08,

with appropriate energy levels. It should also facilitate the study of the influence of extensive delocalization in the central molecular core on the physical and electronic properties of such liquid crystalline semiconductors.

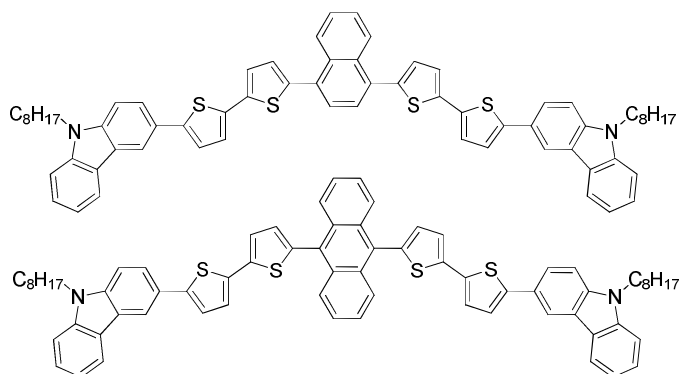


**Figure 2.08** Proposed structures of carbazoles incorporating fused aromatic rings in the middle of the aromatic molecular core.

A number of compounds containing the *N*-alkyl dithieno[3,2-b:2',3'-d]pyrrole aromatic moiety, such as that shown in Figure 2.09, will be synthesised, which should exhibit lower band gaps than those of comparable thiophene compounds due to a higher degree of  $\pi$ -conjugation across the fused thiophene rings.<sup>10</sup> The *N*-alkyl dithieno[3,2-b:2',3'-d]pyrrole (DTPs) appears to be a very promising aromatic building block for organic semiconductors and such materials have been used in prototype OLEDs and OPVs.<sup>16-17</sup> DTP is a strong electron donor and is a very useful building block in the synthesis of donor-acceptor-donor (D-A-D) oligomers. The incorporation of the fused ring DTP unit eliminates rotation around the central thiophene-thiophene bond and the *N*-alkyl side chain of the pyrrole allows for greater solubility without additional steric-interactions that cause deviation from the planarity.<sup>18-19</sup> The presence of fused DTP units in new organic semiconductors should give rise to high charge carrier mobility, high energy levels (HOMO and LUMO) and high conductivity. The planarity of these fused bithiophenes should also lead to lower oxidation potential than the corresponding thiophenes, which should lead to stronger donor properties when incorporated into D-A-D materials. The presence of the DTP moiety reduces the band gap of organic semiconductors by increasing the HOMO energy levels.<sup>20-22</sup>

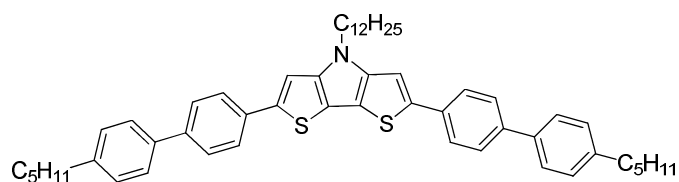


**Figure 2.09** Proposed structure of dithieno[3,2-b:2',3'-d]pyrrole (DTPs).

Isoindigo has strong electron-withdrawing character due to its lactam rings. Recent studies show that isoindigo has broad absorption spectrum across the visible spectrum and that it is an important building block for producing compounds with a low band gap for efficient organic solar cells.<sup>25-26</sup> Isoindigo-based liquid crystals and their applications in electronics have not yet been explored so far, so compounds, such as those shown in Figure 2.10, will be synthesised. The presence of two alkyl chains attached to the central indigo moieties should induce good solubility of these new materials in organic solvents used for spin coating.

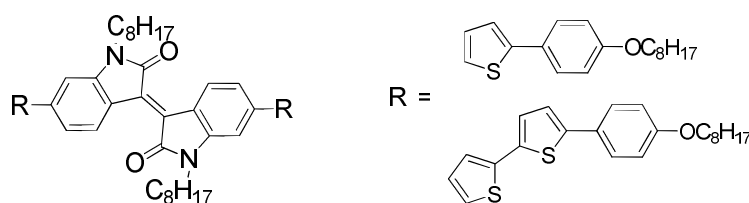


**Figure 2.10** Proposed structures of isoindigo.

A series of novel 9-octyl-2-octyloxy-7-substituted carbazoles incorporating either 2,5-disubstituted 1,3,4-oxadiazole ring and or a 3,3,3-trisubstituted triphenylamine moiety in the centre of the aromatic molecular core, such as those shown in Figure 2.11, will be synthesized in order to yield novel materials with high hole mobility and appropriate energy levels.

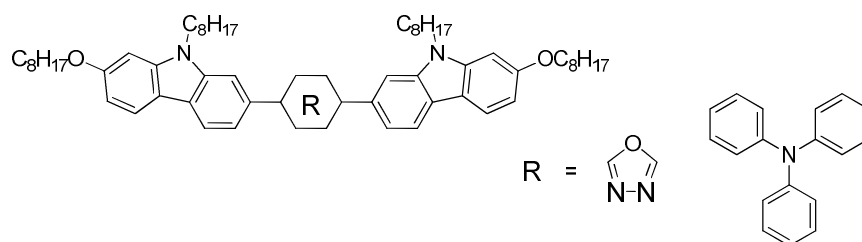


**Figure 2.11** Proposed structures of 9-octyl-2-octyloxy-7-substituted carbazoles.

## 2.1 References

1. T. Yamamoto, *Macromol. Rapid Commun.*, 2002, **23**, 583.
2. M. T. Bernius, M. Inbasekaran, J. O'Brien and W. Wu, *Adv. Mater.*, 2000, **12**, 1737.
3. D. J. Schipper and K. Fagnou, *Chem. Mater.*, 2011, **23**, 1594.
4. Y. Fujinami, J. Kuwabara, W. Lu, H. Hayashi and T. Kanbara, *ACS Macro Lett.*, 2012, **1**, 67.
5. J. Roger, F. Požgan and H. Doucet, *Green Chem.*, 2009, **11**, 425.
6. U. Scherf and E. J. W. List, *Adv. Mater.*, 2002, **14**, 477.
7. T. Miteva, A. Meisel, W. Knoll, H. G. Nothofer, U. Scherf, D. C. Müller, K. Meerholz, A. Yasuda and D. Neher, *Adv. Mater.*, 2001, **13**, 565.
8. Y. Yang and Q. Pei, *J. Appl. Phys.*, 1997, **81**, 3294.
9. D. E. Loy, B. E. Koene and M. E. Thompson, *Adv. Funct. Mater.*, 2002, **12**, 245.
10. M. Redecker, D. D. C. Bradley, M. Inbasekaran and E. P. Woo, *Appl. Phys. Lett.*, 1999, **74**, 1400.
11. A. W. Freeman, M. Urvoy and M. E. Criswell, *J. Org. Chem.*, 2005, **70**, 5014.
12. G. Zotti, G. Schiavon, S. Zecchin, J. F. Morin and M. Leclerc, *Macromol.*, 2002, **35**, 2122.
13. J. Li and A. C. Grimsdale, *Chem. Soc. Rev.*, 2010, **39**, 2399.
14. D. Witker and J. R. Reynolds, *Macromol.*, 2005, **38**, 7636.
15. M. J. Sienkowska, H. Monobe, P. Kaszynski and Y. Shimizu, *J. Mater. Chem.*, 2007, **17**, 1392.
16. K. J. Donovan, K. Scott, M. Somerton, J. Preece and M. Manickam, *Chemical Phys.*, 2006, **322**, 471.
17. E. Perea, F. L. Calahorra and D. Velasco, *Liq Cryst.*, 2002, **29**, 421.
18. M. Manickam, S. Kumar, J. A. Preece and N. Spencer, *Liq Cryst.*, 2000, **27**, 703.
19. A. Dobarro, D. Velasco, V. V. Arnim and H. Finkelmann, *Macromol. Chem. Phys.*, 1997, **198**, 2563.

20. A. Dobarro, D. Velasco, V. V. Arnim and H. Finkelmann, *Macromol. Chem. Phys.*, 1996, **197**, 2729.
21. Y. Koaka and T. Uryu, *Macromol.*, 1995, **28**, 870.
22. Y. Koaka, T. Kato and T. Uryu, *Macromol.*, 1994, **27**, 2658.
23. W. Porzio, C. Botta, S. Destri and M. Pasini, *Synthetic Metals.*, 2001, **122**, 7.
24. Y. Tao, C. Yang and J. Qin, *Chem. Soc. Rev.*, 2011, **40**, 2943.
25. J. Mei, K. R. Graham, R. Stalder and J. R. Reynolds, *Org. Lett.*, 2010, **12**, 660.
26. W. Zhuang, M. Bolognesi, M. Seri, P. Henriksson, D. Gedefaw, R. Kroon, M. Jarvid, A. Lundin, E. Wang, M. Muccini and M. R. Andersson, *Macromol.*, 2013, **46**, 8488.
27. N. Miyaura, T. Yangai and A. Suzuki, *Synth. Commun.*, 1981, **11**, 513.
28. J. K. Stille, *Angew. Chem. Int. Ed. Eng.*, 1986, **25**, 508.
29. K. Tamao, S. Kodama, I. Nakajima and M. Kumada, *Tetrahedron.*, 1982, **38**, 3347.
30. E. Negishi, *Acc. Chem. Res.*, 1982, **15**, 340.

### 3. Experimental

#### 3.1 Evaluation of the Materials

- **<sup>1</sup>H Nuclear Magnetic Resonance (NMR) spectroscopy**

The structures of the intermediates and final products were confirmed by <sup>1</sup>H NMR spectroscopy using a JEOL, JNM-ECP FT NMR spectrometer (400 MHz). An internal standard of tetramethylsilane (TMS) was used.

Abbreviations used to describe the splitting patterns:

s	-	singlet	d	-	doublet	t	-	triplet
dd	-	double doublet	m	-	multiplet	quint	-	quintet

- **<sup>13</sup>C Nuclear Magnetic Resonance (NMR) spectroscopy**

The structures of the final products were confirmed by <sup>13</sup>C NMR spectroscopy using a JEOL, JNM-ECP FT NMR spectrometer, recorded at 100 MHz. An internal standard of tetramethylsilane (TMS) was used.

- **Mass spectroscopy (MS)**

A mass spectrum was recorded for each compound. Compounds with a relative molecular mass (RMM) less than 800 g mol<sup>-1</sup> were analysed using a Gas Chromatography/Mass Spectrometer (GC/MS)-Quadrupole MS/ Perkin Elmer autosystem XL GC with Electron Impact (EI) at a source temperature of 200 °C. Compounds with an RMM greater than 800 g mol<sup>-1</sup> were analysed using a Maldi MS Bruker autoflex speed. A 384 spot anchorchip 800 was used as a target. Samples were dissolved in DCM with HABA (2-(4-hydroxyphenylazo)benzoic acid) matrix (1:10 respectively). The molecular ion of the material is identified as M<sup>+</sup>.

- **Chromatography**

The progress of most reactions was monitored by using thin layer chromatography (TLC). The TLC plates that were used consist of an aluminium back which is coated with silica gel type 60 F<sub>254</sub> from Merck.

The purification of intermediates and final products was mainly achieved by column chromatography using silica gel (Fluorochem, 40-63 micron). Flash column chromatography<sup>1</sup> was carried out where stated using silica gel (Fluorochem, 6-35 micron). Final products were further purified by passing a concentrated solution through a column consisting of a layer of basic alumina, a thin layer of activated charcoal, a layer of neutral alumina and a layer of Hi-Flo filter aid using dichloromethane as the eluent. This was followed by recrystallisation from a suitable solvent, or solvent mixture. All glassware used was thoroughly cleaned by rinsing in base bath followed by distilled water and then drying in an oven at 100 °C for ~ 45 minutes. The purity of the final products was confirmed by elemental analysis (C, H, N and S), which was carried out using a Fisons EA 1108 CHN.

- **Melting point and other transition temperature determinations**

The melting point and other transition temperatures for each final product were determined using a Mettler FP-5 hot-stage and control unit in collaboration with an Olympus BH2 polarising microscope. Differential scanning calorimetry (DSC) using either a Mettler Toledo DSC1 or a Perkin-Elmer DSC 7 differential scanning calorimeter in conjunction with a TAC 7/3 instrument controller was used to calculate the enthalpies of phase transitions for materials exhibiting liquid crystalline phases and to confirm the melting points and transition temperatures of all final products. The calibration of the calorimeter was carried out using an indium standard reference (melting point onset = 156.6 °C,  $\Delta H = 28.45$  J/g). A good agreement with the values observed with the microscope was obtained.

- **Cyclic Voltammetry**

Cyclic voltammetry is an important electrochemical technique to measure the energy levels of an organic semiconductor. The energy levels of a newly developed organic material are key, when evaluating their suitability as an electron acceptor/donor material in an opto-electronic device such as OLEDs. These energy levels are generally represented by the lowest unoccupied molecular orbital (LUMO) and highest occupied molecular orbital (HOMO). Combined measurements of CV and absorption spectra provide the sufficient data to fully assess the compounds suitability into an electronic device as a potential electron donor/acceptor material.

CV measures the current that develops in an electrochemical cell against the voltage applied to give a voltage versus current cycle as shown in Figure 3.01. It is essentially a three electrode system in which glassy carbon used as a working electrode (WE), silver chloride as a reference electrode, platinum wire for the counter electrode (CE) and ferrocene is used as an internal standard. Voltage applied between the reference and working electrodes while the current response is measured between the counter and working electrode. The peak that appears relates to the oxidation and reduction of an organic compound. If it oxidises, that related to the loss of electrons by a molecule, so, can be consider as a electron donor while the compound undergo reduction that means gain of electrons, so, can be seen as an electron acceptor.<sup>33-34</sup>

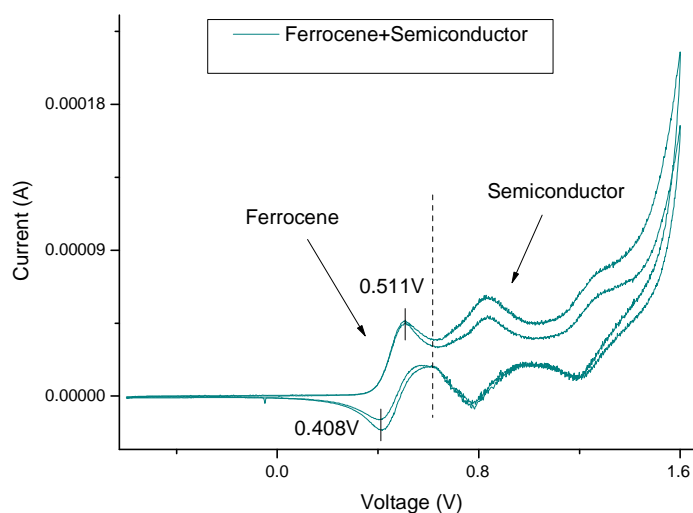


Figure 3.01 Typical cyclic voltammogram.

The following equation is used to calculate the HOMO levels

$$HOMO = E_{ox} - E_{1/2}^{Fe} + 0.425 + 4.7$$

Where,  $E_{ox}$  is the onset on the semiconductor peak.

$E_{1/2}^{Fe}$  is the average value of the ferrocene peaks.

0.425 and 4.7 are constant values for ferrocene standard and silver chloride oxidation level respectively.

- **Conductivity measurements**

The conductivity of the materials was found by spin-coating them onto OFET substrates which were purchased from Ossila. The current-voltage (I-V) characteristics of the devices was taken from the Keithley model 2400 source meter which was computer controlled using a Labview program.

The conductivity ( $\sigma$ ) was found from the following equation:

$$\sigma = \frac{l}{RA}$$

Where,  $l$  is the distance between electrodes.

R is the resistance.

A is the area of the thin-film.

- **Brightness, current density and current efficiency**

The OLEDs were made using the OLED substrates purchased from Ossila. The current density-voltage-luminance (J-V-L) characteristics of the devices (With current efficiency ( $\eta_L=L/J$ )<sup>35</sup> were measured simultaneously with a Minolta LS-110 Luminance meter and a Keithley model 2400 power source using a computer controlled Labview program. All measurements were carried out after the devices had been encapsulated in a glove box under nitrogen conditions.

- **Reagents and reaction solvents**

Reagents that were purchased from Acros organics, Apollo, Sigma Aldrich, Fisher, Alfa Aesar and TCI were used without further purification. Reaction solvents such as diethyl ether, dimethylformamide and tetrahydrofuran, were dried and then stored over molecular sieves (3Å). Triethylamine was distilled over potassium hydroxide pellets then stored over molecular sieves (3Å). Other solvents were used as purchased. All reactions were performed under a dry, nitrogen atmosphere and temperatures were measured internally.

The abbreviations that have been used in this work are described below:

NBS - *N*-Bromosuccinimide

E<sub>g</sub> - Band gap

BINAP - 2,2'-Bis-(diphenylphosphino)-1,1'-binaphthyl

CV - Cyclic Voltammetry

DABCO - 1,4-Diazabicyclo[2.2.2]octane

DMF - *N,N*-Dimethylformamide

DMAc - *N,N*-Dimethylacetamide

DMSO - Dimethylsulphoxide

DCM - Dichloromethane

DME - Dimethoxyethane

DSC - Differential Scanning Calorimetry

EtOH - Ethanol

FT-IR - Fourier transform-infrared

T<sub>g</sub> - Glass transition temperature

I - Isotropic liquid

IR - Infrared spectroscopy

Ir(ppy)<sub>3</sub> - Tris[2-phenylpyridine]iridium(III)

Ir(piq)<sub>3</sub> - Tris[1-phenylisoquinoline]iridium(III)

Ir(mppy)<sub>3</sub> - Tris[2-(*p*-tolyl)pyridine]iridium(III)

Lit - Literature

MeOH - Methanol

MS - Mass spectrometry

NMP - *N*-Methyl-2-pyrrolidone

N - Nematic phase

NMR - Nuclear Magnetic Resonance

NPD - *N,N'*-Di(1-naphthyl)-*N,N'*-diphenyl-(1,1'-biphenyl)-4,4'-diamine

PCBM - Phenyl-C61-butyric acid methyl ester

P3HT - Poly(3-hexylthiophene-2,5-diyl)

RT - Room temperature

Sm - Smectic phase

Cr - Solid crystal

*t*-BuONa - Sodium *t*-butoxide

TLC - Thin layer chromatography

Pd<sub>2</sub>(dba)<sub>3</sub> - Tris(dibenzylideneacetone)dipalladium

PCy<sub>3</sub>·HBF<sub>4</sub> - Tricyclohexylphosphoniumtetrafluoroborate

MeO-TPD - *N,N,N',N'*-Tetrakis(4-methoxyphenyl)benzidine

*p*-TSA - *p*-Toluenesulfonic acid

TEA - Triethylamine

THF - Tetrahydrofuran

UV - Ultra violet

## 3.2 Experimental Discussion

The synthetic pathways to the intermediates and final products are shown in schemes 1-37. A brief discussion of the synthesis and some of the problems encountered are given below.

### Scheme 1, 2, 4 and 5

Bromination in the 3-position of commercially available carbazole **1** using *N*-bromosuccinimide was carried out in a standard bromination procedure in a good yield to give 3-bromocarbazole **2** (73%). It is important to point out that aqueous workup was carried out after the reaction with a saturated Na<sub>2</sub>S<sub>2</sub>O<sub>3</sub> solution in order to quench bromine radicals produced in the reaction. The 3-bromocarbazole **2** was reacted with commercially available 1-bromooctane to give the 3-bromo-*N*-octyl carbazole **3** in good yield (85%). This reaction was carried out at room temperature overnight. Compounds **5**, **7**, **13** and **15** were synthesised by a new pathway, using a one-step palladium-catalysed, direct arylation<sup>2-4</sup> method with potassium carbonate as base, pivalic acid as catalytic proton shuttle and PCy<sub>3</sub>·HBF<sub>4</sub> was used to stabilise the palladium catalyst during the reaction. No preparation of an organometallic derivative is required prior to the coupling reaction compared with the Stille and Suzuki coupling reactions<sup>5</sup>. All these reactions were carried out overnight and all products were recrystallised from ethanol. Compound **5** was synthesised in moderate yield (65%) and **15** in a moderate yield (52%), while compounds **7** and **13** were synthesised in good yield (58% and 86% respectively).

### Scheme 3

The synthesis of compounds 3-bromocarbazole **2** and 3-bromo-*N*-octyl carbazole **3** has been shown in Scheme 1. A Suzuki aryl-aryl cross-coupling was carried out using 4,7-dibromobenzo-1,2,5-thiadiazole **8** and thiophene-2-boronic acid **9**, with palladium acetate as catalyst, tetrahydrofuran as solvent and potassium carbonate as base and the reaction product was recrystallised from ethanol to give compound **10** in a good yield (78%). Compound **11** was synthesised by using a one-step, palladium-catalysed, direct arylation reaction by reacting 3-bromo-*N*-octyl carbazole **3** with 4,7-di(thiophen-2-yl)benzo-1,2,5-thiadiazole **10** to give compound **11** in moderate yield (55%).

## Scheme 6

2,2-Bithiophene **4** was commercially available and was used without further purification. Bromination of compound **4**, in dichloromethane using silica gel with two equivalent quantities of *N*-bromosuccinimide<sup>6</sup> give 5,5'-dibromo-2,2-bithiophene **16** in high yield (89%). NBS was the preferred brominating agent, rather than molecular bromine in this reaction, in an effort to selectively dibrominate the thiophene rings of compound **4** and with monitoring of the reaction (with TLC) to avoid over bromination of the thiophene moieties. In this reaction silica gel was used as a reaction initiator<sup>7</sup>. Compound **18** was synthesised from 5,5'-dibromo-2,2-bithiophene **16** and commercially available tributyl(thiophen-2-yl)stannane **17** in a Stille aryl-aryl cross-coupling reaction<sup>8</sup> using Pd(PPh<sub>3</sub>)<sub>4</sub> as catalyst and DMF as solvent in a good yield (66%). The synthesis of the corresponding 3-bromocarbazole **2** has been described in Scheme 1. Compound **20** was synthesised by alkylating the 9-position of 3-bromocarbazole **2** with 2-[(9-bromononyl)oxy]tetrahydro-2-pyran **19** in an excellent yield (88%). Compound **21** was synthesised by using one step palladium-catalysed, direct arylation reaction by reacting compound **18** with compound **20** in moderate yield (45%).

## Scheme 7

Compound **23** was synthesised by alkylation of the 3-bromocarbazole **2** using commercially available 2-ethylhexyl bromide in excellent yield (90%). Compound **8** was used without any further purification. Compound **22** was synthesised by using a one-step, palladium-catalysed, direct-arylation method between compound **8** and commercially available 2,2-bithiophene **4** in moderate yield (44%). This product was recrystallised from ethanol for the next step. Compound **24** was synthesised by using a one-step, palladium-catalysed, direct arylation reaction by reacting 4,7-di(2,2'-bithiophen-5-yl)benzo-1,2,5-thiadiazole **22** with 3-bromo-*N*-ethylhexyl carbazole **23**. The crude reaction product was recrystallised from a mixture of dichloromethane and methanol to give the final product in moderate yield (62%).

## Scheme 8

2,2-Bithiophene **4** and 2,7-dibromo-9,9-dioctylfluorene **25** was commercially available and was used without further purification. Compound **26** was synthesised by using a one-step, palladium-catalysed, direct arylation method between commercially available

2,2-bithiophene **4** and 2,7-dibromo-9,9-dioctylfluorene **25** in moderate yield (46%). The reaction product was recrystallised from ethanol for the next step of the reaction. Compound **27** was synthesised by using a one-step, palladium-catalysed, direct arylation reaction by reacting with 3-bromo-*N*-octyl carbazole **3** and *bis*-2,7-(2,2'-bithiophen-5-yl)-(9,9-dioctyl)-fluorene **26**. The crude product was recrystallised from a mixture of dichloromethane and methanol to give the final product in moderate yield (64%).

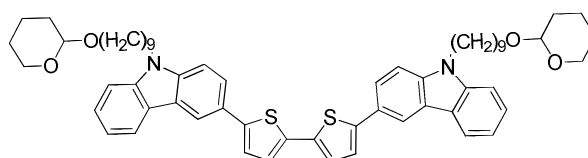
### Scheme 9

2,7-Dibromo-9,9-dioctylfluorene **25** and 2,7-dibromo-9,9-diohexylfluorene **28** are commercially available and were used without further purification. Compound **29** was synthesised by using a one-step, palladium-catalysed, direct arylation reaction between commercially available 2,2-bithiophene **4** (5 equivalences) and 2,7-dibromo-9,9-dihexylfluorene **28** in moderate yield (45%). Excess of bithiophene used in this reaction was recovered during column chromatography. Compound **29** was recrystallised from ethanol for the next step. Compound **30** was synthesised by using a one-step, palladium-catalysed, direct arylation reaction by reacting with commercially available 2,7-dibromo-9,9-dioctylfluorene **25** and *bis*-2,7-(2,2'-bithiophen-5-yl)-(9,9-dihexyl)-fluorene **29** in high yield (73%), which was used for the next step without further purification. The reaction was monitored (TLC) every 40 minutes to avoid the formation of side products (at the reactive thiophene 3 and 4 positions). The reaction was completed in 2 hours. Compound **30** was reacted with commercially available 4-bromoanisole **31** by using a one-step, palladium-catalysed, direct arylation reaction to give compound **32** in an excellent yield (84%). All these reaction steps (**29**, **30**, **32**) were carried out in only 2-3 h.

Compared with typical reaction times of 16-20 h for direct arylation reactions, it was found that 2-3 h was sometimes long enough for these reactions to go to completion. It was noted that when the reaction was run for a longer time, some side-products, such as polymers, were formed, the presence of which rendered it difficult to purify the desired product and so led to a lower reaction yield.

## Scheme 10

The synthesis of compounds 5,5'-dibromo-2,2-bithiophene **16** and compound **20** has already been shown in Scheme 6. Compound **33** was synthesised from compound **20** with commercially available tributyl(thiophen-2-yl)stannane **17** in a Stille, aryl-aryl, cross-coupling reaction using Pd(PPh<sub>3</sub>)<sub>4</sub> as the catalyst and DMF as the solvent in very good yield (85%). Compound **21** was synthesised in a one-step, palladium-catalysed, direct arylation reaction with compound **16** and compound **33** in poor yield (29%), which may be due to what appears to be the presence of a high percentage of homo-coupled compound **A** as an impurity (about 38%). Compound **21** was reacted with commercially available *p*-toluenesulfonic acid monohydrate in DCM to remove the tetrahydropyron groups and provide the bisphenol **34** in very good yield (81%). Compound **35** was synthesised by reacting commercially available methacryloyl chloride with bisphenol **34** and triethylamine in moderate yield (60%).



Compound **A**.

## Scheme 11

The 2,2':5,2''-terthiophene **12** was commercially available and was used without further purification. Bromination of compound **12**, in dichloromethane using silica gel with two equivalent quantities of *N*-bromosuccinimide give 5,5'-dibromo-2,2':5,2''-terthiophene **36** in good yield (67%). NBS was the preferred brominating agent, rather than molecular bromine in this reaction, in an effort to selectively dibrominate the thiophene rings of compound **34**. Monitoring of the reaction (with TLC) to avoid over bromination of the thiophene moieties. Compound **37** was synthesised from 5,5'-dibromo-2,2':5,2''-terthiophene **36** and commercially available tributyl(thiophen-2-yl)stannane **17** in a Stille aryl-aryl cross-coupling using Pd(OAc)<sub>2</sub>, DABCO as catalyst and DMF as solvent in a moderate yield (42%). Purification of the compound **37** was the main synthetic problem of this scheme, as compound **35** was insoluble in most common organic solvents. Therefore, the solution precipitate was triturated with hot water and then hot dichloromethane to remove side products. Synthesis of 3-bromo-*N*-octylcarbazole **3** has been described in Scheme 1. Compound **38** was synthesised by using a one-step

palladium-catalysed, direct arylation reaction of compound **37** with 3-bromo-*N*-octylcarbazole **3** in poor yield (36%).

### Scheme 12

Nitration of commercially available 4,4'-dibromobiphenyl **39** using nitric acid and ethanoic acid gave the dibromo-2-nitrobiphenyl **40** in very good yield (83%). A Cadogan ring-closing condensation reaction<sup>9-10</sup> was carried out using dibromo-2-nitrobiphenyl **40** and commercially available PPh<sub>3</sub> as reagent and DMAc as solvent to give the dibromocarbazole **41** in very good yield (88%). Alkylation of the dibromocarbazole **41** using commercially available NaH as a 60% w/w dispersion in mineral oil and 1-bromooctane in DMF as solvent gave the 9-monoalkylated carbazole **42** in very good yield (87%). The purification of compound **42** was easier due to the presence of the alkyl chain rendering this compound more soluble. The synthesis of compound **3** has been shown in Scheme 1. Compound **43** was synthesised by using a one-step, palladium-catalysed, direct arylation reaction using potassium carbonate, palladium acetate and pivalic acid. It has been found that the phosphine-free system in the presence of pivalic acid was more active than the catalytic system with phosphine ligands.<sup>11</sup> Compound **43** was synthesised in good yield (73%). Compound **44** was synthesised by using a one-step palladium-catalysed, phosphine-free, direct arylation reaction between compound **43** and compound **3** in moderate yield (48%).

### Scheme 13

2,2-Bithiophene **4** and 2,7-dibromo-9,9-dihexylfluorene **28** were commercially available and were used without further purification. Compound **29** was synthesised by using a one-step, palladium-catalysed, direct arylation reaction between commercially available 2,2-bithiophene **4** and 2,7-dibromo-9,9-diohexylfluorene **28** in moderate yield (45%). The crude product was recrystallised from ethanol for the next step of the reaction. Compound **45** was synthesised by using a one-step palladium-catalysed, direct arylation reaction between 3-bromo-*N*-octyl carbazole **3** and *bis*-2,7-(2,2'-Bithiophen-5-yl)-(9,9-dihexyl)-fluorene **29** in moderate yield (66%) of crude material. The crude product was recrystallised from a mixture of dichloromethane and DMSO, then subsequent recrystallisation from a mixture of dichloromethane and methanol, to remove the DMSO present from the previous recrystallisation (yield 58%).

## Scheme 14

3-Bromo-*N*-octyl carbazole **3** was lithiated with *n*-BuLi in tetrahydrofuran at 0 °C followed by quenching with triisopropyl borate, stirring overnight and acidification with hydrochloric acid (20%, v/v), which gave the *n*-octyl carbazole boronic acid **50** in a moderate yield (63%). 4-Bromobenzoyl chloride **47** was synthesised by reacting commercially available 4-bromobenzoic acid with thionyl chloride in excellent yield (95%). 4-Bromo-*N'*-(4-bromobenzoyl)benzohydrazide **48** was synthesised by reacting 4-bromobenzoyl chloride **47** with commercially available 4-bromobenzohydrazide **46** in very good yield (85%). This was followed by the cyclisation of 4-bromo-*N'*-(4-bromobenzoyl)benzohydrazide **48** with SOCl<sub>2</sub> in excellent yield (97%). A Suzuki aryl-aryl cross-coupling was carried out using 2,5-*bis*-(4-bromophenyl)-1,3,4-oxadiazole **49**, 9-(octyl)-carbazol-3-boronic acid **50**, using palladium acetate as catalyst, DMF as solvent and potassium carbonate as base to give 2,5-*bis*-[4-(9-octyl-9-carbazol-3-yl)phenyl]-1,3,4-oxadiazole **51**. The crude product was recrystallised from a mixture of dichloromethane and methanol to give the final product in an excellent yield (95%).

## Scheme 15

The synthesis of 4-bromo-*N'*-(4-bromobenzoyl)benzohydrazide **48** and 2,5-*bis*-(4-bromophenyl)-1,3,4-oxadiazole **49** has been shown in Scheme 14. A Suzuki, aryl-aryl, cross-coupling reaction was carried out using 2,5-*bis*-(4-bromophenyl)-1,3,4-oxadiazole **49**, 4-pentylphenyl boronic acid **52**, palladium acetate as catalyst, DMF as solvent and potassium carbonate as base to give 2,5-*bis*-(4'-pentyl-[1,1'-biphenyl]-4-yl)-1,3,4-oxadiazole **53** in good yield (60%).

## Scheme 16

The synthesis of compounds 4-bromo-*N'*-(4-bromobenzoyl)benzohydrazide **48** and 2,5-*bis*-(4-bromophenyl)-1,3,4-oxadiazole **49** has been shown in Scheme 14. A palladium-catalysed, direct arylation reaction was carried out using commercially available 2-pentylthiophene **54**, 2,5-*bis*-(4-bromophenyl)-1,3,4-oxadiazole **49**, palladium acetate as catalyst, DMF as solvent and potassium carbonate as base to give 2,5-*bis*-(4-(5-pentylthiophen-2-yl)phenyl)-1,3,4-oxadiazole **55**. The crude product was recrystallised from a mixture of dichloromethane and methanol to give the final product in good yield (65%).

## Scheme 17

The synthesis of 4-bromo-*N'*-(4-bromobenzoyl)benzohydrazide **48**, 2,5-*bis*-(4-bromophenyl)-1,3,4-oxadiazole **49** and 3-bromocarbazole **2**, 3-bromo-*N*-octyl carbazole **3** has been shown in Scheme 14 and 1 respectively. A Suzuki aryl-aryl cross-coupling reaction was carried out using 3-bromo-*N*-octyl-carbazole **3**, thiophen-2-boronic acid **9**, Pd(PPh<sub>3</sub>)<sub>4</sub> as catalyst, DME as solvent and sodium carbonate as base to give the 9-octyl-3-(thiophen-2-yl)-9-carbazole **56** in excellent yield (94%). A palladium-catalysed, direct arylation reaction was carried out using 5-*bis*-(4-bromophenyl)-1,3,4-oxadiazole **49**, 9-octyl-3-(thiophen-2-yl)-9-carbazole **56** with palladium acetate as catalyst, DMF as solvent and potassium carbonate as base to give 2,5-*bis*{4-[5-(9-octyl-9-carbazol-3-yl)thiophen-2-yl]phenyl}-1,3,4-oxadiazole **57** in moderate yield (59%), which was recrystallised from a mixture of dichloromethane and methanol to give a moderate yield (51%).

## Scheme 18

3,3',5,5'-Tetrabromo-2,2'-bithiophene **58** was synthesised by bromination of commercially available 2,2'-bithiophene **4** in a standard procedure in almost quantitative yield (98%) using a combination of bromine and glacial acetic acid. This reaction was followed by the elimination of bromine in the 5,5 positions of the 3,3',5,5'-tetrabromo-2,2'-bithiophene **58** using zinc dust in a standard procedure in a good yield (83%) to give 3,3'-dibromo-2,2'-bithiophene **59**. This reaction was followed by the cyclisation of 3,3'-dibromo-2,2'-bithiophene **59** at the 3,3 positions following the work of Reynolds *et al.* exactly, conserving both mole ratios and concentrations<sup>12</sup> using BINAP to give 4-dodecyl-4-dithieno[3,2-b:2',3'-d]pyrrole **60** in excellent yield (95%). 2,6-Dibromo-4-dodecyldithieno[3,2-b:2',3'-d]pyrrole **61** was synthesised using NBS as the brominating agent in a good yield (74%). A Suzuki palladium-catalysed, aryl-aryl cross-coupling reaction was carried out using 2,6-dibromo-4-octyl-4-dithieno[3,2-b:2',3'-d]pyrrole **61** and 4-pentylphenyl boronic acid **52** with Pd(PPh<sub>3</sub>)<sub>4</sub> as the catalyst, DME as solvent and sodium carbonate as base to give 4-dodecyl-2,6-*bis*-(4-pentylphenyl)-4-dithieno[3,2-b:2',3'-d]pyrrole **62** in good yield (70%).

### Scheme 19

The synthesis of 3,3',5,5'-tetrabromo-2,2'-bithiophene **58**, 3,3'-dibromo-2,2'-bithiophene **59**, 4-dodecyl-4-dithieno[3,2-b:2',3'-d]pyrrole **60** and 2,6-dibromo-4-dodecyl-4-dithieno[3,2-b:2',3'-d]pyrrole **61** has been shown in Scheme 18. A Suzuki palladium-catalysed, aryl-aryl cross-coupling reaction was carried out using 2,6-dibromo-4-octyl-4-dithieno[3,2-b:2',3'-d]pyrrole **61** and 6-(octyloxy)pyridin-3-boronic acid **63** with Pd(PPh<sub>3</sub>)<sub>4</sub> as catalyst, DME as solvent and sodium carbonate as the base to give 4-dodecyl-2,6-*bis*-[6-(octyloxy)pyridin-3-yl]-4-dithieno[3,2-b:2',3'-d]pyrrole **64** in good yield (71%).

### Scheme 20

A Suzuki aryl-aryl cross-coupling reaction was carried out using commercially available 1,4-dibromobenzene **65**, thiophen-2-boronic acid **9**, with Pd(PPh<sub>3</sub>)<sub>4</sub> as catalyst, DME as the solvent and sodium carbonate as the base to give 1,4-di(thiophen-2-yl)benzene **66** in excellent yield (97%). A palladium-catalysed, direct arylation reaction was carried out using 1,4-di(thiophen)-2-benzene **66** and 3-bromo-*N*-octyl-carbazole **3**, with palladium acetate as the catalyst, DMF as the solvent and potassium carbonate as the base to give 1,4-*bis*-(5-(9-octyl-9-carbazol-3-yl)thiophen-2-yl)benzene **67**. The crude product was recrystallised from a mixture of dichloromethane and ethanol to give the final product in moderate yield (51%).

### Scheme 21

The synthesis of 3-bromocarbazole **2** and 3-bromo-*N*-octyl carbazole **3** has been shown in Scheme 1. Bithiophene **4** was lithiated using *n*-BuLi in THF at -78 °C and quenched with tributyltin chloride resulting in the formation of the stannyl bithiophene **69** (89%), which was not purified further. 1,4-di(2,2'-bithiophen-5-yl)naphthalene **70** was synthesised from commercially available 1,4-dibromonaphthalene **68** and 2,2'-bithiophen-5-tributylstannane **69** in a stille aryl-aryl cross-coupling using Pd(PPh<sub>3</sub>)<sub>4</sub> as a catalyst and DMF as the solvent in a poor yield (28%). A palladium-catalysed, direct arylation was carried using 1,4-di(2,2'-bithiophen-5-yl)naphthalene **70** and 3-bromo-*N*-octyl-carbazole **3**, with palladium acetate as the catalyst, DMF as the solvent and potassium carbonate as the base to give 1,4-*bis*[5'-(9-octyl-9-carbazol-3-yl)-(2,2'-bithiophen)-5-yl] naphthalene **71** in poor yield (36%).

### Scheme 22

9,10-Di-(2,2'-bithiophen)-5-yl)-anthracene **73** was synthesised by using a one-step, palladium-catalysed, direct arylation reaction between the commercially available 2,2-bithiophene **4** and 9,10-dibromoanthracene **72** in moderate yield (66%). A palladium-catalysed, direct arylation reaction was carried out using 9,10-di-(2,2-bithiophen-5-yl)anthracene **73** and 3-bromo-*N*-octyl-carbazole **3**, with palladium acetate as the catalyst, NMP as the solvent and potassium carbonate as the base to give the 9,10-*bis*-[5'-(9-octyl-9-carbazol-3-yl)-2,2-bithiophen-5-yl]-anthracene **74**. The crude product was recrystallised from a mixture of dichloromethane and methanol to give the final product in moderate yield (48%).

### Scheme 23

A palladium-catalysed, direct arylation reaction was carried out using 9,10-di-(2,2'-bithiophen)-5-yl)-anthracene **73** and 1-bromo-4-(decyloxy)benzene **75**, with palladium acetate as the catalyst, NMP as the solvent and potassium carbonate as the base to give 9,10-*bis*-[5'-(4-(decyloxy)phenyl)-2,2'-bithiophen-5-yl]-anthracene **76**. The crude product was recrystallised from a mixture of dichloromethane and methanol to give the final product in moderate yield (47%).

### Scheme 24

4-Bromo-4'-pentyl-1,1'-biphenyl **77** was lithiated with *n*-BuLi in tetrahydrofuran at -78 °C followed by quenching with trimethyl borate, stirring overnight and then acidification with hydrochloric acid (20%, v/v), which gave 4'-pentyl-1,1'-biphenyl-4-boronic acid **78** in a moderate yield (47%). A Suzuki palladium-catalysed, aryl-aryl cross-coupling reaction was carried out using 2,6-dibromo-4-dodecyldithieno[3,2-*b*:2',3'-*d*]pyrrole **61** and 4'-pentyl-1,1'-biphenyl-4-boronic acid **78**, with Pd(PPh<sub>3</sub>)<sub>4</sub> as catalyst, DME as the solvent and sodium carbonate (20% w/w) as the base to give 4-dodecyl-2,6-*bis*-(4'-pentyl-1,1'-biphenyl-4-yl)-4-dithieno[3,2-*b*:2',3'-*d*]pyrrole **79** in good yield (71%).

## Scheme 25

An Aldol condensation<sup>13</sup> followed by a dehydration reaction of commercially available 6-bromoisatin **80** and 6-bromooxindole **81** in acetic acid under N<sub>2</sub> gave 6,6-dibromoisoidigo **82** in almost quantitative yield (95%). Compound **82** was only slightly soluble in organic solvents perhaps due to the strong intermolecular  $\pi$ - $\pi$  interactions. Alkylation of 6,6-dibromoisoidigo **82** was carried out using 1-bromooctane, resulting in formation of highly soluble 6,6'-dibromo-1,1'-dioctyl-[3,3'-biindolinylidene]-2,2'-dione **83** in very good yield (87%). A Suzuki palladium-catalysed, aryl-aryl cross-coupling reaction was carried out between 1-bromo-4-octyloxybenzene **84** and commercially available thiophene-2-boronic acid (**9**) in DMF with Pd(PPh<sub>3</sub>)<sub>4</sub> to give 2-(4-octyloxyphenyl)thiophene **85** in good yield (69%). The alkoxyphenyl thiophene **85** was lithiated using *n*-BuLi in tetrahydrofuran at -78 °C and quenched with tributyltin chloride resulting in the stannyl thiophene **86** (87%). The Stille tin intermediate was not purified further as it has been shown that the acidic nature of silica gel can protonate the 2-position of the stannyl thiophene and thereby remove the tributyltin moiety<sup>14</sup>. After every Stille coupling an aqueous workup was carried out with a saturated potassium fluoride solution in order to remove the tributyltin chloride by-product. A Stille aryl-aryl cross-coupling reaction was carried out between stannyl thiophene **86** and 6,6'-dibromo-1,1'-dioctyl-[3,3'-biindolinylidene]-2,2'-dione **83** using Pd(PPh<sub>3</sub>)<sub>4</sub> as the catalyst and DMF as the solvent to give compound **87** in a good yield (79%).

## Scheme 26

A direct arylation cross-coupling reaction was carried out between 1-bromo-4-octyloxybenzene **84** and 2,2-bithiophene **4** with palladium acetate as the catalyst, DMF as the solvent and potassium carbonate as the base to give compound **88** in moderate yield (56%). The alkoxyphenyl bithiophene **88** was lithiated using *n*-BuLi in THF at -78 °C and quenched with tributyltin chloride resulting in the formation of the stannyl bithiophene **88** (86%), which was not purified further for reasons explained above. A Stille, aryl-aryl cross-coupling reaction was carried out between stannyl bithiophene **89** and 6,6'-dibromo-1,1'-dioctyl-[3,3'-biindolinylidene]-2,2'-dione **83**, using Pd(PPh<sub>3</sub>)<sub>4</sub> as the catalyst and DMF as the solvent to give compound **90** in a moderate yield (57%).

## Scheme 27

A Suzuki, palladium-catalysed, aryl-aryl cross-coupling was carried out using 9-(octyl)-carbazol-3-boronic acid **50** and 1-bromo-4-iodobenzene **91**, with Pd(PPh<sub>3</sub>)<sub>4</sub> as the catalyst, DME as the solvent and sodium carbonate as the base to give 3-(4-bromophenyl)-9-octyl-9-carbazole **92** in good yield (72%). Compound **92** was lithiated with *n*-BuLi in tetrahydrofuran at -78 °C followed by quenching with triisopropyl borate, stirring overnight and finally acidification with hydrochloric acid (20%, v/v), which gave 4-(9-octyl-9-carbazol-3-yl) phenylboronic acid **93** in a very good yield (87%). A Suzuki palladium-catalysed, aryl-aryl cross-coupling reaction was carried out using 2,5-*bis*-(4-bromophenyl)-1,3,4-oxadiazole **49** and 4-(9-octyl-9-carbazol-3-yl)phenylboronic acid **93** with Pd(PPh<sub>3</sub>)<sub>4</sub> as the catalyst, DME as the solvent and sodium carbonate (20% w/w) as the base to give 2,5-*bis*-(4'-9-octyl-9-carbazol-3-yl-[1,1'-biphenyl]-4-yl)-1,3,4-oxadiazole **94** in moderate yield (66%).

## Scheme 28

A Suzuki, aryl-aryl cross coupling reaction was carried out between 2,5-dibromonitrobenzene **95** and phenylboronic acid **96**, with Pd(PPh<sub>3</sub>)<sub>4</sub> as the catalyst, DME as the solvent and sodium carbonate as the base to give 4-bromo-2-nitrobiphenyl **97** in good yield (72%). A Cadogan ring-closing condensation reaction was carried out using compound **97** and commercially available PPh<sub>3</sub> as reagent to give the 2-bromocarbazole **98** in an excellent yield (90%). Alkylation of the 2-bromocarbazole **98** using commercially available NaH as a 60% w/w dispersion in mineral oil and 1-bromooctane in DMF solution, gave the 2-bromo-9-octylcarbazole **99** in quantitative yield (100%). The purification of compound **99** was easier due to the presence of the alkyl chain rendering this compound more soluble. Compound **99** was lithiated with *n*-BuLi in tetrahydrofuran at -78 °C followed by quenching with triisopropyl borate, stirring overnight and finally acidification with hydrochloric acid (20%, v/v), which gave 9-octyl-9-carbazol-2-boronic acid **100** in a very good yield (87%). A Suzuki, palladium-catalysed, aryl-aryl, cross-coupling reaction was carried out using 2,5-*bis*-(4-bromophenyl)-1,3,4-oxadiazole **49** and compound **100**, with Pd(OAc)<sub>2</sub> as the catalyst, DMF as the solvent and potassium carbonate as the base to give 2,5-*bis*-4-(9-octyl-9-carbazol-2-yl)phenyl-1,3,4-oxadiazole **101** in excellent yield (95%).

## Scheme 29

An Ullman cross coupling reaction<sup>15</sup> was carried out between 2,5-dibromonitrobenzene **102** and 4-iodoanisole **103** with copper as the catalyst to give 4-bromo-4'-methoxy-2-nitrobiphenyl **104** in good yield (75%). A Cadogan ring-closing condensation reaction was carried out using compound **104** and commercially available triethyl phosphite as a reagent to give the 2-bromo-7-methoxycarbazole **105** in moderate yield (60%). Alkylation of the 2-bromo-7-methoxycarbazole **105** using commercially available NaH as a 60% w/w dispersion in mineral oil and 1-bromooctane in DMF as solvent gave the 2-bromo-7-methoxy-9-octylcarbazole **106** in almost quantitative yield (99%). The purification of compound **106** was easier due to the presence of the alkyl chain rendering this compound more soluble. Compound **106** was lithiated with *n*-BuLi in tetrahydrofuran at -78 °C followed by quenching with triisopropyl borate, stirring overnight and finally acidification with hydrochloric acid (20%, v/v), which gave 7-methoxy-9-octyl-9-carbazol-2-boronic acid **107** in an excellent yield (95%). A Suzuki, palladium-catalysed, aryl-aryl cross-coupling reaction was carried out using 2,5-bis-(4-bromophenyl)-1,3,4-oxadiazole **49** and compound **107** with Pd(OAc)<sub>2</sub> as the catalyst, DME as the solvent and sodium carbonate as the base to give 2,5-bis-(4-(7-methoxy-9-octylcarbazol-2-yl)phenyl)-1,3,4-oxadiazole **108** in moderate yield (66%).

## Scheme 30

Alkylation of commercially available 4-iodophenol **109** using 1-bromooctane and potassium carbonate gave the 1-alkoxy-4-iodobenzene **110** in excellent yield (90 %). An Ullman, cross-coupling reaction was carried out between 2,5-dibromonitrobenzene **102** and 1-iodo-4-octyloxybenzene **110** with copper as the catalyst to give 4-bromo-2-nitro-4'-octyloxy-biphenyl **111** in good yield (72%). A Cadogan, ring-closing, condensation reaction was carried out using compound **111** and commercially available PPh<sub>3</sub> as reagent to give the 2-bromo-7-octyloxy-carbazole **112** in moderate yield (54%). Alkylation of the compound **112** using commercially available NaH as a 60% w/w dispersion in mineral oil and 1-bromooctane gave the 2-bromo-9-octyl-7-(octyloxy)-carbazole **113** in almost quantitative yield (99%). Compound **113** was lithiated with *n*-BuLi in tetrahydrofuran at -78 °C followed by quenching with triisopropyl borate, stirring overnight and finally acidification with hydrochloric acid, which gave 9-octyl-7-(octyloxy)-9-carbazol-2-boronic acid **114** in an excellent yield (96%). A Suzuki, palladium-catalysed, aryl-aryl cross-coupling reaction was carried out using 2,5-bis-(4-

bromophenyl)-1,3,4-oxadiazole **49** and compound **114** with Pd(OAc)<sub>2</sub> as the catalyst, DMF as the solvent and potassium carbonate as the base to give 2,5-bis{4-[9-octyl-7-(octyloxy)-9-carbazol-2-yl]phenyl}-1,3,4-oxadiazole **115** in very good yield (85%).

### Scheme 31

A Suzuki, palladium-catalysed, aryl-aryl cross-coupling reaction was carried out using 5,5"-dibromo-2,2':5',2"-terthiophene **36** and compound **114** with Pd(OAc)<sub>2</sub> as the catalyst, DMF as the solvent and potassium carbonate as the base to give 5,5"-bis-(9-octyl-7-(octyloxy)-9-carbazol-2-yl)-2,2':5',2"-terthiophene **116** in good yield (78%).

### Scheme 32

A Suzuki, palladium-catalysed, aryl-aryl cross-coupling reaction was carried out using 9-alkylated carbazole **42** and compound **114** with Pd(OAc)<sub>2</sub> as the catalyst, DMF as the solvent and potassium carbonate as the base to give 9,9',9"-trioctyl-7,7"-bis-(octyloxy)-2,2':7',2"-tercarbazole **117** in good yield (76%).

### Scheme 33

Bromination of carbazole **1** in the 3,6-positions using NBS as the brominating agent in toluene to give 3,6-dibromocarbazole **118** in good yield (70%). Alkylation of 3,6-dibromocarbazole **118** using commercially available tetra-*n*-butylammonium bromide (TBAB), 1-bromooctane and potassium hydroxide in acetone gave 3,6-dibromo-9-octylcarbazole **119** in an excellent yield (95%). A Suzuki palladium-catalysed, aryl-aryl cross-coupling reaction was carried out using 3,6-dibromo-9-octylcarbazole **119** and compound **114**, with Pd(OAc)<sub>2</sub> as the catalyst, DMF as the solvent and potassium carbonate as the base to give 9,9',9"-trioctyl-7,7"-bis-(octyloxy)-2,3':6',2"-tercarbazole **120** in good yield (69%).

### Scheme 34

A Suzuki, palladium-catalysed, aryl-aryl, cross-coupling reaction was carried out using commercially available 4,4-dibromo-biphenyl **39** and compound **114**, with Pd(OAc)<sub>2</sub> as the catalyst, DMF as the solvent and potassium carbonate as the base to give 4,4'-bis-(9-octyl-7-octyloxy-carbazol-2-yl)-1,1'-biphenyl **121** in moderate yield (60%).

### Scheme 35

2,7-dibromo-9,9-dipropylfluorene **123** was synthesised by reacting commercially available 2,7-dibromofluorene **122** with 1-bromopropane in good yield (75%). A palladium catalysed, Suzuki aryl-aryl, cross-coupling was carried out using 2,7-dibromo-9,9-dipropylfluorene **123** and compound **114** with Pd(OAc)<sub>2</sub> as the catalyst, DMF as the solvent and potassium carbonate as the base to give 7,7'-(9,9-dipropylfluorene-2,7-diyl)-bis-(9-octyl-2-octyloxy-carbazole) **124** in good yield (79%).

### Scheme 36

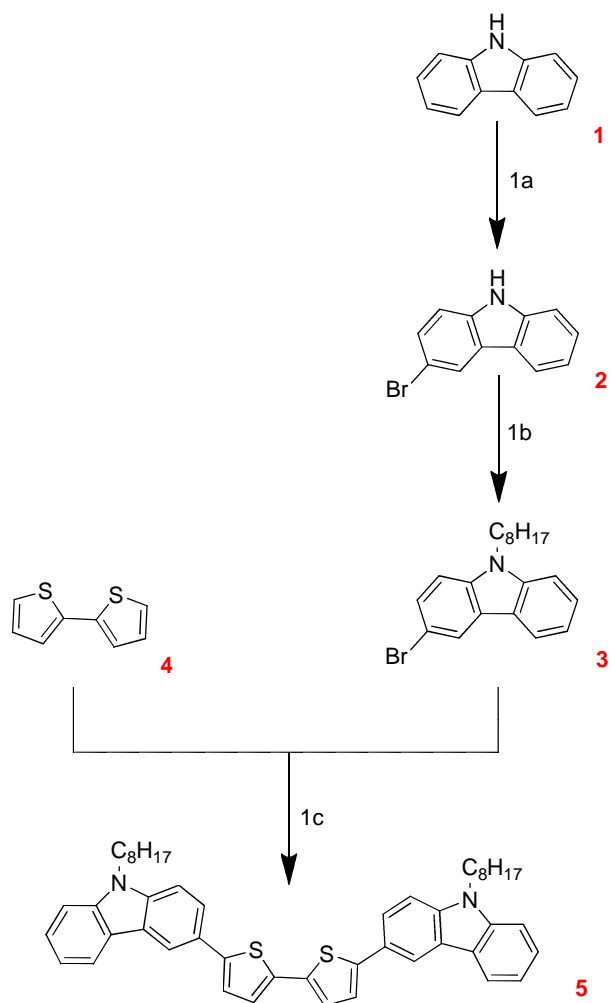
A Suzuki, palladium-catalysed, aryl-aryl, cross-coupling reaction was carried out using commercially available 2,7-dibromofluorene **122** and compound **114** with Pd(OAc)<sub>2</sub> as the catalyst, DMF as the solvent and potassium carbonate as the base to give 2,7-bis-(9-octyl-7-octyloxy-carbazol-2-yl)-fluorene **125** in very good yield (83%).

### Scheme 37

A Suzuki, palladium-catalysed, aryl-aryl cross-coupling reaction was carried out using commercially available *tris*-(4-bromophenyl)amine **126** and compound **114** with Pd(OAc)<sub>2</sub> as the catalyst, DMF as the solvent and potassium carbonate as the base to give *tris*-{4-[9-Octyl-7-(octyloxy)-carbazol-2-yl]phenyl}amine **127** in good yield (75%).

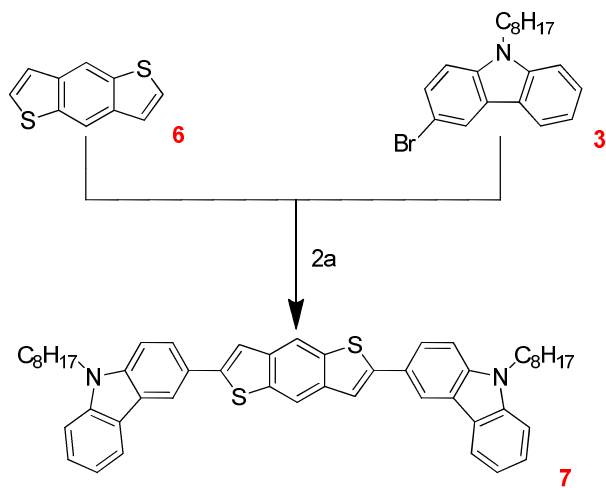
### 3.3 Reaction Schemes

Scheme 1



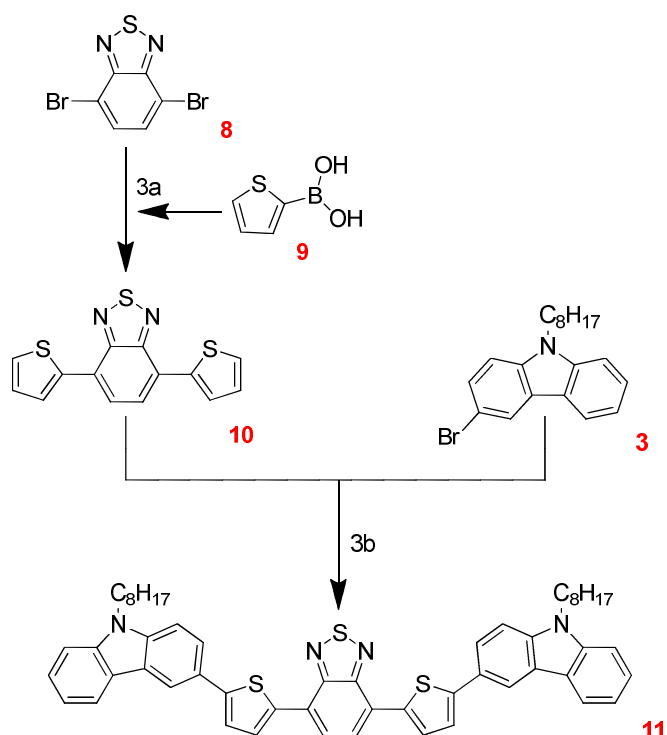
1a: NBS, DMF, 0 °C. 1b: BrC<sub>8</sub>H<sub>17</sub>, DMSO, NaOH. 1c: Pd(OAc)<sub>2</sub>, K<sub>2</sub>CO<sub>3</sub>, PCy<sub>3</sub>·HBF<sub>4</sub>, (CH<sub>3</sub>)<sub>3</sub>CCO<sub>2</sub>H, DMF, 100 °C.

## Scheme 2



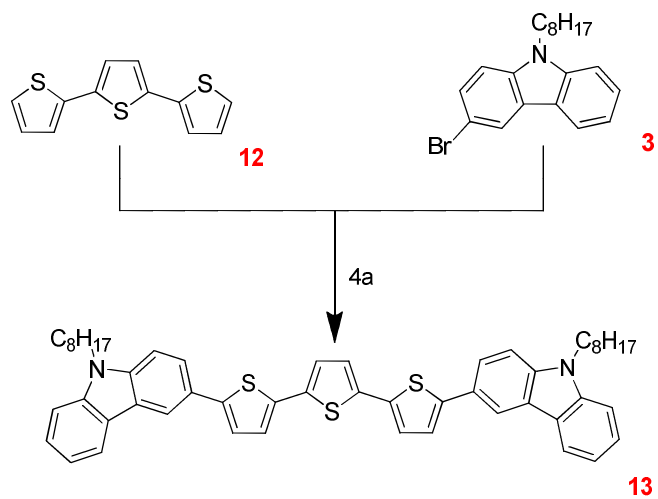
2a: Pd(OAc)<sub>2</sub>, K<sub>2</sub>CO<sub>3</sub>, PCy<sub>3</sub>·HBF<sub>4</sub>, (CH<sub>3</sub>)<sub>3</sub>CCO<sub>2</sub>H, DMF, 100 °C.

## Scheme 3



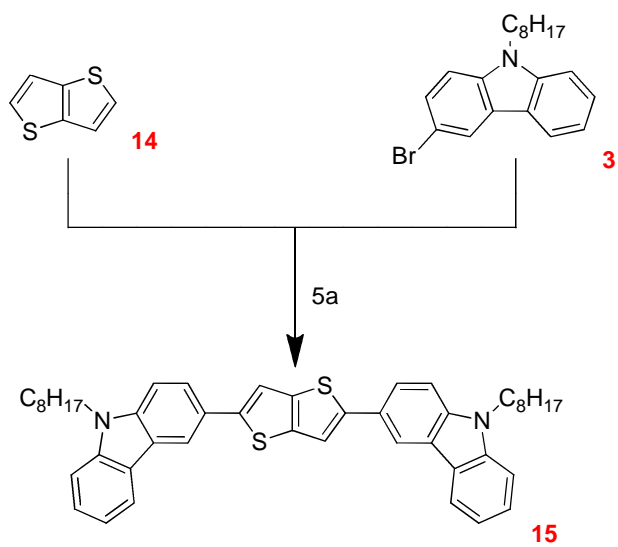
3a: PPh<sub>3</sub>, Pd(OAc)<sub>2</sub>, K<sub>2</sub>CO<sub>3</sub>, THF. 3b: Pd(OAc)<sub>2</sub>, K<sub>2</sub>CO<sub>3</sub>, PCy<sub>3</sub>·HBF<sub>4</sub>, (CH<sub>3</sub>)<sub>3</sub>CCO<sub>2</sub>H, DMF, 100 °C.

### Scheme 4



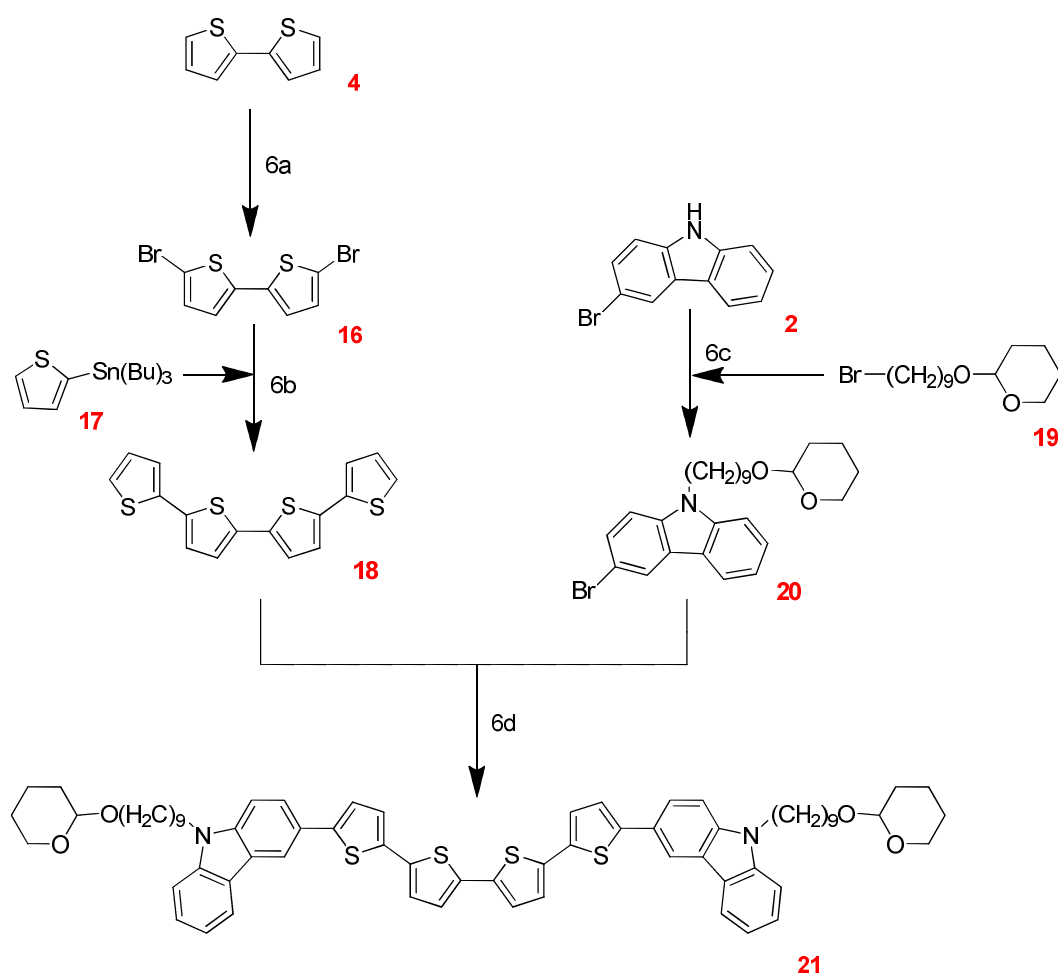
4a: Pd(OAc)<sub>2</sub>, K<sub>2</sub>CO<sub>3</sub>, PCy<sub>3</sub>·HBF<sub>4</sub>, (CH<sub>3</sub>)<sub>3</sub>CCO<sub>2</sub>H, DMF, 100 °C.

### Scheme 5



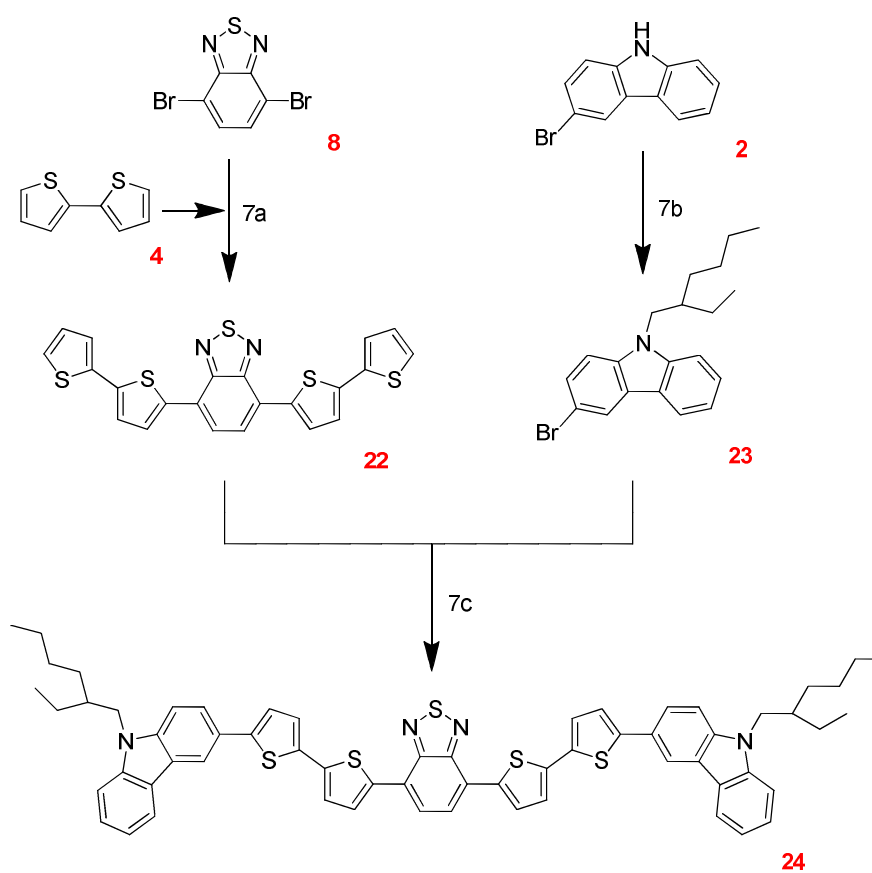
5a: Pd(OAc)<sub>2</sub>, K<sub>2</sub>CO<sub>3</sub>, PCy<sub>3</sub>·HBF<sub>4</sub>, (CH<sub>3</sub>)<sub>3</sub>CCO<sub>2</sub>H, DMF, 100 °C.

### Scheme 6



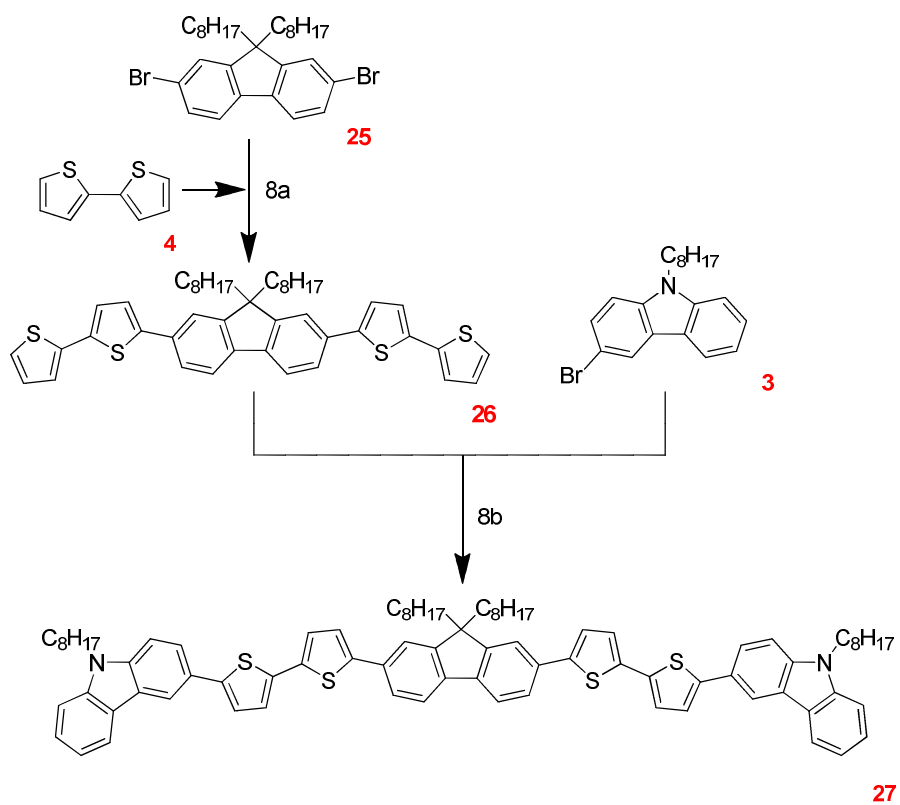
6a: NBS, DCM. 6b: Pd(PPh<sub>3</sub>)<sub>4</sub>, DMF, 100 °C. 6c: DMSO, NaOH. 6d: Pd(OAc)<sub>2</sub>, K<sub>2</sub>CO<sub>3</sub>, PCy<sub>3</sub>·HBF<sub>4</sub>, (CH<sub>3</sub>)<sub>3</sub>CCO<sub>2</sub>H, DMF, 100 °C.

**Scheme 7**



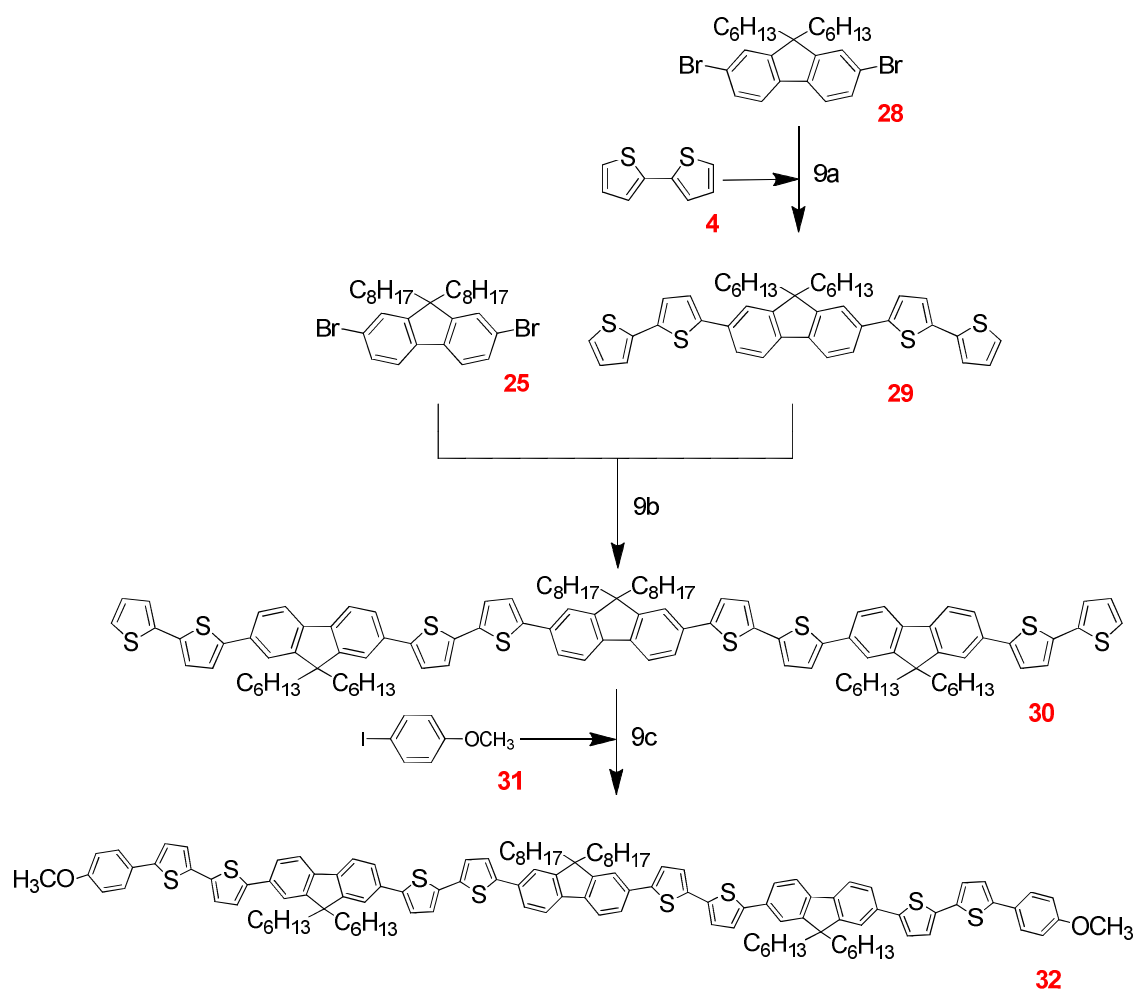
7a: Pd(OAc)<sub>2</sub>, K<sub>2</sub>CO<sub>3</sub>, PCy<sub>3</sub>·HBF<sub>4</sub>, (CH<sub>3</sub>)<sub>3</sub>CCO<sub>2</sub>H, DMF, 100 °C. 7b: NaOH, DMSO, CH<sub>3</sub>(CH<sub>2</sub>)<sub>3</sub>CH(C<sub>2</sub>H<sub>5</sub>)CH<sub>2</sub>Br. 7c: Pd(OAc)<sub>2</sub>, K<sub>2</sub>CO<sub>3</sub>, PCy<sub>3</sub>·HBF<sub>4</sub>, (CH<sub>3</sub>)<sub>3</sub>CCO<sub>2</sub>H, DMF, 100 °C.

## Scheme 8



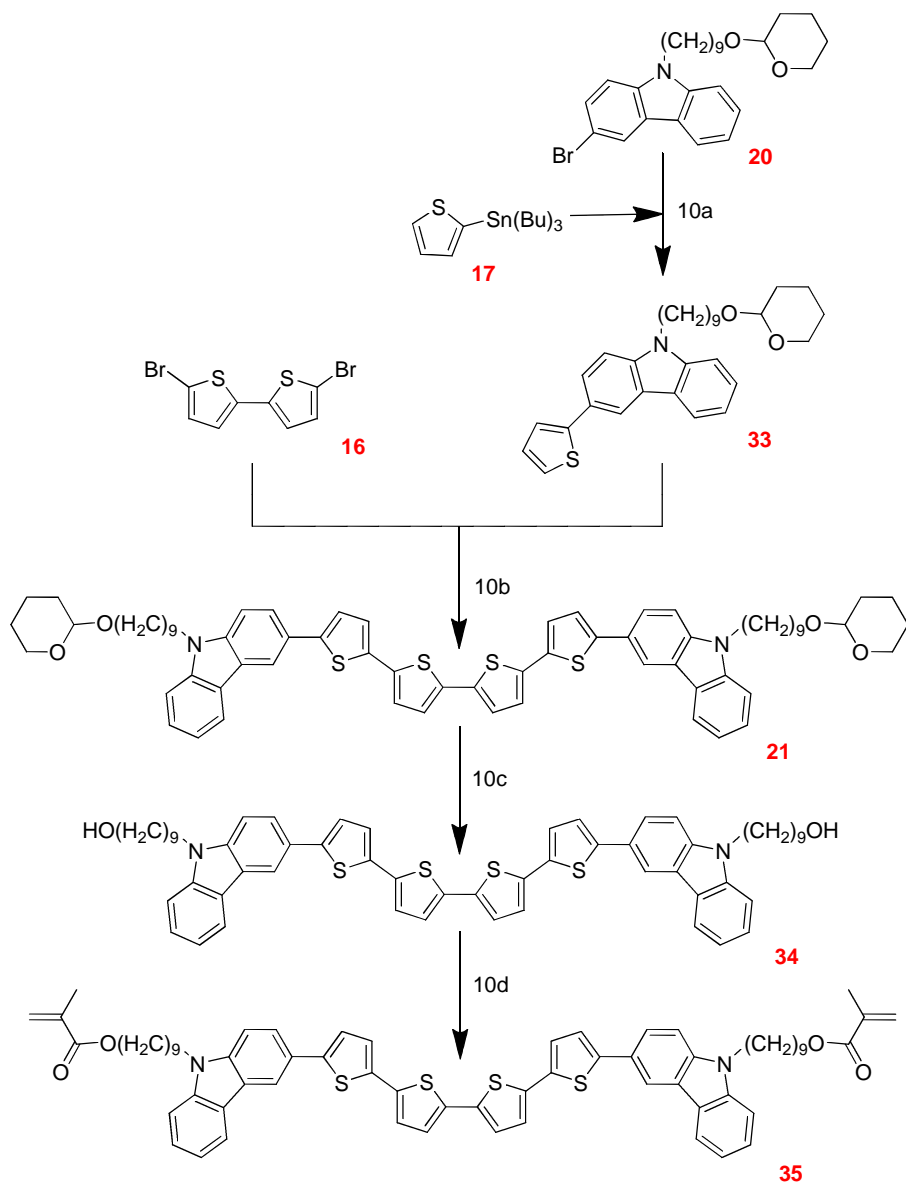
8a: Pd(OAc)<sub>2</sub>, K<sub>2</sub>CO<sub>3</sub>, PCy<sub>3</sub>·HBF<sub>4</sub>, (CH<sub>3</sub>)<sub>3</sub>CCO<sub>2</sub>H, DMF, 100 °C. 8b: Pd(OAc)<sub>2</sub>, K<sub>2</sub>CO<sub>3</sub>, PCy<sub>3</sub>·HBF<sub>4</sub>, (CH<sub>3</sub>)<sub>3</sub>CCO<sub>2</sub>H, DMF, 100 °C.

## Scheme 9



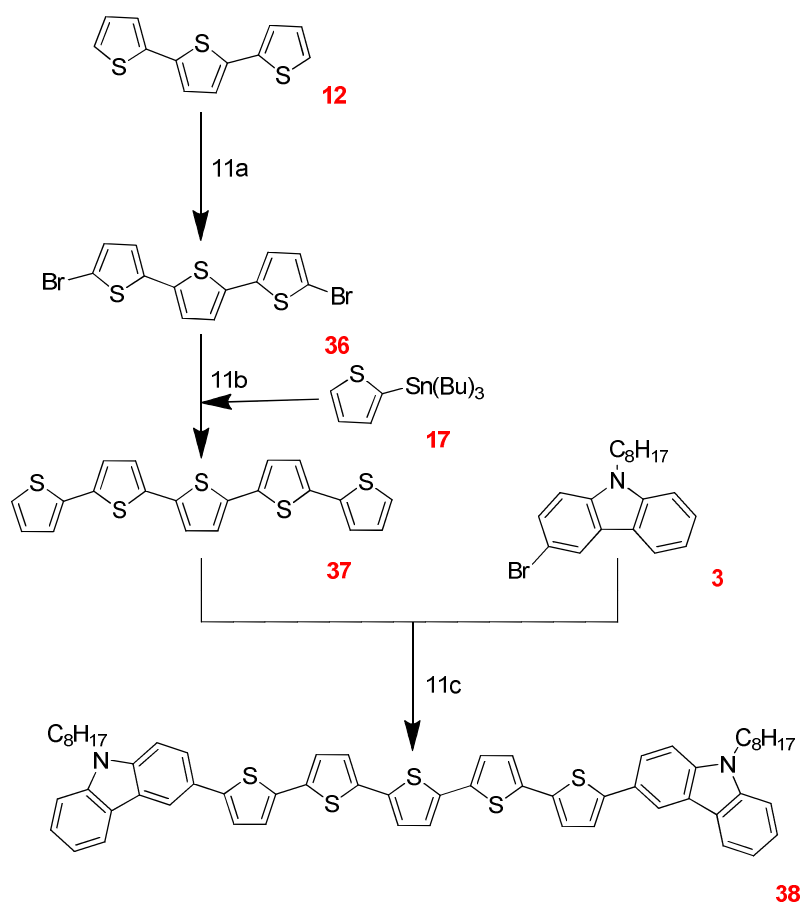
9a: Pd(OAc)<sub>2</sub>, K<sub>2</sub>CO<sub>3</sub>, PCy<sub>3</sub>·HBF<sub>4</sub>, (CH<sub>3</sub>)<sub>3</sub>CCO<sub>2</sub>H, DMF, 100 °C. 9b: Pd(OAc)<sub>2</sub>, K<sub>2</sub>CO<sub>3</sub>, PCy<sub>3</sub>·HBF<sub>4</sub>, (CH<sub>3</sub>)<sub>3</sub>CCO<sub>2</sub>H, DMF, 100 °C. 9c: Pd(OAc)<sub>2</sub>, K<sub>2</sub>CO<sub>3</sub>, PCy<sub>3</sub>·HBF<sub>4</sub>, DMF, (CH<sub>3</sub>)<sub>3</sub>CCO<sub>2</sub>H, 100 °C.

Scheme 10



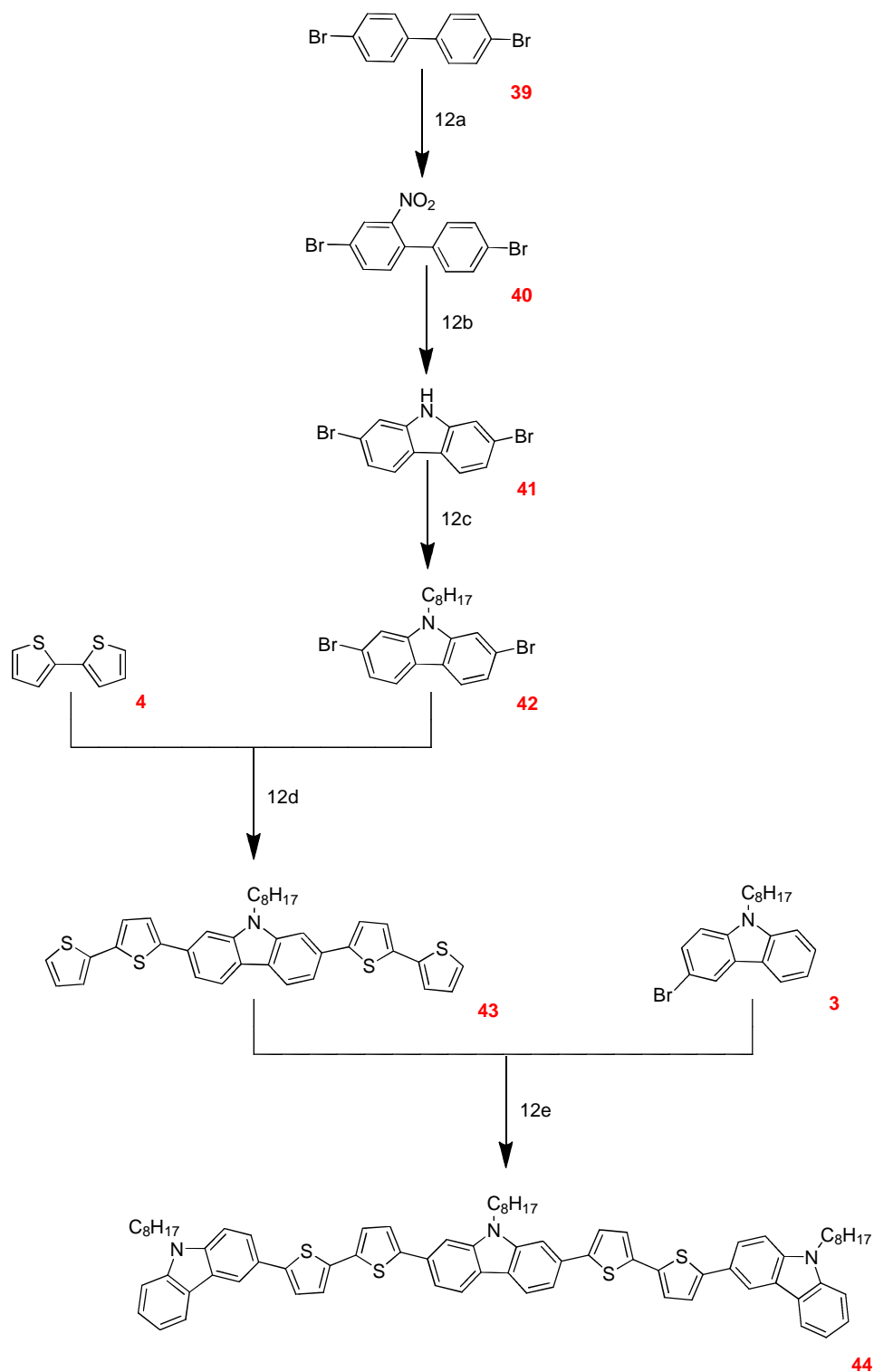
10a: Pd(OAc)<sub>2</sub>, (PPh<sub>3</sub>)<sub>4</sub>, DMF, 100 °C. 10b: Pd(OAc)<sub>2</sub>, K<sub>2</sub>CO<sub>3</sub>, (CH<sub>3</sub>)<sub>3</sub>CCO<sub>2</sub>H, PCy<sub>3</sub>·HBF<sub>4</sub>, DMF, 100 °C. 10c: *p*-TSA, DCM. 10d: C<sub>4</sub>H<sub>5</sub>ClO, TEA, DCM, 0 °C.

### Scheme 11



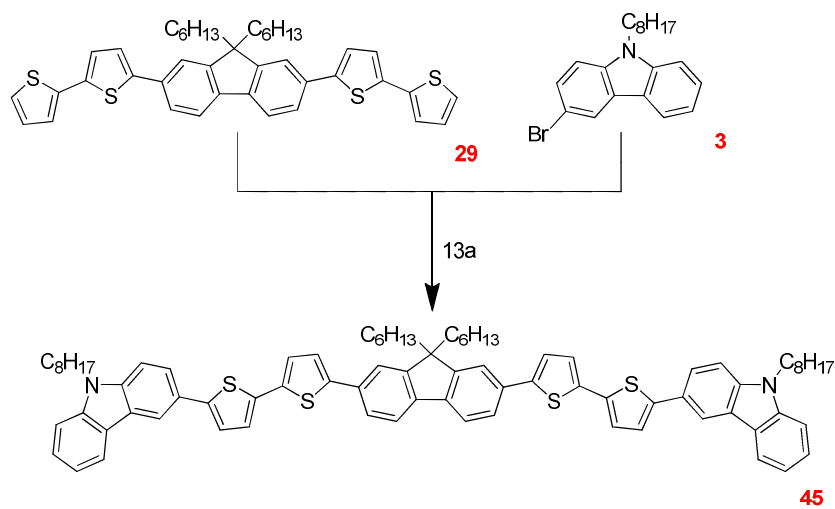
11a: NBS, DCM, silica gel. 11b: Pd(OAc)<sub>2</sub>, DABCO, DMF, 100 °C. 11c: Pd(OAc)<sub>2</sub>, K<sub>2</sub>CO<sub>3</sub>, PCy<sub>3</sub>·HBF<sub>4</sub>, (CH<sub>3</sub>)<sub>3</sub>CCO<sub>2</sub>H, DMF, 100 °C.

**Scheme 12**



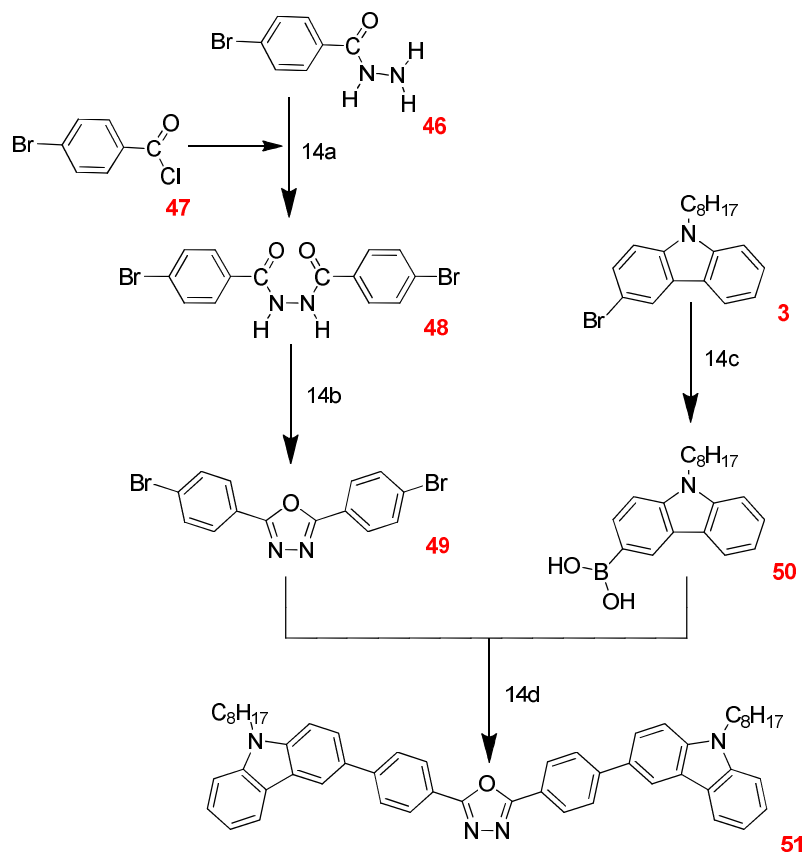
12a:  $\text{CH}_3\text{COOH}$ ,  $\text{HNO}_3$ ,  $\text{H}_2\text{O}$ ,  $100\text{ }^\circ\text{C}$ . 12b:  $\text{PPh}_3$ ,  $\text{DMAc}$ . 12c:  $\text{BrC}_8\text{H}_{17}$ ,  $\text{NaH}$ ,  $\text{DMF}$ . 12d:  $\text{Pd}(\text{OAc})_2$ ,  $\text{K}_2\text{CO}_3$ ,  $(\text{CH}_3)_3\text{CCO}_2\text{H}$ ,  $\text{DMF}$ ,  $100\text{ }^\circ\text{C}$ . 12e:  $\text{Pd}(\text{OAc})_2$ ,  $\text{K}_2\text{CO}_3$ ,  $\text{DMF}$ ,  $(\text{CH}_3)_3\text{CCO}_2\text{H}$ ,  $100\text{ }^\circ\text{C}$ .

### Scheme 13



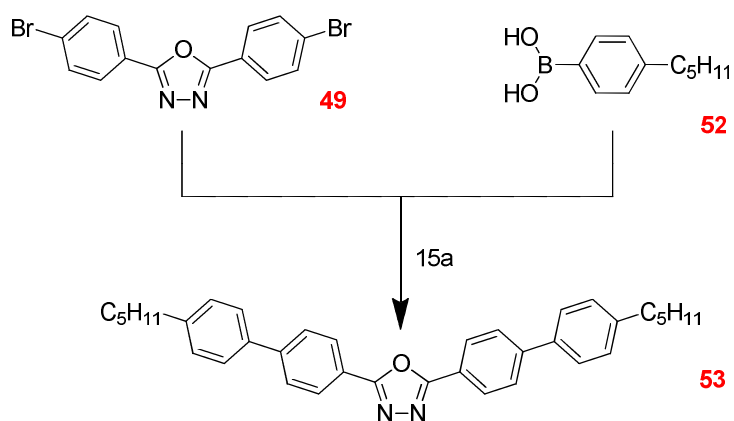
13a: Pd(OAc)<sub>2</sub>, K<sub>2</sub>CO<sub>3</sub>, (CH<sub>3</sub>)<sub>3</sub>CCO<sub>2</sub>H, DMF, 100 °C.

### Scheme 14



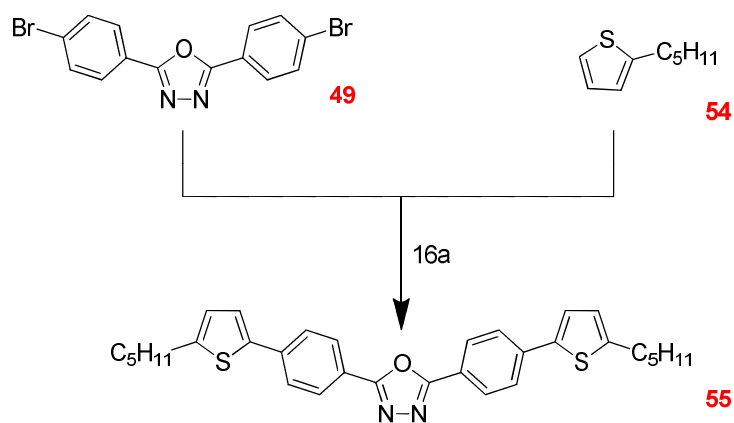
14a: pyridine, 120 °C. 14b: SOCl<sub>2</sub>, 90 °C. 14c: C<sub>6</sub>H<sub>14</sub>, *n*-BuLi, [(CH<sub>3</sub>)<sub>2</sub>CHO]<sub>3</sub>B, THF, 0 °C. 14d: Pd(OAc)<sub>2</sub>, K<sub>2</sub>CO<sub>3</sub>, H<sub>2</sub>O, DMF, 80 °C.

### Scheme 15



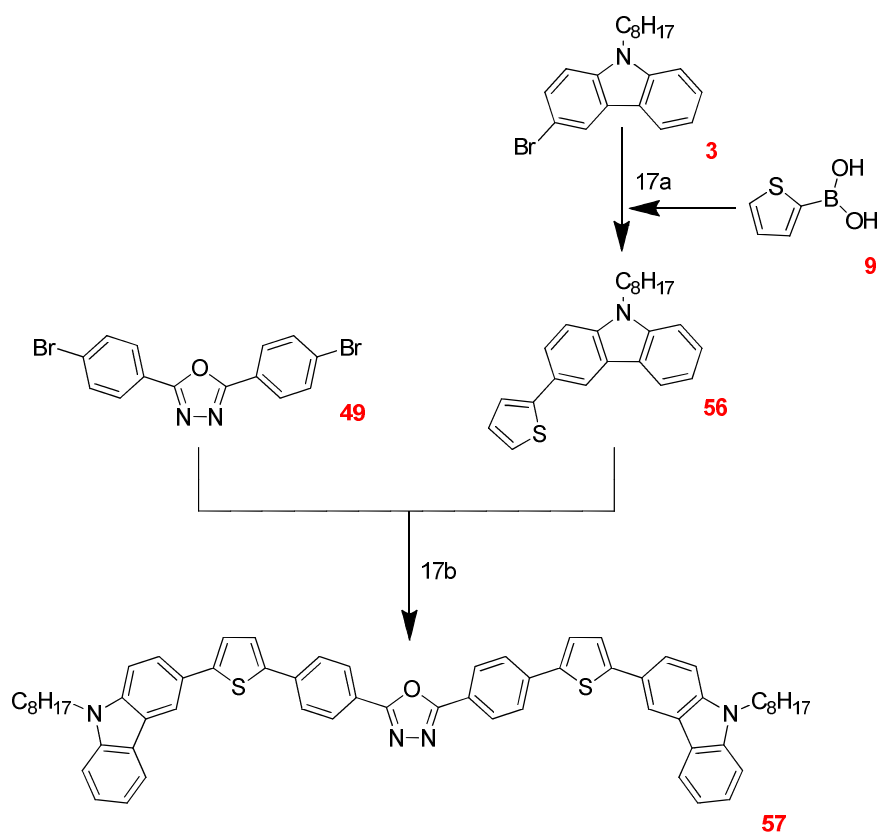
15a: Pd(OAc)<sub>2</sub>, K<sub>2</sub>CO<sub>3</sub>, H<sub>2</sub>O, DMF, 80 °C.

### Scheme 16



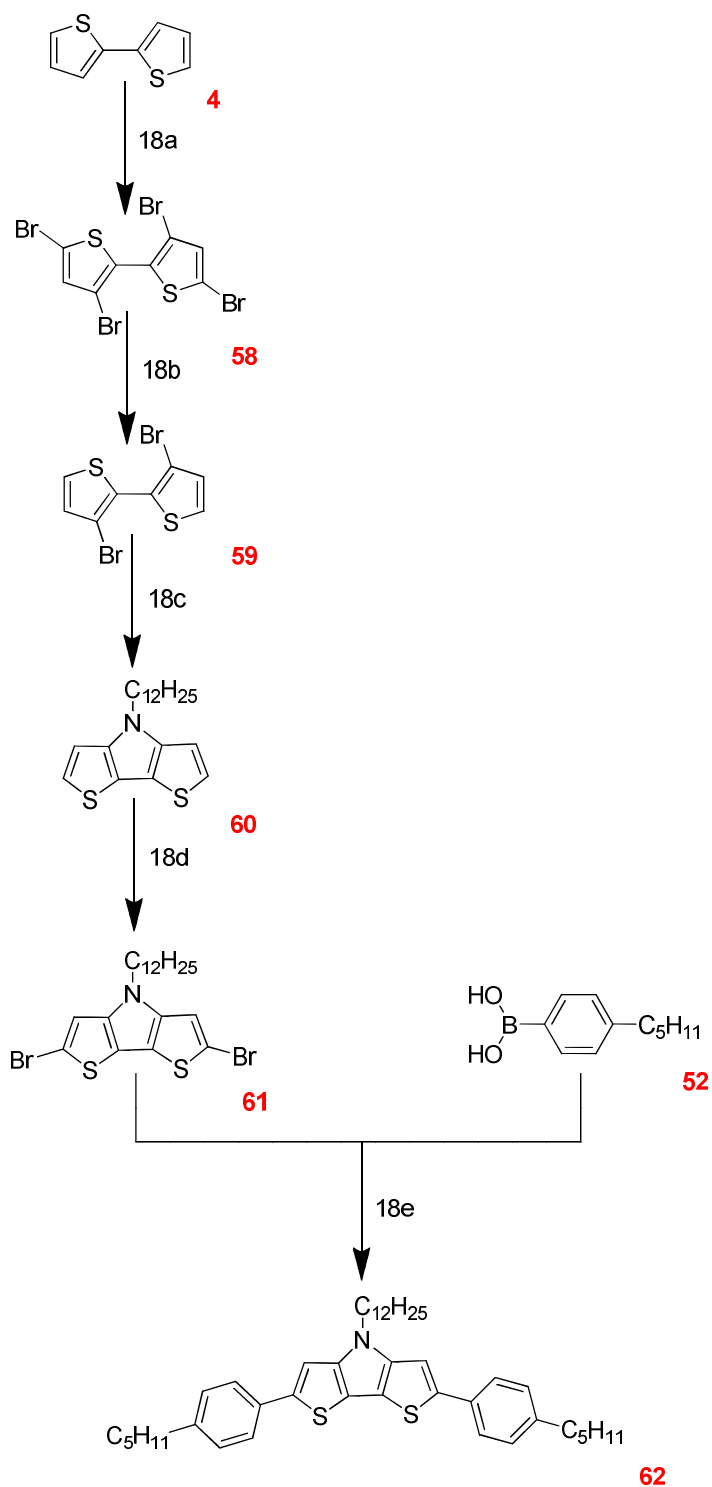
16a: Pd(OAc)<sub>2</sub>, K<sub>2</sub>CO<sub>3</sub>, PCy<sub>3</sub>·HBF<sub>4</sub>, (CH<sub>3</sub>)<sub>3</sub>CCO<sub>2</sub>H, DMF, 100 °C.

### Scheme 17



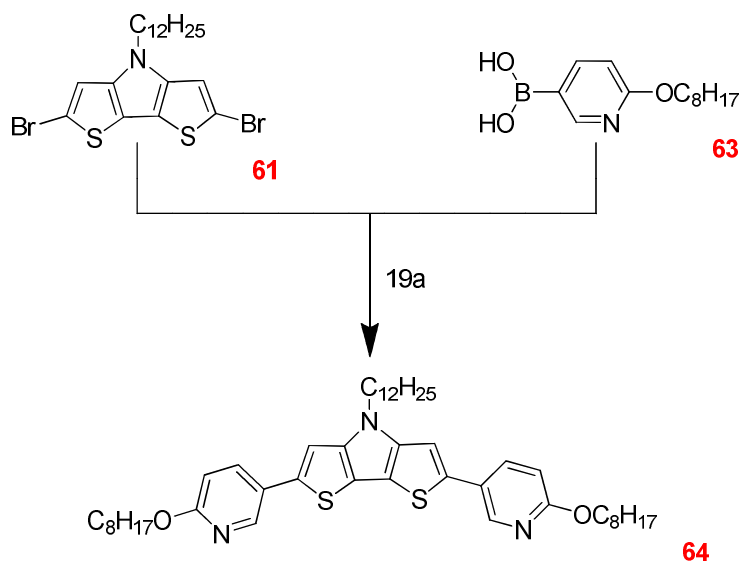
17a: Pd(PPh<sub>3</sub>)<sub>4</sub>, Na<sub>2</sub>CO<sub>3</sub>, DME, H<sub>2</sub>O, 80 °C. 17b: Pd(OAc)<sub>2</sub>, K<sub>2</sub>CO<sub>3</sub>, PCy<sub>3</sub>·HBF<sub>4</sub>, (CH<sub>3</sub>)<sub>3</sub>CCO<sub>2</sub>H, NMP, 100 °C.

Scheme 18



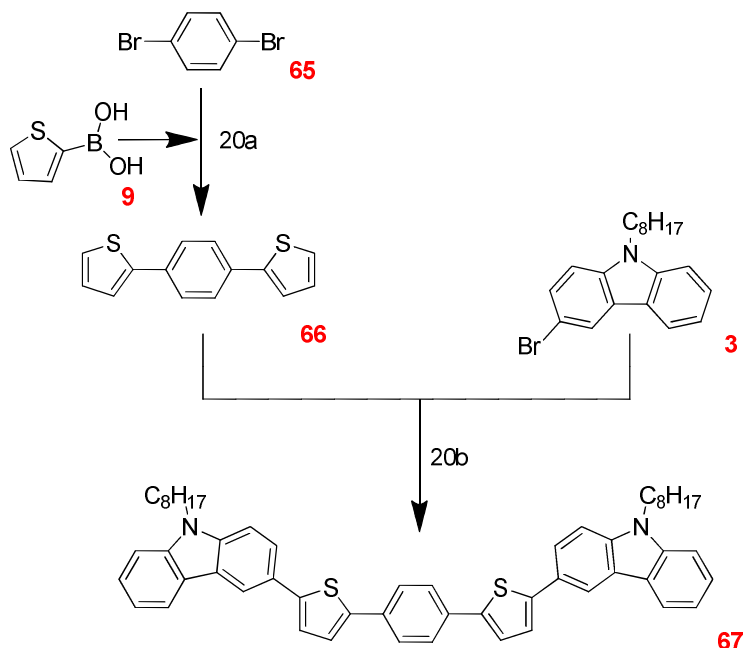
18a: Br<sub>2</sub>, CHCl<sub>3</sub>, CH<sub>3</sub>COOH, KOH. 18b: Zn dust, CH<sub>3</sub>CH<sub>2</sub>CH<sub>2</sub>OH, H<sub>2</sub>O, CH<sub>3</sub>COOH.  
 18c: *t*-BuONa, Pd<sub>2</sub>(dba)<sub>3</sub>, BINAP, *n*-C<sub>12</sub>H<sub>25</sub>NH<sub>2</sub>. 18d: NBS, DMF, CHCl<sub>3</sub>, 0 °C.  
 18e: Pd(PPh<sub>3</sub>)<sub>4</sub>, Na<sub>2</sub>CO<sub>3</sub>, DME, H<sub>2</sub>O, 80 °C.

### Scheme 19



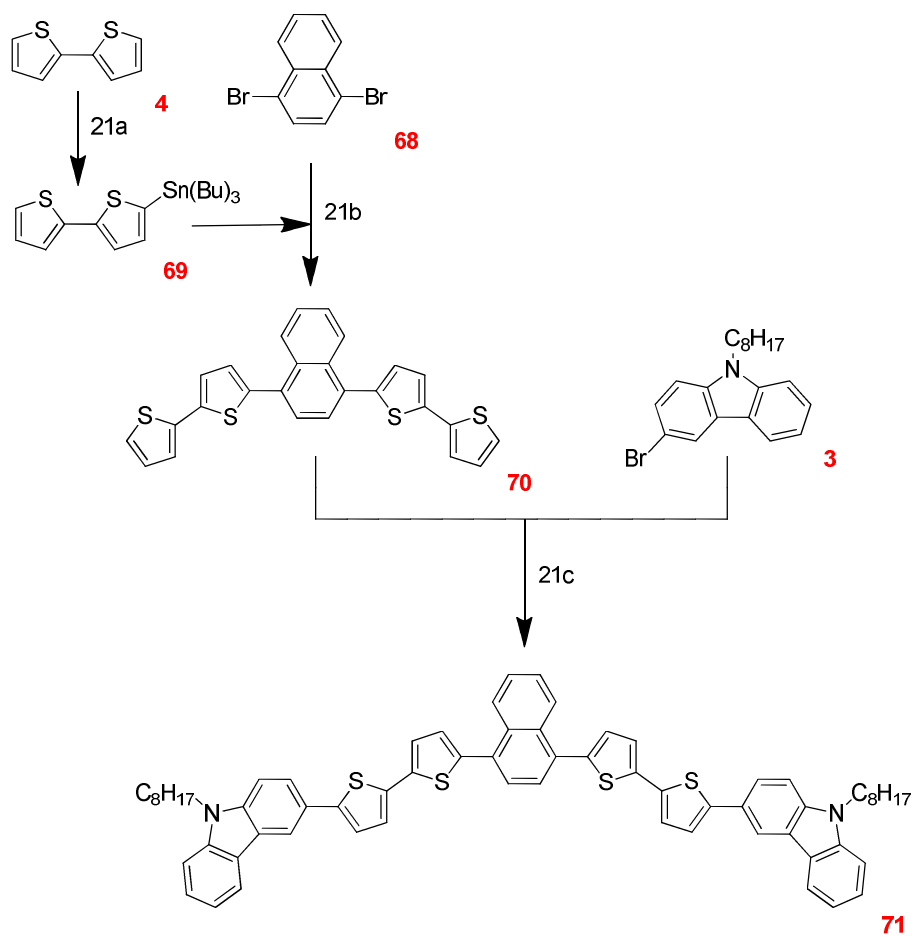
19a: Pd(PPh<sub>3</sub>)<sub>4</sub>, Na<sub>2</sub>CO<sub>3</sub>, DME, H<sub>2</sub>O, 80 °C.

### Scheme 20



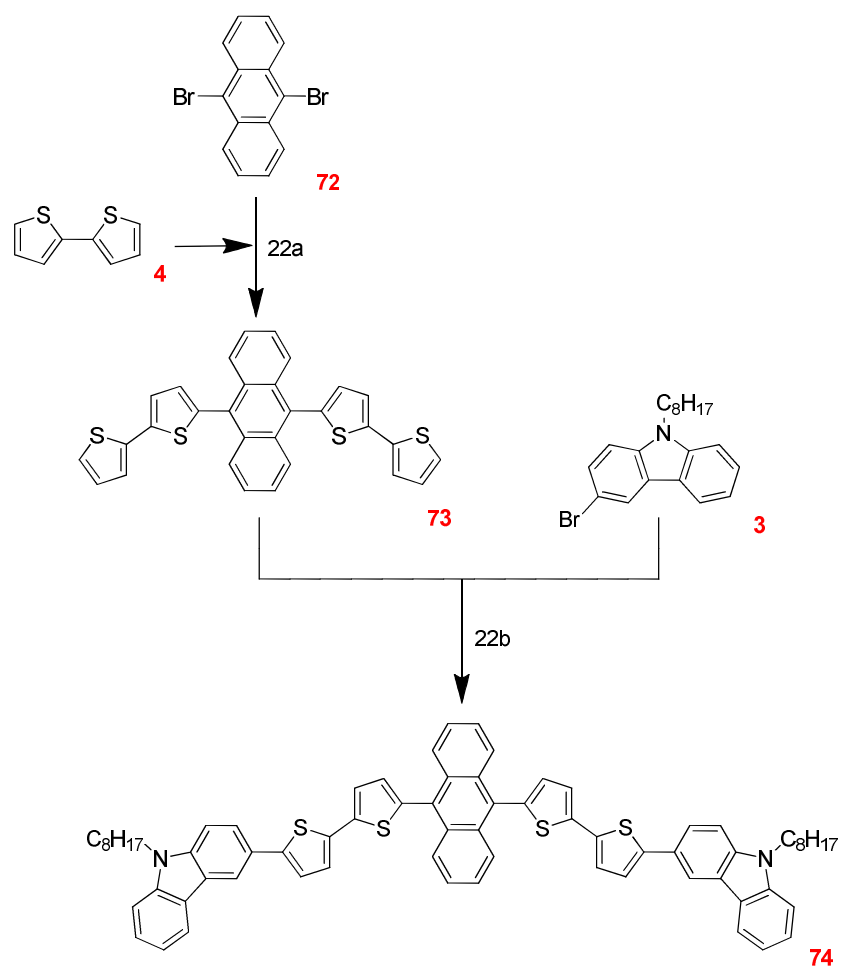
20a: Pd(PPh<sub>3</sub>)<sub>4</sub>, Na<sub>2</sub>CO<sub>3</sub>, DME, H<sub>2</sub>O, 80 °C. 20b: Pd(OAc)<sub>2</sub>, K<sub>2</sub>CO<sub>3</sub>, PCy<sub>3</sub>·HBF<sub>4</sub>, (CH<sub>3</sub>)<sub>3</sub>CCO<sub>2</sub>H, NMP, 100 °C.

**Scheme 21**



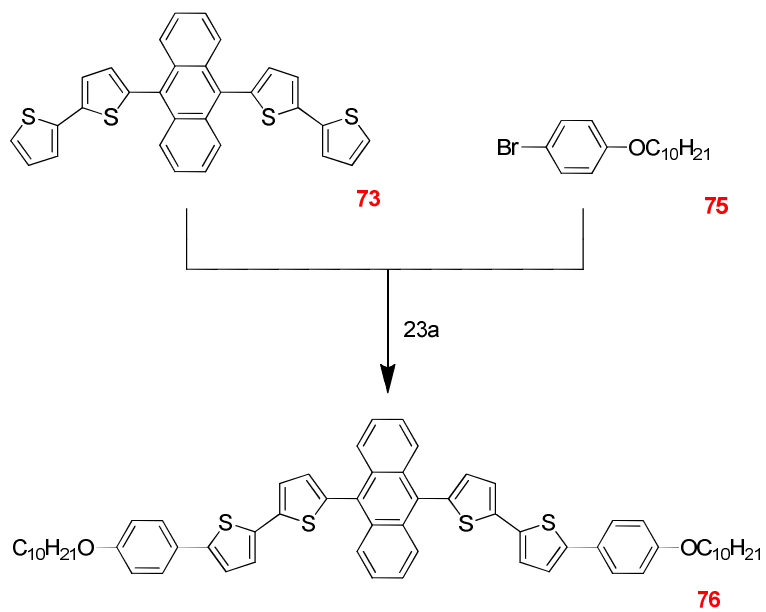
21a: *n*-BuLi, Sn(Bu)<sub>3</sub>Cl, THF, -78 °C. 21b: Pd(OAc)<sub>2</sub>, PPh<sub>3</sub>, DMF. 21c: Pd(OAc)<sub>2</sub>, K<sub>2</sub>CO<sub>3</sub>, PCy<sub>3</sub>·HBF<sub>4</sub>, (CH<sub>3</sub>)<sub>3</sub>CCO<sub>2</sub>H, NMP, 100 °C.

## Scheme 22



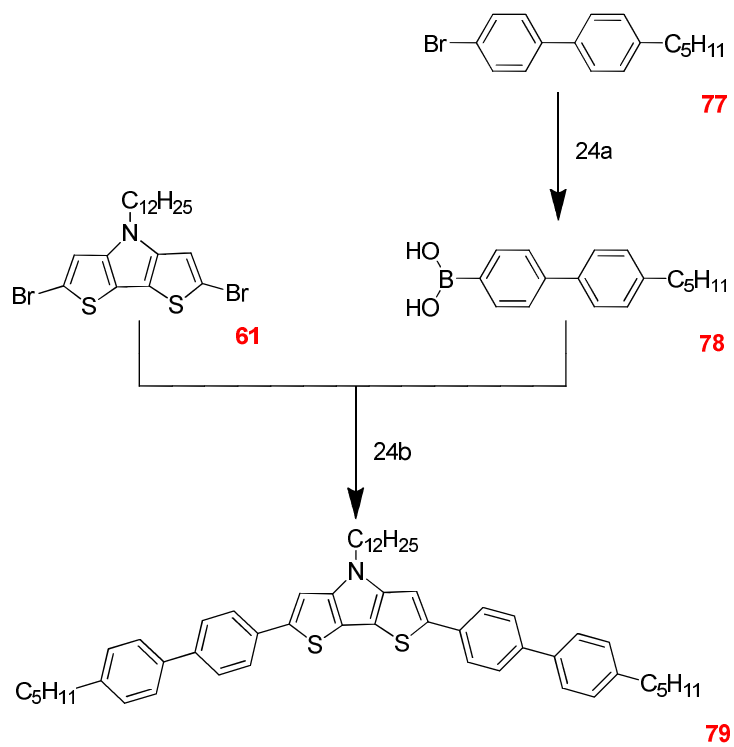
22a: Pd(OAc)<sub>2</sub>, K<sub>2</sub>CO<sub>3</sub>, PCy<sub>3</sub>·HBF<sub>4</sub>, (CH<sub>3</sub>)<sub>3</sub>CCO<sub>2</sub>H, NMP, 100 °C. 22b: Pd(OAc)<sub>2</sub>, K<sub>2</sub>CO<sub>3</sub>, PCy<sub>3</sub>·HBF<sub>4</sub>, (CH<sub>3</sub>)<sub>3</sub>CCO<sub>2</sub>H, NMP, 100 °C.

### Scheme 23



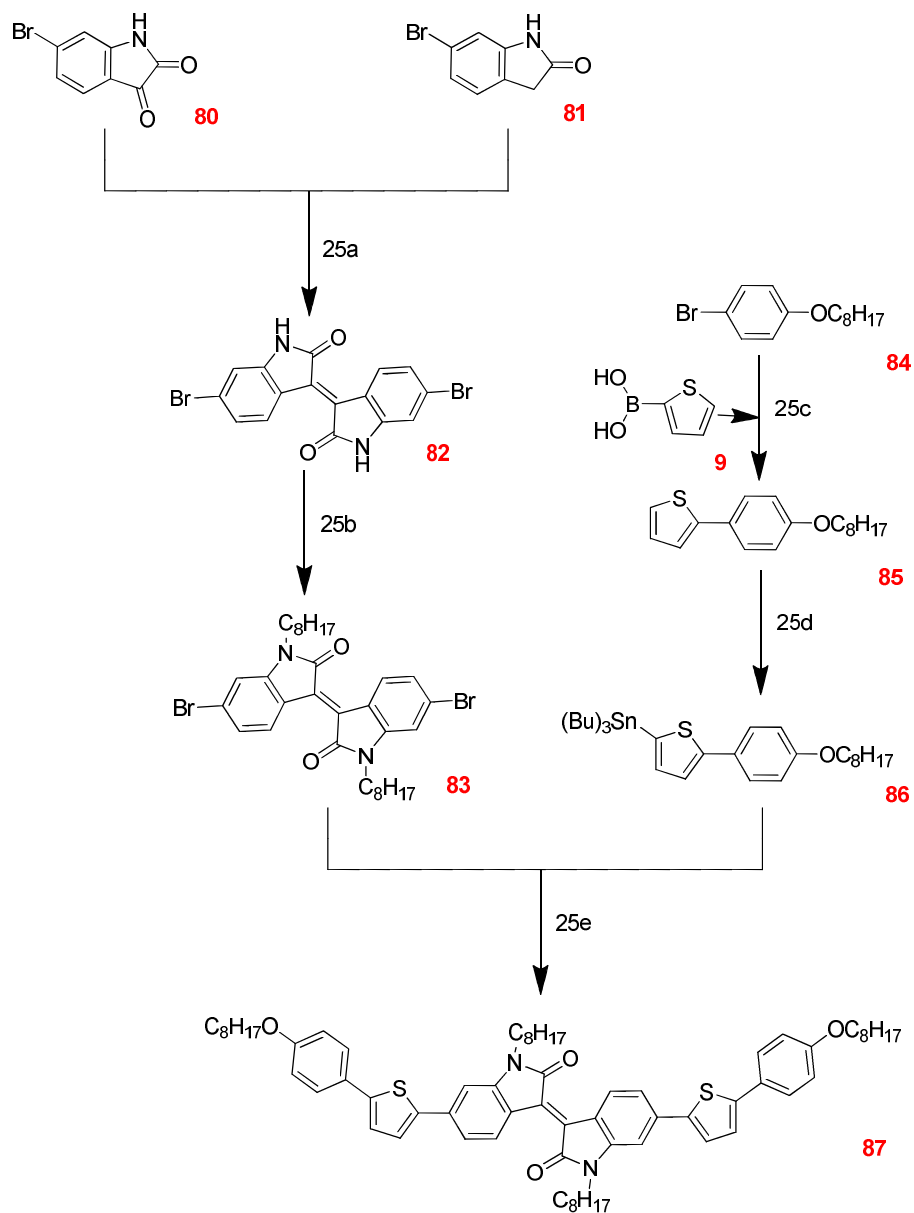
23a: Pd(OAc)<sub>2</sub>, K<sub>2</sub>CO<sub>3</sub>, PCy<sub>3</sub>·HBF<sub>4</sub>, (CH<sub>3</sub>)<sub>3</sub>CCO<sub>2</sub>H, NMP, 100 °C.

### Scheme 24



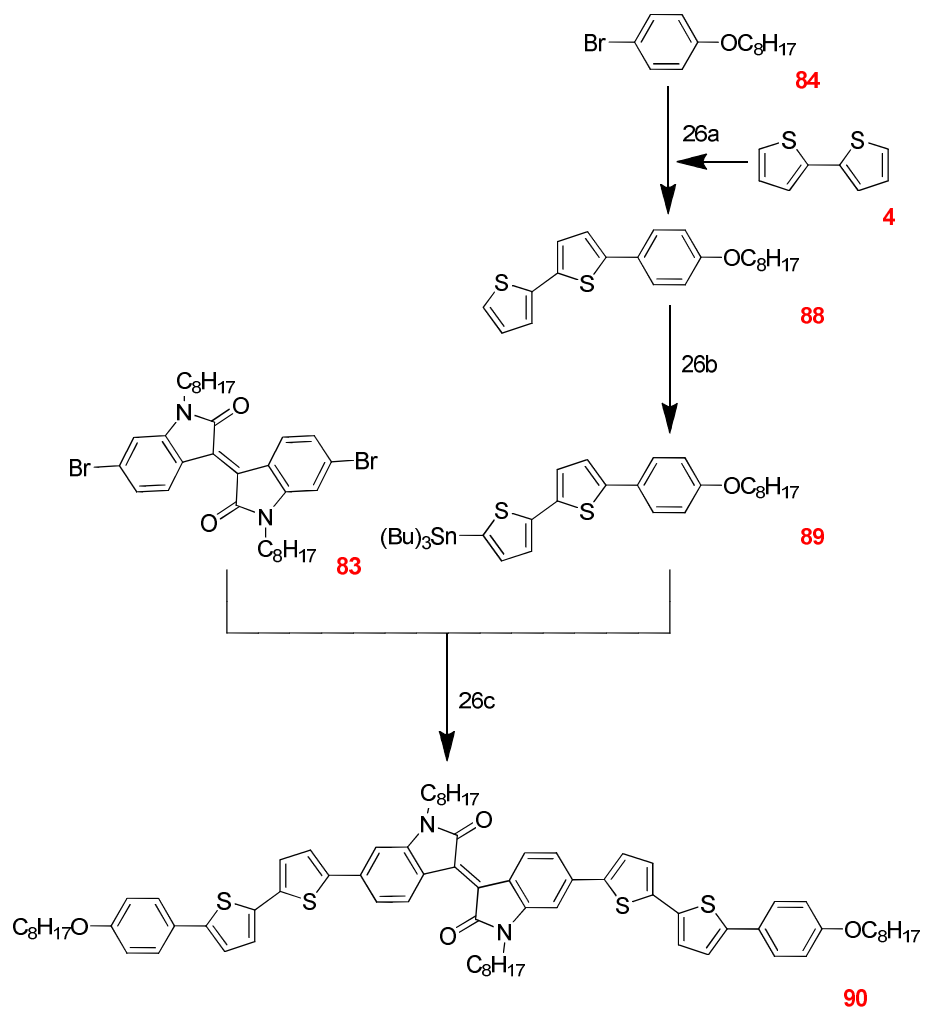
24a: *n*-BuLi, B(OMe)<sub>3</sub>, THF, HCl, -78 °C. 24b: Pd(PPh<sub>3</sub>)<sub>4</sub>, Na<sub>2</sub>CO<sub>3</sub>, DME, H<sub>2</sub>O, 80 °C.

Scheme 25



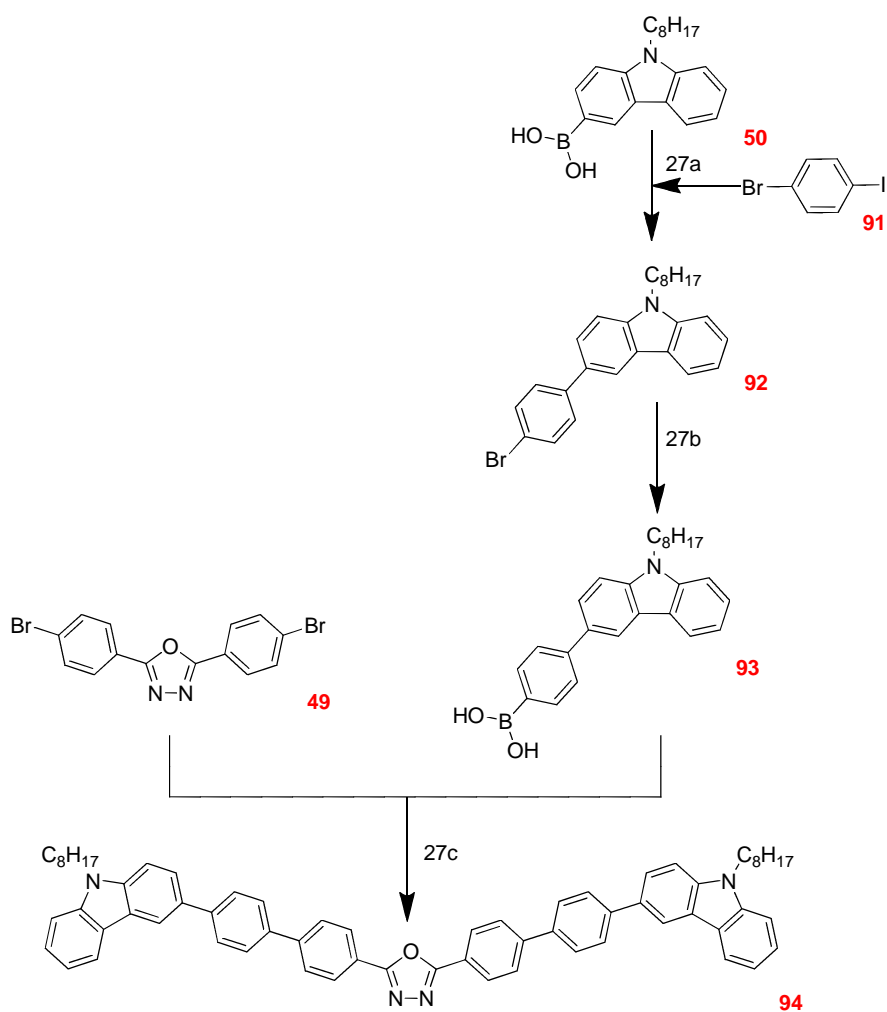
25a: HCl, CH<sub>3</sub>COOH. 25b: BrC<sub>8</sub>H<sub>17</sub>, K<sub>2</sub>CO<sub>3</sub>, DMF, 100 °C. 25c: Pd(PPh<sub>3</sub>)<sub>4</sub>, Na<sub>2</sub>CO<sub>3</sub>, DME, H<sub>2</sub>O, 80°C. 25d: *n*-BuLi, Sn(Bu)<sub>3</sub>Cl, THF, -78 °C. 25e: PPh<sub>3</sub>, Pd(OAc)<sub>2</sub>, DMF, 90 °C.

Scheme 26



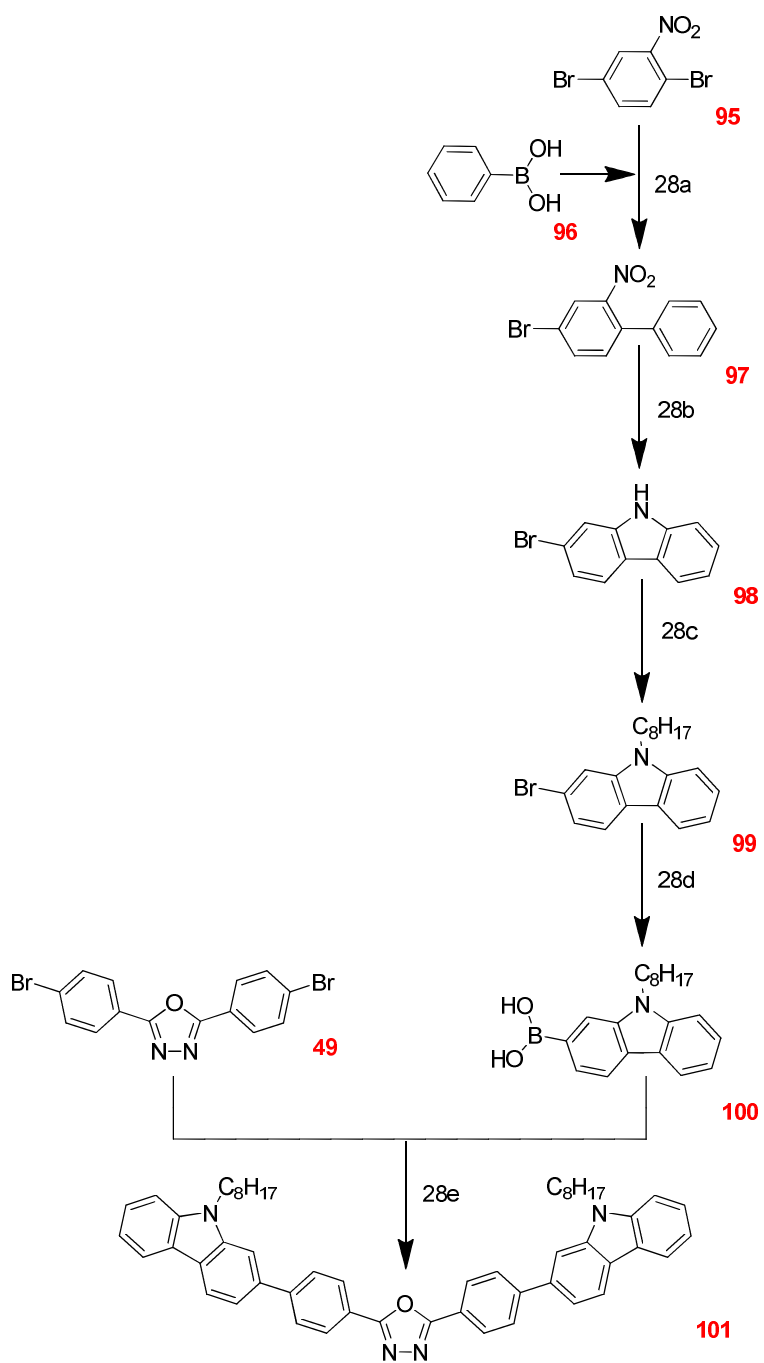
26a: Pd(OAc)<sub>2</sub>, K<sub>2</sub>CO<sub>3</sub>, PCy<sub>3</sub>·HBF<sub>4</sub>, (CH<sub>3</sub>)<sub>3</sub>CCO<sub>2</sub>H, NMP, 100 °C. 26b: *n*-BuLi, Sn(Bu)<sub>3</sub>Cl, THF, -78 °C. 26c: PPh<sub>3</sub>, Pd(OAc)<sub>2</sub>, DMF, 90 °C.

Scheme 27



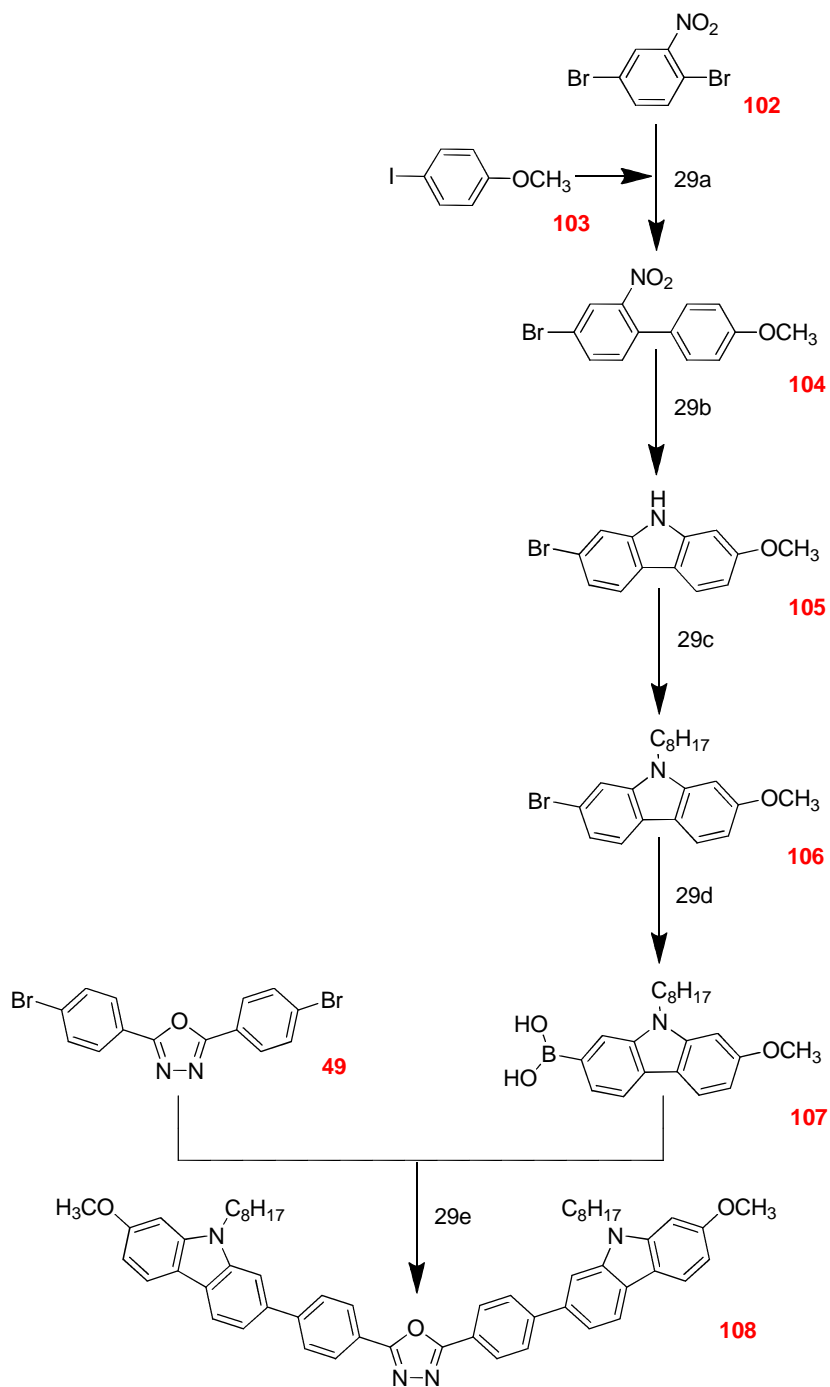
27a: Pd(PPh<sub>3</sub>)<sub>4</sub>, Na<sub>2</sub>CO<sub>3</sub>, DME, H<sub>2</sub>O, 80 °C. 27b: *n*-BuLi, [(CH<sub>3</sub>)<sub>2</sub>CHO]<sub>3</sub>B, THF, -78 °C. 27c: Pd(PPh<sub>3</sub>)<sub>4</sub>, Na<sub>2</sub>CO<sub>3</sub>, DME, H<sub>2</sub>O, 80 °C.

Scheme 28



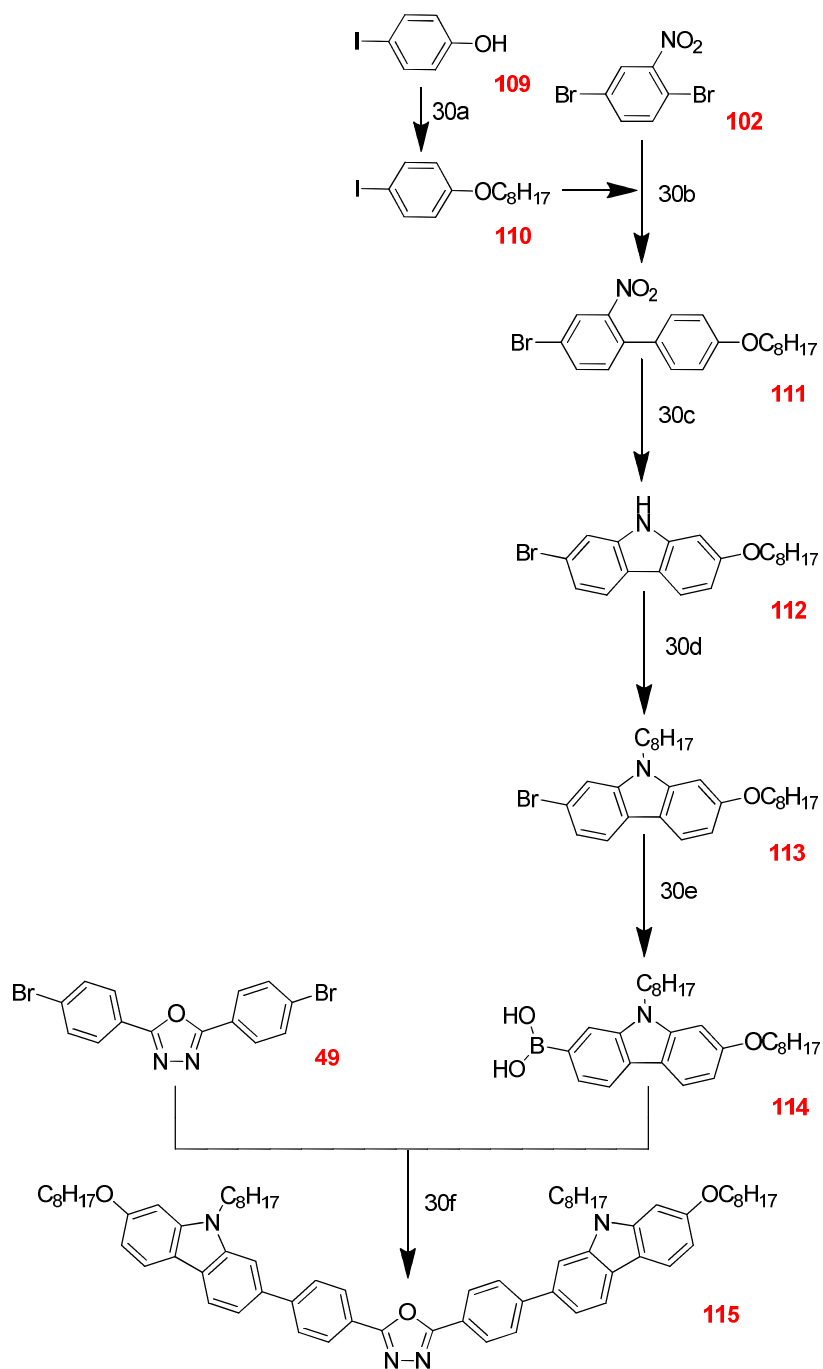
28a: Pd(PPh<sub>3</sub>)<sub>4</sub>, Na<sub>2</sub>CO<sub>3</sub>, toluene, H<sub>2</sub>O, 90 °C. 28b: PPh<sub>3</sub>. 28c: NaH, DMF, BrC<sub>8</sub>H<sub>17</sub>.  
 28d: *n*-BuLi, [(CH<sub>3</sub>)<sub>2</sub>CHO]<sub>3</sub>B, THF, -78 °C. 28e: Pd(OAc)<sub>2</sub>, K<sub>2</sub>CO<sub>3</sub>, H<sub>2</sub>O, DMF, 80 °C.

Scheme 29



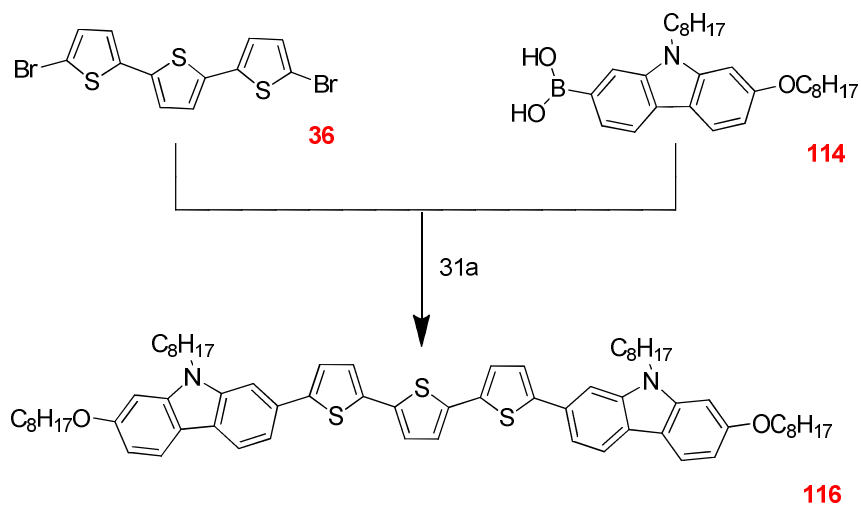
29a: Cu powder. 29b:  $\text{P}(\text{OC}_2\text{H}_5)_3$ . 29c: NaH, DMF,  $\text{BrC}_8\text{H}_{17}$ . 29d: *n*-BuLi,  $[(\text{CH}_3)_2\text{CHO}]_3\text{B}$ , THF,  $-78\text{ }^\circ\text{C}$ . 29e:  $\text{Pd}(\text{OAc})_2$ ,  $\text{K}_2\text{CO}_3$ ,  $\text{H}_2\text{O}$ , DMF,  $80\text{ }^\circ\text{C}$ .

Scheme 30



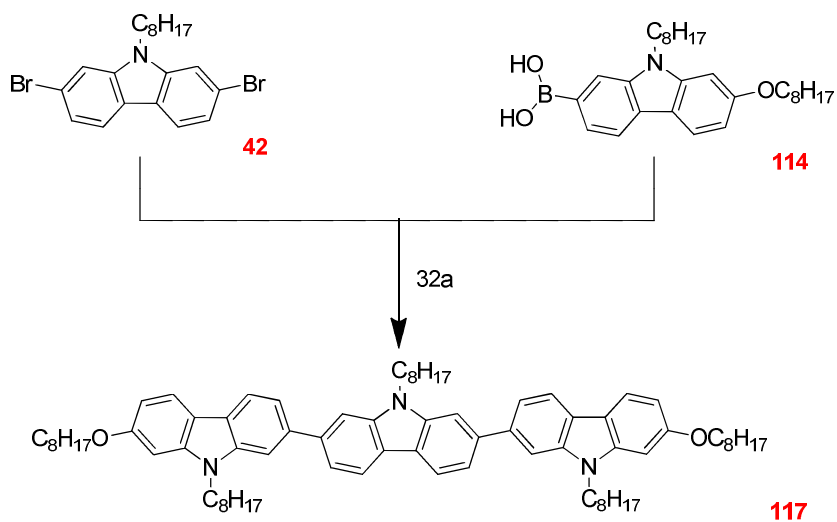
30a:  $\text{BrC}_8\text{H}_{17}$ ,  $\text{K}_2\text{CO}_3$ , DMF. 30b: Cu powder. 30c:  $\text{PPh}_3$ . 30d: NaH, DMF,  $\text{BrC}_8\text{H}_{17}$ .  
 30e: *n*-BuLi,  $[(\text{CH}_3)_2\text{CHO}]_3\text{B}$ , THF,  $-78^\circ\text{C}$ . 30f:  $\text{Pd}(\text{OAc})_2$ ,  $\text{K}_2\text{CO}_3$ ,  $\text{H}_2\text{O}$ , DMF,  $80^\circ\text{C}$ .

### Scheme 31



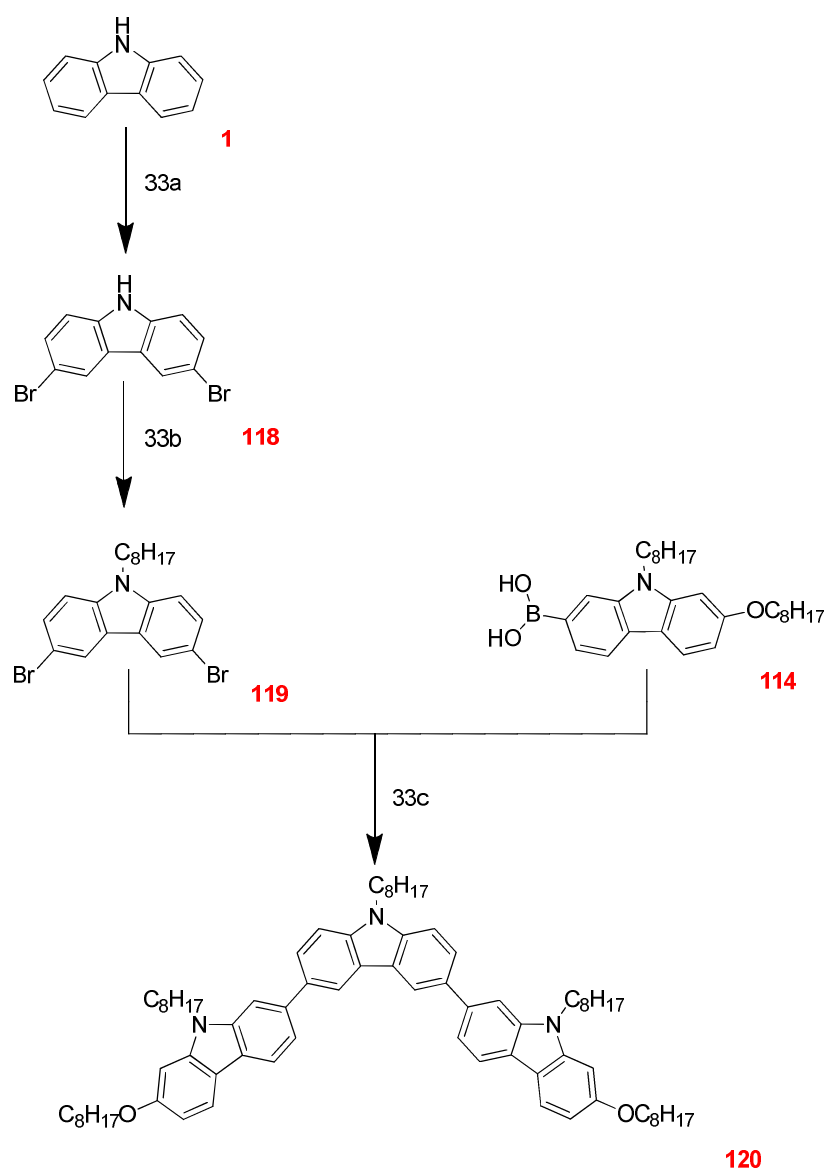
31a: Pd(OAc)<sub>2</sub>, K<sub>2</sub>CO<sub>3</sub>, H<sub>2</sub>O, DMF, 80 °C.

### Scheme 32



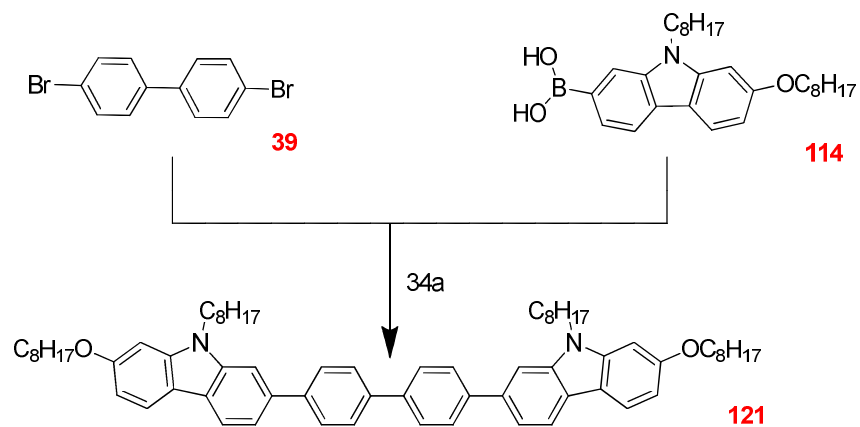
32a: Pd(OAc)<sub>2</sub>, K<sub>2</sub>CO<sub>3</sub>, H<sub>2</sub>O, DMF, 80 °C.

### Scheme 33



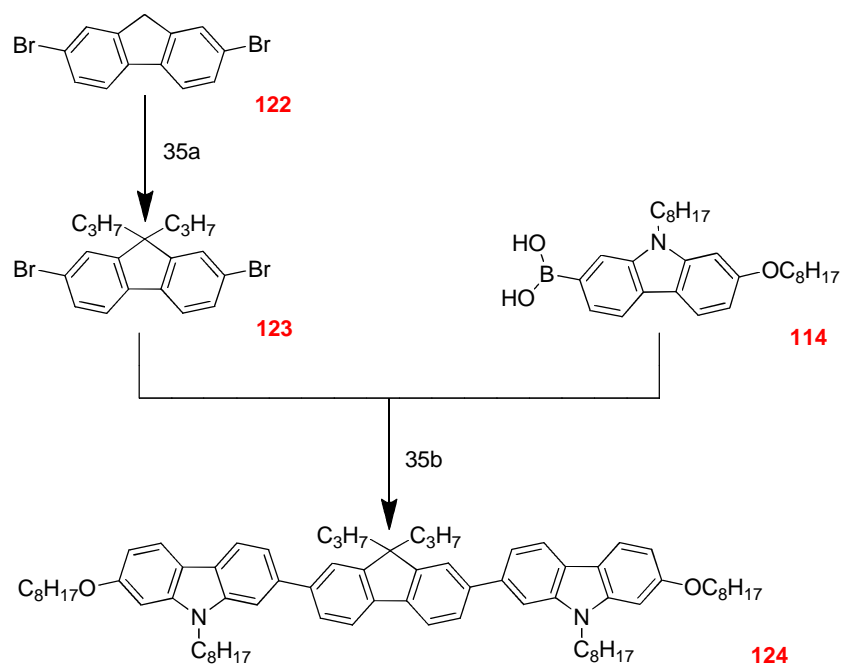
33a: NBS, toluene. 33b: BrC<sub>8</sub>H<sub>17</sub>, KOH, acetone. 33c: Pd(OAc)<sub>2</sub>, K<sub>2</sub>CO<sub>3</sub>, H<sub>2</sub>O, DMF, 80 °C.

### Scheme 34



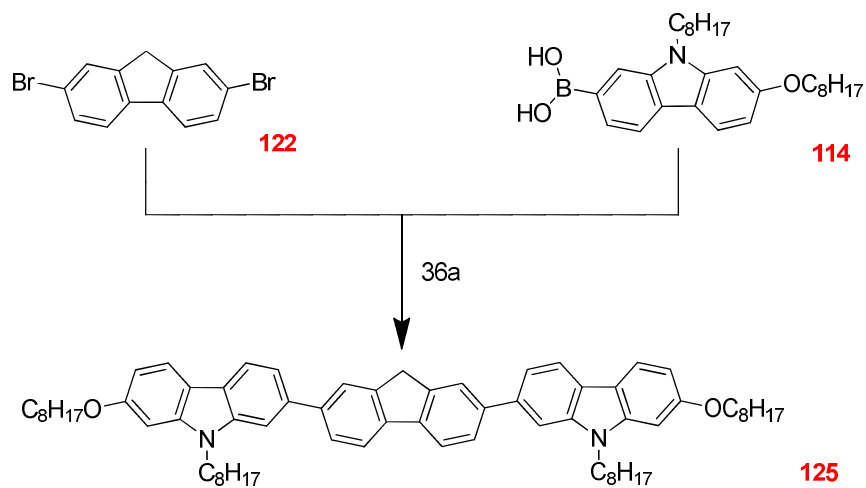
34a: Pd(OAc)<sub>2</sub>, K<sub>2</sub>CO<sub>3</sub>, H<sub>2</sub>O, DMF, 80 °C.

### Scheme 35



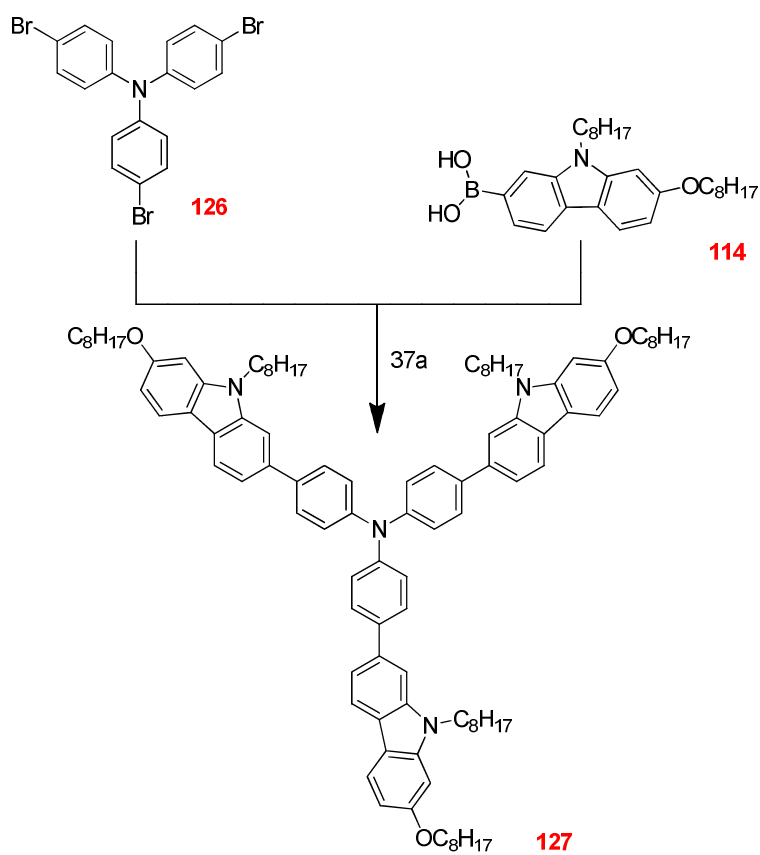
35a: KOH, KI, BrC<sub>3</sub>H<sub>7</sub>, DMSO. 35b: Pd(OAc)<sub>2</sub>, K<sub>2</sub>CO<sub>3</sub>, H<sub>2</sub>O, DMF, 80 °C.

### Scheme 36



36a: Pd(OAc)<sub>2</sub>, K<sub>2</sub>CO<sub>3</sub>, H<sub>2</sub>O, DMF, 80 °C.

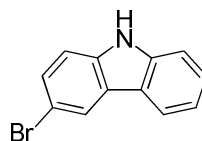
### Scheme 37



37a: Pd(OAc)<sub>2</sub>, K<sub>2</sub>CO<sub>3</sub>, H<sub>2</sub>O, DMF, 80 °C.

### 3.4 Synthesis of the Materials

#### 3-Bromocarbazole (2).



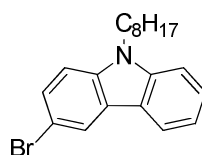
A solution of *N*-bromosuccinimide (NBS) (16.00 g, 0.089 mmol) in DMF (150 cm<sup>3</sup>) was added dropwise to a solution of carbazole (**1**) (15.00 g, 0.089 mmol) and DMF (100 cm<sup>3</sup>) at 0 °C. The mixture was brought to room temperature and stirred for an additional 2 h. The mixture was then poured into a saturated solution of sodium metabisulphite (Na<sub>2</sub>S<sub>2</sub>O<sub>5</sub>) in water (1,000 cm<sup>3</sup>). The resultant precipitate was filtered off, dried and then dissolved in dichloromethane. The resultant organic solution was washed with water (2 x 100 cm<sup>3</sup>), dried (MgSO<sub>4</sub>), filtered and concentrated under reduced pressure. The crude product was recrystallised from ethanol to give the desired product as a white solid (16.21 g, 73%).<sup>27</sup>

Melting point /°C: 195.

<sup>1</sup>H NMR ((CD<sub>3</sub>)<sub>2</sub>SO) δ<sub>H</sub>: 7.16 (1H, t, *J* = 7.3 Hz), 7.40-7.50 (4H, m), 8.15 (1H, d, *J* = 7.9 Hz), 8.34 (1H, d, *J* = 1.6 Hz), 11.41 (1H, s).

MS *m/z* (EI): 82, 113, 123, 139, 166, 245 (M<sup>+</sup>), 247 (M 100).

#### 3-Bromo-*N*-octyl-carbazole (3).

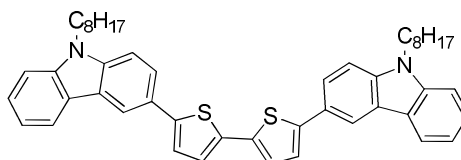


A mixture of 3-bromocarbazole (**2**) (10.00 g, 0.040 mol), 1-bromooctane (8.63 g, 0.044 mol), DMSO (50 cm<sup>3</sup>) and a 50% aqueous NaOH solution (40 cm<sup>3</sup>) was stirred at RT overnight. Water (20 cm<sup>3</sup>) was added and the resulting mixture extracted with diethyl ether (3 x 50 cm<sup>3</sup>). The combined organic extracts were washed with brine (2 x 100 cm<sup>3</sup>), dried (MgSO<sub>4</sub>), filtered and concentrated under reduced pressure. The crude product was purified by flash chromatography (silica gel, hexane) to yield the desired product as colourless oil (12.15 g, 85%).<sup>28</sup>

$^1\text{H}$  NMR ( $\text{CDCl}_3$ )  $\delta_{\text{H}}$ : 0.84 (3H, t,  $J = 6.9$  Hz), 1.21-1.40 (10H, m), 1.87 (2H, quint,  $J = 7.3$  Hz), 4.28 (2H, t,  $J = 7.3$  Hz), 7.21-7.24 (1H, m), 7.26 (1H, d,  $J = 8.7$  Hz), 7.39 (1H, d,  $J = 8.16$  Hz), 7.47 (1H, dd,  $J = 1.0, 6.1$  Hz), 7.53 (1H, dd,  $J = 2.0, 6.7$  Hz), 8.03 (1H, d,  $J = 7.6$  Hz), 8.19 (1H, d,  $J = 1.6$  Hz).

MS  $m/z$  (EI): 125, 160, 325, 341, 352 (M 100), 357 ( $\text{M}^+$ ).

**5,5'-bis-(9-Octyl-9-carbazol-3-yl)-2,2'-bithiophene (5).**



A mixture of potassium carbonate (0.31 g, 0.002 mol), palladium acetate (0.01 g,  $4.4 \times 10^{-5}$  mol),  $\text{PCy}_3 \cdot \text{HBF}_4$  (0.02 g,  $5.4 \times 10^{-5}$  mol), pivalic acid (0.05 g,  $4.9 \times 10^{-4}$  mol), 2,2'-bithiophene (**4**) (0.25 g, 0.001 mol) and 3-bromo-*N*-octyl-carbazole (**3**) (1.35 g, 0.003 mol) in DMF ( $6 \text{ cm}^3$ ) was degassed with  $\text{N}_2$  for 15 minutes and then heated at  $100^\circ\text{C}$  for 16 h. The mixture was allowed to cool to RT, then poured into water ( $100 \text{ cm}^3$ ). The crude product was extracted into dichloromethane ( $3 \times 50 \text{ cm}^3$ ) and the combined organic extracts washed with brine ( $100 \text{ cm}^3$ ), dried ( $\text{MgSO}_4$ ), filtered and concentrated under reduced pressure. Purification of the crude product was carried out *via* column chromatography [silica gel, dichloromethane: hexane, 1 : 1] and recrystallisation from DCM/EtOH to yield the desired product as a yellow solid (0.65 g, 65%).

Transition temp.  $^\circ\text{C}$ : Tg 64 Cr 168 I.

$^1\text{H}$  NMR ( $\text{CDCl}_3$ )  $\delta_{\text{H}}$ : 0.86 (6H, t,  $J = 7.1$  Hz), 1.23-1.39 (20H, m), 1.89 (4H, quint,  $J = 7.5$  Hz), 4.31 (4H, t,  $J = 7.3$  Hz), 7.21 (2H, d,  $J = 3.8$  Hz), 7.25 (2H, s), 7.29 (2H, d,  $J = 3.6$  Hz), 7.40 (4H, d,  $J = 8.7$  Hz), 7.49 (2H, d,  $J = 8.1$  Hz), 7.72 (2H, dd,  $J = 1.4, 7.9$  Hz), 8.14 (2H, d,  $J = 7.7$  Hz), 8.32 (2H, d,  $J = 1.8$  Hz).

$^{13}\text{C}$  NMR ( $\text{CDCl}_3$ ): 14.0, 22.6, 27.3, 28.9, 29.1, 29.3, 31.7, 43.2, 108.9, 109.0, 117.5, 119.0, 120.5, 122.5, 122.7, 123.0, 123.9, 124.1, 125.0, 126.0, 135.8, 140.0, 140.9, 144.3.

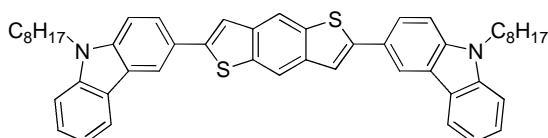
MS  $m/z$  (EI): 306, 400, 556, 720 ( $\text{M}^+$ , M 100).

Combustion analysis:

Expected: C 79.95%, H 7.27%, N 3.88%.

Obtained: C 79.81%, H 7.29%, N 3.83%.

**2,6-bis-(9-Octyl-9-carbazol-3-yl)benzo[1,2-b:4,5-b']dithiophene (7).**



A mixture of potassium carbonate (0.26 g, 0.002 mol), palladium acetate (0.01 g,  $4.4 \times 10^{-5}$  mol),  $\text{PCy}_3 \cdot \text{HBF}_4$  (0.02 g,  $5.4 \times 10^{-5}$  mol), pivalic acid (0.04 g,  $3.9 \times 10^{-4}$  mol), benzo[1,2-b:4,5-b']dithiophene (**6**) (0.25 g, 0.001 mol) and 3-bromo-*N*-octyl-carbazole (**3**) (1.16 g, 0.003 mol) in DMF (6 cm<sup>3</sup>) was degassed with N<sub>2</sub> for 15 minutes and then heated at 100 °C for 16 h. The reaction solution was cooled to RT and then diluted with water (200 cm<sup>3</sup>). The aqueous phase was extracted with dichloromethane (3 x 50 cm<sup>3</sup>). The combined organic layers were dried (MgSO<sub>4</sub>), filtered and concentrated under reduced pressure. Purification of the crude product was carried out *via* column chromatography [silica gel, dichloromethane: hexane, 1 : 1] and recrystallisation from DCM/EtOH to yield the desired product as a light yellow solid (0.56 g, 58%).

Transition temp. /°C: T<sub>g</sub> 76 Cr 190 I.

<sup>1</sup>H NMR (CDCl<sub>3</sub>) δ<sub>H</sub>: 0.86 (6H, t, *J* = 6.7 Hz), 1.19-1.33 (20H, m), 1.89 (4H, quint, *J* = 7.3 Hz), 4.32 (4H, t, *J* = 7.1 Hz), 7.40-7.50 (8H, m), 7.60 (2H, s), 7.85 (2H, dd, *J* = 2.0, 8.2 Hz), 8.17-8.20 (4H, m), 8.45 (2H, d, *J* = 2.3 Hz).

<sup>13</sup>C NMR (CDCl<sub>3</sub>): 14.0, 22.6, 27.2, 28.9, 29.1, 29.3, 31.8, 43.1, 108.9, 109.0, 115.8, 117.0, 118.2, 119.1, 120.5, 122.8, 123.2, 124.4, 125.3, 126, 136.7, 138.5, 140.4, 140.8, 145.3.

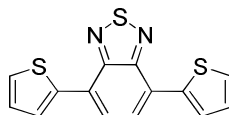
MS *m/z* (EI): 744 (M<sup>+</sup>, M 100), 745.

Combustion analysis:

Expected: C 80.60%, H 7.03%, N 3.76%.

Obtained: C 80.44%, H 7.14%, N 3.73%.

#### 4,7-Di(thiophen-2-yl)benzo-1,2,5-thiadiazole (10).



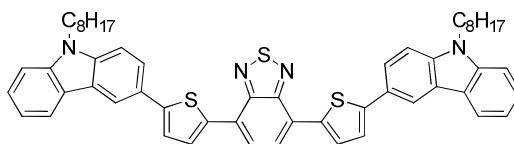
A mixture of 4,7-dibromobenzo-1,2,5-thiadiazole (**8**) (1.00 g, 0.003 mol), thiophen-2-boronic acid (**9**) (1.30 g, 0.010 mol), palladium acetate (0.02 g, 0.0001 mol), triphenylphosphine (0.29 g, 0.001 mol) and potassium carbonate (0.20 g, 0.001 mol) in THF (15 cm<sup>3</sup>) was heated under reflux at 80 °C overnight. The mixture was allowed to cool to RT, then poured into water (100 cm<sup>3</sup>). The crude product was extracted into dichloromethane (2 x 50 cm<sup>3</sup>) and the combined organic extracts washed with brine (100 cm<sup>3</sup>), dried (MgSO<sub>4</sub>), filtered and concentrated under reduced pressure. Purification of the crude product was carried out *via* column chromatography [silica gel, dichloromethane: hexane, 3 : 2]. The compound was further purified by recrystallisation from a mixture of DCM/EtOH to yield the desired product as orange-red solid (0.82 g, 78%).

Melting point /°C: 123-125.

<sup>1</sup>H NMR (CDCl<sub>3</sub>) δ<sub>H</sub>: 7.21 (2H, dd, *J* = 1.7, 4.8 Hz), 7.48 (2H, dd, *J* = 1.8, 4.6 Hz), 7.89 (2H, s), 8.12 (2H, dd, *J* = 1.8, 3.1 Hz).

MS *m/z* (EI): 69, 85, 99, 150, 196, 222, 255, 267, 300 (M<sup>+</sup>, M 100).

#### 4,7-bis-[5-(9-Octyl-9-carbazol-3-yl)thiophen-2-yl]benzo-1,2,5-thiadiazole (11).



A mixture of potassium carbonate (0.10 g, 7.2 x 10<sup>-4</sup> mol), palladium acetate (0.01 g, 4.4 x 10<sup>-5</sup> mol), PCy<sub>3</sub>·HBF<sub>4</sub> (0.01 g, 2.7 x 10<sup>-5</sup> mol), pivalic acid (0.01 g, 9.7 x 10<sup>-5</sup> mol), 4,7-di(thiophen-2-yl)benzo-1,2,5-thiadiazole (**10**) (0.15 g, 0.0005 mol), and 3-bromo-*N*-octyl-carbazole (**3**) (0.45 g, 0.001 mol) in DMF (6 cm<sup>3</sup>) was degassed with N<sub>2</sub> for 15 minutes and then heated at 100 °C for 16 h. The mixture was allowed to cool to RT, then poured into water (100 cm<sup>3</sup>). The crude product was extracted into dichloromethane (2 x 100 cm<sup>3</sup>) and the combined organic extracts washed with brine (100 cm<sup>3</sup>), dried (MgSO<sub>4</sub>), filtered and concentrated under reduced pressure.

Purification of the crude product was carried out *via* column chromatography [silica gel, dichloromethane: hexane, 1 : 1] and recrystallisation from DCM/EtOH to yield the desired product as a reddish brown solid (0.24 g, 55%).

Transition temp. /°C: Tg 56 Cr 307 I.

<sup>1</sup>H NMR (CDCl<sub>3</sub>) δ<sub>H</sub>: 0.86 (6H, t, *J* = 6.7 Hz), 1.25-1.41 (20H, m), 1.89 (4H, quint, *J* = 7.3 Hz), 4.31 (4H, t, *J* = 7.3 Hz), 7.29 (4H, d, *J* = 7.8 Hz), 7.41-7.51 (8H, m), 7.84 (2H, dd, *J* = 3.5, 8.6 Hz), 7.92 (2H, s), 8.16 (2H, d, *J* = 4.0 Hz), 8.43 (2H, d, *J* = 1.8 Hz).

<sup>13</sup>C NMR (CDCl<sub>3</sub>): 14.0, 22.6, 27.3, 29.1, 27.7, 30.5, 31.7, 43.1, 108.9, 117.7, 119.0, 120.5, 121.2, 122.8, 123.2, 123.8, 124.0, 125.2, 126.0, 128.5, 140.1, 140.8, 148.0.

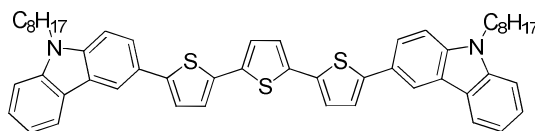
MS *m/z* (EI): 577, 854 (M<sup>+</sup>, M 100).

Combustion analysis:

Expected: C 75.84%, H 6.36%, N 6.55%.

Obtained: C 75.78%, H 6.26%, N 6.48%.

### 5,5''-bis-(9-Octyl-9-carbazol-3-yl)-2,2':5',2''-terthiophene (13).



A mixture of potassium carbonate (0.20 g, 0.001 mol), palladium acetate (0.01 g, 4.4 x 10<sup>-5</sup> mol), PCy<sub>3</sub>·HBF<sub>4</sub> (0.02 g, 5.4 x 10<sup>-5</sup> mol), pivalic acid (0.01 g, 9.7 x 10<sup>-5</sup> mol), 2,2':5',2''-terthiophene (**12**) (0.25 g, 0.001 mol) and 3-bromo-*N*-octyl-carbazole (**3**) (0.90 g, 0.002 mol) in DMF (6 cm<sup>3</sup>) was degassed with N<sub>2</sub> for 15 minutes and then heated at 100 °C for 16 h. The mixture was allowed to cool to RT, then poured into water (100 cm<sup>3</sup>). The crude product was extracted into dichloromethane (2 x 100 cm<sup>3</sup>) and the combined organic extracts washed with brine (100 cm<sup>3</sup>), dried (MgSO<sub>4</sub>), filtered and concentrated under reduced pressure. Purification of the crude product was carried out *via* column chromatography [silica gel, dichloromethane: hexane, 3 : 2] and recrystallisation from DCM/EtOH to yield an orange solid (0.69 g, 86%).

Melting point /°C: 166.

$^1\text{H}$  NMR ( $\text{CDCl}_3$ )  $\delta_{\text{H}}$ : 0.86 (6H, t,  $J = 6.9$  Hz), 1.20-1.40 (20H, m), 1.89 (4H, quint,  $J = 7.5$  Hz), 4.31 (4H, t,  $J = 7.1$  Hz), 7.14 (2H, s), 7.19 (2H, d,  $J = 3.6$  Hz), 7.28 (4H, d,  $J = 3.6$  Hz), 7.42 (4H, dd,  $J = 2.0, 6.5$  Hz), 7.48 (2H, d,  $J = 6.9$  Hz), 7.72 (2H, dd,  $J = 1.8, 6.7$  Hz), 8.14 (2H, d,  $J = 7.7$  Hz), 8.32 (2H, d,  $J = 1.4$  Hz).

$^{13}\text{C}$  NMR ( $\text{CDCl}_3$ ): 14.0, 22.6, 27.3, 28.9, 29.1, 29.3, 31.7, 43.2, 108.9, 109.0, 117.0, 119.0, 120.5, 122.6, 122.7, 123.2, 123.8, 124.5, 125.1, 125.9, 135.0, 136.1, 140.0, 140.9, 144.7.

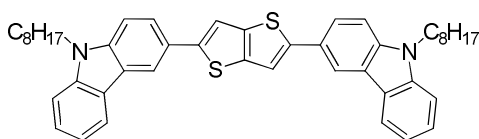
MS  $m/z$  (EI): 306, 384, 690, 802 ( $\text{M}^+$ ,  $\text{M} - 100$ ).

Combustion analysis:

Expected: C 77.76%, H 6.78%, N 3.49%.

Obtained: C 77.86%, H 6.95%, N 3.60%.

### 2,5-bis-(9-Octyl-9-carbazol-3-yl)thieno[3,2-b]thiophene (15).



A mixture of potassium carbonate (0.40 g, 0.003 mol), palladium acetate (0.01 g,  $4.4 \times 10^{-5}$  mol),  $\text{PCy}_3 \cdot \text{HBF}_4$  (0.02 g,  $5.4 \times 10^{-5}$  mol), pivalic acid (0.06 g,  $5.8 \times 10^{-4}$  mol), thieno[3,2-b]thiophene (**14**) (0.15 g, 0.001 mol) and 3-bromo-*N*-octyl-carbazole (**3**) (0.89 g, 0.002 mol) in DMF ( $6 \text{ cm}^3$ ) was degassed with  $\text{N}_2$  for 15 minutes and then heated at  $100^\circ\text{C}$  for 16 h. The mixture was allowed to cool to RT, then poured into water ( $100 \text{ cm}^3$ ). The crude product was extracted into dichloromethane ( $100 \text{ cm}^3$ ) and the combined organic extracts washed with brine ( $100 \text{ cm}^3$ ), dried ( $\text{MgSO}_4$ ), filtered and concentrated under reduced pressure. Purification of the crude product was carried out *via* column chromatography [silica gel, dichloromethane: hexane, 1 : 1] and recrystallisation from DCM/EtOH to yield a light yellow solid (0.36 g, 52%).

Transition temp.  $^\circ\text{C}$ : Tg 46 Cr 187 I.

$^1\text{H}$  NMR ( $\text{CDCl}_3$ )  $\delta_{\text{H}}$ : 0.86 (6H, t,  $J = 6.9$  Hz), 1.24-1.44 (20H, m), 1.89 (4H, quint,  $J = 7.1$  Hz), 4.31 (4H, t,  $J = 6.9$  Hz), 7.28 (2H, s), 7.41 (4H, dd,  $J = 2.3, 6.9$  Hz), 7.49 (2H, d,  $J = 7.1$  Hz), 7.59 (2H, s), 7.76 (2H, dd,  $J = 1.8, 8.1$  Hz), 8.15 (2H, d,  $J = 8.2$  Hz), 8.35 (2H, d,  $J = 1.6$  Hz).

$^{13}\text{C}$  NMR ( $\text{CDCl}_3$ ): 14.0, 22.6, 27.3, 28.6, 29.1, 29.5, 31.8, 43.1, 109.0, 115.8, 117.0, 118.2, 119.2, 121.6, 122.4, 123.5, 124.9, 126.0, 136.8, 138.3, 140.2, 141.0, 145.2.

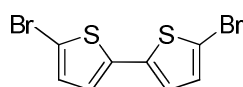
MS  $m/z$  (EI): 623, 694 ( $\text{M}^+$ ,  $\text{M}$  100).

Combustion analysis:

Expected: C 79.49%, H 7.25%, N 4.03%.

Obtained: C 79.36%, H 6.95%, N 3.93%.

### 5,5'-Dibromo-2,2-bithiophene (**16**).



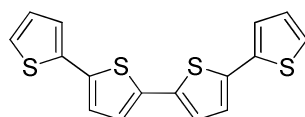
*N*-Bromosuccinimide (9.40 g, 0.052 mol) was added slowly (over a period of 3 hours) to a solution of 2,2-bithiophene (**4**) (4.00 g, 0.024 mol) in DCM (50  $\text{cm}^3$ ) and silica gel (2 g) was added to the resultant solution. Once the addition was complete, the reaction mixture was stirred at RT for 2 hours in the dark. The precipitate formed was filtered off and washed with dichloromethane (100  $\text{cm}^3$ ). The filtrate was washed with sodium metabisulphite solution ( $\text{Na}_2\text{S}_2\text{O}_5$ ) (2 x 50  $\text{cm}^3$ ) and water (100  $\text{cm}^3$ ), dried ( $\text{MgSO}_4$ ), filtered, concentrated under reduced pressure and then purified by recrystallisation from ethanol to yield the desired product as white flakes (6.85 g, 89%).

Melting point / $^\circ\text{C}$ : 145-146 (Lit. 144-146).<sup>16</sup>

$^1\text{H}$  NMR ( $\text{CDCl}_3$ )  $\delta_{\text{H}}$ : 6.85 (2H, d,  $J = 3.9$  Hz), 6.96 (2H, d,  $J = 3.9$  Hz).

MS ( $m/z$ ) (EI): 95, 120, 149, 164, 199, 201, 243, 245, 279, 324 ( $\text{M}^+$ ,  $\text{M}$  100).

### 2,2':5',2'':5'',2'''-Quaterthiophene (**18**).



A mixture of 5,5'-dibromo-2,2-bithiophene (**16**) (2.00 g, 0.006 mol) tributyl(thiophen-2-yl)stannane (**17**) (5.10 g, 0.013 mol) in DMF (50  $\text{cm}^3$ ) was stirred and degassed with  $\text{N}_2$  for 20 minutes. Tetrakis(triphenylphosphine)palladium(0) (0.07 g,  $6 \times 10^{-5}$  mol) was added and the resultant reaction mixture heated at 100  $^\circ\text{C}$  overnight. The reaction

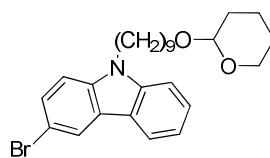
mixture was cooled to RT, water (100 cm<sup>3</sup>) was added and the product extracted with dichloromethane (3 x 50 cm<sup>3</sup>). The combined organic extracts were washed with brine (100 cm<sup>3</sup>), dried (MgSO<sub>4</sub>), filtered and concentrated under reduced pressure. Purification of the crude product was carried out *via* column chromatography [10% potassium carbonate and 90% silica gel, dichloromethane: hexane, 1 : 1] and recrystallised from DCM/EtOH to yield the desired product as a yellow solid (1.34 g, 66%).

Melting point /°C: 211-214.

<sup>1</sup>H NMR (CDCl<sub>3</sub>) δ<sub>H</sub>: 7.03 (2H, dd, *J* = 3.6, 8.6 Hz), 7.08 (4H, d, *J* = 9.1 Hz), 7.18 (2H, dd, *J* = 1.0, 6.1 Hz), 7.23 (2H, dd, *J* = 1.1, 6.1 Hz).

MS (m/z) (EI): 330 (M<sup>+</sup>, M100).

### 3-Bromo-9-{9-[(tetrahydro-2-pyran-2-yl)oxy]nonyl}-9-carbazole (20).

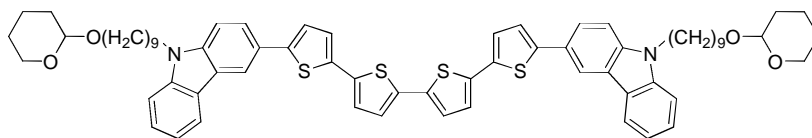


A mixture of 3-bromocarbazole (**2**) (1.90 g, 0.007 mol) and 2-[9-bromo-(nonyloxy)] tetrahydro-2-pyran (**19**) (2.50 g, 0.007 mol) and potassium hydroxide (2.00 g, 0.035 mol) in DMF (20 cm<sup>3</sup>) was heated at 50 °C overnight. Water (20 cm<sup>3</sup>) was added and the resulting mixture extracted with diethyl ether (2 x 50 cm<sup>3</sup>). The combined organic extracts were dried (MgSO<sub>4</sub>), filtered and concentrated under reduced pressure. The crude was purified by flash chromatography (silica gel, ethyl acetate: hexane, 2 : 1) giving the desired product as colourless oil (2.21 g, 88%).

<sup>1</sup>H NMR (CDCl<sub>3</sub>) δ<sub>H</sub>: 1.29-1.43 (10H, m), 1.52-1.62 (6H, m), 1.72 (2H, quint, *J* = 7.3 Hz), 1.82 (2H, quint, *J* = 7.3 Hz), 3.68-3.72 (2H, m), 3.83-3.86 (2H, m), 4.26 (2H, t, *J* = 7.3 Hz), 4.56 (1H, t, *J* = 7.3 Hz), 7.21-7.28 (2H, m), 7.40 (1H, d, *J* = 5.3 Hz), 7.47 (1H, dd, *J* = 1.0, 6.9 Hz), 7.53 (1H, dd, *J* = 2.0, 7.6 Hz), 8.04 (1H, d, *J* = 7.7 Hz), 8.20 (1H, d, *J* = 1.8 Hz).

MS m/z (EI): 472, 473 (M<sup>+</sup>, M100).

**5,5'''-bis-[(9-{9-[(Tetrahydro-2-pyran-2-yl)oxy]nonyl}-carbazol-3-yl)]-2,2':5',2'':5'',2'''-quaterthiophene (21).**



A mixture of potassium carbonate (0.10 g,  $7.2 \times 10^{-4}$  mol), palladium acetate (0.01 g,  $4.4 \times 10^{-5}$  mol), PCy<sub>3</sub>·HBF<sub>4</sub> (0.01 g  $2.7 \times 10^{-5}$  mol), pivalic acid (0.01 g,  $9.7 \times 10^{-5}$  mol), 2,2':5',2'':5'',2'''-quaterthiophene (**18**) (0.20 g, 0.0006 mol) and 3-bromo-9-{9-[(tetrahydro-2-pyran-2-yl)oxy]nonyl}-9-carbazole (**20**) (0.85 g, 0.002 mol) in DMF (2 cm<sup>3</sup>) was degassed with N<sub>2</sub> for 15 minutes and then heated at 100 °C for 16 h. The mixture was allowed to cool to RT, then poured into water (100 cm<sup>3</sup>). The crude product was extracted into dichloromethane (3 x 50 cm<sup>3</sup>) and the combined organic extracts washed with brine (100 cm<sup>3</sup>), dried (MgSO<sub>4</sub>), filtered and concentrated under reduced pressure. Purification of the crude product was carried out *via* column chromatography [silica gel, dichloromethane: hexane, 2 : 3] and recrystallisation from DCM/EtOH to yield the desired product as an orange solid (0.30 g, 45%).

Melting point /°C: 162.

<sup>1</sup>H NMR (CDCl<sub>3</sub>) δ<sub>H</sub>: 1.26-1.39 (20H, m), 1.42-1.59 (12H, m), 1.71 (4H, quint, *J* = 7.3 Hz), 1.86 (4H, m), 3.50-3.60 (4H, m), 3.71-3.80 (4H, m), 4.29 (4H, t, *J* = 7.3 Hz), 4.56 (2H, t, *J* = 4.2 Hz), 7.12 (4H, d, *J* = 3.6 Hz), 7.19 (2H, d, *J* = 3.8 Hz), 7.24 (2H, s), 7.28 (2H, d, *J* = 3.6 Hz), 7.40 (4H, dd, *J* = 1.8, 8.6 Hz), 7.42 (2H, d, *J* = 2.3 Hz), 7.72 (2H, dd, *J* = 3.3, 8.6 Hz), 8.15 (2H, d, *J* = 7.7 Hz), 8.32 (2H, d, *J* = 1.8 Hz).

<sup>13</sup>C NMR (CDCl<sub>3</sub>): 19.7, 25.5, 26.1, 27.2, 29.3, 29.4, 29.7, 30.7, 42.1, 62.3, 67.6, 98.8, 109.5, 110.0, 118.0, 119.4, 122.0, 123.0, 123.4, 123.8, 124.0, 126.6, 128.1, 129.0, 135.0, 136.5, 139.9, 142.7.

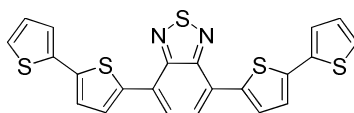
MS *m/z* (EI): 784, 890, 1028, 1112 (M<sup>+</sup>, M 100).

Combustion analysis:

Expected: C 73.34%, H 6.88%, N 2.52%.

Obtained: C 73.42%, H 7.04%, N 2.71%.

#### 4,7-Di-(2,2'-bithiophen-5-yl)benzo-1,2,5-thiadiazole (22).



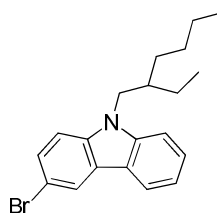
A mixture of potassium carbonate (0.70 g, 0.005 mol), palladium acetate (0.02 g,  $8.8 \times 10^{-5}$  mol),  $\text{PCy}_3 \cdot \text{HBF}_4$  (0.06 g,  $1.6 \times 10^{-4}$  mol), pivalic acid (0.10 g, 0.001 mol), 4,7-dibromobenzo-1,2,5-thiadiazole (**8**) (1.00 g, 0.003 mol) and 2,2-bithiophene (**4**) (1.41 g, 0.008 mol) in DMF (13.6 cm<sup>3</sup>) was degassed with N<sub>2</sub> for 15 minutes and then heated at 100 °C for 16 h. The mixture was allowed to cool to RT, then poured into water (150 cm<sup>3</sup>). The crude product was extracted into dichloromethane (2 x 150 cm<sup>3</sup>) and the combined organic extracts washed with brine (200 cm<sup>3</sup>), dried (MgSO<sub>4</sub>), filtered and concentrated under reduced pressure. Purification of the crude product was carried out *via* column chromatography [silica gel, dichloromethane in hexane, 3 : 1] and recrystallisation from ethanol to yield the desired product as a red solid (0.71 g, 44%).

Melting point /°C: 247.

<sup>1</sup>H NMR (CDCl<sub>3</sub>) δ<sub>H</sub>: 7.07 (2H, dd, *J* = 3.4, 8.6 Hz), 7.27 (4H, m), 7.30 (2H, dd, *J* = 3.5, 8.8 Hz), 7.86 (2H, s), 8.05 (2H, d, *J* = 3.8 Hz).

MS *m/z* (EI): 464 (M<sup>+</sup>, M 100).

#### 3-Bromo-9-(2-ethylhexyl)-carbazole (23).

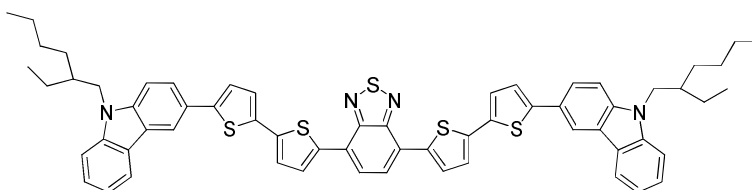


A mixture of 3-bromocarbazole (**2**) (1.50 g, 0.006 mmol), 2-ethylhexyl bromide (1.17 g, 0.006 mol) in DMSO (12 cm<sup>3</sup>) and an aqueous NaOH solution (50% w/w, 6 cm<sup>3</sup>) was stirred at room temperature overnight. Water (20 cm<sup>3</sup>) was added and the resulting mixture extracted with diethyl ether (3 x 50 cm<sup>3</sup>). The combined organic layers were dried (MgSO<sub>4</sub>), filtered and concentrated down under reduced pressure. The crude product was purified by flash chromatography (silica gel, hexane) give the desired product as colourless oil (1.93 g, 90%).

$^1\text{H}$  NMR ( $\text{CDCl}_3$ )  $\delta_{\text{H}}$ : 0.84 (3H, t,  $J = 6.6$  Hz), 0.92 (3H, t,  $J = 6.8$  Hz), 1.21-1.43 (8H, m), 2.05 (1H, m), 4.16 (2H, dd,  $J = 2.7, 7.3$  Hz), 7.24 (1H, s), 7.33 (1H, d,  $J = 8.4$  Hz), 7.44 (1H, d,  $J = 8.0$  Hz), 7.50 (1H, dd,  $J = 1.2, 8.4$  Hz), 7.55 (1H, dd,  $J = 1.6, 8.4$  Hz), 8.06 (1H, d,  $J = 8.1$  Hz), 8.22 (1H, d,  $J = 1.6$  Hz).

MS (m/z) (EI): 129, 158, 329, 342, 348 (M 100), 357 ( $\text{M}^+$ ).

**4,7-bis{(5'-[9-(2-Ethylhexyl)-carbazol-3-yl]-[2,2'-bithiophen]-5-yl)}benzo-1,2,5-thiadiazole (24).**



A mixture of potassium carbonate (0.10 g, 0.0007 mol), palladium acetate (0.01 g,  $4.4 \times 10^{-5}$  mol),  $\text{PCy}_3 \cdot \text{HBF}_4$  (0.01 g,  $2.7 \times 10^{-5}$  mol), pivalic acid (0.15 g, 0.001 mol), 4,7-di(2,2'-bithiophen-5-yl)benzo-1,2,5-thiadiazole (**22**) (0.20 g, 0.0004 mol) and 3-bromo-9-(2-ethylhexyl)-carbazole (**23**) (0.38 g, 0.001 mol) in DMF ( $2 \text{ cm}^3$ ) was degassed with  $\text{N}_2$  for 15 minutes and then heated at  $100^\circ\text{C}$  for 16 h. The mixture was allowed to cool to RT, then poured into water ( $100 \text{ cm}^3$ ). The crude product was extracted into dichloromethane ( $2 \times 100 \text{ cm}^3$ ) and the combined organic extracts washed with brine ( $100 \text{ cm}^3$ ), dried ( $\text{MgSO}_4$ ), filtered and concentrated under reduced pressure. Purification of the crude product was carried out *via* column chromatography [silica gel, dichloromethane: hexane, 1 : 1] and recrystallisation from DCM/EtOH to yield the desired product as a reddish brown solid (0.25 g, 62%).

Transition temp.  $^{\circ}\text{C}$ : Tg 74 Cr 343 I.

$^1\text{H}$  NMR ( $\text{CDCl}_3$ )  $\delta_{\text{H}}$ : 0.84 (6H, t,  $J = 6.6$  Hz), 0.90 (6H, t,  $J = 6.8$  Hz), 1.24-1.34 (16H, m), 1.89 (2H, m), 4.31 (4H, dd,  $J = 2.0, 7.3$  Hz), 7.28-7.38 (8H, m), 7.41 (4H, dd,  $J = 2.0, 7.1$  Hz), 7.53 (2H, d,  $J = 8.6$  Hz), 7.75 (2H, d,  $J = 1.8$  Hz), 7.90 (2H, s), 8.11 (2H, d,  $J = 4.0$  Hz), 8.18 (2H, d,  $J = 1.9$  Hz), 8.35 (2H, d,  $J = 1.8$  Hz).

$^{13}\text{C}$  NMR ( $\text{CDCl}_3$ ): 14.0, 22.6, 27.3, 29.3, 29.6, 30.7, 31.9, 43.4, 108.6, 111.0, 112.8, 117.4, 119.8, 120.9, 122.6, 123.8, 125.0, 126.6, 129.0, 139.9, 142.7, 148.0.

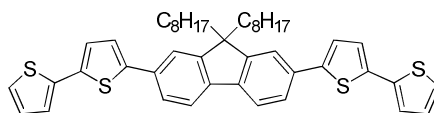
MS m/z (EI): 825, 934, 1018 ( $\text{M}^+$ , M 100).

Combustion analysis:

Expected: C 73.04%, H 5.73%, N 5.50%.

Obtained: C 72.81%, H 5.74%, N 5.38%.

**bis-2,7-(2,2'-Bithiophen-5-yl)-(9,9-dioctyl)-fluorene (26).**



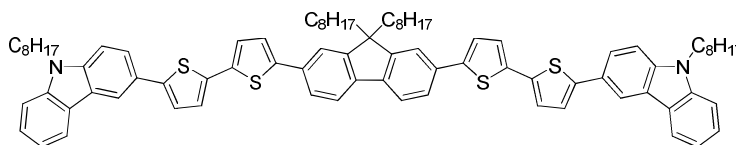
A mixture of potassium carbonate (0.75 g, 0.005 mol), palladium acetate (0.06 g,  $2.6 \times 10^{-4}$  mol),  $\text{PCy}_3 \cdot \text{HBF}_4$  (0.07 g,  $1.9 \times 10^{-4}$  mol), pivalic acid (0.12 g, 0.001 mol), 2,7-dibromo-(9,9-dioctyl)-fluorene (**25**) (2.00 g, 0.003 mol), and 2,2-bithiophene (**4**) (3.00 g, 0.018 mol) in DMF ( $15 \text{ cm}^3$ ) was degassed with  $\text{N}_2$  for 15 minutes and then heated at  $100 \text{ }^\circ\text{C}$  for 3 h. The mixture was allowed to cool to RT, then poured into water ( $200 \text{ cm}^3$ ). The crude product was extracted into dichloromethane ( $2 \times 100 \text{ cm}^3$ ) and the combined organic extracts washed with brine ( $150 \text{ cm}^3$ ), dried ( $\text{MgSO}_4$ ), filtered and evaporated down under reduced pressure. Purification of the crude product was carried out *via* column chromatography [silica gel, dichloromethane: hexane, 2 : 3] to yield the desired product as a yellow solid (1.20 g, 46%).

Melting point / $^\circ\text{C}$ : 144-145.

$^1\text{H}$  NMR ( $\text{CDCl}_3$ )  $\delta_{\text{H}}$ : 0.80 (6H, t,  $J = 7.5$  Hz), 1.26-1.37 (24H, m), 2.04 (4H, m), 7.05 (2H, dd,  $J = 3.6, 8.6$  Hz), 7.18 (2H, d,  $J = 3.8$  Hz), 7.22-7.24 (4H, m), 7.29 (2H, d,  $J = 3.8$  Hz), 7.54 (2H, d,  $J = 1.6$  Hz), 7.59 (2H, dd,  $J = 1.6, 7.8$  Hz), 7.69 (2H, d,  $J = 8.0$  Hz).

MS  $m/z$  (EI): 718 ( $\text{M}^+$ , M100).

**3,3'-[(5',5'''-(9,9-dioctyl-9-fluorene-2,7-diyl)bis-([2,2'-bithiophene]-5',5-diyl)]bis-(9-octyl-9-carbazole) (27).**



A mixture of potassium carbonate (0.05 g, 0.0003 mol), palladium acetate (0.01 g,  $4.4 \times 10^{-4}$  mol),  $\text{PCy}_3 \cdot \text{HBF}_4$  (0.01 g,  $2.7 \times 10^{-5}$  mol), pivalic acid (0.01 g,  $9.7 \times 10^{-5}$  mol),

*bis*-2,7-(2,2'-bithiophen-5-yl)-(9,9-dioctyl)-fluorene (**26**) (0.15 g, 0.0002 mol) and 3-bromo-*N*-octyl-carbazole (**3**) (0.36 g, 0.001 mol) in DMF (15 cm<sup>3</sup>) was degassed with N<sub>2</sub> for 15 minutes and then heated at 100 °C for 16 h. The mixture was allowed to cool to RT, then poured into water (100 cm<sup>3</sup>). The crude product was extracted into dichloromethane (2 x 100 cm<sup>3</sup>) and the combined organic extracts washed with brine (100 cm<sup>3</sup>), dried (MgSO<sub>4</sub>), filtered and concentrated under reduced pressure. Purification of the crude product was carried out *via* column chromatography [silica gel, dichloromethane: hexane, 2 : 3] and recrystallisation from DCM/DMSO followed by DCM/MeOH to yield the desired product as a yellow solid (0.16 g, 64%).

Transition temp. /°C: Tg 18 Cr 107 SmC 123 I.

<sup>1</sup>H NMR (CDCl<sub>3</sub>) δ<sub>H</sub>: 0.84 (6H, t, 7.1 Hz), 0.86 (6H, t, *J* = 6.7 Hz), 0.90-1.05 (10H, m), 1.08-1.30 (34H, m), 1.89 (4H, quint, *J* = 7.2 Hz), 2.06 (4H, m), 4.31 (4H, t, *J* = 7.0 Hz), 7.22 (6H, d, *J* = 7.3 Hz), 7.28 (2H, d, *J* = 3.8 Hz), 7.33 (2H, d, *J* = 3.8 Hz), 7.41 (4H, d, *J* = 7.7 Hz), 7.48 (2H, d, *J* = 8.1 Hz), 7.57 (2H, s), 7.61 (2H, dd, *J* = 2.0, 7.7 Hz), 7.70 (2H, d, *J* = 4.0 Hz), 7.73 (2H, dd, *J* = 1.6 Hz), 8.15 (2H, d, *J* = 7.5 Hz), 8.33 (2H, d, *J* = 1.8 Hz).

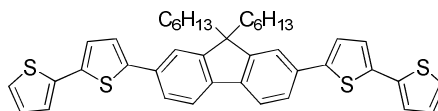
MS *m/z* (EI): 306, 556, 831, 1272 (M<sup>+</sup>, M 100).

Combustion analysis:

Expected: C 80.14%, H 7.60%, N 2.20%, S 10.07%.

Obtained: C 80.01%, H 7.43%, N 2.18%, S 9.97%.

***bis*-2,7-(2,2'-Bithiophen-5-yl)-(9,9-dihexyl)-fluorene (29).**



A mixture of potassium carbonate (0.20 g, 0.001 mol), palladium acetate (0.01 g, 4.4 x 10<sup>-4</sup> mol), PCy<sub>3</sub>·HBF<sub>4</sub> (0.02 g, 5.4 x 10<sup>-5</sup> mol), pivalic acid (0.03 g, 2.9 x 10<sup>-4</sup> mol), 2,7-dibromo-(9,9-dihexyl)-fluorene (**28**) (0.50 g, 0.001 mol) and 2,2-bithiophene (**4**) (0.40 g, 0.002 mol) in DMF (4 cm<sup>3</sup>) was degassed with N<sub>2</sub> for 15 minutes and then heated at 100 °C for 3 h. The mixture was allowed to cool to RT, then poured into water (100 cm<sup>3</sup>). The crude product was extracted into dichloromethane (2 x 50 cm<sup>3</sup>) and the combined organic extracts washed with brine (100 cm<sup>3</sup>), dried (MgSO<sub>4</sub>), filtered and

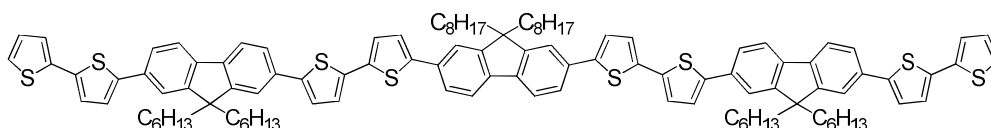
concentrated under reduced pressure. Purification of the crude product was carried out *via* column chromatography [silica gel, dichloromethane: hexane, 2 : 3] and recrystallisation from ethanol to yield the desired product as a yellow solid (0.60 g, 45%).

Melting point /°C: 170.

<sup>1</sup>H NMR (CDCl<sub>3</sub>) δ<sub>H</sub>: 0.75 (6H, t, *J* = 7.8 Hz), 1.01-1.21 (16H, m), 1.98 (4H, t), 7.05 (2H, dd, *J* = 3.6, 8.8 Hz), 7.18 (2H, d, *J* = 3.6 Hz), 7.22-7.24 (4H, m), 7.29 (2H, d, *J* = 3.6 Hz), 7.55 (2H, d, *J* = 5.3 Hz), 7.60 (2H, dd, *J* = 1.6, 7.8 Hz), 7.69 (2H, d, *J* = 7.8 Hz).

MS m/z (EI): 540, 560, 592, 650, 662 (M<sup>+</sup>, M 100).

**5',5'''-(9,9-Dioctyl)-fluoren-2,7-yl)-bis-{5-[7-(2,2'-bithiophen-5-yl)-(9,9-dihexyl)-fluoren-2-yl]-2,2'-bithiophene} (30).**



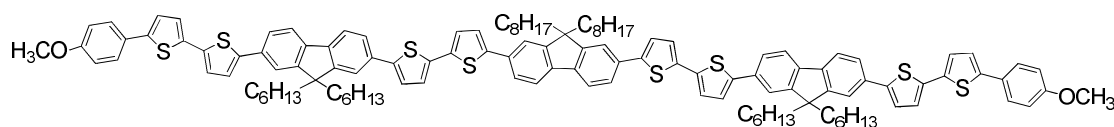
A mixture of potassium carbonate (0.03 g, 2.1 x 10<sup>-4</sup> mol), palladium acetate (0.01 g, 4.4 x 10<sup>-4</sup> mol), PCy<sub>3</sub>·HBF<sub>4</sub> (0.01 g, 2.7 x 10<sup>-5</sup> mol), pivalic acid (0.01 g, 9.7 x 10<sup>-5</sup> mol), *bis*-2,7-(2,2'-bithiophen-5-yl)-(9,9-dihexyl)-fluorene (**29**) (0.60 g, 9.7 x 10<sup>-5</sup> mol) and 2,7-dibromo-(9,9-dioctyl)-fluorene (**25**) (0.10 g, 1.8 x 10<sup>-4</sup> mol) in DMF (2 cm<sup>3</sup>) was degassed with N<sub>2</sub> for 15 minutes and then heated at 100 °C for 3 h. The mixture was allowed to cool to RT, then poured into water (100 cm<sup>3</sup>). The crude product was extracted into dichloromethane (3 x 50 cm<sup>3</sup>) and the combined organic extracts washed with brine (100 cm<sup>3</sup>), dried (MgSO<sub>4</sub>), filtered and concentrated under reduced pressure. Purification of the crude product was carried out *via* column chromatography [silica gel, dichloromethane: hexane, 1 : 4] to yield the desired product as an orange solid (0.22 g, 73%).

Melting point /°C: 229.

<sup>1</sup>H NMR (CDCl<sub>3</sub>) δ<sub>H</sub>: 0.77-0.80 (18H, m), 1.07-1.16 (56H, m), 2.05-2.10 (12H, m), 7.04 (2H, dd, *J* = 3.8, 8.6 Hz), 7.18 (2H, d, *J* = 3.6 Hz), 7.23-7.25 (6H, m), 7.31 (6H, dd, *J* = 3.6, 8.5 Hz), 7.55-7.62 (14H, m), 7.67 (6H, d, *J* = 7.8 Hz).

MS m/z (EI): 1710, 1711 ( $M^+$ , M 100).

**5',5'''-(9,9-Dioctyl-9-fluoren-2,7-yl)-bis-(5-(9,9-dihexyl-7-(5'-(4-methoxyphenyl)-[2,2'-bithiophen]-5-yl)-9-fluoren-2-yl)-2,2'-bithiophene) (32).**



A mixture of potassium carbonate (0.05 g, 0.00021 mol), palladium acetate (0.01 g,  $4.4 \times 10^{-4}$  mol),  $PCy_3 \cdot HBF_4$  (0.01 g,  $2.7 \times 10^{-5}$  mol), pivalic acid (0.01 g,  $9.7 \times 10^{-5}$  mol), 5',5'''-(9,9-Dioctyl)-fluoren-2,7-yl)-bis-{5-[7-(2,2'-bithiophen-5-yl)-(9,9-dihexyl)-fluoren-2-yl]-2,2'-bithiophene} (**30**) (0.40 g,  $2.3 \times 10^{-4}$  mol) and 1-bromo-4-methoxybenzene (**31**) (0.22 g, 0.001 mol) in DMF ( $3 \text{ cm}^3$ ) was degassed with  $N_2$  for 15 minutes and then heated at 100 °C for 3 h. The mixture was allowed to cool to RT, then poured into water ( $200 \text{ cm}^3$ ). The crude product was extracted into dichloromethane ( $2 \times 100 \text{ cm}^3$ ) and the combined organic extracts washed with brine ( $100 \text{ cm}^3$ ), dried ( $MgSO_4$ ), filtered and concentrated under reduced pressure. Purification of the crude product was carried out *via* column chromatography [silica gel, dichloromethane: hexane, 1 : 1] to yield the desired product as an orange solid (0.37 g, 84%).

Transition temp. /°C: Tg 50 Cr 210 N 295 I.

$^1H$  NMR ( $CDCl_3$ )  $\delta_H$ : 0.78-0.82 (18H, m), 1.04-1.14 (56H, m), 2.04-2.10 (12H, m), 3.85 (6H, s), 6.09 (4H, d,  $J = 3.0$  Hz), 7.12 (2H, d,  $J = 3.4$  Hz), 7.18 (2H, d,  $J = 3.6$  Hz), 7.26 (2H, m), 7.35 (6H, dd,  $J = 3.6, 8.4$  Hz), 7.57 (20H, m), 7.70 (6H, d,  $J = 7.8$  Hz).

$^{13}C$  NMR ( $CDCl_3$ ): 14.0, 25.5, 25.6, 29.2, 29.6, 29.8, 31.4, 40.0, 59.0, 94.0, 114.0, 121.0, 122.0, 124.0, 126.9, 129.0, 132.0, 134.0, 139.0, 141.0, 146.0, 150.0, 161.0.

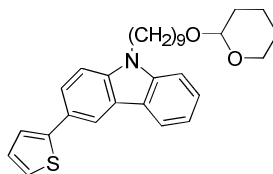
MS m/z (EI): 874, 992, 1096, 1200, 1282, 1392, 1534, 1696, 1779, 1867, 1922, 1923 ( $M^+$ , M 100).

Combustion analysis:

Expected: C 77.99%, H 7.02%, S 13.33%.

Obtained: C 77.88%, H 6.93%, S 13.27%.

**9-{9-[(Tetrahydro-2-pyran-2-yl)oxy]nonyl}-3-(thiophen-2-yl)carbazole (33).**

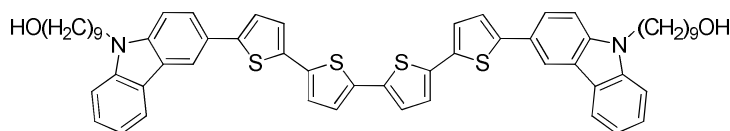


A mixture of 3-bromo-9-{9-[(tetrahydro-2-pyran-2-yl)oxy]nonyl}carbazole (**20**) (2.00 g, 0.004 mol), tributyl(thiophen-2-yl)stannane (**17**) (2.40 g, 0.006 mol) in DMF (25 cm<sup>3</sup>) was stirred and degassed with N<sub>2</sub> for 20 minutes. Palladium acetate (0.20 g, 0.001 mol) and triphenylphosphine (0.30 g, 0.001 mmol) were added and the resultant mixture heated at 100 °C overnight. The mixture was allowed to cool to RT, then poured into water (100 cm<sup>3</sup>). The crude product was extracted into dichloromethane (3 x 50 cm<sup>3</sup>) and the combined organic extracts washed with brine (100 cm<sup>3</sup>), dried (MgSO<sub>4</sub>), filtered and concentrated under reduced pressure. Purification of the crude product was carried out *via* column chromatography [silica gel, ethyl acetate: hexane 1 : 1] to yield the desired product as a colourless liquid (1.71 g, 85%).

<sup>1</sup>H NMR (CDCl<sub>3</sub>) δ<sub>H</sub>: 1.34-1.26 (12H, m), 1.82 (4H, quint, *J* = 7.3 Hz), 3.36 (2H, m), 3.47 (2H, m), 3.70 (2H, m), 3.80 (2H, m), 4.29 (2H, t, *J* = 7.3 Hz), 4.56 (1H, t, *J* = 7.3 Hz), 7.10 (1H, dd, *J* = 3.2, 8.1 Hz), 7.21 (1H, m), 7.24 (1H, d, *J* = 1.2 Hz), 7.33 (1H, dd, *J* = 1.8, 7.6 Hz), 7.37-7.40 (2H, m), 7.46-7.48 (1H, m), 7.73 (1H, dd, *J* = 1.8, 7.6 Hz), 8.14 (1H, d, *J* = 7.3 Hz), 8.31 (1H, d, *J* = 2.2 Hz).

MS (m/z) (EI): 360, 365, 390, 405, 460, 475 (M<sup>+</sup>, M 100).

**5,5'''-bis-[(9-Hydroxynonyl)-carbazol-3-yl]-2,2':5',2'':5'',2'''-quaterthiophene (34).**



5,5'''-bis-[(9-{9-[(tetrahydro-2-pyran-2-yl)oxy]nonyl}-carbazol-3-yl)]-2,2':5',2'':5'',2'''-quaterthiophene (**21**) (0.20 g, 1.7 x 10<sup>-4</sup> mol) and *p*-toluenesulfonic acid monohydrate (0.10 g, 5.2 x 10<sup>-4</sup> mol) were dissolved in DCM (10 cm<sup>3</sup>). The reaction mixture was stirred at RT until the TLC analysis showed the complete conversion, then poured into water (100 cm<sup>3</sup>). The crude product was extracted into dichloromethane (3 x 50 cm<sup>3</sup>) and the combined organic extracts washed with brine (100 cm<sup>3</sup>), dried (MgSO<sub>4</sub>), filtered and concentrated under reduced pressure. Purification of the crude product was carried

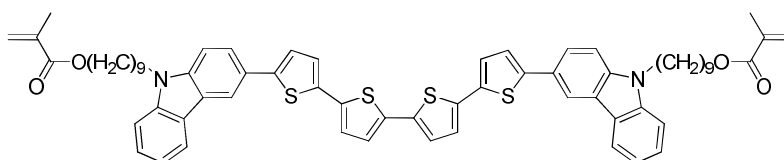
out *via* column chromatography [silica gel, ethyl acetate: hexane, 1 : 1] to yield the desired product (0.13 g, 81%).

Melting point /°C: 235.

<sup>1</sup>H NMR ((CD<sub>3</sub>)<sub>2</sub>SO) δ<sub>H</sub>: 1.26-1.37 (20H, m), 1.53 (4H, quint, *J* = 7.2 Hz), 1.81 (4H, quint, *J* = 7.3 Hz), 4.24 (4H, t, *J* = 8.3 Hz), 4.41 (4H, t, *J* = 8.1 Hz), 7.20 (2H, t, *J* = 6.8 Hz), 7.35 (4H, d, *J* = 3.6 Hz), 7.40 (2H, d, *J* = 3.8 Hz), 7.48 (2H, t, *J* = 6.8 Hz), 7.55 (2H, d, *J* = 8.6 Hz), 7.65 (4H, m), 7.81 (2H, dd, *J* = 1.8, 8.5 Hz), 8.25 (2H, d, *J* = 7.7 Hz), 8.50 (2H, d, *J* = 1.8 Hz).

MS m/z (EI): 402, 719, 944 (M<sup>+</sup>, M 100).

**5,5'''-bis-[9-(Methylacryloyl)nonyl]-carbazol-3-yl]-2,2':5',2'':5'',2'''-quaterthiophene (35).**



Methacryloyl chloride (0.05 g, 9.5 x 10<sup>-4</sup> mol) was added dropwise to a stirred solution of 5,5'''-bis-[9-(9-hydroxynonyl)carbazol-3-yl]-2,2':5',2'':5'',2'''-quaterthiophene (**34**) (0.10 g, 1.4 x 10<sup>-4</sup> mol) and triethylamine (3 cm<sup>3</sup>, 0.02 mol) in DCM (20 cm<sup>3</sup>) at 0 °C. The resultant mixture was stirred and allowed to reach RT overnight. The reaction mixture was then quenched by the addition of methanol (10 cm<sup>3</sup>) in order to remove the excess methacryloyl chloride. After 1 h, the clear solution was poured into saturated solution of sodium bicarbonate (NaHCO<sub>3</sub>) in water (100 cm<sup>3</sup>). The crude product was extracted into dichloromethane (2 x 50 cm<sup>3</sup>) and the combined organic extracts washed with brine (50 cm<sup>3</sup>), dried (MgSO<sub>4</sub>), filtered and concentrated under reduced pressure. Purification was carried out *via* column chromatography [silica gel, dichloromethane: hexane, 3 : 2] to yield the desired product as an orange solid (0.06 g, 60%).

Transition temp. /°C: Cr 164 N 178 I.

<sup>1</sup>H NMR (CDCl<sub>3</sub>) δ<sub>H</sub>: 1.28-1.47 (20H, m), 1.85 (4H, quint, *J* = 7.1 Hz), 1.94 (4H, quint, *J* = 7.3 Hz), 2.01 (6H, s), 3.41 (4H, t, *J* = 7.5 Hz), 4.14 (4H, t, *J* = 8.1 Hz), 5.55 (2H, m), 6.36 (2H, s), 7.20 (2H, t, *J* = 6.8 Hz), 7.35 (4H, d, *J* = 3.6 Hz), 7.41 (2H, d, *J* = 3.8 Hz), 7.48 (2H, t, *J* = 6.8 Hz), 7.55 (2H, d, *J* = 8.6 Hz), 7.65 (4H, m), 7.80 (2H, dd, *J* = 1.8, 8.5 Hz), 8.25 (2H, d, *J* = 7.7 Hz), 8.50 (2H, d, *J* = 1.8 Hz).

$^{13}\text{C}$  NMR ( $\text{CDCl}_3$ ): 19.8, 23.2, 25.9, 27.1, 28.9, 30.9, 42.2, 62.3, 98.8, 109.5, 118.0, 119.4, 121.9, 123.2, 123.6, 123.5, 123.9, 126.4, 129.0, 129.2, 135.2, 137.4, 134.0, 141.5, 167.4.

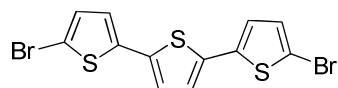
MS  $m/z$  (EI): 886, 890, 920, 960, 975, 990, 1080 ( $\text{M}^+$ ,  $\text{M}$  100).

Combustion analysis:

Expected: C 73.30%, H 6.34%, N 2.59%, S 11.86%.

Obtained: C 73.18%, H 6.21%, N 2.54%, S 11.68%.

### 5,5''-Dibromo-2,2':5',2''-terthiophene (**36**).



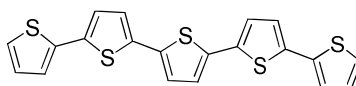
*N*-bromosuccinimide (1.77 g, 0.01 mol) was added slowly (over a period of 3 hours) to a mixture of 2,2':5',2''-terthiophene (**12**) (1.00 g, 0.004 mol) in dichloromethane (15  $\text{cm}^3$ ) and silica gel (1 g) was added to the resultant solution. Once the addition was complete, the reaction mixture was stirred at room temperature for 2 hours in the dark. The precipitate formed was filtered off and washed with dichloromethane (100  $\text{cm}^3$ ). The filtrate was washed with sodium metabisulphite solution (2 x 50  $\text{cm}^3$ ) and water (100  $\text{cm}^3$ ), dried ( $\text{MgSO}_4$ ), filtered and concentrated under reduced pressure. The crude product was purified further by recrystallisation from ethanol to yield the desired product as a dark yellow powder (1.10 g, 67%).

Melting point  $^{\circ}\text{C}$ : 150-153.

$^1\text{H}$  NMR ( $\text{CDCl}_3$ )  $\delta_{\text{H}}$ : 6.90 (2H, d,  $J = 4.1$  Hz), 6.97 (2H, d,  $J = 4.4$  Hz), 7.01 (2H, s).

MS  $m/z$  (EI): 405 ( $\text{M}^+$ ,  $\text{M}$  100).

### 2,2':5',2'':5''',2''':5''''-Quinquethiophene (**37**).

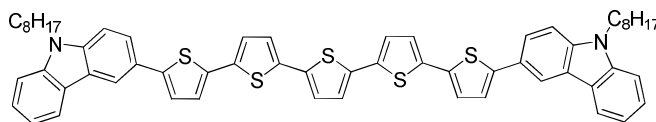


A mixture of 5,5''-dibromo-2,2':5',2''-terthiophene (**36**) (1.00 g, 0.002 mol) tributyl (thiophen-2-yl)stannane (**17**) (2.02 g, 0.005 mol) in DMF (10  $\text{cm}^3$ ) was stirred and degassed with  $\text{N}_2$  for 20 minutes. Palladium acetate (0.01 g,  $4.4 \times 10^{-4}$  mol) and

DABCO (0.01 g,  $1.5 \times 10^{-4}$  mol) was added and the resulting reaction mixture was heated at 100 °C overnight. The reaction mixture was cooled to RT. The mixture was poured into methanol giving a suspension of an orange powder. After filtering off the crude product, it was washed twice with warm water and washed with dichloromethane (200 cm<sup>3</sup>). The residue was first dissolved in warm dioxane and then precipitated with a small volume of water, affording the desired product as an orange powder (0.43 g, 42%).<sup>29</sup>

Melting point /°C: 253.

**5,5''''-bis-(9-Octyl-9-carbazol-3-yl)-2,2':5',2'':5'',2''':5''',2''''-quinquethiophene (38).**



A mixture of potassium carbonate (0.05 g,  $3.6 \times 10^{-4}$  mol), palladium acetate (0.01 g,  $4.4 \times 10^{-4}$  mol), PCy<sub>3</sub>·HBF<sub>4</sub> (0.01 g,  $2.7 \times 10^{-5}$  mol), pivalic acid (0.01 g,  $9.7 \times 10^{-5}$  mol), 2,2':5',2'':5'',2''':5''',2''''-quinquethiophene (**37**) (0.15 g, 0.0002 mol) and 3-bromo-*N*-octyl-carbazole (**3**) (0.2 g, 0.0005 mol) in DMF (2 cm<sup>3</sup>) was degassed with N<sub>2</sub> for 15 minutes. The reaction mixture was then heated at 100 °C for 16 h. The reaction mixture allowed to cool to RT, poured into water (50 cm<sup>3</sup>) and the crude product extracted into dichloromethane (2 x 50 cm<sup>3</sup>). The combined organic extracts were washed with brine (50 cm<sup>3</sup>), dried (MgSO<sub>4</sub>), filtered and concentrated under reduced pressure. Purification of the crude product was carried out *via* column chromatography [silica gel, dichloromethane: hexane, 4 : 1] to yield the desired product as a red solid (0.07 g, 36%).

Transition temp. /°C: T<sub>g</sub> 119 Cr 170 N 215 I.

<sup>1</sup>H NMR (CDCl<sub>3</sub>) δ<sub>H</sub>: 0.84 (6H, t, *J* = 6.9 Hz), 1.22-1.24 (20H, m), 1.88 (4H, quint, *J* = 7.3 Hz), 4.29 (4H, t, *J* = 7.8 Hz), 7.31-7.39 (10H, m), 7.40-7.50 (4H, m), 7.73 (2H, d, *J* = 8.1 Hz), 7.90 (2H, s), 8.09 (2H, d, *J* = 7.6 Hz), 8.19 (2H, d, *J* = 8.1 Hz), 8.30 (2H, d, *J* = 4.5 Hz).

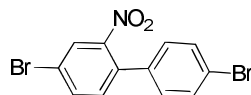
MS *m/z* (EI): 306, 379, 444, 556, 689, 966 (M<sup>+</sup>, M 100).

Combustion analysis:

Expected: C 74.49%, H 6.04%, N 2.90%, S 16.57%.

Obtained: C 74.35%, H 5.96%, N 2.99%, S 16.47%.

#### 4,4'-Dibromo-2-nitrobiphenyl (**40**).



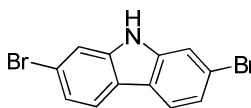
A mixture of fuming nitric acid (100%, 20 cm<sup>3</sup>) and water (2 cm<sup>3</sup>) was added dropwise to a solution of 4,4'-dibromobiphenyl (**39**) (5.00 g, 0.016 mol) in glacial acetic acid (60 cm<sup>3</sup>) at 100 °C. Once addition was complete the mixture was heated at 100 °C for 1 h, then allowed to cool to RT. The yellow precipitate formed was filtered off and washed with copious amounts of water. The dried crude product was purified by recrystallisation from ethanol to yield the desired product as a pale yellow crystalline solid (4.22 g, 83%).

Melting Point /°C: 125-126 (Lit. 125-127).<sup>7</sup>

<sup>1</sup>H NMR (CDCl<sub>3</sub>) δ<sub>H</sub>: 7.16 (2H, d, *J* = 4.7 Hz), 7.31 (1H, d, *J* = 8.2 Hz), 7.57 (2H, d, *J* = 4.7 Hz), 7.76 (1H, dd, *J* = 2.2, 8.4 Hz), 8.03 (1H, d, *J* = 2.2 Hz),

MS *m/z* (EI): 355 (M<sup>+</sup>, M 100).

#### 2,7-Dibromocarbazole (**41**).



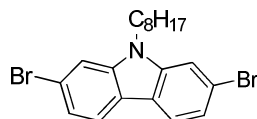
A solution of 4,4'-dibromo-2-nitrobiphenyl (**40**) (3.00 g, 0.008 mol), triphenylphosphine (5.50 g, 0.021 mol) and DMAc (20 cm<sup>3</sup>) was heated under reflux for 20 h. The crude product was extracted into dichloromethane (3 x 50 cm<sup>3</sup>) and the combined organic extracts washed with brine (2 x 50 cm<sup>3</sup>), dried (MgSO<sub>4</sub>), filtered and evaporated down under reduced pressure. Purified *via* column chromatography [silica gel, ethyl acetate: hexane, 2 : 3] to yield the desired product as a pale yellow solid (2.40 g, 88%).

Melting Point /°C: 238-239 (Lit. 236-238).<sup>17</sup>

$^1\text{H}$  NMR ( $\text{CDCl}_3$ )  $\delta_{\text{H}}$ : 7.35 (2H, dd,  $J = 8.2, 1.6$  Hz), 7.57 (2H, d,  $J = 1.6$  Hz), 7.87 (2H, d,  $J = 8.2$  Hz), 8.13 (1H, s).

MS  $m/z$  (EI): 323 ( $\text{M}^+$ ,  $M$  100).

### 2,7-Dibromo-9-octylcarbazole (42).



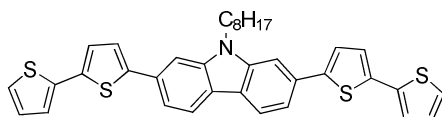
NaH (0.18 g, 60% dispersion in mineral oil, 0.007 mol) was added in small portions to a solution of 2,7-dibromocarbazole (**41**) (2.00 g, 0.006 mol) in DMF (25  $\text{cm}^3$ ). The resultant mixture was stirred for 30 minutes, 1-bromooctane (1.31 g, 0.007 mol) was added and the resulting mixture was heated at 50  $^\circ\text{C}$  for 3 h, then stirred overnight at RT. The reaction mixture allowed to cool to RT, poured into water (200  $\text{cm}^3$ ) and the crude product extracted into dichloromethane (3 x 50  $\text{cm}^3$ ). The combined organic extracts were washed with brine (2 x 50  $\text{cm}^3$ ), dried ( $\text{MgSO}_4$ ), filtered and concentrated under reduced pressure. Purification of the crude product was carried out *via* column chromatography [silica gel, dichloromethane: hexane, 1 : 4] to yield the desired product as a white crystalline solid (2.33 g, 87%).

Melting Point  $^\circ\text{C}$ : 67-68 (Lit. 66-67)<sup>18</sup>.

$^1\text{H}$  NMR ( $\text{CDCl}_3$ )  $\delta_{\text{H}}$ : 0.87 (3H, t,  $J = 7.0$  Hz), 1.22-1.38 (10H, m), 1.82 (2H, quint), 4.20 (2H, t,  $J = 7.2$  Hz), 7.34 (2H, dd,  $J = 1.4, 8.2$  Hz), 7.57 (2H, d,  $J = 1.5$  Hz), 7.89 (2H, d,  $J = 8.4$  Hz).

MS  $m/z$  (EI): 435, 437 ( $\text{M}^+$ ,  $M$  100).

### 2,7-bis-(2,2'-Bithiophen-5-yl)-9-octylcarbazole (43).



A mixture of potassium carbonate (1.17 g, 0.008 mol), palladium acetate (0.05 g, 2.2 x 10<sup>-4</sup> mol), pivalic acid (0.01 g, 9.7 x 10<sup>-5</sup> mol), 2,7-dibromo-9-octylcarbazole (**42**) (1.50 g, 0.003 mol) and 2,2-bithiophene (**4**) (3.00 g, 0.018 mol) in DMF (15  $\text{cm}^3$ ) was

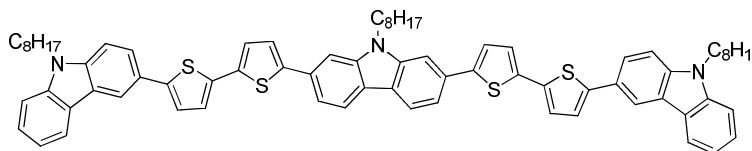
degassed with N<sub>2</sub> for 15 minutes. The reaction mixture was then heated at 100 °C for 3 h. The reaction mixture was then heated at 100 °C for 3 h. The reaction mixture allowed to cool to RT, poured into water (200 cm<sup>3</sup>) and the crude product extracted into dichloromethane (2 x 150 cm<sup>3</sup>). The combined organic extracts were washed with brine (200 cm<sup>3</sup>), dried (MgSO<sub>4</sub>), filtered and concentrated under reduced pressure. Purification of the crude product was carried out *via* column chromatography [silica gel, dichloromethane: hexane, 1 : 1] and recrystallisation from toluene to yield the desired product as a yellow solid (1.54 g, 73%).

Melting Point /°C: >300.

<sup>1</sup>H NMR (CDCl<sub>3</sub>) δ<sub>H</sub>: 0.87 (3H, t, *J* = 6.9 Hz), 1.19-1.38 (10H, m), 1.85 (2H, quint, *J* = 7.2 Hz), 4.29 (2H, t, *J* = 7.0 Hz), 6.98 (2H, dd, *J* = 2.8, 6.1 Hz), 7.13 (2H, d, *J* = 3.8 Hz), 7.16 (4H, d, *J* = 4.4 Hz), 7.26 (2H, d, *J* = 3.6 Hz), 7.42 (2H, dd, *J* = 1.4, 8.7 Hz), 7.50 (2H, d, *J* = 1.0 Hz), 7.97 (2H, d, *J* = 8.1 Hz).

MS *m/z* (EI): 413, 549, 579, 607 (M<sup>+</sup>, M 100).

**3,3'-[(5',5'''-(9-Octyl-9-carbazole-2,7-diyl)-bis-([2,2'-bithiophene]-5',5-diyl)]-bis-(9-octyl-9-carbazole) (44).**



A mixture of potassium carbonate (0.15 g, 0.001 mol), palladium acetate (0.01 g, 4.4 x 10<sup>-4</sup> mol), pivalic acid (0.01 g, 9.7 x 10<sup>-5</sup> mol), 2,7-bis-(2,2'-bithiophen-5-yl)-9-octylcarbazole (0.25 g, 0.0004 mol) (**43**) and 3-bromo-*N*-octyl-carbazole (**3**) (0.36 g, 0.001 mol) in DMF (3 cm<sup>3</sup>) was degassed with N<sub>2</sub> for 15 minutes. The reaction mixture was then heated at 100 °C for 3 h. The reaction mixture allowed to cool to RT, poured into water (200 cm<sup>3</sup>) and the crude product extracted into dichloromethane (2 x 100 cm<sup>3</sup>). The combined organic extracts were washed with brine (100 cm<sup>3</sup>), dried (MgSO<sub>4</sub>), filtered and concentrated under reduced pressure. Purification of the crude product was carried out *via* column chromatography [silica gel, dichloromethane: hexane, 1 : 1] and then recrystallised from the DCM/DMSO followed by DCM/MeOH to yield the desired product as a yellow solid (0.22 g, 48%).

Transition temp. /°C: Cr 160 SmC 180 I.

$^1\text{H}$  NMR ( $\text{CDCl}_3$ )  $\delta_{\text{H}}$ : 0.84 (9H, t,  $J = 6.9$  Hz), 1.24-1.68 (24H, m), 1.88 (6H, quint,  $J = 7.3$  Hz), 1.92 (6H, m), 4.28 (6H, t,  $J = 7.1$  Hz), 7.24 (4H, d,  $J = 4.7$  Hz), 7.25 (2H, d,  $J = 3.8$  Hz), 7.29 (2H, d,  $J = 3.8$  Hz), 7.32 (4H, d,  $J = 2.0$  Hz), 7.37 (2H, d,  $J = 8.1$  Hz), 7.46 (4H, m), 7.47 (2H, dd,  $J = 1.6, 8.8$  Hz), 7.69 (2H, dd,  $J = 1.8, 8.7$  Hz), 7.98 (2H, d,  $J = 8.1$  Hz), 8.14 (2H, d,  $J = 7.7$  Hz), 8.30 (2H, d,  $J = 1.6$  Hz).

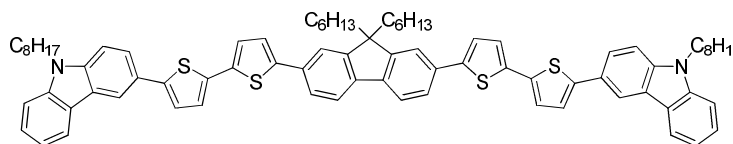
MS  $m/z$  (EI): 1161 ( $\text{M}^+$ ,  $\text{M} 100$ ), 1062.

Combustion analysis:

Expected: C 78.51%, H 6.85%, N 3.61%, S 11.03%.

Obtained: C 78.39%, H 6.96%, N 3.72%, S 11.07%.

***bis*-2,7-{5-[9-(Octyl)-carbazol-3-yl]-2,2'-bithiophen-5'-yl}-(9,9-dihexyl)-fluorene (45).**



A mixture of potassium carbonate (0.17 g, 0.001 mol), palladium acetate (0.01 g,  $4.4 \times 10^{-4}$  mol), pivalic acid (0.01 g,  $9.7 \times 10^{-5}$  mol), *bis*-2,7-(2,2'-bithiophen-5-yl)-(9,9-dihexyl)-fluorene (**29**) (0.25 g,  $4.7 \times 10^{-4}$  mol) and 3-bromo-*N*-octyl-carbazole (**3**) (0.4 g, 0.001 mol) in DMF (3  $\text{cm}^3$ ) was degassed with  $\text{N}_2$  for 15 minutes. The reaction mixture was then heated at 100  $^\circ\text{C}$  for 3 h. The reaction mixture allowed to cool to RT, poured into water (200  $\text{cm}^3$ ) and the crude product extracted into dichloromethane (2 x 100  $\text{cm}^3$ ). The combined organic extracts were washed with brine (100  $\text{cm}^3$ ), dried ( $\text{MgSO}_4$ ), filtered and concentrated under reduced pressure. Purification of the crude product was carried out *via* column chromatography [silica gel, dichloromethane: hexane, 2 : 3] and recrystallisation from DCM/DMSO followed by DCM/MeOH to yield the desired product as a yellow solid (0.26 g, 58%).

Transition temp.  $^\circ\text{C}$ : Tg 26 Cr 109 N 125 I.

$^1\text{H}$  NMR ( $\text{CDCl}_3$ )  $\delta_{\text{H}}$ : 0.86 (6H, t,  $J = 6.7$  Hz), 0.90-1.05 (6H, m), 1.08-1.12 (16H, m), 1.14-1.38 (20H, m), 1.89 (4H, quint,  $J = 7.2$  Hz), 2.06 (4H, m), 4.31 (4H, t,  $J = 7.3$  Hz), 7.22 (4H, d,  $J = 7.3$  Hz), 7.24 (2H, d,  $J = 7.3$  Hz), 7.29 (2H, d,  $J = 3.8$  Hz), 7.34 (2H, d,  $J = 3.8$  Hz), 7.41 (4H, d,  $J = 2.0$  Hz), 7.48 (2H, d,  $J = 8.1$  Hz), 7.57 (2H, s), 7.63 (2H,

dd,  $J = 2.4, 7.7$  Hz), 7.71 (2H, d,  $J = 4.0$  Hz), 7.73 (2H, dd,  $J = 1.8, 9.5$  Hz), 8.14 (2H, d,  $J = 7.5$  Hz), 8.30 (2H, d,  $J = 1.8$  Hz).

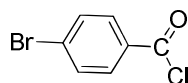
MS  $m/z$  (EI): 998, 1020, 1069, 1120, 1140, 1190, 1216 ( $M^+$ ,  $M - 100$ ).

Combustion analysis:

Expected: C 79.88%, H 7.28%, N 2.30%, S 10.53%.

Obtained: C 79.77%, H 7.01%, N 2.25%, S 10.68%.

#### 4-Bromobenzoyl chloride (**47**).

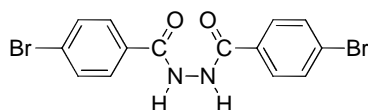


Thionyl chloride (7.25 cm<sup>3</sup>, 0.010 mol) was added dropwise to slurry of 4-bromobenzoic acid (5.00 g, 0.025 mol) in toluene (50 cm<sup>3</sup>). The resultant reaction mixture was heated at 70 °C for 2 h and then evaporated down under vacuum. Hexane (20 cm<sup>3</sup>) was added to the reaction mixture and concentrated again under reduced pressure to afford a yellow-brown solid, which was used without further purification (5.20 g, 95%).<sup>30</sup>

Melting point /°C: 36-41.

<sup>1</sup>H NMR (CDCl<sub>3</sub>)  $\delta_H$ : 7.68 (2H, d,  $J = 8.5$  Hz), 8.00 (2H, d,  $J = 8.5$  Hz).

#### 4-Bromo-*N'*-(4-bromobenzoyl)benzohydrazide (**48**).

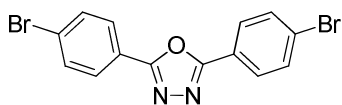


A solution of 4-bromobenzohydrazide (**46**) (2.40 g, 0.011 mol), 4-bromobenzoyl chloride (**47**) (2.45 g, 0.011) and pyridine (50 cm<sup>3</sup>) was heated under reflux for 6 h. After cooling to RT, the reaction mixture was poured into ethanol (200 cm<sup>3</sup>). The mixture was cooled to 0 °C and the resultant precipitate filtered off and dried to afford title compound as white crystals (3.75 g, 85%).

Melting point /°C: >300.<sup>10</sup>

$^1\text{H NMR}$  ( $(\text{CD}_3)_2\text{SO}$ )  $\delta_{\text{H}}$ : 7.66 (4H, d,  $J = 8.5$  Hz), 7.78 (4H, d,  $J = 8.5$  Hz), 10.57 (2H, s).

**2,5-bis-(4-Bromophenyl)-1,3,4-oxadiazole (49).**



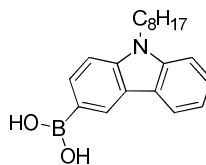
A solution of 4-bromo- $N'$ -(4-bromobenzoyl)benzohydrazide (**48**) (3.50 g, 0.009 mol) in thionyl chloride ( $10 \text{ cm}^3$ ) was heated under reflux for 7 h. Excess thionyl chloride was distilled off and then the residue was slowly poured into water ( $100 \text{ cm}^3$ ). The resultant precipitate was filtered off and then purified *via* stirring in hexane before being filtered off and dried to yield the desired product as white crystals (3.26 g, 97%).

Melting point  $^{\circ}\text{C}$ : 258.<sup>19</sup>

$^1\text{H NMR}$  ( $\text{CDCl}_3$ )  $\delta_{\text{H}}$ : 7.69 (4H, d,  $J = 8.7$  Hz), 8.01 (4H, d,  $J = 8.7$  Hz).

MS  $m/z$  (EI): 157, 164, 166, 183 (M 100), 185, 190, 219, 243, 246, 299, 323, 377 ( $\text{M}^+$ ).

**9-(Octyl)-carbazol-3-boronic acid (50).**



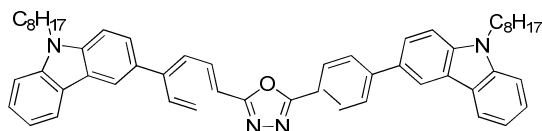
A solution of 3-bromo- $N$ -octyl-carbazole (**3**) (0.75 g, 0.002 mol) in THF ( $10 \text{ cm}^3$ ) was added dropwise to a cooled ( $0 \text{ }^{\circ}\text{C}$ ) solution of 2.5 M  $n$ -BuLi (in hexanes) ( $1.5 \text{ cm}^3$ , 0.003 mol) and hexane ( $50 \text{ cm}^3$ ) at  $0 \text{ }^{\circ}\text{C}$  over a period of 10 minutes. The resultant reaction mixture was stirred for 1 h at  $0 \text{ }^{\circ}\text{C}$ . Triisopropyl borate ( $1.20 \text{ cm}^3$ , 0.006 mol) was added dropwise to the reaction mixture, which was then allowed to warm to RT and stirred for an additional 40 minutes before being quenched with 20% hydrochloric acid ( $20 \text{ cm}^3$ ) and then stirred vigorously for 1 h. The crude product was extracted into dichloromethane ( $3 \times 50 \text{ cm}^3$ ). The combined organic extracts were washed with brine ( $2 \times 100 \text{ cm}^3$ ), dried ( $\text{MgSO}_4$ ), filtered and concentrated under reduced pressure. Purification of the crude product was carried out *via* stirring in hexane ( $100 \text{ cm}^3$ ) to yield the desired product as a white crystalline solid (0.64 g, 63%).

Melting point  $^{\circ}\text{C}$ : 173-175.

$^1\text{H}$  NMR ( $(\text{CD}_3)_2\text{SO}$ )  $\delta_{\text{H}}$ : 0.79 (3H, t,  $J = 7.3$  Hz), 1.20-1.30 (10H, m), 1.75 (2H, quint,  $J = 7.1$  Hz), 4.37 (2H, t,  $J = 6.9$  Hz), 7.20 (1H, t,  $J = 7.3$  Hz), 7.44 (1H, t,  $J = 7.1$  Hz), 7.54 (1H, d,  $J = 8.3$  Hz), 7.57 (1H, d,  $J = 8.3$  Hz), 7.90 (1H, dd,  $J = 1.0, 7.8$  Hz), 8.10 (1H, d,  $J = 7.5$  Hz), 8.59 (1H, s).

MS  $m/z$  (EI): 322, 323 ( $\text{M}^+$ ,  $\text{M} - 100$ ).

**2,5-bis-{4-[9-(Octyl)-carbazol-3-yl]phenyl}-1,3,4-oxadiazole (51).**



A mixture of palladium acetate (0.01 g,  $4.4 \times 10^{-4}$  mol), 2,5-bis-(4-bromophenyl)-1,3,4-oxadiazole (**49**), (0.20 g,  $5.2 \times 10^{-4}$  mol), 9-(octyl)-carbazol-3-boronic acid (**50**) (0.42 g, 0.001 mol), potassium carbonate (0.35 g, 0.002 mol) and water ( $5 \text{ cm}^3$ ) in DMF ( $5 \text{ cm}^3$ ) was heated under reflux at  $80^\circ\text{C}$  overnight. The reaction mixture allowed to cool to RT, poured into water ( $200 \text{ cm}^3$ ) and the crude product extracted into dichloromethane ( $2 \times 150 \text{ cm}^3$ ). The combined organic extracts were washed with brine ( $200 \text{ cm}^3$ ), dried ( $\text{MgSO}_4$ ), filtered and concentrated under reduced pressure. Purification of the crude product was carried out *via* column chromatography [silica gel, dichloromethane:hexane, 1 : 4] and recrystallisation first from a mixture of DCM/DMSO and then from a mixture of DCM/MeOH to yield the desired product as a white solid (0.38 g, 95%).

Melting point  $^{\circ}\text{C}$ : 195-204.

$^1\text{H}$  NMR ( $\text{CDCl}_3$ )  $\delta_{\text{H}}$ : 0.85 (6H, t,  $J = 6.1$  Hz), 1.25-1.42 (20H, m), 1.91 (4H, quint,  $J = 7.2$  Hz), 4.34 (4H, t,  $J = 7.2$  Hz), 7.28 (2H, d,  $J = 7.7$  Hz), 7.43 (2H, d,  $J = 8.0$  Hz), 7.50-7.52 (4H, m), 7.80 (2H, dd,  $J = 1.6, 8.7$  Hz), 7.92 (4H, d,  $J = 8.7$  Hz), 8.17 (2H, d,  $J = 7.5$  Hz), 8.28 (4H, d,  $J = 8.7$  Hz), 8.40 (2H, d,  $J = 1.3$  Hz).

$^{13}\text{C}$  NMR ( $\text{CDCl}_3$ ): 14.0, 22.6, 27.3, 28.9, 29.1, 29.3, 31.7, 43.2, 108.9, 109.0, 118.9, 119.1, 120.4, 121.7, 122.8, 123.4, 125.0, 126.0, 127.3, 127.5, 130.6, 140.4, 140.9, 145.3, 164.6.

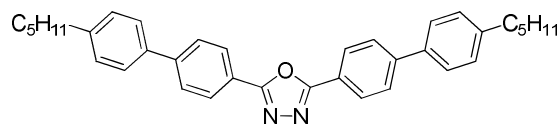
MS  $m/z$  (EI): 335, 439, 505, 551, 573, 628, 677, 776 ( $\text{M}^+$ ,  $\text{M} - 100$ ).

Combustion analysis:

Expected: C 83.47%, H 7.26%, N 7.21%.

Obtained: C 83.34%, H 6.35%, N 7.15%.

**2,5-bis-(4'-Pentyl-[1,1'-biphenyl]-4-yl)-1,3,4-oxadiazole (53).**



A mixture of palladium acetate (0.01 g,  $4.4 \times 10^{-5}$  mol), 2,5-bis-(4-bromophenyl)-1,3,4-oxadiazole (**49**) (0.3 g,  $7.8 \times 10^{-4}$  mol), 4-pentylphenyl boronic acid (**52**) (0.38 g, 0.002 mol), potassium carbonate (0.54 g, 0.004 mol) and water (6 cm<sup>3</sup>) in DMF (8 cm<sup>3</sup>) was heated under reflux at 80 °C overnight. The reaction mixture allowed to cool to RT, poured into water (200 cm<sup>3</sup>) and the crude product extracted into dichloromethane (2 x 100 cm<sup>3</sup>). The combined organic extracts were washed with brine (150 cm<sup>3</sup>), dried (MgSO<sub>4</sub>), filtered and concentrated under reduced pressure. Purification of the crude product was carried out *via* column chromatography [silica gel, ethyl acetate: dichloromethane, 1 : 4] and recrystallisation from DCM/MeOH to yield the desired product as a white solid (0.24 g, 60%).

Transition temp. /°C: Cr 225 SmA 247 I.

<sup>1</sup>H NMR (CDCl<sub>3</sub>) δ<sub>H</sub>: 0.92 (6H, t, *J* = 5.6 Hz), 1.36-1.38 (8H, m), 1.68 (4H, quint, *J* = 7.8 Hz), 2.68 (4H, t, *J* = 7.8 Hz), 7.30 (4H, d, *J* = 8.3 Hz), 7.60 (4H, d, *J* = 8.3 Hz), 7.77 (4H, d, *J* = 4.7 Hz), 7.83 (4H, d, *J* = 4.7 Hz).

<sup>13</sup>C NMR (CDCl<sub>3</sub>): 14.0, 22.5, 31.1, 31.5, 35.6, 122.4, 126.9, 127.3, 127.4, 129.0, 137.0, 143.2, 144.4, 164.5.

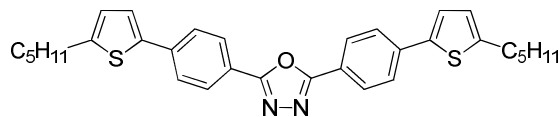
MS *m/z* (EI): 365, 457, 513, 515 (M<sup>+</sup>, M 100).

Combustion analysis:

Expected: C 84.01%, H 7.44%, N 5.44%.

Obtained: C 84.21%, H 7.68%, N 5.26%.

**2,5-bis-[4-(5-Pentylthiophen-2-yl)phenyl]-1,3,4-oxadiazole (55).**



A mixture of palladium acetate (0.01 g,  $4.4 \times 10^{-5}$  mol), 5-bis-(4-bromophenyl)-1,3,4-oxadiazole (**49**) (0.30 g,  $7.8 \times 10^{-4}$  mol), 2-pentylthiophene (**54**) (0.38 g, 0.002 mol), potassium carbonate (0.30 g, 0.002 mol),  $\text{PCy}_3 \cdot \text{HBF}_4$  (0.01 g,  $2.7 \times 10^{-5}$  mol) and pivalic acid (0.02 g,  $1.9 \times 10^{-4}$  mol) in DMF ( $5 \text{ cm}^3$ ) was degassed with  $\text{N}_2$  for 15 minutes at RT and then heated at  $100^\circ\text{C}$  for 16 h. The reaction mixture allowed to cool to RT, poured into water ( $200 \text{ cm}^3$ ) and the crude product extracted into dichloromethane ( $2 \times 100 \text{ cm}^3$ ). The combined organic extracts were washed with brine ( $150 \text{ cm}^3$ ), dried ( $\text{MgSO}_4$ ), filtered and concentrated under reduced pressure. Purification of the crude product was carried out *via* column chromatography [silica gel, dichloromethane: hexane, 1 : 4] and recrystallisation from DCM/MeOH to yield the desired product as a white solid (0.27 g, 65%).

Transition temp.  $^\circ\text{C}$ : Cr 175 N 199 I.

$^1\text{H}$  NMR ( $\text{CDCl}_3$ )  $\delta_{\text{H}}$ : 0.92 (6H, t,  $J = 5.9$  Hz), 1.34-1.42 (8H, m), 1.72 (4H, quint,  $J = 7.8$  Hz), 2.84 (4H, t,  $J = 7.8$  Hz), 6.80 (2H, d,  $J = 3.6$  Hz), 7.26 (2H, d,  $J = 3.6$  Hz), 7.72 (4H, d,  $J = 8.7$  Hz), 8.12 (4H, d,  $J = 8.7$  Hz).

$^{13}\text{C}$  NMR ( $\text{CDCl}_3$ ): 14.0, 22.4, 30.3, 31.2, 31.3, 122.0, 124.1, 125.5, 125.6, 127.4, 137.9, 140.0, 147.5, 164.3.

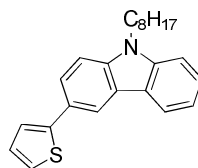
MS  $m/z$  (EI): 365, 469, 493, 527 ( $\text{M}^+$ , M 100).

Combustion analysis:

Expected: C 72.96%, H 6.51%, N 5.32%, S 12.17%.

Obtained: C 72.85%, H 6.67%, N 5.49%, S 12.28%.

### 9-Octyl-3-(thiophen-2-yl)carbazole (**56**).

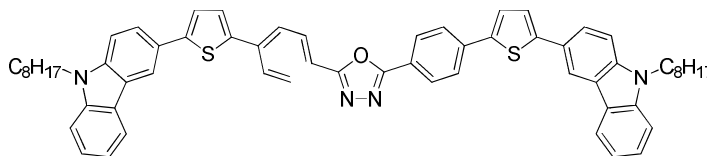


A mixture of Tetrakis(triphenylphosphine)palladium(0) (0.01 g,  $8.6 \times 10^{-6}$  mol), 3-bromo-*N*-octyl-carbazole (**3**) (2.00 g, 0.005 mol), thiophen-2-boronic acid (**9**) (0.85 g, 0.007 mol), sodium carbonate (1.78 g, 0.017 mol) and water (20 cm<sup>3</sup>) in DME (20 cm<sup>3</sup>) was heated under reflux at 80 °C overnight. The reaction mixture allowed to cool to RT, poured into water (200 cm<sup>3</sup>) and the crude product extracted into dichloromethane (2 x 100 cm<sup>3</sup>). The combined organic extracts were washed with brine (150 cm<sup>3</sup>), dried (MgSO<sub>4</sub>), filtered and concentrated under reduced pressure. Purification of the crude product was carried out *via* column chromatography [silica gel, dichloromethane: hexane, 1 : 1] to yield the desired product as a colourless liquid (1.90 g, 94%).

<sup>1</sup>H NMR (CDCl<sub>3</sub>)  $\delta$ <sub>H</sub>: 0.85 (3H, t,  $J = 7.1$  Hz), 1.25-1.42 (10H, m), 1.87 (2H, quint,  $J = 7.3$  Hz), 4.29 (2H, t,  $J = 7.3$  Hz), 7.10 (1H, dd,  $J = 3.3, 7.9$  Hz), 7.25 (2H, m), 7.33 (1H, dd,  $J = 1.2, 3.0$  Hz), 7.37 (1H, d,  $J = 5.1$  Hz), 7.40 (1H, d,  $J = 4.7$  Hz), 7.46 (1H, dd,  $J = 1.1, 8.1$  Hz), 7.73 (1H, dd,  $J = 1.8, 4.7$  Hz), 8.13 (1H, d,  $J = 7.7$  Hz), 8.32 (1H, d,  $J = 3.8$  Hz).

MS  $m/z$  (EI): 41, 131, 151, 180, 189, 217, 228, 248, 262 (M 100), 263, 264, 275, 289, 316, 359, 361 (M<sup>+</sup>).

### 2,5-bis-{4-[5-(9-Octyl-carbazol-3-yl)thiophen-2-yl]phenyl}-1,3,4-oxadiazole (**57**).



A mixture of palladium acetate (0.01 g,  $4.4 \times 10^{-5}$  mol), 5-bis-(4-bromophenyl)-1,3,4-oxadiazole (**49**) (0.20 g,  $5.2 \times 10^{-4}$  mol), 9-octyl-3-(thiophen-2-yl)carbazole (**56**) (0.47 g, 0.001 mol), potassium carbonate (0.20 g, 0.001 mol), PCy<sub>3</sub>·HBF<sub>4</sub> (0.01 g,  $2.7 \times 10^{-5}$  mol) and pivalic acid (0.02 g,  $1.8 \times 10^{-4}$  mol) in NMP (5 cm<sup>3</sup>) was degassed with N<sub>2</sub> for 15 minutes at RT and then heated at 100 °C for 16 h. The reaction mixture allowed to cool to RT, poured into water (100 cm<sup>3</sup>) and the crude product extracted into

dichloromethane (2 x 100 cm<sup>3</sup>). The combined organic extracts were washed with brine (100 cm<sup>3</sup>), dried (MgSO<sub>4</sub>), filtered and concentrated under reduced pressure. Purification of the crude product was carried out *via* column chromatography [silica gel, ethyl acetate: dichloromethane, 1 : 4] and recrystallisation from DCM/EtOH to yield the desired product as a yellow solid (0.25 g, 51%).

Transition temp. /°C: T<sub>g</sub> 80 Cr 171 I.

<sup>1</sup>H NMR (CDCl<sub>3</sub>) δ<sub>H</sub>: 0.86 (6H, t, *J* = 7.7 Hz), 1.20-1.45 (20H, m), 1.90 (4H, quint, *J* = 6.1 Hz), 4.30 (4H, t, *J* = 7.3 Hz), 7.29 (4H, d, *J* = 7.1 Hz), 7.37 (2H, d, *J* = 3.6 Hz), 7.43 (4H, d, *J* = 8.3 Hz), 7.46 (2H, d, *J* = 3.6 Hz), 7.75 (2H, dd, *J* = 1.8, 8.2 Hz), 7.81 (4H, d, *J* = 7.3 Hz), 8.17 (6H, d, *J* = 8.5 Hz), 8.37 (2H, d, *J* = 1.4 Hz).

<sup>13</sup>C NMR (CDCl<sub>3</sub>): 14.0, 22.5, 27.2, 28.9, 19.1, 29.3, 31.7, 40.9, 43.0, 108.8, 117.0, 119.0, 120.4, 121.7, 122.7, 122.8, 123.1, 123.6, 124.9, 125.0, 125.1, 125.9, 127.0, 137.2, 140.0, 140.2, 140.8, 146.4, 164.0.

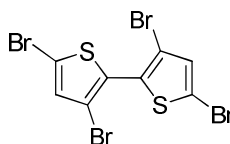
MS *m/z* (EI): 337, 373, 379, 436, 551, 581, 841, 863, 941 (M<sup>+</sup>, M 100).

Combustion analysis:

Expected: C 79.11%, H 6.42%, N 5.95%, S 6.81%.

Obtained: C 79.22%, H 5.77%, N 6.24%, S 6.67%.

### 3,3',5,5'-Tetrabromo-2,2'-bithiophene (58).



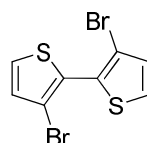
A solution of bromine (26.84 g, 0.168 mol) in chloroform (50 cm<sup>3</sup>) was added dropwise to a cooled solution of 2,2'-bithiophene (**4**) (7.00 g, 0.042 mol), glacial acetic acid (56 cm<sup>3</sup>) and chloroform (50 cm<sup>3</sup>) at 0 °C over a period of 2 h. The resultant reaction mixture was stirred at RT overnight and then heated under reflux for a further 24 h. The reaction mixture was allowed to cool to RT, poured into aqueous KOH solution (50 cm<sup>3</sup>) and the crude product was extracted into dichloromethane (2 x 100 cm<sup>3</sup>). A solution of Na<sub>2</sub>S<sub>2</sub>O<sub>3</sub> (20%, 100 cm<sup>3</sup>) was added to the combined organic layers and the resultant mixture stirred until the solution was colourless in order to remove the excess

bromine. The organic layer was then washed with water (3 x 100 cm<sup>3</sup>), dried (MgSO<sub>4</sub>), filtered and concentrated under reduced pressure. Recrystallization from ethanol afforded the desired product as off-white crystals (19.96 g, 98%).<sup>11</sup>

Melting point /°C: 140.

<sup>1</sup>H NMR (CDCl<sub>3</sub>) δ<sub>H</sub>: 7.02 (2H, s).

### 3,3'-Dibromo-2,2'-bithiophene (**59**).

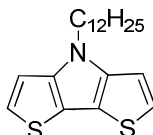


Zinc dust (14.14 g, 0.216 mol) was added in small portions over 5 minutes to a solution under reflux of 3,3',5,5'-tetrabromo-2,2'-bithiophene (**58**) (18.80 g, 0.039 mol), *n*-propanol (400 cm<sup>3</sup>), water (10 cm<sup>3</sup>) and glacial acetic acid (20 cm<sup>3</sup>). After heating under reflux overnight, the mixture was cooled to RT, filtered and then the solvent was removed. The resultant residue was dissolved in diethyl ether (100 cm<sup>3</sup>). The resultant solution was washed with water (50 cm<sup>3</sup>), saturated sodium bicarbonate (50 cm<sup>3</sup>) solution and brine (50 cm<sup>3</sup>), dried (MgSO<sub>4</sub>), filtered and concentrated under reduced pressure. The crude product was recrystallised from hexane to give the desired product as light yellow crystals (10.60 g, 83%).<sup>20</sup>

Melting point /°C: 98-101.

<sup>1</sup>H NMR (CDCl<sub>3</sub>) δ<sub>H</sub>: 7.05 (2H, d, *J* = 5.3 Hz), 7.39 (2H, d, *J* = 5.3 Hz).

### 4-Dodecyl-4-dithieno[3,2-b:2',3'-d]pyrrole (**60**).



A solution of, 3,3'-dibromo-2,2'-bithiophene (**59**) (3.00 g, 0.009 mol), sodium *t*-butoxide (2.36 g, 0.024 mol), BINAP (0.60 g, 9.6 x 10<sup>-4</sup> mol) and toluene (50 cm<sup>3</sup>) was degassed with N<sub>2</sub> for 10 minutes. Tris(dibenzylideneacetone)dipalladium(0) (0.2 g, 2.5 x 10<sup>-4</sup> mol) and dodecylamine (2.00 g, 0.010 mol) were added and the resultant reaction mixture was heated under reflux overnight. The reaction mixture allowed to

cool to RT, poured into water (50 cm<sup>3</sup>) and the crude product extracted into diethyl ether (2 x 80 cm<sup>3</sup>). The combined organic extracts were washed with brine (2 x 50 cm<sup>3</sup>), dried (MgSO<sub>4</sub>), filtered and concentrated under reduced pressure. The crude product was purified by column chromatography (Silica gel, hexane: dichloromethane, 1 : 3) to give the desired product as a light yellow oil (3.95 g, 95%).<sup>11</sup>

<sup>1</sup>H NMR (CDCl<sub>3</sub>) δ<sub>H</sub>: 0.87 (3H, t, *J* = 6.7 Hz), 1.22-1.30 (18H, m), 1.87 (2H, quint, *J* = 7.1 Hz), 4.19 (2H, t, *J* = 7.1 Hz), 7.00 (2H, d, *J* = 5.3 Hz), 7.12 (2H, d, *J* = 5.3 Hz).

MS m/z (EI): 41, 43, 69, 81, 100, 121 134, 152, 178, 179, 192 (M 100), 194, 206, 234, 248, 290, 304, 318, 347 (M<sup>+</sup>).

### 2,6-Dibromo-4-dodecyldithieno[3,2-b:2',3'-d]pyrrole (61).



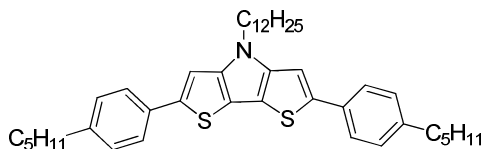
A solution of *N*-bromosuccinimide (2.99 g, 0.017 mol) in DMF (50 cm<sup>3</sup>) was added dropwise to a solution of 4-dodecyl-4-dithieno[3,2-b:2',3'-d]pyrrole (**60**) (2.80 g, 0.008 mol) and chloroform (100 cm<sup>3</sup>) at 0 °C. After stirring for 1 hr at 0 °C (at which point no starting material was observed by TLC), water (50 cm<sup>3</sup>) was added to the reaction mixture and the crude product extracted into chloroform (100 cm<sup>3</sup>). The combined organic extracts were washed with brine (2 x 100 cm<sup>3</sup>), dried (MgSO<sub>4</sub>), filtered and concentrated under reduced pressure. The crude product was purified by column chromatography [silica gel, hexane] to give the desired product as a light yellow solid (3.10 g, 74%).<sup>20</sup>

Melting point /°C: 55.

<sup>1</sup>H NMR (CDCl<sub>3</sub>) δ<sub>H</sub>: 0.89 (3H, t, *J* = 6.1 Hz), 1.23-1.31 (18H, m), 1.81 (2H, quint, *J* = 6.9 Hz), 4.08 (2H, t, *J* = 6.9 Hz), 7.02 (2H, s).

MS m/z (EI): 505 (M<sup>+</sup>, M 100).

#### 4-Dodecyl-2,6-bis-(4-pentylphenyl)-4-dithieno[3,2-b:2',3'-d]pyrrole (**62**).



A mixture of tetrakis(triphenylphosphine)palladium(0) (0.01 g,  $8.6 \times 10^{-6}$  mol), 2,6-dibromo-4-dodecyldithieno[3,2-b:2',3'-d]pyrrole (**61**) (0.20 g, 0.0004 mol), 4-pentylphenyl-boronic acid (**52**) (0.21 g, 0.001 mol), sodium carbonate (0.12 g, 0.001 mol) and water (5 cm<sup>3</sup>) in DME (5 cm<sup>3</sup>) was heated under reflux at 80 °C overnight. The reaction mixture allowed to cool to RT, poured into water (150 cm<sup>3</sup>) and the crude product extracted into dichloromethane (2 x 100 cm<sup>3</sup>). The combined organic extracts were washed with brine (2 x 100 cm<sup>3</sup>), dried (MgSO<sub>4</sub>), filtered and concentrated under reduced pressure. Purification of the crude product was carried out *via* column chromatography [silica gel, dichloromethane: hexane, 2 : 3] to yield the desired product as a yellow solid (0.16 g, 70%).

Melting point /°C: 98.

<sup>1</sup>H NMR (CDCl<sub>3</sub>) δ<sub>H</sub>: 0.84-0.90 (9H, m), 1.23-1.36 (26H, m), 1.63 (4H, quint, *J* = 6.1 Hz), 1.90 (2H, quint, *J* = 7.7 Hz), 2.62 (4H, t, *J* = 7.5 Hz), 4.20 (2H, t, *J* = 6.6 Hz), 7.18 (4H, d, *J* = 8.3 Hz), 7.20 (2H, s), 7.56 (4H, d, *J* = 8.3 Hz).

<sup>13</sup>C NMR (CDCl<sub>3</sub>): 14.0, 22.6, 27.0, 29.2, 29.3, 31.8, 35.6, 47.3, 66.4, 106.0, 114.0, 125.2, 128.9, 135.9, 137.1, 141.0, 142.0, 161.0.

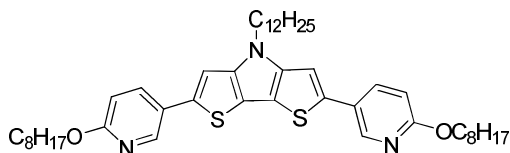
MS *m/z* (EI): 637, 639 (M<sup>+</sup>, M 100).

Combustion analysis:

Expected: C 78.82%, H 8.98%, N 2.19%, S 10.02%.

Obtained: C 78.63%, H 9.07%, N 2.24%, S 9.87%.

**4-Dodecyl-2,6-bis-[6-(octyloxy)pyridin-3-yl]-4-dithieno[3,2-b:2',3'-d]pyrrole (64).**



A mixture of tetrakis(triphenylphosphine)palladium(0) (0.01 g,  $8.6 \times 10^{-6}$  mol), 2,6-dibromo-4-dodecyldithieno[3,2-b:2',3'-d]pyrrole (**61**) (0.25 g, 0.0005 mol), 6-(octyloxy)pyridin-3-boronic acid (**63**) (0.37 g, 0.001 mol), sodium carbonate (0.16 g, 0.001 mol) and water (5 cm<sup>3</sup>) in DME (10 cm<sup>3</sup>) was heated under reflux at 80 °C overnight. The reaction mixture allowed to cool to RT, poured into water (200 cm<sup>3</sup>) and the crude product extracted into dichloromethane (2 x 200 cm<sup>3</sup>). The combined organic extracts were washed with brine (2 x 200 cm<sup>3</sup>), dried (MgSO<sub>4</sub>), filtered and concentrated under reduced pressure. Purification of the crude product was carried out *via* column chromatography [silica gel, dichloromethane: hexane, 2 : 3] to yield the desired product as a yellow solid (0.25 g, 71%).

Melting point /°C: 81.

<sup>1</sup>H NMR (CDCl<sub>3</sub>) δ<sub>H</sub>: 0.84-0.90 (9H, m), 1.23-1.31 (38H, m), 1.79 (4H, quint, *J* = 6.9 Hz), 1.90 (2H, quint, *J* = 6.9 Hz), 4.20 (2H, t, *J* = 6.9 Hz), 4.32 (4H, t, *J* = 6.8 Hz), 6.78 (2H, d, *J* = 6.5 Hz), 7.11 (2H, s), 7.80 (2H, dd, *J* = 2.4, 8.0 Hz), 8.43 (2H, d, *J* = 1.8 Hz).

<sup>13</sup>C NMR (CDCl<sub>3</sub>): 14.0, 22.6, 29.0, 29.2, 29.4, 29.5, 31.8, 47.3, 66.4, 106.5, 111.0, 114.0, 125.0, 135.9, 138.2, 143.4, 144.7, 163.2.

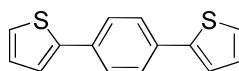
MS *m/z* (EI): 459, 551, 757 (M<sup>+</sup>, M 100).

Combustion analysis:

Expected: C 72.87%, H 8.91%, N 5.54%, S 8.46%.

Obtained: C 72.63%, H 9.10%, N 5.60%, S 8.34%.

### 1,4-Di-(thiophen-2-yl)benzene (**66**).



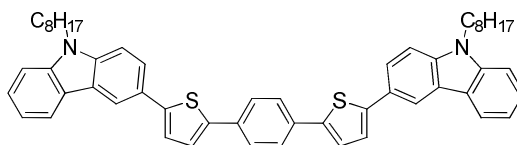
A mixture of Pd(PPh<sub>3</sub>)<sub>4</sub> (0.30 g, 2.6 x 10<sup>-4</sup> mol), 1,4-dibromobenzene (**65**) (3.00 g, 0.127 mol), thiophene-2-boronic acid (**9**) (4.07 g, 0.031 mol), sodium carbonate (4.00 g, 0.037 mol) and water (15 cm<sup>3</sup>) in DME (40 cm<sup>3</sup>) was heated under reflux at 80 °C overnight. The reaction mixture allowed to cool to RT, poured into water (200 cm<sup>3</sup>) and the crude product extracted into dichloromethane (2 x 200 cm<sup>3</sup>). The combined organic extracts were washed with brine (2 x 200 cm<sup>3</sup>), dried (MgSO<sub>4</sub>), filtered and concentrated under reduced pressure. Purification of the crude product was carried out *via* column chromatography [silica gel, dichloromethane: hexane, 1 : 4] to yield the desired product as a yellow solid (2.97 g, 97%).<sup>26</sup>

Melting point /°C: 206.

<sup>1</sup>H NMR (CDCl<sub>3</sub>) δ<sub>H</sub>: 7.08 (2H, dd, *J* = 1.1, 3.6 Hz), 7.29 (2H, dd, *J* = 1.0, 3.8 Hz), 7.34 (2H, dd, *J* = 1.0, 3.8 Hz), 7.61 (4H, s).

MS *m/z* (EI): 45, 51, 69, 115, 121, 122, 139, 152, 165, 197, 208, 240, 242 (M<sup>+</sup>, M 100).

### 1,4-bis-[5-(9-Octyl-carbazol-3-yl)thiophen-2-yl]benzene (**67**).



A mixture of palladium acetate (0.01 g, 2.5 x 10<sup>-5</sup> mol), 1,4-di(thiophen-2-yl)benzene (**66**) (0.50 g, 0.002 mol), 3-bromo-*N*-octyl-carbazole (**3**) (1.85 g, 0.005 mol), potassium carbonate (0.82 g, 0.006 mol), PCy<sub>3</sub>·HBF<sub>4</sub> (0.03 g, 8.5 x 10<sup>-5</sup> mol) and pivalic acid (0.02 g, 1.9 x 10<sup>-4</sup> mol) in NMP (10 cm<sup>3</sup>) was degassed with N<sub>2</sub> for 15 minutes at RT. The reaction mixture was then heated at 100 °C for 16 h. The reaction mixture allowed to cool to RT, poured into water (200 cm<sup>3</sup>) and the crude product extracted into dichloromethane (2 x 200 cm<sup>3</sup>). The combined organic extracts were washed with brine (2 x 200 cm<sup>3</sup>), dried (MgSO<sub>4</sub>), filtered and concentrated under reduced pressure. Purification of the crude product was carried out *via* column chromatography [silica gel, dichloromethane: hexane, 1 : 1] and recrystallisation from DCM/EtOH to yield the desired product as a yellow solid (0.25 g, 51%).

Melting point /°C: 179-215.

<sup>1</sup>H NMR (CDCl<sub>3</sub>) δ<sub>H</sub>: 0.86 (6H, t, *J* = 6.3 Hz), 1.19-1.41 (20H, m), 1.89 (4H, quint, *J* = 6.7 Hz), 4.31 (4H, t, *J* = 7.1 Hz), 7.28 (2H, s), 7.35 (4H, dd, *J* = 3.8, 6.3 Hz), 7.41 (4H, d, *J* = 8.5 Hz), 7.49 (2H, d, *J* = 8.1 Hz), 7.70 (4H, s), 7.78 (2H, dd, *J* = 1.6, 6.7 Hz), 8.15 (2H, d, *J* = 7.7 Hz), 8.35 (2H, d, *J* = 1.5 Hz).

<sup>13</sup>C NMR (CDCl<sub>3</sub>): 13.9, 22.5, 27.3, 29.0, 29.1, 29.4, 31.8, 43.2, 108.0, 109.0, 117.0, 119.0, 120.6, 122.0, 123.0, 124.0, 125.6, 125.8, 126.0, 133.0, 140.2, 141.0, 141.9, 145.0.

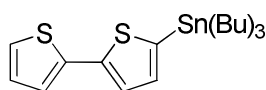
MS *m/z* (EI): 551, 796 (M<sup>+</sup>, M 100).

Combustion analysis:

Expected: C 81.36%, H 7.08%, N 3.51%, S 8.04%.

Obtained: C 81.55%, H 7.23%, N 3.55%, S 8.11%.

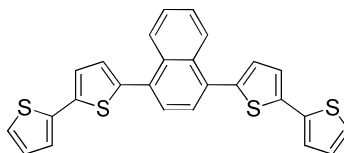
### 2,2'-Bithiophen-5-tributylstannane (69).



A solution of 2.5 M *n*-BuLi (in hexanes) (18.50 cm<sup>3</sup>) was added slowly to a solution of 2,2'-bithiophene (**4**) (7.00 g, 0.0421 mol) in THF (dry, 200 cm<sup>3</sup>) at -78 °C. After stirring for 1 h at -78 °C, tri *n*-butyltin chloride (15.10 g, 0.046 mol) was added slowly and the temperature of the reaction mixture was allowed to reach RT after completion of the addition. The reaction mixture was stirred overnight. Water (150 cm<sup>3</sup>) was added and the product extracted into diethyl ether (300 cm<sup>3</sup>). The combined ethereal extracts were dried (MgSO<sub>4</sub>), filtered and concentrated under reduced pressure to yield the desired product as a pale brown oil, which was not purified further (17.15 g, 89%).

<sup>1</sup>H NMR (CDCl<sub>3</sub>) δ<sub>H</sub>: 0.84-0.96 (9H, m), 1.07-1.12 (6H, m), 1.29-1.38 (6H, m), 1.53-1.61 (6H, m), 6.98-7.01 (1H, m), 7.05 (1H, t, *J* = 3.4 Hz), 7.20-7.16 (2H, m), 7.29 (1H, d, *J* = 2.6 Hz).

### 1,4-Di-(2,2'-bithiophen-5-yl)-naphthalene (70).



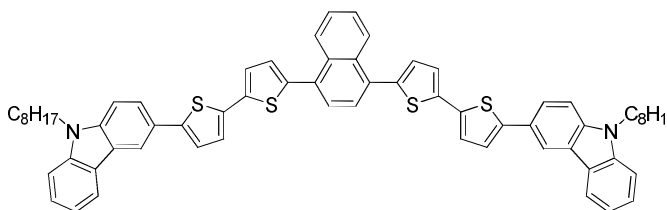
A solution of 1,4-dibromonaphthalene (**68**) (1.00 g, 0.003 mol), 2,2'-bithiophen-5-tributylstannane (**69**) (4.30 g, 0.001 mol), palladium acetate (0.03 g,  $1.3 \times 10^{-4}$  mol) and triphenylphosphine (0.50 g, 0.002 mol) in DMF (15 cm<sup>3</sup>) was degassed with N<sub>2</sub> for 15 minutes and then heated at 100 °C for 18 h. The reaction mixture allowed to cool to RT, poured into water (200 cm<sup>3</sup>) and the crude product extracted into dichloromethane (2 x 150 cm<sup>3</sup>). The combined organic extracts were washed with brine (2 x 200 cm<sup>3</sup>), dried (MgSO<sub>4</sub>), filtered and concentrated under reduced pressure. Purification of the crude product was carried out *via* column chromatography [silica gel, dichloromethane: hexane, 1 : 4] to give the desired product as a yellow solid (0.45 g, 28%).<sup>21</sup>

Melting point /°C: 177.

<sup>1</sup>H NMR (CDCl<sub>3</sub>) δ<sub>H</sub>: 7.06 (2H, dd, *J* = 3.6, 4.2 Hz), 7.19 (2H, d, *J* = 3.0 Hz), 7.24-7.26 (6H, m), 7.55 (2H, dd, *J* = 3.2, 7.3 Hz), 7.61 (2H, s), 8.38 (2H, dd, *J* = 3.2, 7.3 Hz).

MS *m/z* (EI): 456 (M<sup>+</sup>, M 100).

### 1,4-bis-[5'-(9-Octyl-carbazol-3-yl)-(2,2'-bithiophen)-5-yl]naphthalene (71).



A mixture of palladium acetate (0.01 g,  $4.4 \times 10^{-4}$  mol), 1,4-di-(2,2'-bithiophen-5-yl)-naphthalene (**70**) (0.25 g,  $5.2 \times 10^{-4}$  mol), 3-bromo-*N*-octyl-carbazole (**3**) (0.50 g, 0.001 mol), potassium carbonate (0.22 g, 0.001 mol), PCy<sub>3</sub>·HBF<sub>4</sub> (0.01 g,  $2.7 \times 10^{-5}$  mol) and pivalic acid (0.02 g,  $1.8 \times 10^{-4}$  mol) in NMP (5 cm<sup>3</sup>) was degassed with N<sub>2</sub> for 15 minutes at RT and then heated at 100 °C for 16 h. The reaction mixture allowed to cool to RT, poured into water (200 cm<sup>3</sup>) and the crude product extracted into dichloromethane (2 x 100 cm<sup>3</sup>). The combined organic extracts were washed with brine (2 x 100 cm<sup>3</sup>), dried (MgSO<sub>4</sub>), filtered and concentrated under reduced pressure.

Purification of the crude product was carried out *via* column chromatography [silica gel, dichloromethane: hexane, 2 : 3] and recrystallisation from DCM/EtOH to yield the desired product as a yellow solid (0.22 g, 36%).

Transition temp. /°C: Tg 62 Cr 121 I.

<sup>1</sup>H NMR (CDCl<sub>3</sub>) δ<sub>H</sub>: 0.86 (6H, t, *J* = 6.5 Hz), 1.24-1.40 (20H, m), 1.88 (4H, quint, *J* = 7.7 Hz), 4.32 (4H, t, *J* = 7.3 Hz), 7.23-7.25 (6H, d, *J* = 3.2 Hz), 7.31 (4H, dd, *J* = 3.2, 8.1 Hz), 7.42 (4H, d, *J* = 8.3 Hz), 7.48 (2H, d, *J* = 7.7 Hz), 7.58 (2H, dd, *J* = 3.6, 8.1 Hz), 7.65 (2H, s), 7.75 (2H, dd, *J* = 1.6, 9.3 Hz), 8.16 (2H, d, *J* = 7.7 Hz), 8.35 (2H, d, *J* = 1.8 Hz), 8.43 (2H, dd, *J* = 3.2, 8.1 Hz).

<sup>13</sup>C NMR (CDCl<sub>3</sub>): 14.0, 22.6, 27.3, 28.9, 29.1, 29.4, 31.8, 43.2, 108.0, 109.0, 117.6, 119.0, 120.5, 122.6, 122.7, 123.2, 123.5, 123.9, 124.7, 125.2, 126.0, 126.2, 126.6, 127.4, 128.4, 132.1, 129.9, 132.4, 135.0, 138.0, 140.0, 140.9, 144.9.

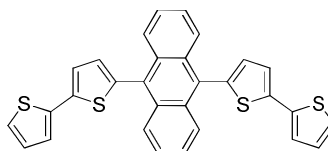
MS *m/z* (EI): 551, 815, 1010 (M<sup>+</sup>, M100).

Combustion analysis:

Expected: C 78.37%, H 6.18%, N 2.77%, S 12.68%.

Obtained: C 78.47%, H 6.36%, N 2.72%, S 12.80%.

### 9,10-Di-(2,2'-bithiophen-5-yl)-anthracene (**73**).



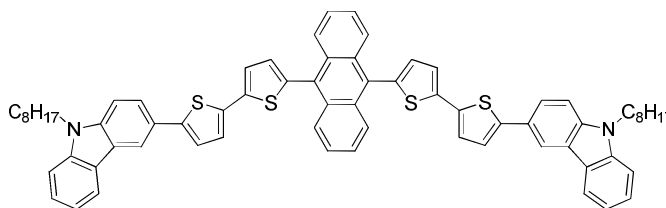
A mixture of palladium acetate (0.02 g, 8.8 x 10<sup>-4</sup> mol), 9,10-dibromoanthracene (**72**) (1.00 g, 0.003 mol), 2,2'-bithiophene (**4**) (2.50 g, 0.015 mol), potassium carbonate (1.25 g, 0.009 mol), PCy<sub>3</sub>·HBF<sub>4</sub> (0.01 g, 2.7 x 10<sup>-5</sup> mol) and pivalic acid (0.02 g, 1.8 x 10<sup>-4</sup> mol) in NMP (10 cm<sup>3</sup>) was degassed with N<sub>2</sub> for 15 minutes at RT and then heated at 100 °C for 18 h. The reaction mixture allowed to cool to RT, poured into water (200 cm<sup>3</sup>) and the crude product extracted into dichloromethane (2 x 150 cm<sup>3</sup>). The combined organic extracts were washed with brine (2 x 150 cm<sup>3</sup>), dried (MgSO<sub>4</sub>), filtered and concentrated under reduced pressure. Purification of the crude product was carried out *via* column chromatography [silica gel, dichloromethane: hexane, 2 : 3] to give the desired product as a yellow solid (1.02 g, 66%).<sup>12</sup>

Melting point /°C: >300.

<sup>1</sup>H NMR (CDCl<sub>3</sub>) δ<sub>H</sub>: 7.07 (2H, dd, *J* = 3.8, 4.4 Hz), 7.11 (2H, d, *J* = 2.6 Hz), 7.27-7.28 (4H, m), 7.39 (2H, d, *J* = 3.4 Hz), 7.45 (4H, dd, *J* = 3.4, 6.7 Hz), 8.02 (4H, dd, *J* = 3.4, 6.5 Hz).

MS *m/z* (EI): 507 (M<sup>+</sup>, M 100).

**9,10-bis-[5'-(9-Octyl-9-carbazol-3-yl)-2,2'-bithiophen-5-yl]-anthracene (74).**



A mixture of palladium acetate (0.01 g, 4.4 x 10<sup>-4</sup> mol), 9,10-di-(2,2'-bithiophen-5-yl)-anthracene (**73**) (0.40 g, 0.00079 mol), 3-bromo-*N*-octyl-carbazole (**3**) (0.70 g, 0.002 mol), potassium carbonate (0.33 g, 0.002 mol), PCy<sub>3</sub>·HBF<sub>4</sub> (0.01 g, 2.7 x 10<sup>-5</sup> mol) and pivalic acid (0.02 g, 1.8 x 10<sup>-4</sup> mol) in NMP (10 cm<sup>3</sup>) was degassed with N<sub>2</sub> for 15 minutes at RT and then heated at 100 °C for 18 h. The reaction mixture allowed to cool to RT, poured into water (200 cm<sup>3</sup>) and the crude product extracted into dichloromethane (2 x 100 cm<sup>3</sup>). The combined organic extracts were washed with brine (2 x 100 cm<sup>3</sup>), dried (MgSO<sub>4</sub>), filtered and concentrated under reduced pressure. Purification of the crude product was carried out *via* column chromatography [silica gel, dichloromethane: hexane, 2 : 3] and recrystallisation from DCM/EtOH to yield the desired product as a yellow solid (0.41 g, 48%).

Melting point /°C: 245.

<sup>1</sup>H NMR (CDCl<sub>3</sub>) δ<sub>H</sub>: 0.87 (6H, t, *J* = 6.5 Hz), 1.20-1.42 (20H, m), 1.89 (4H, quint, *J* = 7.3 Hz), 4.32 (4H, t, *J* = 7.1 Hz), 7.16 (2H, d, *J* = 3.4 Hz), 7.25-7.27 (8H, m), 7.31 (2H, d, *J* = 3.8 Hz), 7.42-7.44 (4H, m), 7.48 (4H, dd, *J* = 3.0, 8.1 Hz), 7.78 (2H, dd, *J* = 1.8, 6.7 Hz), 8.08 (4H, dd, *J* = 3.2, 8.1 Hz), 8.15 (2H, d, *J* = 7.7 Hz), 8.36 (2H, d, *J* = 1.8 Hz).

$^{13}\text{C}$  NMR ( $\text{CDCl}_3$ ): 14.0, 22.6, 27.3, 28.9, 29.2, 29.4, 31.7, 43.2, 108.9, 109.0, 117.6, 119.0, 120.5, 122.6, 122.7, 123.2, 123.3, 123.9, 124.7, 125.2, 125.9, 126.0, 126.2, 126.7, 129.9, 130.4, 131.4, 135.0, 137.3, 139.3, 140.0, 140.9, 144.9.

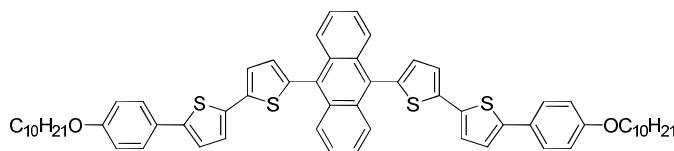
MS  $m/z$  (EI): 551, 815, 859, 1060 ( $\text{M}^+$ ,  $\text{M} - 100$ ).

Combustion analysis:

Expected: C 79.20%, H 6.08%, N 2.64%, S 12.08%.

Obtained: C 79.38%, H 6.24%, N 2.42%, S 12.07%.

**9,10-bis{5'-[4-(Decyloxy)phenyl]-[2,2'-bithiophen]-5-yl}anthracene (76).**



A mixture of palladium acetate (0.01 g,  $4.4 \times 10^{-4}$  mol), 9,10-di[(2,2'-bithiophen)-5-yl]anthracene (**73**) (0.20 g, 0.0004 mol), 1-bromo-4-(decyloxy)benzene (**75**) (0.30 g, 0.0009 mol), potassium carbonate (0.33 g, 0.001 mol),  $\text{PCy}_3 \cdot \text{HBF}_4$  (0.02 g,  $5.4 \times 10^{-5}$  mol) and pivalic acid (0.02 g,  $1.8 \times 10^{-4}$  mol) in NMP (5  $\text{cm}^3$ ) was degassed with  $\text{N}_2$  for 15 minutes at RT and then heated at 100  $^\circ\text{C}$  for 18 h. The reaction mixture allowed to cool to RT, poured into water (200  $\text{cm}^3$ ) and the crude product extracted into dichloromethane (2 x 100  $\text{cm}^3$ ). The combined organic extracts were washed with brine (2 x 100  $\text{cm}^3$ ), dried ( $\text{MgSO}_4$ ), filtered and concentrated under reduced pressure. Purification of the crude product was carried out *via* column chromatography [silica gel, dichloromethane: hexane, 2 : 3] and recrystallisation from DCM/EtOH to yield the desired product as a yellow solid (0.18 g, 47%).

Melting point  $^\circ\text{C}$ : 222.

$^1\text{H}$  NMR ( $\text{CDCl}_3$ )  $\delta_{\text{H}}$ : 0.89 (6H, t,  $J = 6.7$  Hz), 1.20-1.50 (28H, m), 1.80 (4H, quint,  $J = 7.9$  Hz), 4.00 (4H, t,  $J = 6.7$  Hz), 6.94 (4H, d,  $J = 8.1$  Hz), 7.12 (2H, d,  $J = 3.4$  Hz), 7.15 (2H, d,  $J = 3.6$  Hz), 7.21 (2H, d,  $J = 3.8$  Hz), 7.38 (2H, d,  $J = 3.6$  Hz), 7.46 (4H, dd,  $J = 3.2, 6.5$  Hz), 7.57 (4H, d,  $J = 8.7$  Hz), 8.04 (4H, dd,  $J = 3.2, 6.5$  Hz).

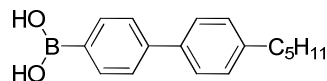
MS  $m/z$  (EI): 551, 815, 970 ( $\text{M}^+$ ,  $\text{M} - 100$ ).

Combustion analysis:

Expected: C 76.66%, H 6.85%, S 13.20%.

Obtained: C 76.40%, H 6.59%, S 12.96%.

#### 4'-Pentyl-1,1'-biphenyl-4-boronic acid (**78**).

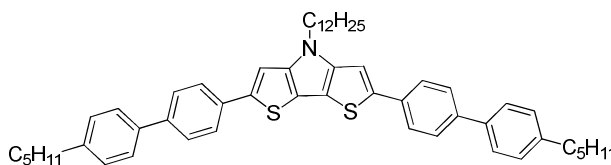


A solution of 2.5 M *n*-BuLi (in hexanes) (15.2 cm<sup>3</sup>, 0.020 mol) was added dropwise to a solution of 4-bromo-4'-pentyl-1,1'-biphenyl (**77**) (5.00 g, 0.016 mol) in THF (100 cm<sup>3</sup>) at -75 °C. The reaction mixture was stirred at this temperature for 1 h and then trimethyl borate (10 cm<sup>3</sup>, 0.066 mol) was added. The reaction mixture was brought to RT and then stirred at this temperature overnight. Aqueous hydrochloric acid (20%, 100 cm<sup>3</sup>) was added and the resultant mixture stirred for a further 2 h. The reaction mixture was extracted with dichloromethane (3 x 100 cm<sup>3</sup>). The combined organic layers were dried (MgSO<sub>4</sub>), filtered and concentrated under reduced pressure. The crude product was washed with hexane, filtered off and then dried to afford the desired product as a white solid (2.12 g, 47%).

Melting point /°C: 154.

<sup>1</sup>H NMR (CDCl<sub>3</sub>) δ<sub>H</sub>: 0.92 (3H, t, *J* = 6.9 Hz), 1.30-1.38 (4H, m), 1.69 (2H quint, *J* = 7.5 Hz), 2.68 (2H, t, *J* = 7.5 Hz), 7.30 (2H, d, *J* = 7.9 Hz), 7.61 (2H, d, *J* = 7.9 Hz), 7.75 (2H, d, *J* = 7.9 Hz), 8.32 (2H, d, *J* = 7.6 Hz).

#### 4-Dodecyl-2,6-bis-(4'-pentyl-1,1'-biphenyl-4-yl)-4-dithieno[3,2-b:2',3'-d]pyrrole (**79**).



A mixture of Tetrakis(triphenylphosphine)palladium(0) (0.01 g, 8.6 x 10<sup>-6</sup> mol), 2,6-dibromo-4-dodecylthieno[3,2-b:2',3'-d]pyrrole (**61**) (0.45 g, 0.001 mol), 4'-pentyl-1,1'-biphenyl-4-boronic acid (**78**) (0.7 g, 0.002 mol), sodium carbonate (0.3 g, 0.003 mol) and water (7 cm<sup>3</sup>) in DME (10 cm<sup>3</sup>) was heated under reflux at 80 °C overnight. The reaction mixture allowed to cool to RT, poured into water (200 cm<sup>3</sup>) and the crude

product extracted into dichloromethane (2 x 100 cm<sup>3</sup>). The combined organic extracts were washed with brine (2 x 100 cm<sup>3</sup>), dried (MgSO<sub>4</sub>), filtered and concentrated under reduced pressure. Purification of the crude product was carried out *via* column chromatography [silica gel, dichloromethane: hexane, 4 : 1] to yield the desired product as an orange solid (0.51 g, 71%).

Transition temp. /°C: Cr 200 N 299 I.

<sup>1</sup>H NMR (CDCl<sub>3</sub>) δ<sub>H</sub>: 0.86 (3H, t, *J* = 7.1 Hz), 0.91 (6H, t, *J* = 6.9 Hz), 1.20-1.40 (26H, m), 1.64 (4H, quint, *J* = 7.5 Hz), 1.92 (2H, quint, *J* = 7.3 Hz), 2.65 (4H, t, *J* = 7.5 Hz), 4.20 (2H, t, *J* = 6.5 Hz), 7.25-7.27 (6H, m), 7.55 (4H, d, *J* = 8.3 Hz), 7.61 (4H, d, *J* = 8.3 Hz), 7.69 (4H, d, *J* = 8.3 Hz).

<sup>13</sup>C NMR (CDCl<sub>3</sub>): 14.0, 22.6, 29.5, 29.6, 31.5, 35.6, 38.7, 47.3, 68.1, 106.7, 114.6, 125.5, 126.8, 127.3, 128.8, 134.3, 137.8, 139.7, 142.2.

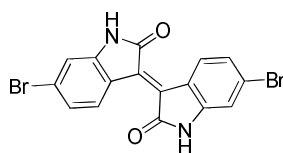
MS *m/z* (EI): 446, 551, 790, 791 (M<sup>+</sup>, M 100).

Combustion analysis:

Expected: C 81.87%, H 8.27%, N 1.77%, S 8.09%.

Obtained: C 81.62%, H 8.46%, N 1.68%, S 7.87%.

### 6,6'-Dibromoisindigo (**82**).



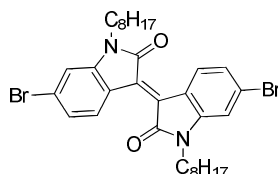
Concentrated hydrochloric acid solution (0.6 cm<sup>3</sup>) was added to a suspension of 6-bromoisatin (**80**) (3.20 g, 0.013 mol) and 6-bromooxindole (**81**) (3.00 g, 0.014 mol) in acetic acid (90 cm<sup>3</sup>) and the resultant reaction heated under reflux for 24 h. The reaction mixture was allowed to cool to RT and resultant solid material filtered off, washed with water, ethanol and ethyl acetate and then dried under vacuum to yield 6,6'-dibromoisindigo as a reddish-purple solid (5.18 g, 95%).<sup>13</sup>

Melting point /°C: >300.

$^1\text{H}$  NMR ( $(\text{CD}_3)_2\text{SO}$ )  $\delta_{\text{H}}$ : 6.98 (2H, d,  $J = 2.0$  Hz), 7.18 (2H, dd,  $J = 1.8, 8.2$  Hz), 8.98 (2H, d,  $J = 8.7$  Hz), 11 (2H, s).

MS  $m/z$  (EI): 315, 320 (M 100), 329, 417 ( $\text{M}^+$ ).

### 6,6'-Dibromo-1,1'-dioctyl-[3,3'-biindolinylidene]-2,2'-dione (**83**).



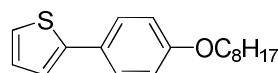
1-Bromooctane (5.04 g, 0.026 mol) was injected through a septum under nitrogen into a suspension of 6,6'-dibromoisoindigo (**82**) (5.00 g, 0.012 mol) and potassium carbonate (9.84 g, 0.071 mol) in DMF (20  $\text{cm}^3$ ) and the resultant reaction mixture stirred for 15 h at 100  $^\circ\text{C}$ . The reaction mixture allowed to cool to RT, poured into water (200  $\text{cm}^3$ ) and the crude product extracted into dichloromethane (2 x 150  $\text{cm}^3$ ). The combined organic extracts were washed with brine (2 x 200  $\text{cm}^3$ ), dried ( $\text{MgSO}_4$ ), filtered and concentrated under reduced pressure. Purification of the crude product was carried out *via* stirring in methanol to give title compound as deep-red solid (6.80 mg, 87%).

Melting point  $^\circ\text{C}$ : 140.

$^1\text{H}$  NMR ( $\text{CDCl}_3$ )  $\delta_{\text{H}}$ : 0.87 (6H, t,  $J = 6.9$  Hz), 1.26-1.35 (20H, m), 1.68 (4H, quint,  $J = 6.5$  Hz), 3.73 (4H, t,  $J = 7.5$  Hz), 6.93 (2H, d,  $J = 1.8$  Hz), 7.17 (2H, dd,  $J = 1.8, 8.5$  Hz), 9.08 (2H, d,  $J = 8.5$  Hz).

MS  $m/z$  (EI): 321 (M 100), 325, 365, 567, 349, 607, 643 ( $\text{M}^+$ ).

### 2-(4-Octyloxyphenyl)thiophene (**85**).



Tetrakis(triphenylphosphine)palladium(0) (0.37 g,  $3.2 \times 10^{-4}$  mol), sodium carbonate (3.00 g, 0.028 mol) and water (12  $\text{cm}^3$ ) were added to a mixture of the 1-bromo-4-octyloxybenzene (**84**) (5.00 g, 0.016 mol) and thiophene-2-boronic acid (**9**) (3.06 g, 0.024 mol) in DME (40  $\text{cm}^3$ ) and the resultant reaction mixture heated under reflux at 80  $^\circ\text{C}$  overnight. The reaction mixture allowed to cool to RT, poured into water (200  $\text{cm}^3$ ) and the crude product extracted into dichloromethane (2 x 100  $\text{cm}^3$ ). The

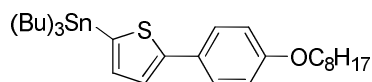
combined organic extracts were washed with brine (2 x 200 cm<sup>3</sup>), dried (MgSO<sub>4</sub>), filtered and concentrated under reduced pressure. Purification of the crude product was carried out *via* column chromatography [silica gel, dichloromethane: hexane, 1 : 6] to yield the desired product as a light yellow solid (3.20 g, 69%).

Melting point /°C: 69-71 (Lit 68-70).<sup>22</sup>

<sup>1</sup>H NMR (CDCl<sub>3</sub>) δH: 0.88 (3H, t), 1.27-1.36 (8H, m), 1.42-1.49 (2H, m), 1.80 (2H, quint, *J* = 6.7 Hz), 3.99 (2H, t, *J* = 6.5 Hz), 6.89 (2H, d, *J* = 9.0 Hz), 7.04 (1H, dd, *J* = 1.4, 3.6 Hz), 7.18-7.21 (2H, m), 7.52 (2H, d, *J* = 9.0 Hz).

MS m/z (EI): 177, 178, 210, 213, 279, 288 (M<sup>+</sup>, M 100).

### 2-[(4-Octyloxyphenyl)-5-tributylstannyl]thiophene (86).

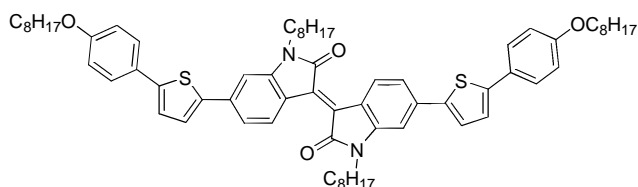


A solution of 2.5 M *n*-BuLi (in hexanes) (5 cm<sup>3</sup>, 0.012 mol) was added slowly to a solution of 2-(4-octyloxyphenyl)thiophene (**85**) (2.80 g, 0.001 mol) in THF (dry, 100 cm<sup>3</sup>) at -78 °C. After stirring for 1 h at -78 °C, tri *n*-butyltin chloride (3.47 g, 0.011 mol) was added slowly and the temperature of the reaction mixture was allowed to reach RT after completion of the addition. The reaction mixture was stirred overnight. Water (100 cm<sup>3</sup>) was added and the product extracted into diethyl ether (200 cm<sup>3</sup>). The combined ethereal extracts were dried (MgSO<sub>4</sub>), filtered and concentrated under reduced pressure to yield the desired product as a pale brown oil, which was not purified further (4.9 g, 87%).

<sup>1</sup>H NMR (CDCl<sub>3</sub>) δH: 0.86-0.94 (12H, m), 1.11 (6H, m), 1.27-1.43 (16H, m), 1.58-1.60 (6H, m), 3.96 (2H, t, *J* = 6.7 Hz), 6.89 (2H, d, *J* = 9.0 Hz), 7.10 (1H, d, *J* = 3.4 Hz), 7.31 (1H, d, *J* = 3.4 Hz), 7.53 (2H, d, *J* = 9.0 Hz).

MS m/z (EI): 533, 551, 555 (M 100), 575, 576 (M<sup>+</sup>).

### 1,1'-Dioctyl-6,6'-bis-(5-4-(octyloxyphenyl)thiophen-2-yl)-[3,3'-biindolinylidene]-2,2'-dione (87).



Palladium acetate (0.01 g,  $4.4 \times 10^{-4}$  mol) was added to a degassed solution of 6,6'-dibromo-1,1'-dioctyl-[3,3'-biindolylidene]-2,2'-dione (**83**) (0.25 g, 0.0002 mol), 2-[(4-Octyloxyphenyl)-5-tributylstannyl]thiophene (**86**) (0.40 g, 0.0007 mol) and triphenylphosphine (0.10 g,  $3.8 \times 10^{-4}$  mol) in DMF (5 cm<sup>3</sup>). The mixture was heated at 90 °C overnight, allowed to cool to RT, poured into a saturated aqueous KF solution (50 cm<sup>3</sup>) and the crude product extracted into dichloromethane (100 cm<sup>3</sup>) and water (100 cm<sup>3</sup>). The combined organic extracts were dried (MgSO<sub>4</sub>), filtered and concentrated under reduced pressure. The crude dark red solids were purified *via* column chromatography [silica gel, dichloromethane: hexane, 1 : 1] to give the desired product as a brown solid (0.19 g, 79 %).

Melting point /°C: 195.

<sup>1</sup>H NMR (CDCl<sub>3</sub>) δ: 0.88 (12H, t, *J* = 6.9 Hz), 1.20-1.54 (40H, m), 1.80 (8H, m), 3.83 (4H, t, *J* = 6.7 Hz), 3.99 (4H, t, *J* = 6.5 Hz), 6.91 (4H, d, *J* = 8.7 Hz), 6.97 (2H, d, *J* = 1.4 Hz), 7.21 (2H, d, *J* = 3.6 Hz), 7.28 (2H, dd, *J* = 1.6, 7.5 Hz), 7.39 (2H, d, *J* = 3.6 Hz), 7.58 (4H, d, *J* = 8.7 Hz), 9.18 (2H, d, *J* = 8.3 Hz).

<sup>13</sup>C NMR (CDCl<sub>3</sub>): 14.1, 22.7, 27.3, 29.1, 29.2, 29.3, 29.4, 31.8, 68.1, 105.0, 114.9, 118.0, 120.0, 123.0, 125.3, 126.0, 130.3, 131.0, 135.0, 142.0, 145.0, 145.2, 159.1, 168.0.

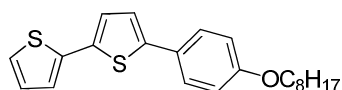
MS *m/z* (EI): 560, 781, 890, 950, 1058 (M<sup>+</sup>, M 100), 1059.

Combustion analysis:

Expected: C 77.08%, H 8.18%, N 2.64%, S 6.05%.

Obtained: C 76.88%, H 8.21%, N 2.59%, S 6.15%.

#### 5-(4-Octyloxyphenyl)-2,2'-bithiophene (**88**).



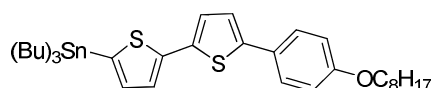
A mixture of palladium acetate (0.02 g,  $8.9 \times 10^{-5}$  mol), 1-bromo-4-(octyloxy)benzene (**84**) (2.00 g, 0.007 mol), 2,2'-bithiophene (**4**) (7.00 g, 0.024 mol), potassium carbonate (2.30 g, 0.018 mol),  $\text{PCy}_3 \cdot \text{HBF}_4$  (0.02 g,  $2.7 \times 10^{-4}$  mol) and pivalic acid (0.2 g, 0.002 mol) in NMP (20  $\text{cm}^3$ ) was degassed with  $\text{N}_2$  for 15 minutes at RT and then heated at 100 °C for 18 h. The reaction mixture was allowed to cool to RT and then diluted with dichloromethane (100  $\text{cm}^3$ ) and water (100  $\text{cm}^3$ ). The aqueous phase was extracted with dichloromethane (2 x 100  $\text{cm}^3$ ). The combined organic extracts were dried ( $\text{MgSO}_4$ ), filtered and concentrated under reduced pressure. Purification of the crude product was carried out *via* column chromatography [silica gel, dichloromethane: hexane, 1 : 4] to yield a yellow solid (1.45 g, 56%).

Melting point /°C: 63-64.

$^1\text{H}$  NMR ( $\text{CDCl}_3$ )  $\delta\text{H}$ : 0.89 (3H, t,  $J = 6.9$  Hz), 1.29-1.48 (8H, m), 1.42-1.48 (2H, m), 1.79 (2H, quint,  $J = 6.7$  Hz), 3.97 (2H, t,  $J = 6.5$  Hz), 6.90 (2H, d,  $J = 8.5$  Hz), 7.02 (1H, dd,  $J = 1.4, 3.6$  Hz), 7.11 (2H, d,  $J = 3.8$  Hz), 7.17 (1H, dd,  $J = 1.2, 4.1$  Hz), 7.19 (1H, dd,  $J = 1.0, 4.0$  Hz), 7.51 (2H, d,  $J = 8.5$  Hz).

MS  $m/z$  (EI): 41, 55, 69, 98, 121, 127, 152, 184, 213, 229, 240, 257, 258 (M 100), 259, 260, 261, 284, 326, 341, 368, 370 ( $\text{M}^+$ ), 371.

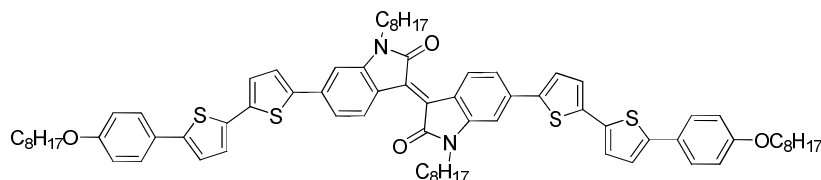
#### Tributyl(5'-(4-octyloxyphenyl)-[2,2'-bithiophen]-5-yl)stannane (**89**).



A solution of 2.5 M *n*-BuLi (in hexanes) (2  $\text{cm}^3$ , 0.004 mol) was added slowly to a solution of 5-(4-octyloxyphenyl)-2,2'-bithiophene (**88**) (0.85 g, 0.002 mol) in THF (50  $\text{cm}^3$ ) at -78 °C. After stirring for 1 h at -78 °C, tributyltin chloride (1.70 g, 0.005 mol) was added slowly and the temperature of the reaction mixture was allowed to reach RT after completion of the addition. The reaction mixture was stirred overnight. Water (50  $\text{cm}^3$ ) was added and the product extracted into diethyl ether (100  $\text{cm}^3$ ). The combined ethereal extracts were dried ( $\text{MgSO}_4$ ), filtered and concentrated under reduced pressure to yield the desired product as a light brown liquid, which was not purified further (1.30 g, 86%).

$^1\text{H}$  NMR ( $\text{CDCl}_3$ )  $\delta$ H: 0.89 (3H, t,  $J = 6.9$  Hz), 1.10-1.48 (37H, m), 1.54 (2H, quint,  $J = 6.7$  Hz), 3.97 (2H, t,  $J = 6.5$  Hz), 6.90 (2H, d,  $J = 8.7$  Hz), 7.08 (1H, d,  $J = 3.2$  Hz), 7.10 (2H, d,  $J = 3.6$  Hz), 7.28 (1H, d,  $J = 3.2$  Hz), 7.51 (2H, d,  $J = 8.7$  Hz).

**1,1'-Dioctyl-6,6'-bis-(5'-4-octyloxyphenyl)-[2,2'-bithiophen]-5-yl)-[3,3'-biindolinylidene]-2,2'-dione (90).**



Palladium acetate (0.01 g,  $4.4 \times 10^{-4}$  mol) was added to a degassed solution of 6,6'-dibromo-1,1'-dioctyl-[3,3'-biindolinylidene]-2,2'-dione (**83**) (0.20 g, 0.0002 mol), tributyl(5'-(4-octyloxyphenyl)-[2,2'-bithiophen]-5-yl)stannane (**89**) (0.20 g, 0.0003 mol) and triphenylphosphine (0.05 g,  $1.9 \times 10^{-4}$  mol) in DMF (5  $\text{cm}^3$ ). The mixture was heated at 90  $^\circ\text{C}$  overnight, allowed to cool to RT, poured into a saturated aqueous KF solution (50  $\text{cm}^3$ ) and the crude product extracted into dichloromethane (100  $\text{cm}^3$ ) and water (100  $\text{cm}^3$ ). The combined organic extracts were dried ( $\text{MgSO}_4$ ), filtered and concentrated under reduced pressure. The crude dark red solids were purified *via* column chromatography [silica gel, dichloromethane: hexane, 1 : 1] to give the desired product as a brown solid (0.16 g, 57%).

Transition temp.  $^\circ\text{C}$ : Tg 96 Cr 238 N 281 I.

$^1\text{H}$  NMR ( $\text{CDCl}_3$ )  $\delta$ : 0.89 (12H, t,  $J = 6.9$  Hz), 1.56-1.24 (40H, m), 1.80 (8H, m), 3.83 (4H, t,  $J = 6.7$  Hz), 3.99 (4H, t,  $J = 6.5$  Hz), 6.92 (6H, d,  $J = 6.2$  Hz), 7.13 (2H, d,  $J = 3.6$  Hz), 7.16 (4H, dd,  $J = 3.7, 8.1$  Hz), 7.25 (2H, m), 7.35 (2H, dd,  $J = 3.8, 7.6$  Hz), 7.52 (4H, d,  $J = 8.7$  Hz), 9.25 (2H, d,  $J = 7.1$  Hz).

$^{13}\text{C}$  NMR ( $\text{CDCl}_3$ ): 14.1, 22.5, 27.8, 29.3, 29.8, 30.2, 30.8, 31.6, 68.1, 105.0, 115.2, 118.2, 120.0, 122.6, 124.9, 125.6, 126.0, 126.7, 130.3, 131.0, 135.0, 142.0, 145.0, 145.2, 159.1, 168.0.

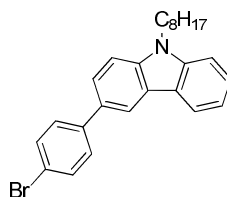
MS  $m/z$  (EI): 551 (M 100), 815, 859, 1223 ( $\text{M}^+$ ).

Combustion analysis:

Expected: C 74.59%, H 7.41%, N 2.29%, S 10.48%.

Obtained: C 74.37%, H 7.29%, N 2.36%, S 10.26%.

### 3-(4-Bromophenyl)-9-octyl-9-carbazole (92).



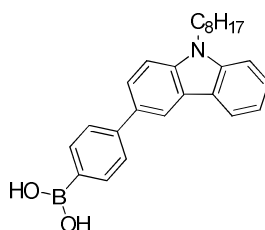
A mixture of tetrakis(triphenylphosphine)palladium(0) (0.05 g,  $4.3 \times 10^{-4}$  mol), 9-(octyl)-9-carbazol-3-boronic acid (**50**), (0.63 g, 0.002 mol), 1-bromo-4-iodobenzene (**91**) (0.50 g, 0.001 mol), sodium carbonate (0.60 g, 0.005 mol) and water (10 cm<sup>3</sup>) in DME (20 cm<sup>3</sup>) was heated under reflux at 80 °C overnight. The reaction mixture allowed to cool to RT, poured into water (100 cm<sup>3</sup>) and the crude product extracted into dichloromethane (2 x 50 cm<sup>3</sup>). The combined organic extracts were washed with brine (2 x 50 cm<sup>3</sup>), dried (MgSO<sub>4</sub>), filtered and concentrated under reduced pressure. Purification of the crude product was carried out *via* flash column chromatography [silica gel, dichloromethane: hexane, 5%→10%→15%→20%] to yield the desired product as a colourless solid (0.55 g, 72%).

Melting point /°C: 94-95.

<sup>1</sup>H NMR (CDCl<sub>3</sub>)  $\delta_{\text{H}}$ : 0.85 (3H, t,  $J = 6.9$  Hz), 1.27-1.42 (10H, m), 1.89 (2H, quint,  $J = 7.3$  Hz), 4.32 (2H, t,  $J = 7.3$  Hz), 7.25 (2H, s), 7.43 (1H, d,  $J = 4.0$  Hz), 7.47 (1H, d,  $J = 8.7$  Hz), 7.55 (4H, s), 7.65 (1H, dd,  $J = 1.4, 7.1$  Hz), 8.14 (1H, d,  $J = 7.7$  Hz), 8.27 (1H, d,  $J = 1.8$  Hz).

MS  $m/z$  (EI): 41, 43, 55, 57, 101, 126, 127, 128, 140, 168, 189, 202, 217, 226, 240, 254, 255, 256, 257, 322, 334 (M 100), 336, 337, 354, 356, 431, 433 (M<sup>+</sup>).

### 4-(9-Octyl-9-carbazol-3-yl)phenylboronic acid (93).



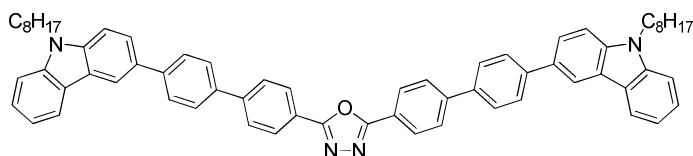
A solution of 3-(4-bromophenyl)-9-octyl-9-carbazole (**92**) (0.86 g, 0.002 mol) in dry THF (20 cm<sup>3</sup>) was added dropwise to a cooled (-78 °C) solution of 2.5 M *n*-BuLi (in hexanes) (4 cm<sup>3</sup>, 0.009 mol) over a period of 10 minutes. The resultant reaction mixture was stirred for 1 h at -78 °C. Triisopropyl borate (1.5 cm<sup>3</sup>, 0.008 mol) was added dropwise to the reaction mixture, which was then allowed to warm to RT and stirred for an additional 40 minutes before being quenched with 20% hydrochloric acid (30 cm<sup>3</sup>) and then stirred vigorously for 1 h. The crude product was extracted into dichloromethane (3 x 50 cm<sup>3</sup>). The combined organic layers were washed with brine (3 x 50 cm<sup>3</sup>), dried (MgSO<sub>4</sub>), filtered and concentrated under reduced pressure to yield the crude product, which was used without further purification (0.71 g, 87%).

Melting point /°C: 94-96.

<sup>1</sup>H NMR (CDCl<sub>3</sub>) δ<sub>H</sub>: 0.85 (3H, t, *J* = 6.9 Hz), 1.27-1.42 (10H, m), 1.89 (2H, quint, *J* = 7.3 Hz), 4.32 (2H, t, *J* = 7.3 Hz), 7.46 (3H, m), 7.76-7.85 (3H, m), 7.90 (1H, d, *J* = 7.9 Hz), 7.17 (1H, m), 8.26 (1H, d, *J* = 7.9 Hz), 8.39 (2H, m).

MS *m/z* (EI): 43, 77, 78, 115, 127, 128, 151, 178, 189, 226, 228, 241, 254, 256 (M 100), 257.

#### 2,5-bis-(4'-9-Octyl-9-carbazol-3-yl)-[1,1'-biphenyl]-4-yl)-1,3,4-oxadiazole (**94**).



$^1\text{H}$  NMR ( $\text{CDCl}_3$ )  $\delta_{\text{H}}$ : 0.86 (6H, t,  $J = 6.9$  Hz), 1.25-1.44 (20H, m), 1.91 (4H, quint,  $J = 7.3$  Hz), 4.34 (4H, t,  $J = 7.1$  Hz), 7.27 (2H, s), 7.44 (2H, d,  $J = 8.1$  Hz), 7.51 (4H, dd,  $J = 5.3, 3.8$  Hz), 7.77-7.83 (6H, m), 7.85 (8H, dd,  $J = 2.0, 6.3$  Hz), 8.18 (2H, d,  $J = 7.7$  Hz), 8.28 (4H, d,  $J = 8.3$  Hz), 8.40 (2H, d,  $J = 1.1$  Hz).

$^{13}\text{C}$  NMR ( $\text{CDCl}_3$ ): 14.0, 22.6, 27.3, 29.0, 29.1, 29.3, 31.8, 43.2, 108.8, 109.0, 118.7, 118.9, 120.0, 122.5, 122.9, 123.4, 124.9, 125.8, 127.2, 127.4, 131.3, 137.6, 140.1, 140.9, 142.0, 144.0, 164.5.

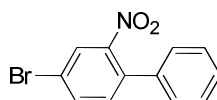
MS  $m/z$  (EI): 926, 928 ( $\text{M}^+$ , M 100), 929.

Combustion analysis:

Expected: C 85.37%, H 6.94%, N 6.03%.

Obtained: C 85.46%, H 7.05%, N 6.05%.

#### 4-Bromo-2-nitrobiphenyl (**97**).

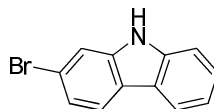


Phenylboronic acid (**96**) (6.10 g, 0.049 mol), 2,5-dibromonitrobenzene (**95**) (11.20 g, 0.040 mol) and Tetrakis(triphenylphosphine)palladium(0) (1.02 g, 0.010 mol) were dissolved in a mixture of toluene (150  $\text{cm}^3$ ), sodium carbonate (13 g, 0.122 mol) and water (50  $\text{cm}^3$ ). The degassed mixture was heated at 90  $^\circ\text{C}$  for 5 h, cooled to RT and then diluted with distilled water (100  $\text{cm}^3$ ). The organic phase was separated and the organic products were extracted into diethyl ether (100  $\text{cm}^3$ ). The combined organic extracts were dried ( $\text{MgSO}_4$ ), filtered and concentrated under reduced pressure to give a dark brown liquid. The product was purified by flash column chromatography [silica gel, dichloromethane: hexane, 5% $\rightarrow$ 10% $\rightarrow$ 15% $\rightarrow$ 20%] to give the desired product (8.20 g, 72%).

$^1\text{H}$  NMR ( $\text{CDCl}_3$ )  $\delta_{\text{H}}$ : 7.29-7.30 (2H, m), 7.33 (1H, d,  $J = 8.1$  Hz), 7.41-7.43 (3H, m), 7.73 (1H, dd,  $J = 4.2, 2.0$  Hz), 8.00 (1H, d,  $J = 2.0$  Hz).

MS  $m/z$  (EI): 32, 51, 63, 75, 76, 77, 98, 102, 115, 126, 139, 150, 151, 152 (M 100), 153, 167, 168, 181, 207, 219, 231, 247, 261, 277 ( $\text{M}^+$ ).

## 2-Bromocarbazole (**98**).



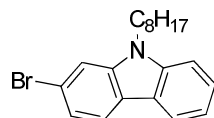
A mixture of 4-bromo-2-nitrophenyl (**97**) (4.00 g, 0.014 mol) and triphenylphosphine (13.00 g, 0.051 mol) was heated at 200 °C under reflux for 10 h. The cooled reaction mixture was poured into hexane and filtered. The remaining residue was diluted with a 1 : 1 mixture of methanol and distilled water to give a precipitate, which was filtered off and washed several times with a 1 : 1 mixture of methanol and water, followed by hexane (150 cm<sup>3</sup>). Column chromatography using hexane as eluent gave the title compound as a white solid (3.10 g, 90%).

Melting point /°C: 251-253.

<sup>1</sup>H NMR ((CD<sub>3</sub>)<sub>2</sub>SO) δ<sub>H</sub>: 7.17 (1H, t, *J* = 7.1 Hz), 7.28 (1H, dd, *J* = 1.8, 6.5 Hz), 7.40 (1H, t, *J* = 6.9 Hz), 7.48 (1H, d, *J* = 8.1 Hz), 7.65 (1H, d, *J* = 1.6 Hz), 8.07 (1H, d, *J* = 8.3 Hz), 8.13 (1H, d, *J* = 7.7 Hz), 11.39 (1H, s).

MS m/z (EI): 75, 76, 77, 98, 102, 115, 126, 245 (M<sup>+</sup>, M 100), 246.

## 2-Bromo-9-octylcarbazole (**99**).



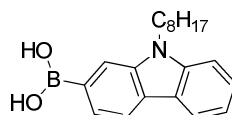
NaH (0.30 g, 0.008 mol) was added in a small portions to a solution of 2-bromocarbazole (**98**) (1.90 g, 0.007 mol) in DMF (20 cm<sup>3</sup>). The resultant mixture was stirred for 30 minutes and then the reaction temperature was increased to 50 °C. 1-Bromooctane (1.78 g, 0.009 mol) was added and the resultant reaction mixture heated at 50 °C for 3 h and then stirred overnight at RT. The reaction mixture was added to the water (200 cm<sup>3</sup>) and extracted into diethylether (150 cm<sup>3</sup>). The combined organic extracts were washed with brine (2 x 100 cm<sup>3</sup>), dried (MgSO<sub>4</sub>), filtered and concentrated under reduced pressure. The crude product was purified using flash chromatography to yield the desired product as a colourless liquid (2.90 g, 100%).

<sup>1</sup>H NMR (CDCl<sub>3</sub>) δ<sub>H</sub>: 0.86 (3H, t, *J* = 6.9 Hz), 1.24-1.39 (10H, m), 1.86 (2H, quint, *J* = 7.3 Hz), 4.24 (2H, t, *J* = 7.3 Hz), 7.22 (1H, d, *J* = 7.1 Hz), 7.31 (1H, dd, *J* = 1.6, 6.5

Hz), 7.38 (1H, d,  $J = 8.1$  Hz), 7.46 (1H, dd,  $J = 1.2, 7.1$  Hz), 7.54 (1H, d,  $J = 1.6$  Hz), 7.93 (1H, d,  $J = 8.3$  Hz), 8.06 (1H, d,  $J = 7.7$  Hz).

MS  $m/z$  (ED): 41, 43, 55, 69, 75, 89, 137, 139, 150, 151, 152, 164, 178, 179, 180, 193, 206, 235, 258 (M 100), 260, 261, 262, 277, 314, 355, 357 ( $M^+$ ).

### 9-Octyl-9-carbazol-2-boronic acid (**100**).



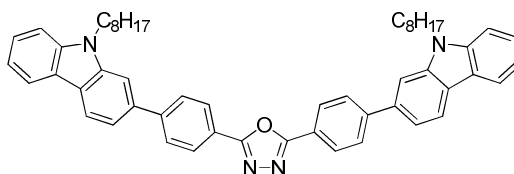
2.5 M *n*-BuLi (in hexanes) (6 cm<sup>3</sup>, 0.014 mol) was added dropwise to a solution of 2-bromo-9-octylcarbazole (**99**) (2.80 g, 0.007 mol) in THF (30 cm<sup>3</sup>) at -78 °C under N<sub>2</sub> and the mixture was stirred for 1 h. Triisopropyl borate (3.6 cm<sup>3</sup>, 0.019 mol) was added dropwise to the reaction mixture, which was then allowed to warm to RT and stirred overnight. 20% Hydrochloric acid (20 cm<sup>3</sup>) was added to the reaction mixture, which was stirred for 1 h to give a clear, blue solution. The reaction mixture was extracted into dichloromethane (2 x 50 cm<sup>3</sup>). The combined organic layers were washed with brine (2 x 50 cm<sup>3</sup>), dried (MgSO<sub>4</sub>), filter and concentrated under reduced pressure. Purification of the crude product was carried out *via* stirring in hexane (100 cm<sup>3</sup>) to yield the desired product as a white solid, which was filtered off and dried (2.20 g, 87%).

Melting point /°C: 173-175.

<sup>1</sup>H NMR (CDCl<sub>3</sub>) δ<sub>H</sub>: 0.86 (3H, t,  $J = 7.1$  Hz), 1.20-1.30 (10H, m), 1.98 (2H, quint,  $J = 7.1$  Hz), 4.40, (2H, t,  $J = 7.1$  Hz), 7.26 (2H, t,  $J = 7.5$  Hz), 7.49 (3H, m), 8.18 (2H, d,  $J = 7.7$  Hz), 8.26 (1H, d,  $J = 7.7$  Hz), 8.36 (1H, s).

MS  $m/z$  (EI): 41, 43, 55, 69, 115, 127, 140, 152, 151, 166, 180 (M 100), 181.

### 2,5-bis-4-(9-Octyl-9-carbazol-2-yl)phenyl-1,3,4-oxadiazole (**101**).



A mixture of palladium acetate (0.01 g, 4.4 x 10<sup>-5</sup> mol), 2,5-bis-(4-bromophenyl)-1,3,4-oxadiazole (**49**) (0.55 g, 0.003 mol), 9-octyl-9-carbazol-2-boronic acid (**100**) (1.17 g,

0.001 mol), potassium carbonate (1.00 g, 0.007 mol) and water (5 cm<sup>3</sup>) in DMF (10 cm<sup>3</sup>) was heated under reflux at 80 °C overnight. The reaction mixture allowed to cool to RT, poured into water (300 cm<sup>3</sup>) and the crude product extracted into dichloromethane (2 x 200 cm<sup>3</sup>). The combined organic extracts were washed with brine (2 x 250 cm<sup>3</sup>), dried (MgSO<sub>4</sub>), filtered and concentrated under reduced pressure. Purification of the crude product was carried out *via* column chromatography [silica gel, dichloromethane: ethyl acetate, 1 : 9] and recrystallisation first from a mixture of DCM/DMSO and then from a mixture of DCM/MeOH to yield a white solid (0.38 g, 95%).

Melting point /°C: 205.

<sup>1</sup>H NMR (CDCl<sub>3</sub>) δ<sub>H</sub>: 0.86 (6H, t, *J* = 6.9 Hz), 1.25-1.47 (20H, m), 1.93 (4H, quint, *J* = 7.5 Hz), 4.38 (4H, t, *J* = 7.1 Hz), 7.26 (2H, m), 7.48 (2H, d, *J* = 8.1 Hz), 7.50 (2H, d, *J* = 7.1 Hz), 7.53 (2H, dd, *J* = 6.5, 1.6 Hz), 7.65 (2H, s), 7.91 (4H, d, *J* = 8.7 Hz), 8.14 (2H, d, *J* = 7.5 Hz), 8.20 (2H, d, *J* = 7.9 Hz), 8.28 (4H, d, *J* = 8.5 Hz).

<sup>13</sup>C NMR (CDCl<sub>3</sub>): 14.0, 22.6, 22.7, 27.3, 29.0, 29.1, 29.3, 30.8, 31.8, 43.1, 64.0, 94.0, 107.0, 107.8, 116.2, 118.3, 119.8, 122.0, 122.2, 123.0, 127.3, 127.9, 136.0, 141.1, 141.9, 145.6, 158.8, 164.6.

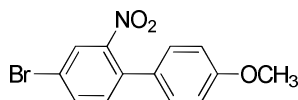
MS *m/z* (EI): 667, 699, 774, 776 (M<sup>+</sup>, M 100).

Combustion analysis:

Expected: C 83.47%, H 7.26%, N 7.21%.

Obtained: C 83.60%, H 7.36%, N 7.24%.

#### 4-Bromo-4'-methoxy-2-nitrobiphenyl (**104**).



Copper powder (17.00 g, 0.101 mol) was added over 1 h to a stirred molten mixture of 2,5-dibromonitrobenzene (**102**) (25.00 g, 0.091 mol) and 4-iodoanisole (**103**) (25.00 g, 0.102 mol) maintained at 175 °C. The reaction mixture was maintained at 175 °C for another 6 h. The reaction mixture was extracted into hot toluene and the extract was filtered through silica. The filtrate was washed with water 400 (cm<sup>3</sup>), dried (MgSO<sub>4</sub>),

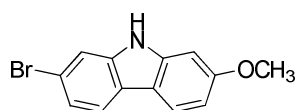
filtered and concentrated under reduced pressure. The crude material was recrystallized from ethanol to give title compound as yellow needles (20.46 g, 75%).

Melting point /°C: 125-126 (Lit 125-127 °C).<sup>23</sup>

<sup>1</sup>H NMR (CDCl<sub>3</sub>) δ<sub>H</sub>: 3.84 (3H, s), 6.94 (2H, d, *J* = 7.5 Hz), 7.22 (2H, d, *J* = 7.9 Hz), 7.29 (1H, d, *J* = 8.1 Hz), 7.70 (1H, dd, *J* = 2.4, 8.7 Hz), 7.94 (1H, d, *J* = 2.0 Hz).

MS m/z (ED): 39, 51, 63, 69, 75, 89, 111, 113, 138, 139 (M 100), 140, 155, 167, 182, 185, 208, 224, 248, 264, 290, 307 (M<sup>+</sup>).

### 2-Bromo-7-methoxycarbazole (105).



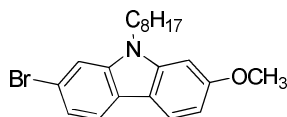
A solution of 4-bromo-4-methoxy-2-nitrobiphenyl (**104**) (10.00 g, 0.032 mol) in triethyl phosphite (25 cm<sup>3</sup>, 0.150 mol) was stirred at reflux under nitrogen overnight. Then the excess triethyl phosphite was distilled off under reduced pressure. After this the residue was washed with ethanol and recrystallized with a 1 : 1 mixture of dichloromethane and ethanol to give title compound as ivory crystals (5.30 g, 60%).<sup>23</sup>

Melting point /°C: 286.

<sup>1</sup>H NMR ((CD<sub>3</sub>)<sub>2</sub>SO) δ<sub>H</sub>: 3.74 (3H, s), 6.71 (1H, dd, *J* = 2.2, 6.3 Hz), 6.90 (1H, d, *J* = 2.2 Hz), 7.15 (1H, dd, *J* = 1.8, 8.3 Hz), 7.50 (1H, d, *J* = 1.2 Hz), 7.86 (1H, d, *J* = 7.1 Hz), 7.89 (1H, d, *J* = 7.7 Hz), 11.16 (1H, s).

MS m/z (ED): 39, 50, 62, 63, 74, 87, 99, 101, 125, 126, 137, 152, 153, 181, 196, 206, 217, 231, 232, 235, 246, 260, 275 (M<sup>+</sup>, M 100).

### 2-Bromo-7-methoxy-9-octylcarbazole (106).



NaH (0.6 g of a 60 % dispersed in mineral oil) was added in a small portions to a solution of 2-bromo-7-methoxycarbazole (**105**) (2.15 g, 0.007 mol) in DMF (20 cm<sup>3</sup>). The resultant mixture was stirred for 30 minutes. 1-bromooctane (1.60 gm, 0.008 mol) was added and the resulting mixture was heated at 50 °C for 3 h, then stirred overnight

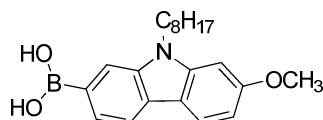
at RT. The reaction mixture was poured into ice-water (250 cm<sup>3</sup>). The precipitate was collected by filtration followed by flash column chromatography [silica gel, dichloromethane: hexane, 5%→10%→15%→20%] to give a colourless solid (2.95 g, 99%).<sup>23</sup>

Melting point /°C: 57.

<sup>1</sup>H NMR (CDCl<sub>3</sub>) δ<sub>H</sub>: 0.87 (3H, t, *J* = 6.9 Hz), 1.24-1.39 (10H, m), 1.83 (2H, quint, *J* = 7.5 Hz), 3.93 (3H, s), 4.17 (2H, t, *J* = 7.3 Hz), 6.84 (2H, d, *J* = 6.3 Hz), 7.27 (1H, dd, *J* = 1.6, 8.7 Hz), 7.47 (1H, d, *J* = 1.6 Hz), 7.82 (1H, d, *J* = 8.3 Hz), 7.91 (1H, d, *J* = 8.1 Hz).

MS m/z (EI): 41, 43, 55, 69, 75, 113, 126, 139, 166, 167, 194, 210, 233, 245, 275, 288 (M 100), 290, 291, 307, 344, 372, 387 (M<sup>+</sup>).

#### 7-Methoxy-9-octyl-9-carbazol-2-boronic acid (107).



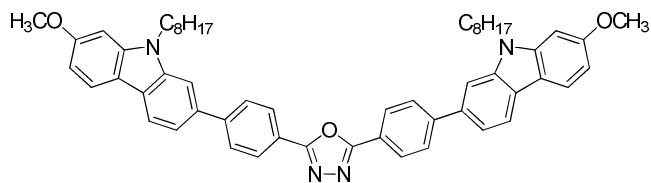
2.5 M *n*-BuLi (in hexanes) (10 cm<sup>3</sup>, 0.024 mol) was added dropwise to a solution of 2-bromo-7-methoxy-9-octylcarbazole (**106**) (3.00 g, 0.007 mol) in dry THF (30 cm<sup>3</sup>) at -78 °C under N<sub>2</sub> and the mixture was stirred for 1 h. Triisopropyl borate (7 cm<sup>3</sup>, 0.037 mol) was added dropwise to the reaction mixture, which was then allowed to warm to RT and stirred for overnight. Aqueous hydrochloric acid (20%, 50 cm<sup>3</sup>) was added and stirring continued for 1 h. The reaction mixture was extracted into dichloromethane (2 × 50 cm<sup>3</sup>). The combined organic layers were washed with brine (2 × 50 cm<sup>3</sup>), dried (MgSO<sub>4</sub>), filter and concentrated under reduced pressure. Purification of the crude product was carried out *via* stirring in hexane (100 cm<sup>3</sup>) to yield a white solid (2.60 g, 95%).

Melting point /°C: 78.

<sup>1</sup>H NMR (CDCl<sub>3</sub>) δ<sub>H</sub>: 0.86 (3H, t, *J* = 6.8 Hz), 1.24-1.39 (10H, m), 1.86 (2H, quint, *J* = 7.2 Hz), 3.96 (3H, s), 4.27 (2H, t, *J* = 7.3 Hz), 6.85 (2H, d, *J* = 6.9 Hz), 7.50 (1H, d, *J* = 7.5 Hz), 7.99-8.09 (2H, m), 8.11 (1H, t, *J* = 7.2 Hz), 8.18 (1H, d, *J* = 7.3 Hz).

MS m/z (EI): 43, 55, 57, 77, 127, 139, 153, 167, 196, 210, 223, 256 (M 100), 258, 283, 312, 354 (M<sup>+</sup>).

**2,5-bis-(4-7-methoxy-9-octylcarbazol-2-yl)phenyl-1,3,4-oxadiazole (108).**



A mixture of palladium acetate (0.05 g,  $4.3 \times 10^{-4}$  mol), 2,5-bis-(4-bromophenyl)-1,3,4-oxadiazole (**49**) (1.00 g, 0.002 mol), 7-methoxy-9-octyl-9-carbazol-2-boronic acid (**107**) (2.50 g, 0.007 mol), sodium carbonate (1.11 g, 0.010 mol) and water (10 cm<sup>3</sup>) in DME (20 cm<sup>3</sup>) was heated under reflux at 80 °C overnight. The reaction mixture allowed to cool to RT, poured into water (300 cm<sup>3</sup>) and the crude product extracted into dichloromethane (2 x 250 cm<sup>3</sup>). The combined organic extracts were washed with brine (2 x 250 cm<sup>3</sup>), dried (MgSO<sub>4</sub>), filtered and concentrated under reduced pressure. Purification of the crude product was carried out *via* column chromatography [silica gel, ethyl acetate: dichloromethane 1 : 4] to yield a light yellow solid (1.45 g, 66%).

Transition temp. °C: Cr 118 Cr 178 I.

<sup>1</sup>H NMR (CDCl<sub>3</sub>) δ<sub>H</sub>: 0.86 (6H, t, *J* = 7.1 Hz), 1.27-1.45 (20H, m), 1.91 (4H, quint, *J* = 7.5 Hz), 3.95 (6H, s), 4.30 (4H, t, *J* = 7.1 Hz), 6.87-6.89 (4H, m), 7.51 (2H, dd, *J* = 1.0, 8.1 Hz), 7.56 (2H, s), 7.88 (4H, d, *J* = 8.1 Hz), 7.99 (2H, d, *J* = 6.1 Hz), 8.07 (2H, d, *J* = 8.1 Hz), 8.25 (4H, d, *J* = 8.3 Hz).

<sup>13</sup>C NMR (CDCl<sub>3</sub>): 14.0, 22.6, 27.3, 28.8, 29.1, 29.3, 31.8, 43.0, 55.7, 93.3, 107.0, 107.8, 116.4, 118.4, 119.8, 121.2, 122.2, 123.0, 127.3, 128.0, 136.0, 141.0, 142.5, 145.6, 159.3, 164.0.

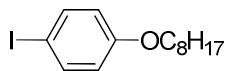
MS m/z (EI): 835, 836 (M<sup>+</sup>, M 100).

Combustion analysis:

Expected: C 80.35%, H 7.22%, N 6.69%.

Obtained: C 80.60%, H 7.40%, N 6.70%.

### 1-Iodo-4-octyloxybenzene (110)

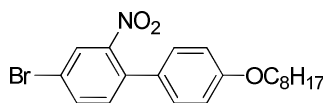


A mixture of 4-iodophenol (**109**) (14.65 g, 0.066 mol), potassium carbonate (23.00 g, 0.166 mol), 1-bromooctane (13.00 g, 0.067 mol) and DMF (150 cm<sup>3</sup>) was heated under reflux overnight. The cooled reaction mixture was poured into water (250 cm<sup>3</sup>) and the crude product extracted into hexane (2 × 100 cm<sup>3</sup>). The combined organic extracts were washed with an aqueous NaOH solution and brine (200 cm<sup>3</sup>), dried (MgSO<sub>4</sub>), filtered and concentrated under reduced pressure. Purification was carried out *via* column chromatography [silica gel, hexane] to yield a colourless liquid (20.00 g, 90%).<sup>31</sup>

<sup>1</sup>H NMR (CDCl<sub>3</sub>) δ<sub>H</sub>: 0.88 (3H, t, *J* = 6.7 Hz), 1.28-1.49 (10H, m), 1.76 (2H, quint, *J* = 6.7 Hz), 3.90 (2H, t, *J* = 6.7 Hz), 6.65 (2H, d, *J* = 7.1 Hz), 7.54 (2H, d, *J* = 7.1 Hz).

MS m/z (EI): 41, 43, 57, 65, 93, 106, 107, 109, 133, 165, 191, 203, 220 (M 100), 221, 233, 260, 288, 304, 332 (M<sup>+</sup>), 333.

### 4-Bromo-2-nitro-4'-octyloxy-biphenyl (111).

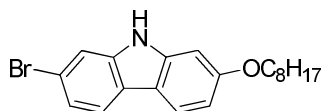


Copper powder (15.00 g, 0.056 mol) was added over 1 h to a stirred molten mixture of 2,5-dibromonitrobenzene (**102**) (16.00 g, 0.080 mol) and 1-iodo-4-octyloxybenzene (**110**) (18.92 g, 0.056 mol) maintained at 175 °C. The reaction mixture was maintained at 175 °C for another 6 h. The reaction mixture was extracted into hot toluene and the extract was filtered through silica. The filtrate was washed with water 400 (cm<sup>3</sup>), dried (MgSO<sub>4</sub>), filter and concentrated under reduced pressure. Purification of the crude product was carried out *via* flash column chromatography [silica gel, ethyl acetate: hexane, 5%→10%→15%→20%] to yield a light yellow liquid (16.00 g, 72%).

<sup>1</sup>H NMR (CDCl<sub>3</sub>) δ<sub>H</sub>: 0.82 (3H, t, *J* = 7.2 Hz), 1.20-1.48 (10H, m), 1.79 (2H, quint, *J* = 6.5 Hz), 3.97 (2H, t, *J* = 6.5 Hz), 6.92 (2H, d, *J* = 7.3 Hz), 7.19 (2H, d, *J* = 7.1 Hz), 7.30 (1H, d, *J* = 8.1 Hz), 7.69 (1H, dd, *J* = 1.8, 8.1 Hz), 7.93 (1H, d, *J* = 2.0 Hz).

MS m/z (EI): 43, 57, 71, 75, 102, 113, 128, 139, 140, 150 (M 100), 168, 184, 197, 222, 226, 248, 263, 276, 293, 296, 375, 405 (M<sup>+</sup>).

## 2-Bromo-7-octyloxy-carbazole (**112**).



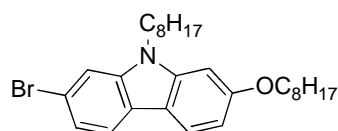
A solution of 4-bromo-2-nitro-4'-octyloxy-biphenyl (**111**) (16.00 g, 0.039 mol) in triphenylphosphine (25.00 g, 0.095 mol) was stirred at 200 °C under nitrogen overnight. The reaction mixture was poured onto hexane and filtered. The remaining residue was diluted with a 1 : 1 mixture of methanol and water to give a precipitate which was filtered off and washed several times with a 1 : 1 mixture of methanol and water, followed by hexane 100 (cm<sup>3</sup>). This was used without further purification (8.05 g, 54%).

Melting point /°C: 265.

<sup>1</sup>H NMR (CDCl<sub>3</sub>) δ<sub>H</sub>: 0.87 (3H, t, *J* = 6.7 Hz), 1.29-1.52 (10H, m), 1.82 (2H, quint, *J* = 6.7 Hz), 4.01 (2H, t, *J* = 6.5 Hz), 6.84-6.86 (2H, m), 7.30 (1H, dd, *J* = 2.4, 6.5 Hz), 7.48 (1H, d, *J* = 3.8 Hz), 7.78 (1H, d, *J* = 7.7 Hz), 7.87 (1H, d, *J* = 7.3 Hz), 7.96 (1H, s).

MS *m/z* (EI): 41, 43, 71, 75, 113, 125, 126, 138, 152, 183, 208, 235, 261 (*M* 100), 263, 364, 294, 363, 373 (*M*<sup>+</sup>).

## 2-Bromo-9-octyl-7-(octyloxy)-9-carbazole (**113**).

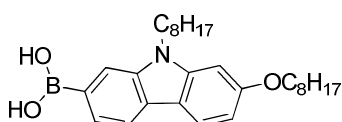


NaH (1.50 g of a 60 % dispersed in mineral oil) was added in a small portions to a solution of 2-bromo-7-(octyloxy)-carbazole (**112**) (6.75 g, 0.018 mol) in DMF (60 cm<sup>3</sup>). The resultant mixture was stirred for 30 minutes. 1-Bromooctane (4.18 g, 0.021 mol) was added and the resulting mixture heated at 50 °C for 3 h, then stirred overnight at RT. The reaction mixture was poured into water (200 cm<sup>3</sup>) and the crude product extracted into dichloromethane (2 x 250 cm<sup>3</sup>). The combined organic extracts were washed with brine (2 x 200 cm<sup>3</sup>), dried (MgSO<sub>4</sub>), filtered and concentrated under reduced pressure. Purification of the crude product was carried out *via* flash column chromatography [silica gel, dichloromethane: hexane, 5%→10%→15%→20%] to yield a colourless liquid (8.67 g, 99%).

$^1\text{H}$  NMR ( $\text{CDCl}_3$ )  $\delta_{\text{H}}$ : : 0.89 (6H, t,  $J = 8.5$  Hz), 1.25 (18H, m), 1.50 (2H, quint,  $J = 7.3$  Hz), 1.84 (4H, quint,  $J = 8.1$  Hz), 4.06 (2H, t,  $J = 6.5$  Hz), 4.16 (2H, t,  $J = 7.3$  Hz), 6.85 (2H, d,  $J = 1.6$  Hz), 7.28 (1H, dd,  $J = 1.2, 7.9$  Hz), 7.46 (1H, d,  $J = 1.4$  Hz), 7.81 (1H, d,  $J = 8.3$  Hz), 7.90 (1H, d,  $J = 8.5$  Hz).

MS  $m/z$  (EI): 43, 57 (M 100), 71, 73, 139, 153, 167, 180, 195, 196, 222, 260, 274, 277, 308, 372, 373, 407, 426, 478, 487 ( $\text{M}^+$ ), 488.

#### 9-Octyl-7-(octyloxy)-9-carbazol-2-boronic acid (**114**).



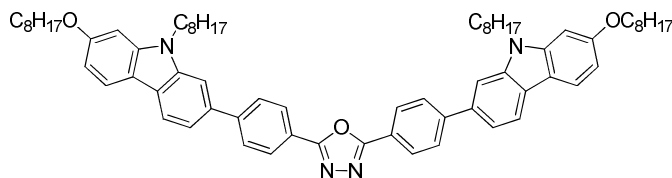
2.5 M *n*-BuLi (in hexanes) (10  $\text{cm}^3$ , 0.025 mol) was added dropwise to a solution of 2-bromo-9-octyl-7-(octyloxy)-9-carbazole (**113**) (4.00 g, 0.006 mol) in THF (30  $\text{cm}^3$ ) at  $-78$   $^\circ\text{C}$ . The resultant reaction mixture was stirred for 1 h. Triisopropyl borate (3.4  $\text{cm}^3$ , 0.018 mol) was added dropwise to the reaction mixture, which was then allowed to warm to RT and stirred for overnight. 20% Hydrochloric acid (70  $\text{cm}^3$ ) was added and the resultant mixture stirred for 1 h and then extracted into diethyl ether (3  $\times$  50  $\text{cm}^3$ ). The combined organic layers were washed with brine (2  $\times$  100  $\text{cm}^3$ ), dried ( $\text{MgSO}_4$ ), and concentrated under reduced pressure. Purification of the crude product was carried out *via* stirring in hexane (100  $\text{cm}^3$ ) to yield the desired product as a white solid (2.70 g, 96%).

Melting point  $^\circ\text{C}$ : 120-122.

$^1\text{H}$  NMR ( $\text{CDCl}_3$ )  $\delta_{\text{H}}$ : 0.88 (6H, t,  $J = 8.5$  Hz), 1.24-1.51 (20H, m), 1.84 (4H, quint,  $J = 8.1$  Hz), 4.08 (2H, t,  $J = 6.7$  Hz), 4.26 (2H, t,  $J = 7.1$  Hz), 6.85 (2H, d,  $J = 6.9$  Hz), 7.50 (1H, d,  $J = 7.9$  Hz), 7.79 (1H, s), 7.95-8.08 (2H, m), 8.15 (1H, t,  $J = 7.1$  Hz), 8.32 (1H, d,  $J = 7.1$  Hz).

MS  $m/z$  (EI): 43, 55, 77, 115, 128, 165, 202, 226, 228, 242, 256 (M 100), 257.

**2,5-bis-{4-[9-octyl-7-(octyloxy)-9-carbazol-2-yl]phenyl}-1,3,4-oxadiazole (115).**



A mixture of palladium acetate (0.01 g,  $4.4 \times 10^{-4}$  mol), 2,5-bis-(4-bromophenyl)-1,3,4-oxadiazole (**49**) (0.25 g,  $6.5 \times 10^{-3}$  mol), 9-octyl-7-(octyloxy)-9-carbazol-2-boronic acid (**114**) (0.75 g, 0.001 mol), potassium carbonate (0.50 g, 0.003 mol) and water (3 cm<sup>3</sup>) in DMF (5 cm<sup>3</sup>) was heated under reflux at 80 °C overnight. The reaction mixture allowed to cool to RT, poured into water (200 cm<sup>3</sup>) and the crude product extracted into dichloromethane (2 x 200 cm<sup>3</sup>). The combined organic extracts were washed with brine (2 x 200 cm<sup>3</sup>), dried (MgSO<sub>4</sub>), filtered and concentrated under reduced pressure. Purification of the crude product was carried out *via* column chromatography [silica gel, dichloromethane: ethyl acetate), 1 : 4] and recrystallisation from a DCM/MeOH to yield a light yellow solid (0.57 g, 85%).

Transition temp. /°C: Cr 138 Cr 148 I.

<sup>1</sup>H NMR (CDCl<sub>3</sub>) δ<sub>H</sub>: 0.84 (6H, t, *J* = 6.9 Hz), 0.92 (6H, t, *J* = 7.1 Hz), 1.31-1.65 (40H, m), 1.91 (8H, quint, *J* = 7.7 Hz), 4.10 (4H, t, *J* = 6.5 Hz), 4.30 (4H, t, *J* = 7.1 Hz), 6.84-6.88 (4H, m), 7.51 (2H, dd, *J* = 1.0, 8.1 Hz), 7.59 (2H, s), 7.90 (4H, d, *J* = 8.1 Hz), 7.96 (2H, d, *J* = 8.3 Hz), 8.06 (2H, d, *J* = 8.1 Hz), 8.26 (4H, d, *J* = 8.1 Hz).

<sup>13</sup>C NMR (CDCl<sub>3</sub>): 14.0, 22.6, 27.3, 28.8, 29.2, 31.8, 43.0, 68.5, 94.0, 106.9, 107.8, 116.2, 118.3, 119.8, 121.1, 122.1, 123.1, 127.3, 127.9, 136.0, 141.0, 142.5, 145.5, 158.9, 164.5.

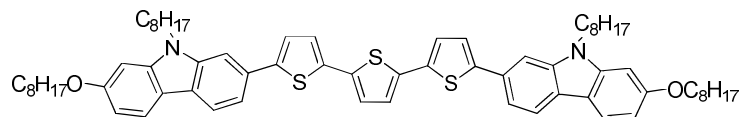
MS *m/z* (EI): 627, 1033 (M<sup>+</sup>, M 100).

Combustion analysis:

Expected: C 81.35%, H 8.58%, N 5.42%.

Obtained: C 81.36%, H 8.77%, N 5.36%.

**5,5''-bis-[9-Octyl-7-(octyloxy)-9-carbazol-2-yl]-2,2':5',2''-terthiophene (116).**



A mixture of palladium acetate (0.01 g,  $4.4 \times 10^{-4}$  mol), 5,5''-dibromo-2,2':5',2''-terthiophene (**36**) (0.25 g,  $6.1 \times 10^{-3}$  mol), 9-octyl-7-(octyloxy)-9-carbazol-2-boronic acid (**114**) (0.70 g, 0.001 mol), potassium carbonate (0.42 g, 0.003 mol) and water (3 cm<sup>3</sup>) in DMF (5 cm<sup>3</sup>) was heated under reflux at 80 °C overnight. The reaction mixture allowed to cool to RT, poured into water (200 cm<sup>3</sup>) and the crude product extracted into dichloromethane (2 x 150 cm<sup>3</sup>). The combined organic extracts were washed with brine (2 x 200 cm<sup>3</sup>), dried (MgSO<sub>4</sub>), filtered and concentrated under reduced pressure. Purification of the crude product was carried out *via* column chromatography [silica gel, dichloromethane: hexane, 3 : 4] and recrystallisation from a DCM/MeOH to yield the desired product as an orange solid (0.50 g, 78%).

Transition temp. /°C: Cr 165 N 198 I.

<sup>1</sup>H NMR (CDCl<sub>3</sub>) δ<sub>H</sub>: 0.87 (6H, t, *J* = 7.1 Hz), 0.91 (6H, t, *J* = 6.5 Hz), 1.30-1.48 (40H, m), 1.86 (8H, quint, *J* = 6.5 Hz), 4.08 (4H, t, *J* = 6.5 Hz), 4.25 (4H, t, *J* = 7.1 Hz), 6.83-6.85 (4H, m), 7.14 (2H, s), 7.19 (2H, d, *J* = 3.8 Hz), 7.31 (2H, d, *J* = 3.8 Hz), 7.45 (2H, dd, *J* = 1.2, 8.3 Hz), 7.52 (2H, s), 7.91 (2H, d, *J* = 7.9 Hz), 7.96 (2H, d, *J* = 8.9 Hz).

<sup>13</sup>C NMR (CDCl<sub>3</sub>): 14.0, 22.6, 27.2, 28.7, 29.2, 29.4, 30.9, 31.8, 43.0, 68.5, 94.0, 105.4, 107.8, 116.5, 117.1, 119.7, 121.0, 122.8, 123.4, 124.0, 124.5, 130.2, 135.7, 136.1, 140.9, 142.5, 144.8, 158.7.

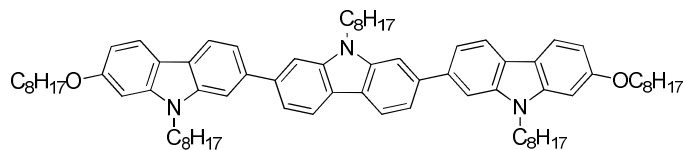
MS *m/z* (EI): 551, 812, 1059 (M<sup>+</sup>, M 100).

Combustion analysis:

Expected: C 77.08%, H 8.18%, N 2.64%.

Obtained: C 77.16%, H 8.25%, N 2.52%.

**9,9',9''-Trioctyl-7,7''-bis-(octyloxy)-2,2':7',2''-tercarbazole (117).**



A mixture of palladium acetate (0.01 g,  $4.4 \times 10^{-4}$  mol), 2,7-dibromo-9-octyl-9-carbazole (**42**) (0.25 g, 0.0006 mol), 9-octyl-7-(octyloxy)-9-carbazol-2-boronic acid (**114**) (0.60 g, 0.001 mol), potassium carbonate (0.32 g, 0.002 mol) and water (3 cm<sup>3</sup>) in DMF (5 cm<sup>3</sup>) was heated under reflux at 80 °C overnight. The reaction mixture allowed to cool to RT, poured into water (200 cm<sup>3</sup>) and the crude product extracted into dichloromethane (2 x 150 cm<sup>3</sup>). The combined organic extracts were washed with brine (2 x 200 cm<sup>3</sup>), dried (MgSO<sub>4</sub>), filtered and concentrated under reduced pressure. Purification of the crude product was carried out *via* column chromatography [silica gel, dichloromethane: hexane, 1 : 9] and recrystallisation from acetone to yield the desired product as a colourless solid (0.50 g, 76%).

Transition temp. /°C: Tg 72 Cr 90 N 109 I.

<sup>1</sup>H NMR (CDCl<sub>3</sub>) δ<sub>H</sub>: 0.82 (3H, t, *J* = 6.9 Hz), 0.85 (6H, t, *J* = 6.7 Hz), 0.90 (6H, t, *J* = 6.7 Hz), 1.25-1.54 (48H, m), 1.83-2.01 (12H, m), 4.10 (4H, t, *J* = 6.5 Hz), 4.32 (4H, t, *J* = 7.3 Hz), 4.45 (2H, t, *J* = 6.9 Hz), 6.80-6.89 (4H, m), 7.57 (2H, dd, *J* = 1.1, 6.1 Hz), 7.61 (2H, dd, *J* = 1.1, 5.9 Hz), 7.65 (2H, s), 7.69 (2H, s), 7.98 (2H, d, *J* = 8.3 Hz), 8.07 (2H, d, *J* = 7.9 Hz), 8.20 (2H, d, *J* = 7.9 Hz).

<sup>13</sup>C NMR (CDCl<sub>3</sub>): 14.0, 22.6, 26.1, 27.3, 29.2, 29.3, 29.4, 29.5, 31.8, 43.0, 68.5, 94.0, 107.5, 107.6, 116.5, 119.1, 119.6, 120.4, 121.0, 121.7, 122.2, 138.9, 140.3, 141.1, 141.5, 142.4, 158.5.

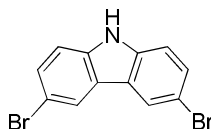
MS *m/z* (EI): 978, 1090 (M<sup>+</sup>, M 100), 1091.

Combustion analysis:

Expected: C 83.69%, H 9.52%, N 3.85%.

Obtained: C 83.88%, H 9.78%, N 3.83%.

### 3,6-Dibromocarbazole (**118**).



A solution of *N*-bromosuccinimide (NBS) (10.85 g, 0.060 mmol) in toluene (70 cm<sup>3</sup>) was added dropwise to a solution of carbazole (**1**) (5.00 g, 0.036 mmol) in toluene (100 cm<sup>3</sup>) and stirred at room temperature for 30 minutes. The reaction mixture was poured into cold methanol (200 cm<sup>3</sup>) and the resulting precipitate was filtered off. This precipitate was then purified *via* stirring in methanol before being filtered off and dried to yield the desired product as a light gray solid (4.10 g, 70%).<sup>32</sup>

Melting point /°C: 204-208.

<sup>1</sup>H NMR ((CD<sub>3</sub>)<sub>2</sub>SO) δ<sub>H</sub>: 7.39 (2H, d, *J* = 8.1 Hz), 7.46 (2H, dd, *J* = 2.2, 8.3 Hz), 8.35 (2H, d, *J* = 2.0 Hz), 11.59 (1H, s).

MS *m/z* (EI): 323 (M<sup>+</sup>, M 100).

### 3,6-Dibromo-9-octyl-carbazole (**119**).



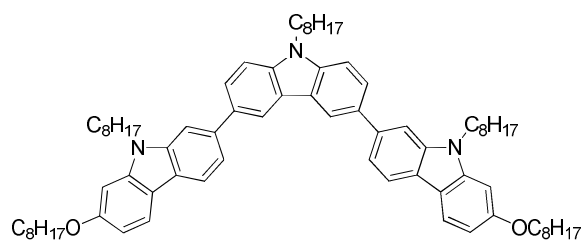
A solution of compound 3,6-dibromocarbazole (**118**) (2.51 g, 0.008 mol), tetra-*n*-butylammonium bromide (TBAB) (0.10 g, 0.0003 mol), 1-bromooctane (2.40 g, 0.012 mol), potassium hydroxide (0.82 g, 0.014 mol) in acetone (25 cm<sup>3</sup>) was refluxed for 6 h. The reaction mixture allowed to cool to RT, the resulting reaction mixture was filtered and the filtrate was concentrated under reduced pressure. The crude product was purified by recrystallization with ethanol to afford the desired product as a white solid (3.21 g, 95%).<sup>32</sup>

Melting point /°C: 84-87.

<sup>1</sup>H NMR (CDCl<sub>3</sub>) δ<sub>H</sub>: 0.86 (3H, t, *J* = 6.7 Hz), 1.25-1.22 (10H, m), 1.85-1.78 (2H, quint, *J* = 7.1 Hz), 4.23 (2H, t, *J* = 7.2 Hz), 7.25 (2H, d, *J* = 8.8 Hz), 7.54 (2H, d, *J* = 8.8 Hz), 8.13 (2H, s).

MS m/z (EI): 436 ( $M^+$ , M 100).

**9,9',9''-Trioctyl-7,7''-bis-(octyloxy)-2,3':6',2''-tercarbazole (120).**



A mixture of palladium acetate (0.01 g,  $4.4 \times 10^{-4}$  mol), 3,6-dibromo-9-octylcarbazole (**119**) (0.20 g, 0.0006 mol), 9-octyl-7-(octyloxy)-9-carbazol-2-boronic acid (**114**) (0.60 g, 0.001 mol), potassium carbonate (0.32 g, 0.002 mol) and water (3 cm<sup>3</sup>) in DMF (5 cm<sup>3</sup>) was heated under reflux at 80 °C overnight. The reaction mixture allowed to cool to RT, poured into water (200 cm<sup>3</sup>) and the crude product extracted into dichloromethane (2 x 100 cm<sup>3</sup>). The combined organic extracts were washed with brine (2 x 100 cm<sup>3</sup>), dried (MgSO<sub>4</sub>), filtered and concentrated under reduced pressure. Purification of the crude product was carried out *via* column chromatography [silica gel, dichloromethane: hexane, 1 : 9] to yield the desired product as a colourless solid (0.46 g, 69%).

Melting point /°C: 57.

<sup>1</sup>H NMR (CDCl<sub>3</sub>) δ<sub>H</sub>: 0.82 (3H, t,  $J = 6.9$  Hz), 0.86 (6H, t,  $J = 6.9$  Hz), 0.87 (6H, t,  $J = 6.9$  Hz), 1.26-1.51 (48H, m), 1.83-1.97 (12H, m), 4.10 (4H, t,  $J = 6.5$  Hz), 4.31 (4H, t,  $J = 7.3$  Hz), 4.38 (2H, t,  $J = 7.1$  Hz), 6.84-6.88 (4H, m), 7.53 (2H, d,  $J = 8.5$  Hz), 7.59 (2H, dd,  $J = 1.8, 7.1$  Hz), 7.64 (2H, s), 7.85 (2H, dd,  $J = 1.6, 7.7$  Hz), 7.96 (2H, d,  $J = 8.3$  Hz), 8.06 (2H, d,  $J = 8.1$  Hz), 8.49 (2H, d,  $J = 1.6$  Hz).

<sup>13</sup>C NMR (CDCl<sub>3</sub>): 14.0, 26.1, 29.2, 29.3, 29.4, 29.5, 31.8, 43.0, 68.5, 94.0, 107.1, 107.4, 109.0, 116.6, 118.9, 119.2, 119.6, 120.8, 121.7, 123.5, 127.0, 133.6, 138.8, 140.2, 141.3, 142.2, 158.5.

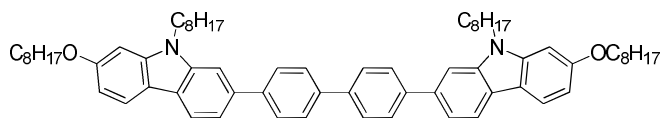
MS m/z (EI): 1090 ( $M^+$ , M 100), 1091.

Combustion analysis:

Expected: C 83.69%, H 9.52%, N 3.85%.

Obtained: C 83.89%, H 9.81%, N 3.67%.

**4,4'-bis-(9-Octyl-7-octyloxy-carbazol-2-yl)-1,1'-biphenyl (121).**



A mixture of palladium acetate (0.01 g,  $4.4 \times 10^{-4}$  mol), 4,4'-dibromo-1,1'-biphenyl (**39**) (0.20 g, 0.0006 mol), 9-octyl-7-(octyloxy)-9-carbazol-2-boronic acid (**114**) (0.72 g, 0.001 mol), potassium carbonate (0.45 g, 0.003 mol) and water (3 cm<sup>3</sup>) in DMF (5 cm<sup>3</sup>) was heated under reflux at 80 °C overnight. The reaction mixture allowed to cool to RT, poured into water (150 cm<sup>3</sup>) and the crude product extracted into dichloromethane (2 x 100 cm<sup>3</sup>). The combined organic extracts were washed with brine (2 x 100 cm<sup>3</sup>), dried (MgSO<sub>4</sub>), filtered and concentrated under reduced pressure. Purification of the crude product was carried out *via* column chromatography [silica gel, dichloromethane: hexane, 2 : 4] to yield the desired product as a white solid (0.41 g, 60%).

Transition temp. /°C: Cr 141 N 222 I.

<sup>1</sup>H NMR (CDCl<sub>3</sub>) δ<sub>H</sub>: 0.86 (6H, t, *J* = 6.9 Hz), 0.92 (6H, t, *J* = 6.7 Hz), 1.25-1.50 (40H, m), 1.86 (8H, quint, *J* = 7.5 Hz), 4.09 (4H, t, *J* = 6.5 Hz), 4.29 (4H, t, *J* = 7.0 Hz), 6.84-6.87 (4H, m), 7.51 (2H, dd, *J* = 2.6, 7.9 Hz), 7.59 (2H, s), 7.82 (8H, d, *J* = 8.3 Hz), 7.96 (2H, d, *J* = 8.1 Hz), 8.06 (2H, d, *J* = 7.9 Hz).

<sup>13</sup>C NMR (CDCl<sub>3</sub>): 14.1, 22.6, 29.2, 29.3, 29.4, 29.5, 31.8, 57.0, 68.5, 94.0, 106.8, 107.6, 116.4, 118.4, 119.6, 121.0, 122.4, 127.3, 128.0, 137.1, 139.2, 141.1, 141.3, 142.4, 158.6.

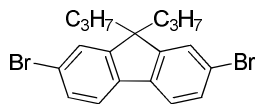
MS *m/z* (EI): 964, 965 (M<sup>+</sup>, M 100).

Combustion analysis:

Expected: C 84.60%, H 9.19%, N 2.90%.

Obtained: C 84.37%, H 9.32%, N 2.85%.

### 2,7-Dibromo-9,9-dipropyl-fluorene (**123**).



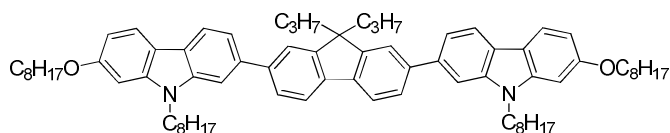
Powdered potassium hydroxide (7.37 g, 0.130 mol) was added in small portions to a solution of 2,7-dibromofluorene (**122**) (5.00 g, 0.015 mol), 1-bromopropane (3.81 g, 0.031 mol) and potassium iodide (0.25 g, 0.0015 mol) in DMSO (50 cm<sup>3</sup>) at RT. The deep purple reaction mixture was stirred for 3 h then poured into water (200 cm<sup>3</sup>). The crude product extracted into hexane (2 x 100 cm<sup>3</sup>). The combined organic extracts were washed with brine (200 cm<sup>3</sup>), dried (MgSO<sub>4</sub>), filtered and concentrated under reduced pressure. Purification was carried out *via* column chromatography [silica gel, hexane] and recrystallisation from EtOH to yield the desired product as a white crystalline solid (4.58 g, 75%).

Melting Point /°C: 136-138 (Lit 137-138).<sup>24-25</sup>

<sup>1</sup>H NMR (CDCl<sub>3</sub>) δ<sub>H</sub>: 0.66 (6H, t, *J* = 7.3 Hz), 0.71 (4H, m), 2.00 (4H, t, *J* = 8.0 Hz), 7.45 (2H, d, *J* = 8.4 Hz), 7.48 (2H, dd, *J* = 1.0, 8.0 Hz), 7.51 (2H, d, *J* = 1.0 Hz).

MS *m/z* (EI): 163, 176, 189, 202, 248, 256, 284, 323, 336, 365, 411, 409 (M<sup>+</sup>, M 100).

### 7,7'-(9,9-Dipropyl-fluorene-2,7-diyl)-bis-(9-octyl-2-octyloxy-carbazole) (**124**).



A mixture of palladium acetate (0.01 g, 4.4 x 10<sup>-4</sup> mol), 2,7-dibromo-9,9-dipropyl-fluorene (**123**) (0.20 g, 0.0005 mol), 9-octyl-7-(octyloxy)-9-carbazol-2-boronic acid (**114**) (0.55 g, 0.001 mol), potassium carbonate (0.45 g, 0.003 mol) and water (5 cm<sup>3</sup>) in DMF (10 cm<sup>3</sup>) was heated under reflux at 80 °C overnight. The reaction mixture allowed to cool to RT, poured into water (200 cm<sup>3</sup>) and the crude product extracted into dichloromethane (2 x 100 cm<sup>3</sup>). The combined organic extracts were washed with brine (2 x 100 cm<sup>3</sup>), dried (MgSO<sub>4</sub>), filtered and concentrated under reduced pressure. Purification of the crude product was carried out *via* column chromatography [silica gel, dichloromethane: hexane, 1 : 9] to yield the desired product as a colourless solid (0.42 g, 79%).

Transition temp. /°C: Cr 52 N 60 I.

<sup>1</sup>H NMR (CDCl<sub>3</sub>) δ<sub>H</sub>: 0.73 (6H, t, *J* = 7.3 Hz), 0.84 (6H, t, *J* = 6.9 Hz), 0.94 (6H, t, *J* = 6.7 Hz), 1.27-1.37 (44H, m), 1.83-1.94 (8H, m), 2.07-2.11 (4H, quint, *J* = 6.5 Hz), 4.09 (4H, t, *J* = 6.5 Hz), 4.31 (4H, t, *J* = 7.3 Hz), 6.85-6.88 (4H, m), 7.52 (2H, dd, *J* = 2.2, 8.1 Hz), 7.59 (2H, s), 7.71 (4H, d, *J* = 8.3 Hz), 7.82 (2H, d, *J* = 7.7 Hz), 7.98 (2H, d, *J* = 8.3 Hz), 8.06 (2H, d, *J* = 8.6 Hz).

<sup>13</sup>C NMR (CDCl<sub>3</sub>): 14.1, 14.6, 17.0, 22.6, 26.0, 27.3, 29.2, 29.3, 29.4, 31.8, 42.9, 43.0, 55.4, 68.5, 94.0, 106.9, 107.6, 116.5, 118.6, 119.6, 119.8, 121.0, 122.0, 122.3, 126.4, 138.2, 139.7, 141.2, 142.4, 151.7, 158.6.

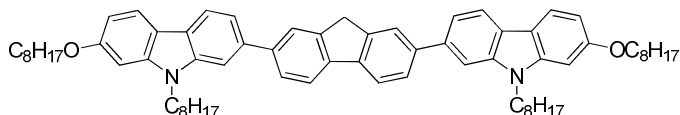
MS *m/z* (EI): 1059, 1061 (M<sup>+</sup>, M 100).

Combustion analysis:

Expected: C 84.85%, H 9.49%, N 2.64%.

Obtained: C 85.01%, H 9.78%, N 2.60%.

### 2,7-bis-(9-Octyl-7-octyloxy-carbazol-2-yl)-fluorene (125).



A mixture of palladium acetate (0.01 g,  $4.4 \times 10^{-4}$  mol), 2,7-dibromo-fluorene (**122**) (0.06 g,  $1.8 \times 10^{-3}$  mol), 9-octyl-7-(octyloxy)-9-carbazol-2-boronic acid (**114**) (0.20 g,  $4.4 \times 10^{-3}$  mol), potassium carbonate (0.06 g,  $4.3 \times 10^{-4}$  mol) and water (5 cm<sup>3</sup>) in DMF (10 cm<sup>3</sup>) was heated under reflux at 80 °C overnight. The reaction mixture allowed to cool to RT, poured into water (100 cm<sup>3</sup>) and the crude product extracted into dichloromethane (2 x 50 cm<sup>3</sup>). The combined organic extracts were washed with brine (2 x 50 cm<sup>3</sup>), dried (MgSO<sub>4</sub>), filtered and concentrated under reduced pressure. Purification of the crude product was carried out *via* column chromatography [silica gel, dichloromethane: hexane, 2 : 4] to yield the desired product as a colourless solid (0.15 g, 83%).

Transition temp. /°C: Cr 127 N 198 I.

$^1\text{H}$  NMR ( $\text{CDCl}_3$ )  $\delta_{\text{H}}$ : 0.86 (6H, t,  $J = 7.1$  Hz), 0.90 (6H, t,  $J = 6.5$  Hz), 1.25-1.39 (40H, m), 1.90 (8H, quint,  $J = 6.7$  Hz), 4.07-4.10 (6H, m), 4.28 (4H, t,  $J = 7.1$  Hz), 6.84-6.87 (4H, m), 7.52 (2H, dd,  $J = 1.0, 7.1$  Hz), 7.59 (2H, s), 7.74 (2H, d,  $J = 8.9$  Hz), 7.91 (4H, d,  $J = 7.3$  Hz), 8.94 (2H, d,  $J = 8.1$  Hz), 8.03 (2H, d,  $J = 8.1$  Hz).

$^{13}\text{C}$  NMR ( $\text{CDCl}_3$ ): 14.0, 22.6, 28.8, 29.1, 29.3, 29.4, 31.8, 37.1, 43.0, 68.5, 94.0, 107.0, 107.5, 116.6, 118.6, 119.6, 120.0, 121.0, 122.2, 124.1, 126.4, 138.0, 140.3, 141.0, 141.1, 142.3, 144.0, 158.5.

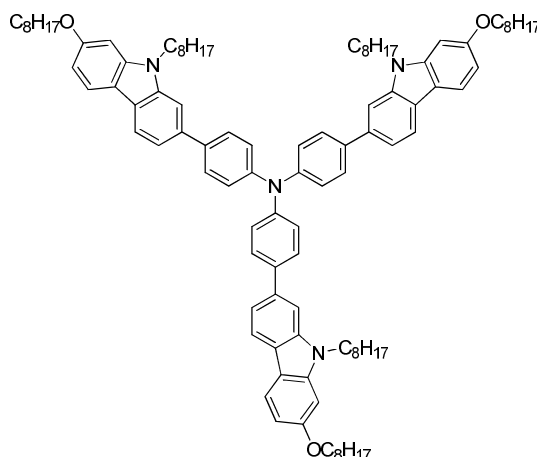
MS  $m/z$  (EI): 864, 977 ( $\text{M}^+$ ,  $\text{M} 100$ ), 978.

Combustion analysis:

Expected: C 84.79%, H 9.07%, N 2.87%.

Obtained: C 84.63%, H 9.36%, N 2.75%.

***tris***-{4-[9-Octyl-7-(octyloxy)-carbazol-2-yl]phenyl}amine (**127**).



A mixture of palladium acetate (0.01 g,  $4.4 \times 10^{-4}$  mol), *tris*-(4-bromophenyl)amine (**126**) (0.20 g, 0.0004 mol), 9-octyl-7-(octyloxy)-9-carbazol-2-boronic acid (**114**) (0.66 g, 0.001 mol), potassium carbonate (0.41 g, 0.003 mol) and water (5  $\text{cm}^3$ ) in DMF (10  $\text{cm}^3$ ) was heated under reflux at 80  $^\circ\text{C}$  overnight. The reaction mixture allowed to cool to RT, poured into water (200  $\text{cm}^3$ ) and the crude product extracted into dichloromethane (2 x 100  $\text{cm}^3$ ). The combined organic extracts were washed with brine (2 x 100  $\text{cm}^3$ ), dried ( $\text{MgSO}_4$ ), filtered and concentrated under reduced pressure. Purification of the crude product was carried out *via* column chromatography [silica gel, dichloromethane: hexane, 1 : 4] to yield the desired product as a light yellow solid (0.45 g, 75%).

Melting point /°C: 111.

<sup>1</sup>H NMR (CDCl<sub>3</sub>) δ<sub>H</sub>: 0.82-0.90 (18H, m), 1.20-1.42 (60H, m), 1.88 (12H, quint, *J* = 6.73 Hz), 4.08 (6H, t, *J* = 6.7 Hz), 4.29 (6H, t, *J* = 7.1 Hz), 6.83-6.86 (6H, m), 7.32 (6H, d, *J* = 8.5 Hz), 7.44 (3H, dd, *J* = 1.2, 8.1 Hz), 7.51 (3H, s), 7.65 (6H, d, *J* = 8.5 Hz), 7.96 (3H, d, *J* = 8.3 Hz), 8.03 (3H, d, *J* = 8.1 Hz).

<sup>13</sup>C NMR (CDCl<sub>3</sub>): 14.1, 19.5, 22.6, 22.7, 27.3, 29.2, 29.4, 31.8, 43.0, 68.5, 94.0, 105.0, 107.5, 116.5, 118.0, 119.6, 120.9, 122.0, 127.0, 129.0, 136.0, 138.0, 141.2, 142.3, 148.0, 158.5.

MS m/z (EI): 813, 980, 1056, 1349, 1461 (M<sup>+</sup>, M 100).

Combustion analysis:

Expected: C 83.79%, H 9.10%, N 3.83%.

Obtained: C 84.01%, H 9.22%, N 3.60%.

### 3.5 References

1. A. J. Shusterman, N. G. Mcdougal and A. Glasfeld, *J. Chem. Educ.*, 1997, **74**, 1222.
2. D. J. Schipper and K. Fagnou, *Chem. Mater.*, 2011, **23**, 1594.
3. H. Y. Fu, L. Chen and H. Doucet, *J. Org. Chem.*, 2012, **77**, 4473.
4. L. G. Mercier and M. Leclerc, *Acc. Chem. Res.*, 2013, **46**, 597.
5. N. Miyaura, T. Yangai and A. Suzuki, *Synth. Commun.*, 1981, **11**, 513.
6. R. M. Kellog, A. P. Schapp, E. T. Harper and H. Wynberg, *J. Org. Chem.*, 1968, **33**, 2902.
7. A. G. Mistry, K. Smith and M. R. Bye, *Tetrahedron. Lett.*, 1986, **9**, 1051.
8. J. K. Stille, *Angew. Chem. Int. Ed. Eng.*, 1986, **25**, 508.
9. P. T. Boudreault, S. Beaupre and M. Leclerc, *Polym. Chem.*, 2010, **1**, 27.
10. A. W. Freeman, M. Urvoy and M. E. Criswell, *J. Org. Chem.*, 2005, **70**, 5014.
11. Y. Fujinami, J. Kuwabara, W. Lu, H. Hayashi and T. Kanbara, *Macromol. Lett.*, 2012, **1**, 67.
12. P. M. Beaujuge, H. N. Tsao, M. R. Hansen, C. M. Amb, C. Risko, J. Subbiah, K. R. Choudhury, A. Mavrinskiy, W. Pisula, J. L. Brédas, F. So, K. Müllen and J. R. Reynolds, *J. Am. Chem. Soc.*, 2012, **134**, 8944.
13. J. Mei, K. R. Graham, R. Stalderand and J. R. Reynolds, *Org. Lett.*, 2010, **12**, 660.
14. L. L. Miller and Y. Yu, *J. Org. Chem.*, 1995, **60**, 6813.
15. <http://www.organic-chemistry.org>, (accessed January 2014).
16. R. M. Kellog, A. Schapp and H. Wynberg, *J. Org. Chem.*, 1969, **34**, 343.
17. F. Dierschke, A. C. Grimsdale and K. Müllen, *Synthesis*, 2003, **16**, 2470.
18. J. Bouchard, S. Wakim and M. Leclerc, *J. Org. Chem.*, 2004, **69**, 5705.
19. X. Zhan, Y. Liu, X. Wu, S. Wang and D. Zhu, *Macromol.*, 2002, **35**, 2529.
20. P. Imin, M. Imit and A. Adronov, *Macromol.*, 2011, **44**, 9138.
21. A. M. Fraind and J. D. Tover, *J. Phys. Chem.*, 2010, **114**, 3104.

22. M. P. Aldred, P. Vlachos, A. E. A. Contoret, S. R. Farrar, B. Mansoor, K. L. Woon, R. Hudson, S. M. Kelly and M. O'Neill, *J. Mater. Chem.*, 2005, **15**, 3208.
23. J. W. Choi, C. Kulshreshtha, G. P. Kennedy, J. H. Kwona, S.H. Jung and M. Chae, *Solar. Energy. Mat and Solar Cells.*, 2011, **95**, 2069.
24. C. J. Kelley, A. Ghiorghis and J. M. Kauffman, *J. Chem. Res.*, 1997, **12**, 2701.
25. M. P. Aldred, R. Hudson, S. P. Kitney, P. Vlachos, A. Liedtke, K. L. Woon, M. O'Neill and S. M. Kelly, *Liq. Cryst.*, 2008, **35**, 413.
26. S. Lois, J. C. Florès, J. P. L. Porte, F. S. Spirau, J. J. E. Moreau, K. Miqueu, J. M. Sotiropoulos, P. Baylère, M. Tillard and C. Belin, *Euro. J. Org. Chem.*, 2007, **24**, 4019.
27. A. Midya, Z. Xie, J. X. Yang, Z. K. Chen, D. J. Blackwood, J. Wang, S. Adams and K. P. Loh, *Chem. Commun.*, 2010, **46**, 2091.
28. R. Grisorio, A. D. Aquila, G. Romanazzi, G. P. Suranna, P. Mastrorilli, P. Cosma, D. Acierno, E. Amendola, G. Ciccarella and C. F. Nobile, *Tetrahedron.*, 2006, **62**, 627.
29. M. Melucci, G. Barbarella, M. Zambianchi, P. Di Pietro and A. Bongini, *J. Org. Chem.*, 2004, **69**, 4821.
30. A. Kudelko and M. Wróblowska, *Tetrahedron. Lett.*, 2011, **55**, 3252.
31. S. R. Gagné, C. Curutchet, F. Grenier, G. Scholes and J. F. Morin, *Tetrahydron.*, 2010, **66**, 4230.
32. L. Zhang, S. Zeng, L. Yin, C. Ji, K. Li, Y. Li and Y. Wang, *New. J. Chem.*, 2013, **37**, 632.
33. G. A. Mabbott, *J. Chem. Educ.*, 1983, **60**, 697.
34. P. A. Christensen and A. Hamnett, "Techniques and mechanisms in electro chemistry" Springer, 1994.
35. B. Geffroy, P. I. Roy and C. Prat, *Polym Int.*, 2006, **55**, 572.

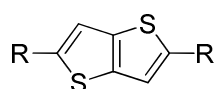
## 4. Results and Discussion

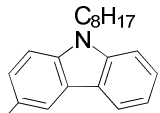
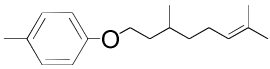
### 4.1 Derivatives incorporating 3-substituted carbazole rings

#### 4.1.1 Fused rings/carbazoles

The melting temperatures of 2,5-disubstituted-thieno[3,2-b]thiophenes **15** and **MD85**, differing in the nature of the moiety R in a terminal position of the aromatic core, are collated in Table 4.01.<sup>1</sup>

**Table 4.01** The melting temperatures (°C) of compounds **15** and **MD85**.



Compound	R	T <sub>g</sub>	Cr	I		
<b>15</b>		•	46	•	187	•
<b>MD85</b>		•	-	•	229	•

The presence of two 3-substituted carbazole moieties on the both ends of the molecule in **15** leads to a much lower melting point (by 42 °C) than that of **MD85** with alkyloxy benzene groups on the both ends of the molecule. Compound **15** exhibits a melting transition at 187 °C and forms a glassy state on cooling from the isotropic liquid after melting. Unfortunately, the presence of the branching alkyl groups attached to the carbazole also decreases the tendency for mesophase formation. Due to the bulky nature and ineffective packing of the carbazole moieties it decreases the melting point. Therefore, the compound **15** has a longer length-to-breadth ratio than the compound **MD85**. In contrast the DSC thermograph of **MD85** shows a melting transition at a much higher temperature (229 °C). No glass transition could be observed for this compound.

The presence of the two 3-substituted carbazole moieties on both ends of the molecule reduces the van der Waals forces of attraction between the molecular cores of adjacent molecules of compound **15**. The electron-donating strength of the 3-carbazole is stronger than the alkoxy benzebe groups of the compound **MD85**, in which the alkyl chain is attached to the oxygen atom. Compound **15** is expected to facilitate inter-

molecular interactions arising from  $\pi$ - $\pi$  stacking, due to the presence of the nitrogen atom, stronger intra-molecular charge transfer and more-planar conjugated backbone, and therefore improve the hole mobility. Therefore, the alkyl chain attached to the nitrogen atom is responsible for the lower melting point for compound **15**.

Compound **MD85** was found not to exhibit any liquid crystalline mesophases. The high degree of chain branching in the side chains of compound **MD85** probably hinders effective packing of the molecules as compared to compound **15**. This effect reduces the sum of van der Waals forces of attraction between the aromatic cores of adjacent molecules. The melting point of compound **MD85** is high, although the combined effect of four branching methyl groups in the chain should lead to relatively low melting points for such compounds with three aromatic rings, one of which is fused, in the aromatic core.

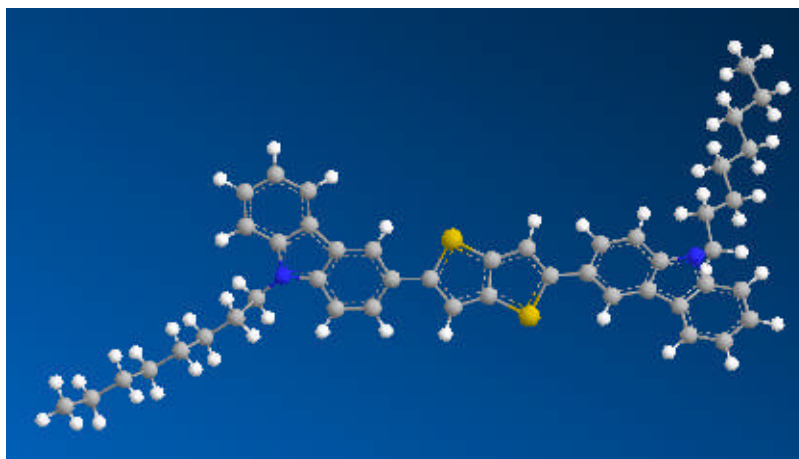


**Figure 4.01** MMFF94 optimised geometry of compound **15**.

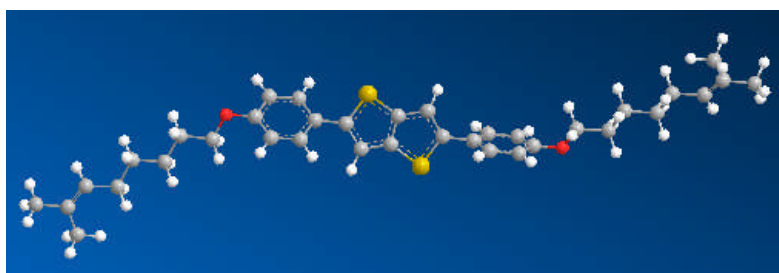


**Figure 4.02** MMFF94 optimised geometry of compound **MD85**.<sup>19</sup>

The glass transition and melting temperatures of the fused ring/carbazoles **5**, **7** and **15**, differing in the nature of the sulphur-containing rings in the centre of the aromatic core, are collated in Table 4.02.

**Table 4.02** Melting temperatures (°C) of the fused ring/carbazoles **5**, **7** and **15**.

Compound	R	T <sub>g</sub>	Cr	I		
<b>5</b>		•	64	•	168	•
<b>7</b>		•	76	•	190	•
<b>15</b>		•	46	•	187	•

None of the compounds shown in Table **4.02** exhibits an observable liquid crystalline mesophase. However, a glass transition above room temperature could be determined for each of these compounds after cooling from the isotropic liquid.

Compounds **7** and **15**, which incorporate a fused aromatic ring, have much higher melting temperatures than those of the compound **5** containing two 2,5-disubstituted thiophene rings. The low melting point of compound **5**, compared to that of the compounds **7** and **15**, is probably attributable to the lack of planarity of the two thiophene rings in the phases studied, due to freedom to rotate about the thiophene-thiophene bond, i.e., the higher melting points of compounds **7** and **15** are probably attributable to better  $\pi$ - $\pi$  stacking interactions arising from the cores that is not present in **5**.

These differences are more difficult to explain taking into account the non-coaxial and non-co-linear nature of the thiophene bonds in compounds **7** and **15**, whereas in compound **5** the thiophene ring bonds are parallel and co-linear, Figure 4.01 and 4.03. Therefore, the compound **5** has a longer length-to-breadth ratio than the compounds **7** and **15**. A combination of these steric effects leads to weaker van der Waals forces of attraction between neighbouring molecules and the anisotropy of dispersion forces and

the anisotropy of polarisability. A combination of these factors would lead to a much lower melting point of the compound **5**.<sup>2</sup>

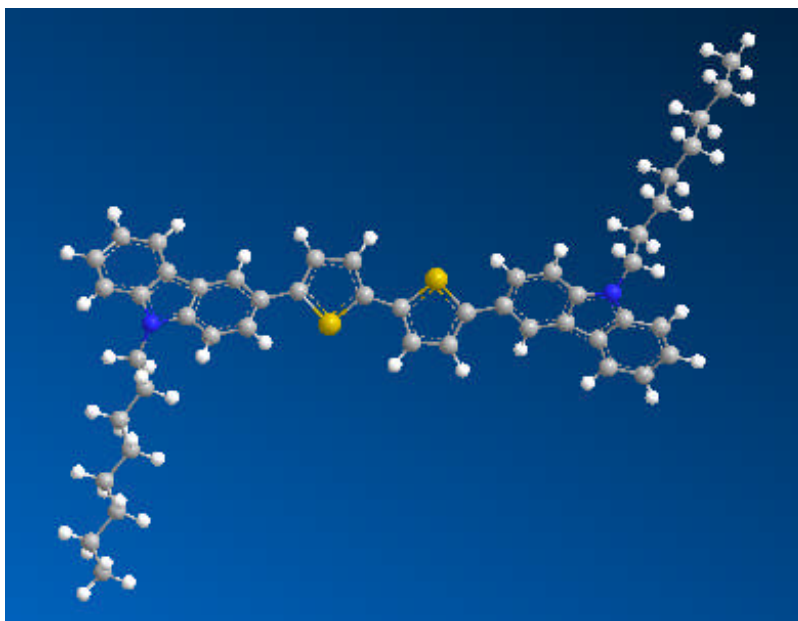


**Figure 4.03** MMFF94 optimised geometry of compound **5**.

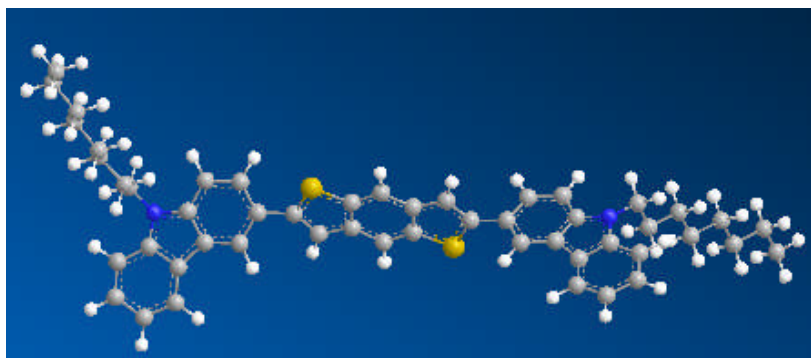


**Figure 4.04** MMFF94 optimised geometry of compound **7**.

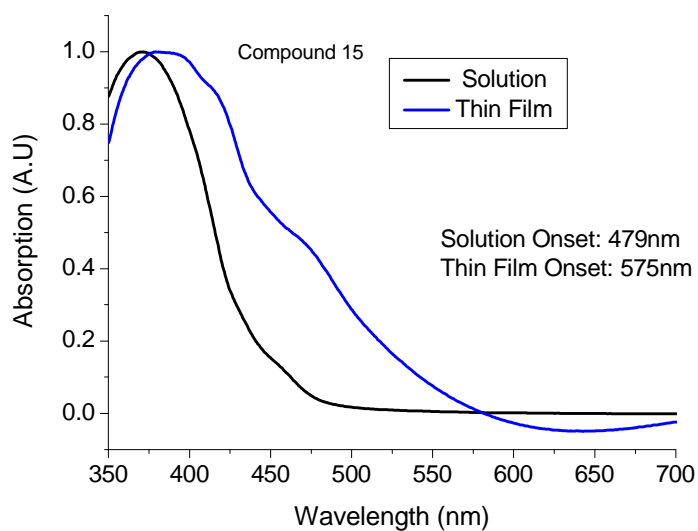


**Figure 4.05** UV-vis absorption spectra of compound **15**.

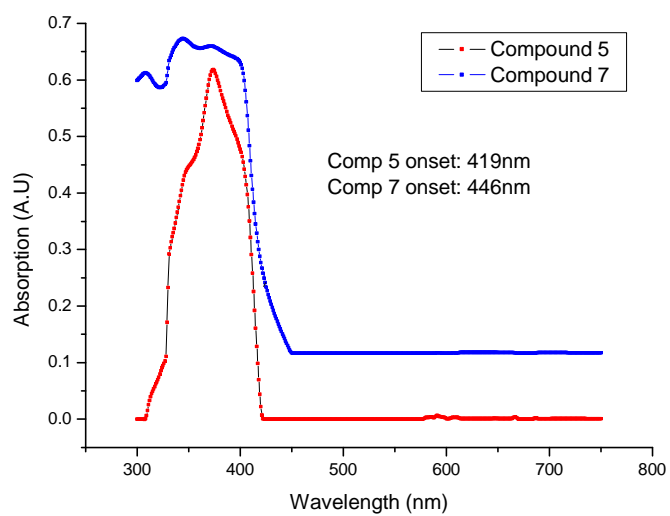


**Figure 4.06** UV-vis absorption spectra of compounds **5** (red) and **7** (blue) in solution.

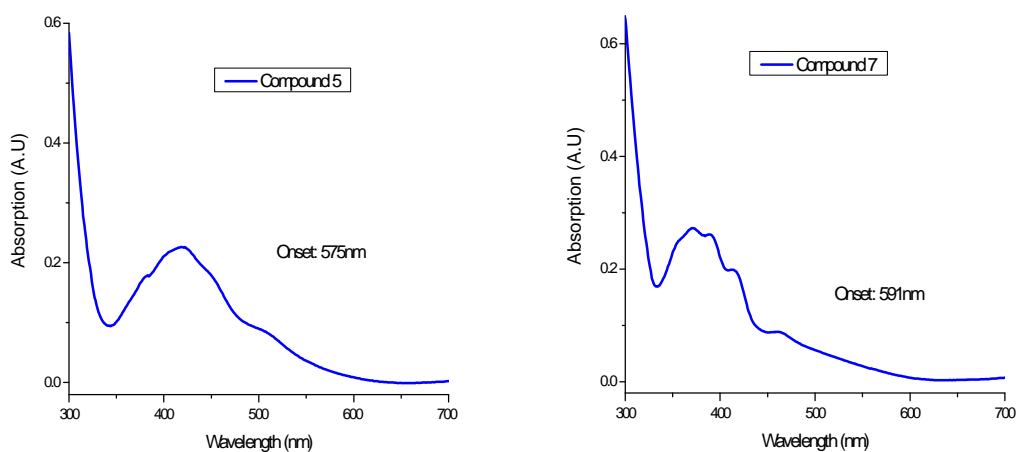
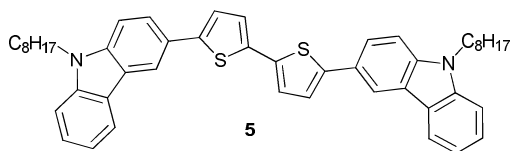


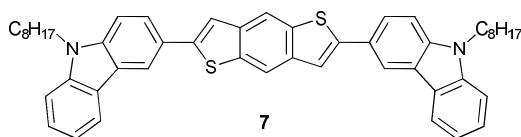
**Figure 4.07** UV-vis absorption spectra of compounds **5** and **7** in a thin film.

**Table 4.03** Band gap ( $E_g$ ), ionisation potential (IP) and electron affinity (EA) in eV of compound **5**.



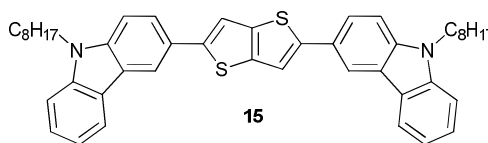
Compound <b>5</b>	IP	$E_g$	EA
Solution	5.30	2.96	2.33
Thin Film	5.30	2.00	3.30

**Table 4.04** Band gap ( $E_g$ ), ionisation potential (IP) and electron affinity (EA) in eV of compound **7**.



Compound <b>7</b>	IP	$E_g$	EA
Solution	5.41	2.78	2.62
Thin Film	5.41	2.10	3.30

**Table 4.05** Band gap ( $E_g$ ), ionisation potential (IP) and electron affinity (EA) in eV of compound **15** measured as a thin film and in solution.



Compound <b>15</b>	IP	$E_g$	EA
Solution	5.31	2.59	2.72
Thin Film	5.31	2.15	3.15

Tables 4.03-4.05 show the band gap ( $E_g$ ), ionisation potential (IP) and electron affinity (EA) determined in solution and in a thin film for the thiophene derivatives **5**, **7** and **15**, respectively. The UV-vis absorption spectra of compounds **5** and **7** in solution and in a thin film are shown in Figures 4.06 and 4.07, respectively.

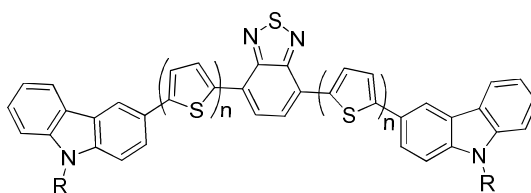
The band gap in solution of compound **15** is significantly smaller than that of compound **7**, which is in turn lower than that of compound **5**, as shown by the UV-vis absorption spectra of compounds **5** and **7** in solution and as a thin film, Figures 4.06 and 4.07. The differences in the band gap of the thin films for these compounds are much less significant. However, the differences between the values for each of the compounds **5**, **7** and **15** measured in a thin film are much lower than those measured in solution. These differences in the band gap may be due to strong van der Waal forces of attraction between the planar aromatic molecular cores, Figures 4.03 and 4.04, of these thiophene derivatives.

The ionisation potential of compounds **5** and **15** are very similar and a little lower than that of compound **7**. The similar ionisation potential of compounds **5** and **15** shows that when the two 2,5-disubstituted thiophene rings are fused to form the thienothiophene group it does not affect the IP, within the limits of experimental error.

#### 4.1.2 Benzothiadiazole/carbazoles

The glass transition and melting temperatures of the 4,7-disubstituted-benzo-1,2,5-thiadiazoles **11** and **24**, differing in the number (n) of the 2,5-disubstituted thiophene rings in the aromatic core and the chain R attached to the carbazole groups, are collated in Table 4.06.

**Table 4.06** The melting temperatures (°C) of 4,7-disubstituted-benzo-1,2,5- thiadiazoles **11** and **24**.



Compound	n	R	Tg	Cr	I		
<b>11</b>	1	C <sub>8</sub> H <sub>17</sub> -	•	56	•	307	•
<b>24</b>	2	(C <sub>2</sub> H <sub>5</sub> ) <sub>2</sub> CHC <sub>3</sub> H <sub>6</sub> -	•	74	•	343	•

The 4,7-disubstituted-benzo-1,2,5-thiadiazole **24**, with four 2,5-disubstituted thiophene rings in the centre of the aromatic molecular core (n = 2), exhibits a higher melting point (343 °C) and higher glass transition temperature (74 °C) than those (307 °C and 56 °C, respectively) of the corresponding benzothiadiazole compound **11**, with only two 2,5-disubstituted thiophene rings in the centre of the aromatic molecular core (n = 1), despite the presence of a branched ethylhexyl chain attached to the carbazole groups. The lower melting and glass transition temperatures of compound **11** as compared to those of compound **24** is probably due to the presence of thiophene rings of the benzothiadiazole lie more in the plane of the molecule with less inter-annular twisting, Figure 4.08 and 4.09 respectively. The modelling structure shows there is a much greater degree of inter-annular twisting between the benzothiadiazole and thiophene in the compound **24**.

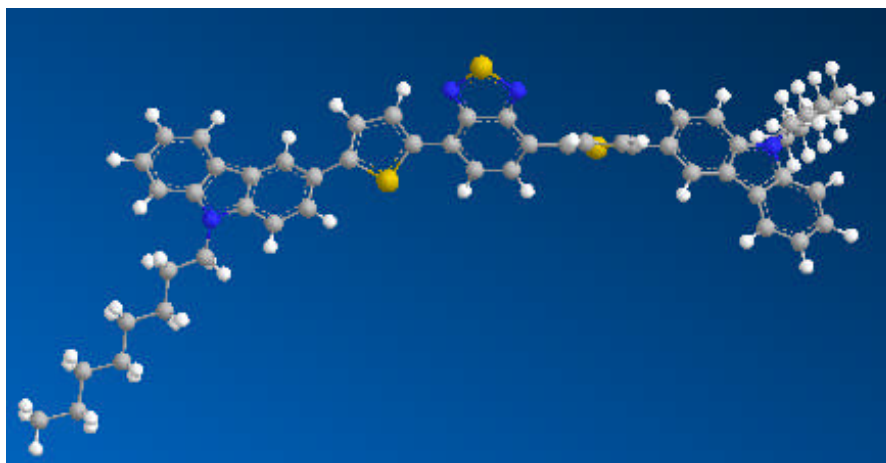


**Figure 4.08** MMFF94 optimised geometry of compound **11**.

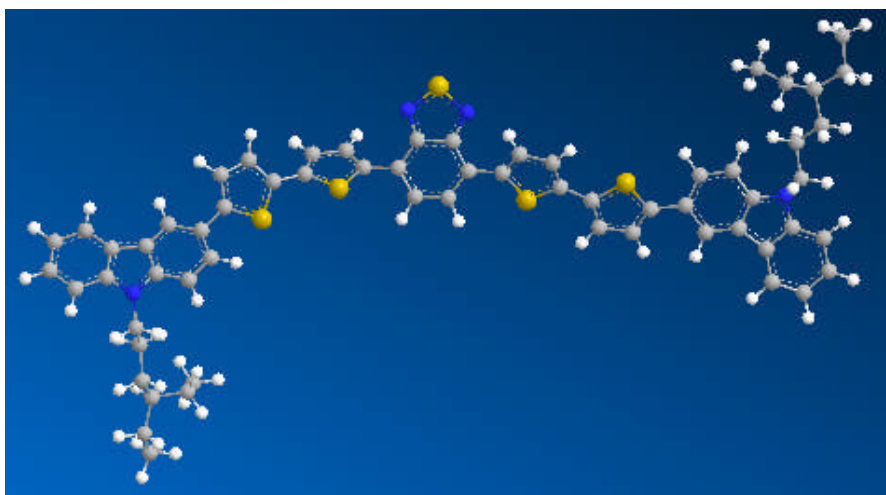


**Figure 4.09** MMFF94 optimised geometry of compound **24**.

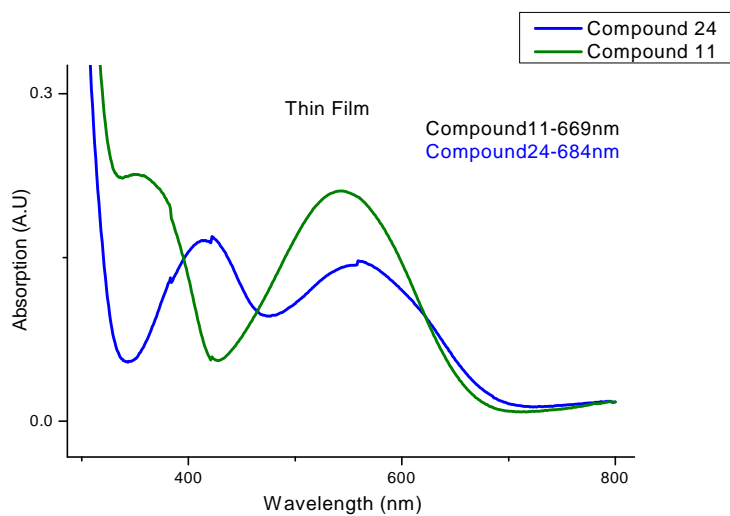
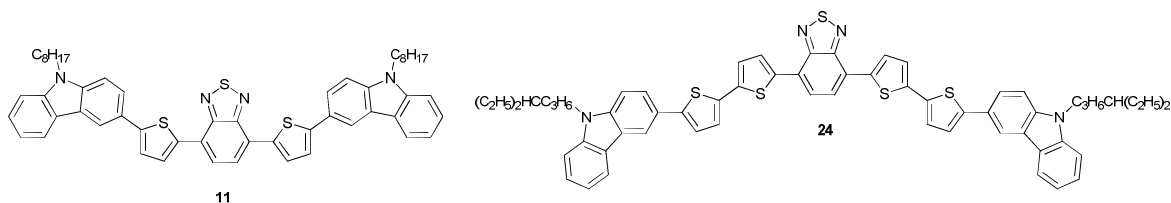


**Figure 4.10** UV-vis absorption spectra of compounds **11** and **24**.

**Table 4.07** Band gap ( $E_g$ ), ionisation potential (IP) and electron affinity (EA) in eV of compounds **11** and **24**.



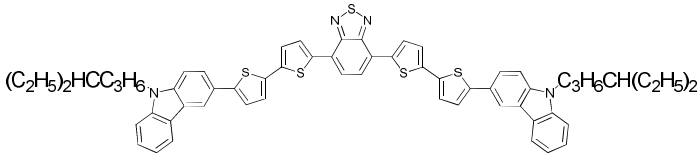
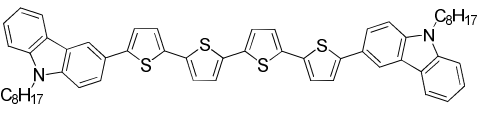
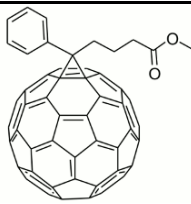
Compound (Thin Film)	IP	$E_g$	EA
<b>11</b>	5.31	1.85	3.45
<b>24</b>	5.25	1.81	3.44

The ionisation potential, electron affinity and band gap of the benzothiadiazole **11** and **24** are very similar as confirmed by UV-vis and cyclic voltammetry. Therefore, the presence of two additional 2,5-disubstituted thiophene rings in the molecular core of compound **24** compared to that of compound **11**, do not appear to affect the molecular energy levels to any significant degree. Similarly, the presence of the branched alkyl chain of compound **24** compared to the linear alkyl chain of compound **11**, does not appear to affect the molecular energy levels to any significant degree. This behaviour is consistent with the melting temperatures collated in Table 4.06. Both of these phenomena suggest that the presence of the alkyl chain does not affect the intermolecular separation of the aromatic molecular cores of the benzothiadiazoles **11** and **24**.

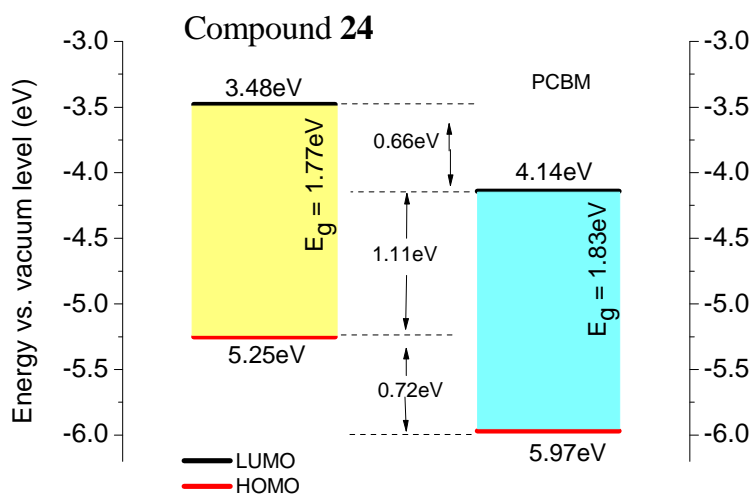
The UV-vis absorption spectrum shows that there are two main peaks of absorption with maximum of 420 nm and 660 nm. The first one at 660 nm is due to the interaction of carbazole moiety and the second one at 420 nm is due to benzothiadiazole moiety, Figure 4.10.<sup>3</sup>

Although the benzothiadiazoles **11** and **24** do not exhibit an observable mesophase, each one of them forms a stable glass and, as such, they are still suitable as an electron donor in organic solar cells. Therefore, a photovoltaic device was made using compound **24** as an electron donor and PCBM as an electron acceptor. A comparison of the performance

of OPV devices made using either compound **24** or **WB52** without a benzothiadiazole moiety in the centre of the molecular structure shows how the presence of the benzothiadiazole in the molecular core affects the performance of the device. The energy level diagram for both of the donor materials (compound **24** and **WB52**) with PCBM shows that the presence of the benzothiadiazole unit in the centre of the molecule reduces the energy band gap from 2.22 eV to 1.77 eV. A low band gap is one of the significant requirements for an organic photovoltaic device.<sup>4-5</sup>

Name	Structure	Energy levels (eV) CV Data
<b>24</b> (Donor)		HOMO = 5.25 LUMO = 3.48
<b>WB52<sup>a</sup></b> (Donor)		HOMO = 5.27 LUMO = 3.05
<b>PCBM</b> (Acceptor)		HOMO = 5.97 LUMO = 4.14

Notes for table<sup>a</sup>: Data from Weixiao Bao of the University of Hull.



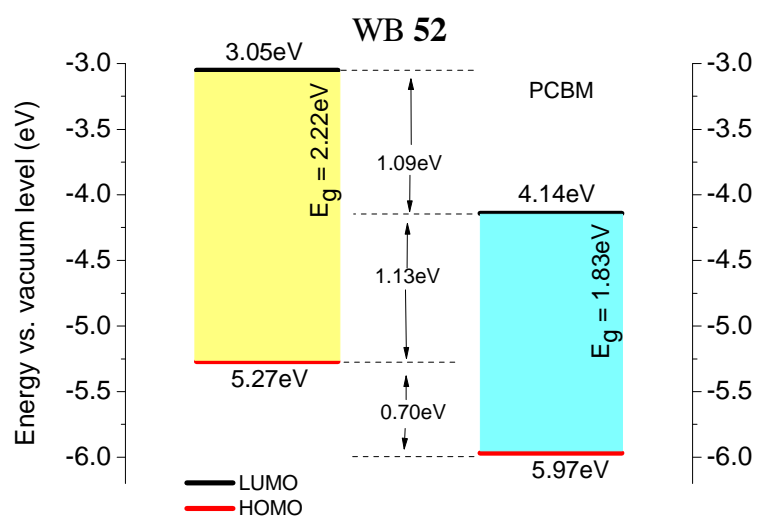


**Figure 4.11** Energy level diagram of compounds **24** and **WB52**.

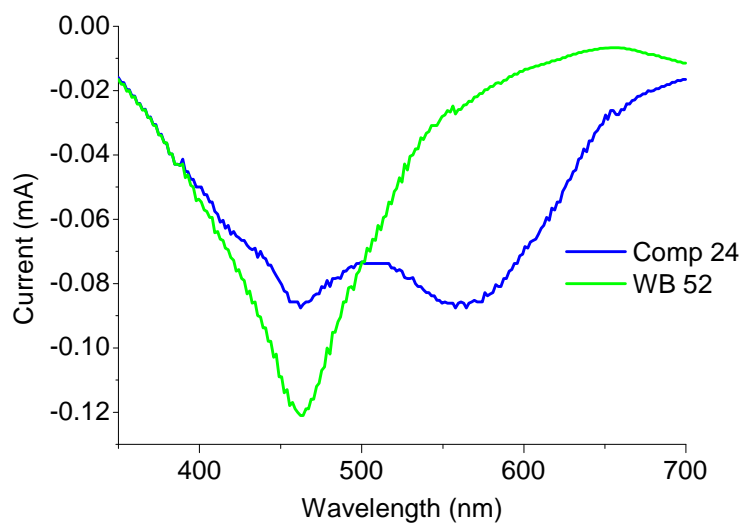


**Figure 4.12** Graph showing the difference in the current produced by photoelectric material composed of either compound **24** or **WB52**.

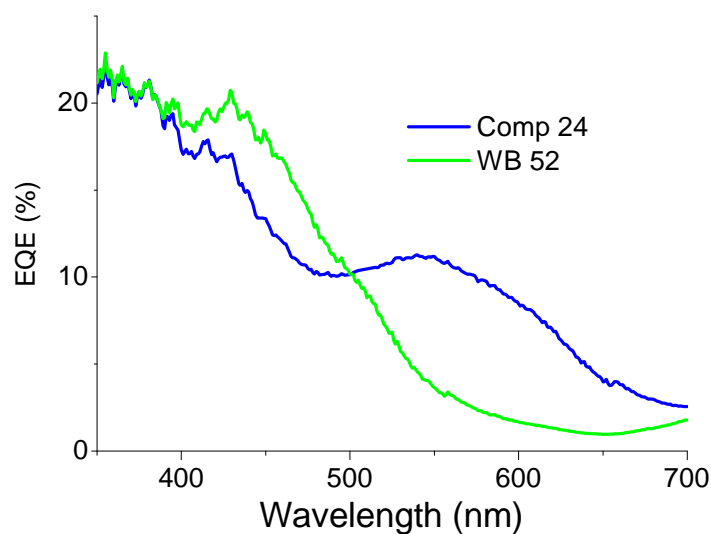


**Figure 4.13** A graph showing variation of external quantum efficiency, and reflectance with wavelength of **24** and **WB52**.

The graph in the Figure 4.12 shows the current produced by the compound **24** is much higher than that of compound **WB52**. Compound **24** strongly absorbs across most regions of the visible spectrum. External quantum efficiency has been observed to be high as well for compound **24**, Figures 4.13.

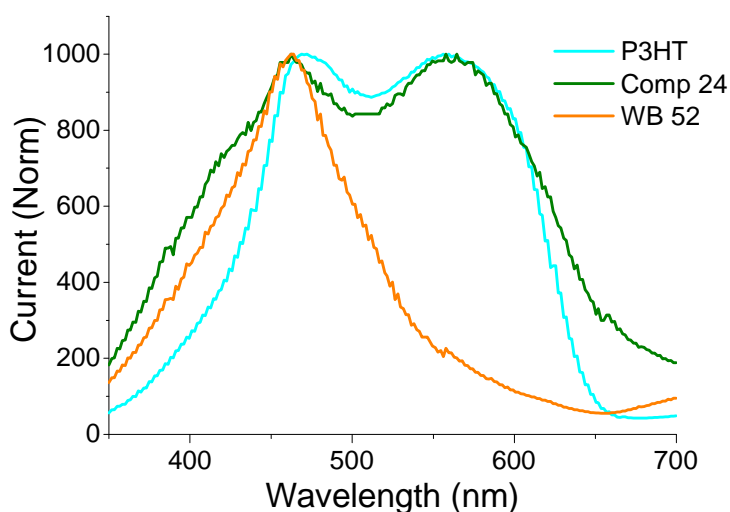


**Figure 4.14** Graph showing difference of current produced by photoelectric material between **24**, **WB52** and **P3HT**.

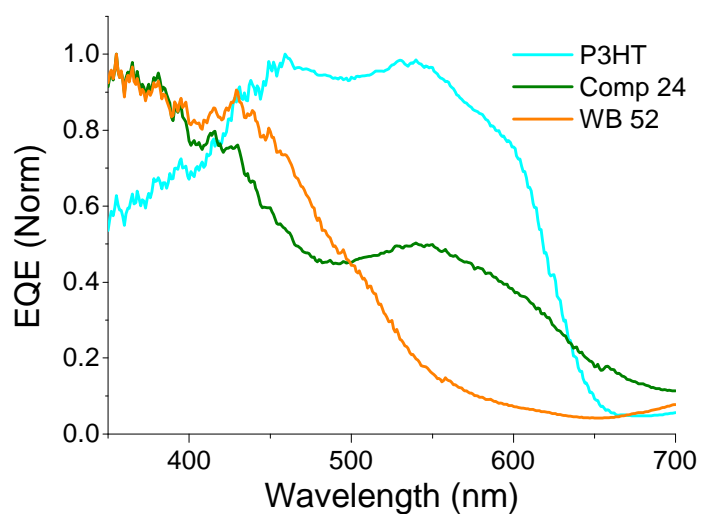


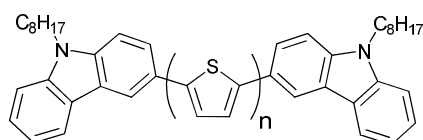
**Figure 4.15** A graph showing variation of external quantum efficiency and reflectance with wavelength of compounds **24**, **WB52** and **P3HT**.

Comparisons have been made between the compounds **24**, **WB52** and Poly(3-hexylthiophene-2,5-diyl) (**P3HT**). **P3HT** is commonly used as donor material in solar cells. The current produced by the compound **24** and external quantum efficiency are much higher than **WB52** and are very much comparable to **P3HT**, which absorbs through most of the visible spectrum. Figure 4.14 and 4.15. A maximum power conversion efficiency of  $\eta = 1.6\%$  was achieved from this device.

### 4.1.3 Oligothiophene/carbazoles

The mesomorphic behaviour and liquid crystalline temperatures of the oligothiophenes **WB48**, **5**, **13**, **WB52** and **38**, differing in the number (n) of the 2,5-disubstituted thiophene rings in the middle of the aromatic core, are collated in Table 4.08.

**Table 4.08** The mesomorphic behaviour and liquid crystalline transition temperatures (°C) of the carbazoles **WB48**, **5**, **13**, **WB52** and **38**.



Compound	n	Tg	Cr	N	I
<b>WB48</b> <sup>b</sup>	1	•	62	• -	• -
<b>5</b>	2	•	64	• 168	• -
<b>13</b>	3	•	-	• 166	• -
<b>WB52</b> <sup>c</sup>	4	•	-	• 162	• -
<b>38</b>	5	•	119	• 170	• 215

Notes for table<sup>b, c</sup>: Data obtained by Weixiao Bao of the University of Hull.

Only compound **38** of all of the compounds shown in Table 4.08, exhibits an observable liquid crystalline phase, i.e., a nematic phase. Compounds **WB48**, **WB52**, **5** and **13** were found to exhibit no observable liquid crystal phases despite significant supercooling below the melting point, although a glass transition above room temperature could be observed for compound **WB48**. The melting point of compound **5** is much higher than that of the glass transition temperature of compound **WB48** perhaps as could be expected, on the basis of increased molecular interactions for polyaromatic molecules and a much more linear molecular shape. However, the melting point is remarkably similar to that of each of the oligomers number (n = 2-4). All these compounds should have a planar structure that would facilitate short inter-molecular

distances requisite for  $\pi$ - $\pi$  interactions, which may be responsible for the high melting point of the compounds shown in Table 4.08, due to strong van der Waals forces of attraction.

Analysis by a combination of optical microscopy and DSC thermography of the mesomorphic behaviour and the liquid crystalline transition temperatures of compound **38** reveals a high melting point (170 °C) and a nematic phase (Figure 4.16 and 4.17) up to the clearing point (215 °C). In addition to which, compound **38** also exhibits a glass transition above room temperature (119 °C). Compound **38** ( $n = 5$ ) has a higher length-to-breadth ratio than that of the other compounds **WB48**, **WB52**, **5** and **13** ( $n > 5$ ) and this is probably responsible for the manifestation of liquid crystalline mesophases at high temperatures. The anisotropy of the intermolecular forces of attraction will be greater for compound **38** ( $n = 5$ ) compared to that of the compounds **WB48**, **WB52**, **5** and **13** ( $n > 5$ ).

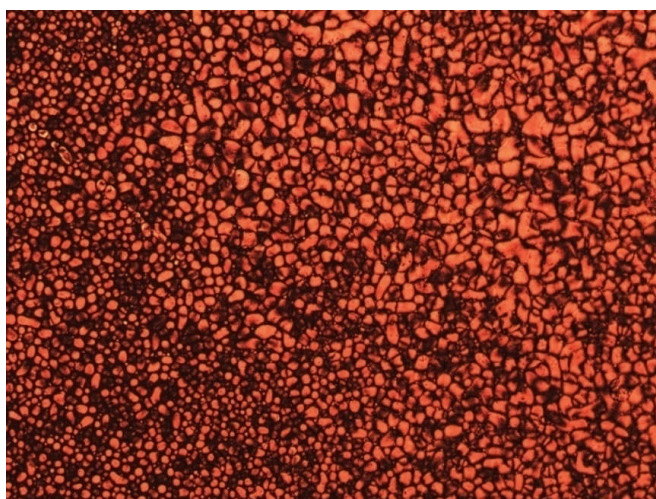


**Figure 4.16** Nematic droplets observed on cooling the isotropic phase of compound **38** to just below its clearing point.

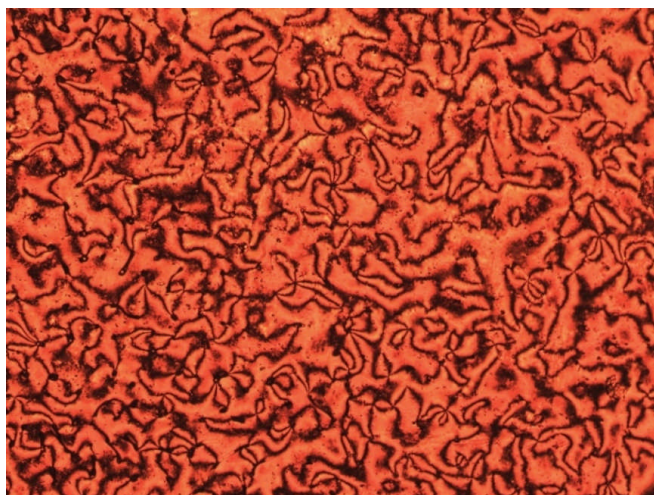


**Figure 4.17** Schlieren texture of the nematic phase of compound **38**.

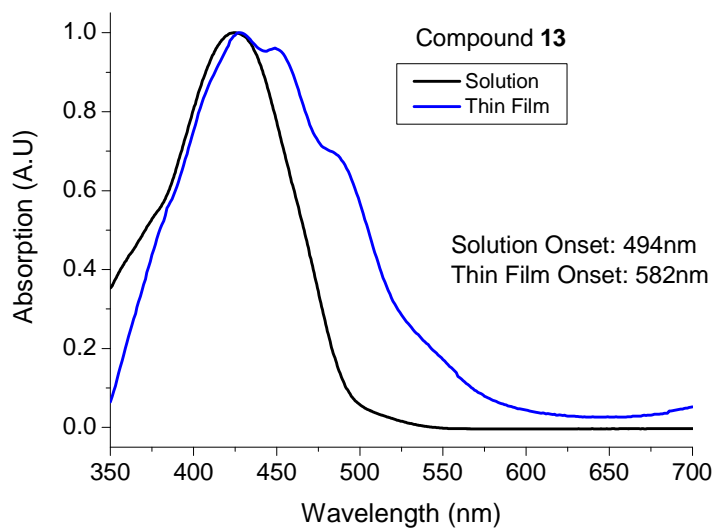


**Figure 4.18** UV-vis absorption spectra of compound **13**.

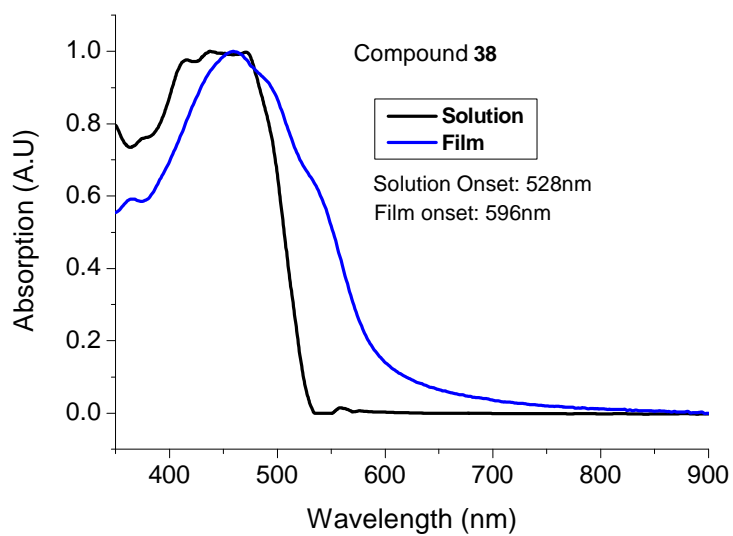
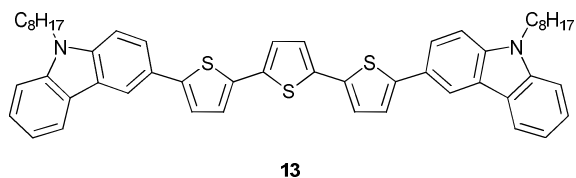


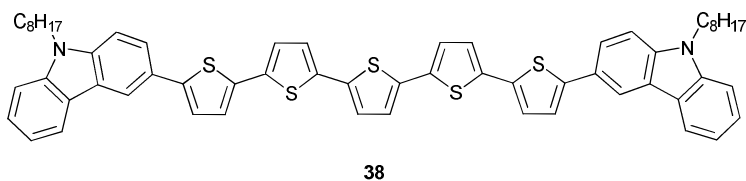
**Figure 4.19** UV-vis absorption spectra of compound **38**.

**Table 4.09** Band gap ( $E_g$ ), ionisation potential (IP) and electron affinity (EA) in eV of compound **13**.



Compound <b>13</b>	IP	$E_g$	EA
Solution	5.28	2.51	2.77
Thin Film	5.28	2.13	3.15

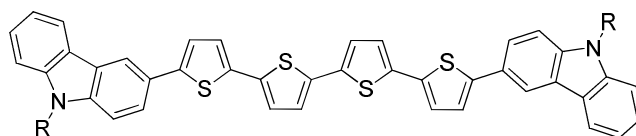
**Table 4.10** Band gap ( $E_g$ ), ionisation potential (IP) and electron affinity (EA) in eV of compound **38**.



Compound <b>38</b>	IP	$E_g$	EA
Solution	5.19	2.35	2.84
Thin Film	5.19	2.09	3.10

The mesomorphic behaviour and liquid crystalline temperatures of the additional thiophene/carbazoles **21**, **34**, **35** and **WB52**, differing in the nature of the substituent R on the carbazole moieties, are collated in Table 4.11.

**Table 4.11** The mesomorphic behaviour and liquid crystalline transition temperatures (°C) of the compounds **21**, **34**, **35** and **WB52**.



Compound	R	Cr	N	I		
<b>WB52</b>	C <sub>8</sub> H <sub>17</sub>	•	162	•	-	•
<b>21</b>	-(CH <sub>2</sub> ) <sub>9</sub> O- 	•	162	•	-	•
<b>34</b>	-(CH <sub>2</sub> ) <sub>9</sub> OH	•	235	•	-	•
<b>35</b>	-(CH <sub>2</sub> ) <sub>9</sub> O- 	•	164	•	178	•

Compound **35** exhibits a nematic phase, whereas compound **21** is found not to exhibit any liquid crystalline behaviour, as shown by a combination of analysis by DSC and optical microscopy. Compounds **WB52** and compound **21** both exhibit the same melting point (162 °C) without any observable glass transition, despite substantial super-cooling below the melting point from the isotropic liquid. Compound **21**, in spite of having a long alkyl chain with a pyran group at the terminus of the chain, does not seem to be influence the melting point of the compound. It might be due to the non-conjugative and non-polymerisable nature of the pyran group as compared to the polymerisable end groups. Compound **35** with methacrylate group has slightly higher melting temperature than the compounds **WB52** and **21** and a much lower temperature than that of the compound **34**. A nematic mesophase was observed for the compound **35** below the clearing point (178 °C). This fact is probably due to steric effects that are attributable to the bulky nature of the photopolymerisable methacrylate group at the end of the terminal aliphatic groups of the reactive mesogens **35**. The presence of these bulky groups will lead to broadening of the molecular rotation volume and a lower

length-to-breadth ratio. These differences in molecular shape will lead to weaker van der Waals forces of attraction between neighbouring molecules for the methacrylate **35** compared to that of the corresponding **WB52**, **21** and **34** with the same aromatic core. The terminal chains of the reactive mesogens **35** are longer than that of the compounds **WB52**, **21** and **34**.

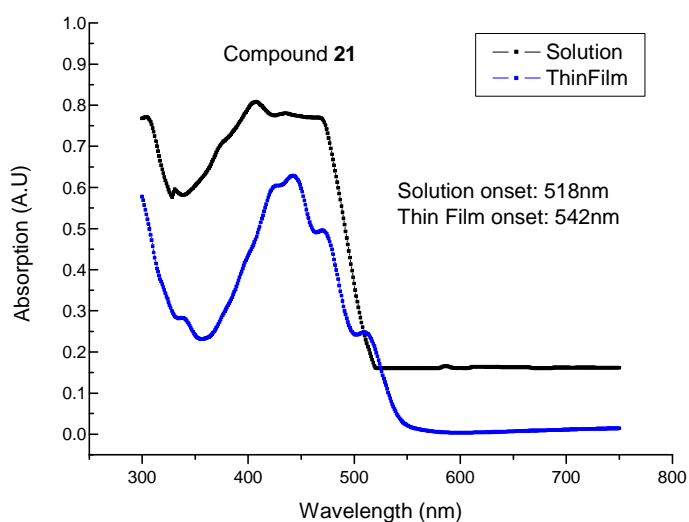
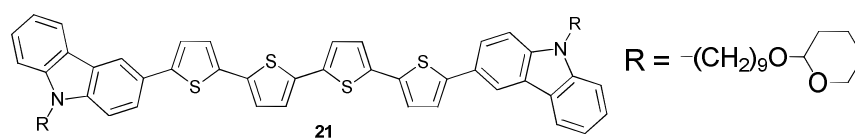


**Figure 4.20** UV-vis absorption spectra of compound **21**.

**Table 4.12** Band gap ( $E_g$ ), ionisation potential (IP) and electron affinity (EA) in eV of compound **21**.



Compound <b>21</b>	IP	$E_g$	EA
Solution	5.30	2.39	2.90
Thin Film	5.30	2.29	3.00

A key requirement to obtain high charge carrier mobility is high quality thin film morphology of the deposited active organic layer. The main challenge of solution-processable organic semiconductors is to overcome the poor solubility in common organic solvents that is caused by the strong  $\pi$ - $\pi$  interactions. Many methods are considered to increase the solubility of new semiconductors, incorporation of terminal n-alkyl carbazole chain into the conjugated thiophene backbone to increase the solubility as well as charge transport.

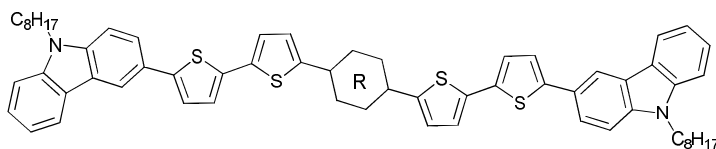
One of the most important requirements for solar cell application is low band gap and thermal stability. Thiophene is an ideal core which can provide all the requirements for solar cell. So a series of thiophene based carbazole end groups have been synthesised and are successfully used in devices.

The value of the band gap ( $E_g$ ) of the compounds **38**, **WB52**, **13** and **5** decrease with increasing number of thiophene rings between the two terminal carbazole moieties as shown by the UV-vis absorption spectra. This indicates that it is the presence of the conjugated 2,5-disubstituted thiophene rings being the dominant factor in determining the band gap of this class of materials<sup>6</sup>. The electron donating and withdrawing nature of the compounds is determined by the terminal carbazoles. The electron-donating ability of the carbazole moiety is also influenced by the presence of the electron-rich thiophene groups.

## 4.2 2,7-Disubstituted-9-alkylcarbazoles

The mesomorphic behaviour and liquid crystalline temperatures of compound **27** and **44** differing in the nature of the moiety R in the middle of the aromatic core, are collated in Table 4.13.

**Table 4.13** The mesomorphic behaviour and liquid crystalline transition temperatures (°C) of the compounds **27** and **44**.



Compound	R	T <sub>g</sub>	Cr	SmC	I
<b>27</b>		• 18	• 107	• 123	•
<b>44</b>		• -	• 160	• 180	•

A comparison of the thermal data for the fluorene **27** and the carbazole **44**, Table 4.13, shows that replacing the 2,7-disubstituted-9,9-(dioctyl)fluorene unit with a 2,7-disubstituted-9-octyl-carbazole unit has a large effect on the temperature range of the phase transitions for these compounds, although both of these compounds exhibit an enantiotropic smectic C mesophase. The melting and clearing point (160 °C and 180 °C, respectively) of the carbazole **44** are much higher than those (107 °C and 123 °C, respectively) of the corresponding 9,9-dioctyl-substituted fluorine **27**. This phenomenon is clearly attributable to steric effects, which are much lower for the carbazole **44**, where the octyl chain is likely to lie in the plane of the aromatic core of the molecule, Figure 4.22. The two octyl chains attached to position 9 of the fluorene **27** lie out of the plane of the aromatic core, Figure 4.21. In this configuration this would lead to significant increase of the molecular rotation volume, a lower length-to-breadth ratio as well as greater intermolecular separation between neighbouring molecules. A combination of these steric effects would lead to weaker van der Waals forces of attraction between neighbouring molecules and the anisotropy of dispersion forces and the anisotropy of polarisability. A combination of these factors should lead to much lower liquid crystalline transition temperatures for the 9,9-(dioctyl)-substituted fluorene **27**

compared to those of the related carbazole **44**. In addition to which, the fluorene **27** also exhibits a glass transition just below room temperature (18 °C). Most liquid crystalline 2,7-disubstituted-9,9-(dialky)fluorene polymers exhibit a high glass transition temperature that allows them to be quenched to form a nematic glass below room temperature, in which the liquid crystalline order is preserved and remains stable. Compound **27** may have meta-stable glass transition as it has a low glass temperature.

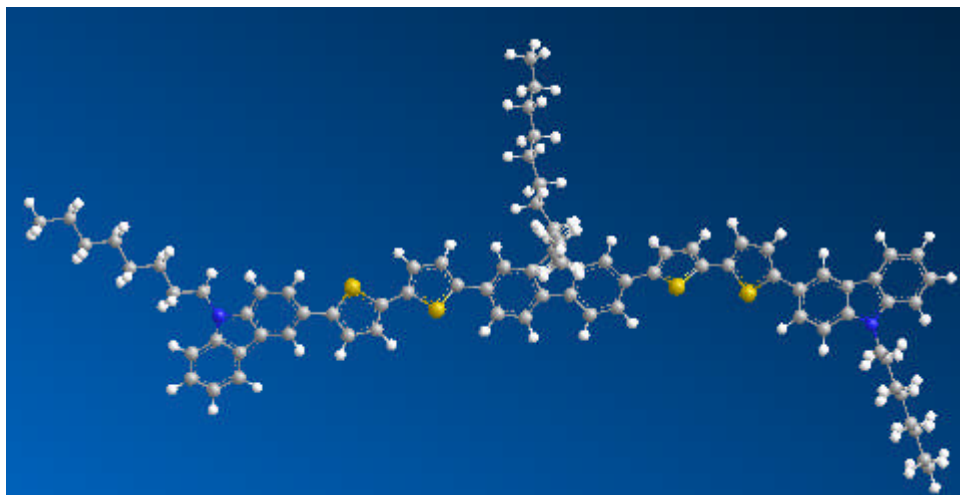


**Figure 4.21** MMFF94 optimised geometry of compound **27**.

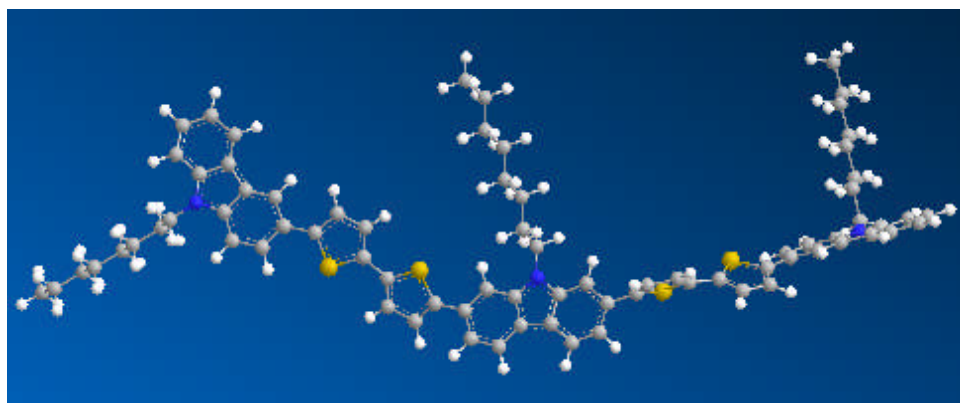


**Figure 4.22** MMFF94 optimised geometry of compound **44**.

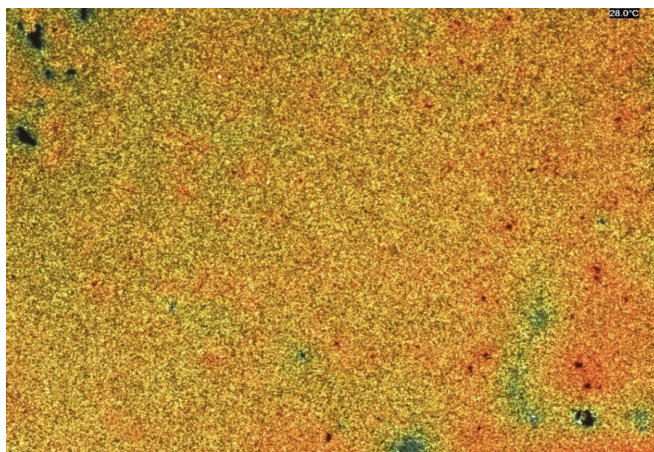


**Figure 4.23** Schlieren texture of the smectic phase below the clearing point of compound **44** after cooling from the isotropic liquid.

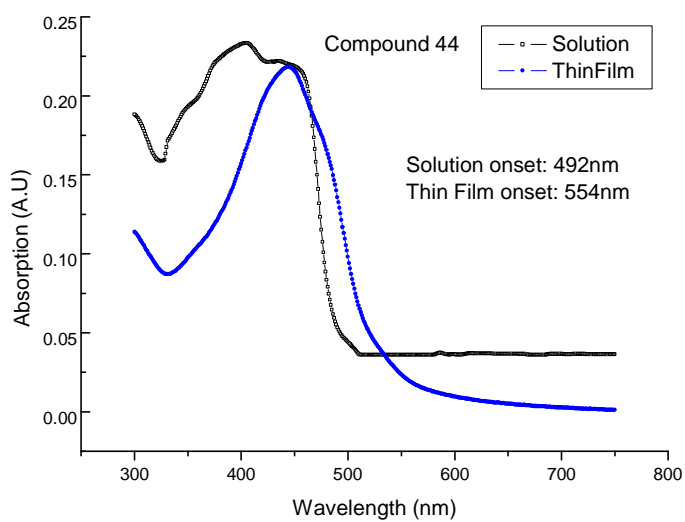


**Figure 4.24** UV-vis absorption spectra of Compound **44**.

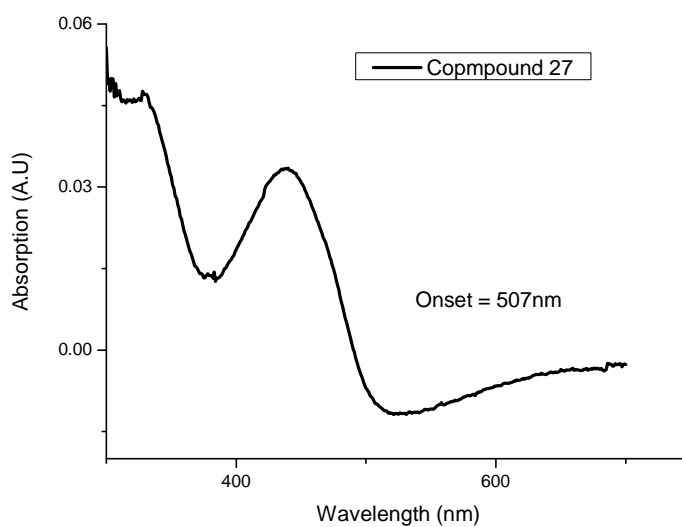
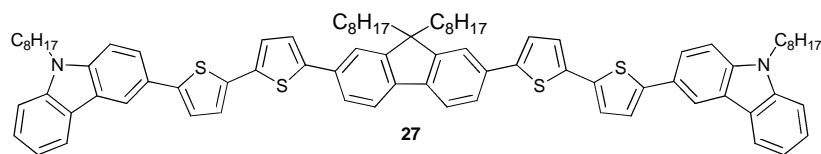


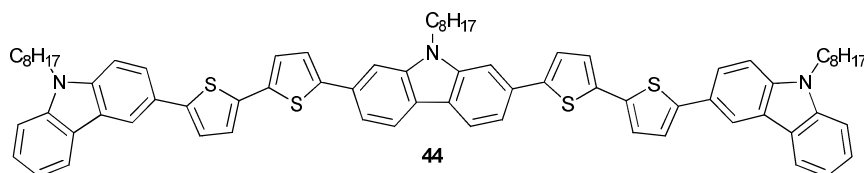
**Figure 4.25** UV-vis absorption spectra of Compound **27**.

**Table 4.14** Band gap ( $E_g$ ), ionisation potential (IP) and electron affinity (EA) in eV of compound **27**.



Compound <b>27</b>	IP	$E_g$	EA
Thin Film	5.38	2.44	2.94

**Table 4.15** Band gap ( $E_g$ ), ionisation potential (IP) and electron affinity (EA) in eV of compound **44**.



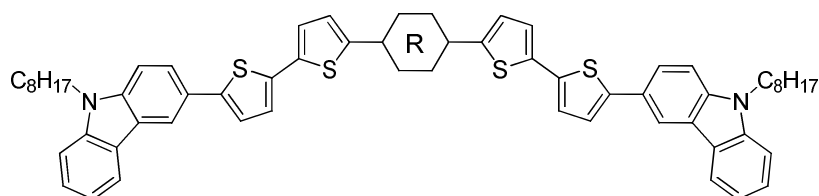
Compound <b>44</b>	IP	$E_g$	EA
Solution	5.28	2.52	2.93
Thin Film	5.28	2.24	3.03

It is clear from Tables 4.14 and 4.15 that the presence of the 2,7-disubstituted carbazole moiety in compound **44** leads to a lower ionisation potential and a lower band gap than those of the corresponding compound **27** with a 2,7-disubstituted fluorene unit in place of the 2,7-disubstituted carbazole moiety. The lowest HOMO and LUMO values are found when R is carbazole as a result of its electron-withdrawing nature. The nitrogen atom in carbazole lowers the oxidation potential and hence raises the HOMO energy level. It has also been shown recently that organic semiconductors containing a 2,7-disubstituted carbazole moiety attached to 2,5-disubstituted thiophene rings exhibit lower HOMO and the LUMO energy levels than those values observed the analogous compounds incorporating a 3,6-disubstituted carbazole unit instead of the 2,7-disubstituted carbazole moiety. This was attributed to an enhancement of the electron-donating ability of the carbazole moiety by the increased influence of the electron-rich thiophene groups.<sup>7-8</sup>

### 4.3 2,7-Disubstituted-9,9-dialkylfluorenes

The mesomorphic behaviour and liquid crystalline temperatures of the oligothiophene **WB52** and the 2,7-disubstituted-9,9-dialkylfluorenes **27** and **45**, differing in the nature of the moiety R in a central position, are collated in Table 4.16.

**Table 4.16** The mesomorphic behaviour and liquid crystalline transition temperatures (°C) of the compounds **WB52**, **27** and **45**.



Compound	R	Tg	Cr	SmC	I			
<b>WB52</b>	-	•	-	•	162	•	-	•
<b>27</b>		•	18	•	107	•	123	•
<b>45</b>		•	26	•	109	•	125	•

Compound **WB52** with four 2,5-disubstituted-thiophene rings in the middle of the aromatic core (R = 0) is a high melting crystal (162 °C). The glass transition temperature, the melting point and the clearing point (26 °C, 109 °C and 125 °C, respectively) of the 9,9-dihexyl-substituted fluorene **45** shown in Table 4.16 are significantly higher than those (18 °C, 107 °C and 123 °C, respectively) of the corresponding 9,9-dioctyl-substituted fluorene **27** with the same aromatic core, but longer alkyl substituents attached to the non-central carbazoles. The lower transition temperatures are also probably due to steric effects. The two octyl groups attached at the 9-position on the fluorene in **27** will project further from the plane of the conjugated molecular core than the two hexyl chains in **45**. This will lead to a greater intermolecular separation for the compound **27**. This will in turn lead to weaker van der Waals forces of attraction between the aromatic core of adjacent molecules and lower transition temperatures.

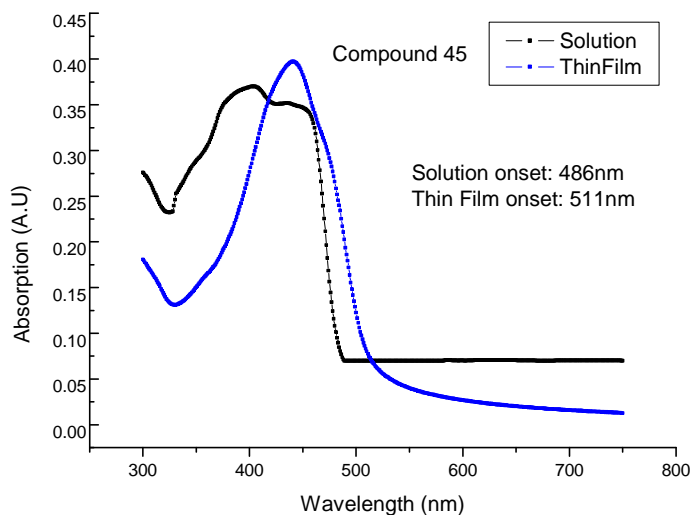
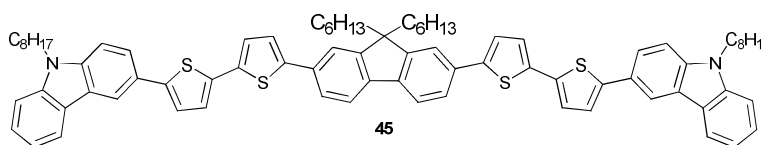


**Figure 4.26** UV-vis absorption spectra of compound **45**.

**Table 4.17** Band gap ( $E_g$ ), ionisation potential (IP) and electron affinity (EA) in eV of compound **45**.

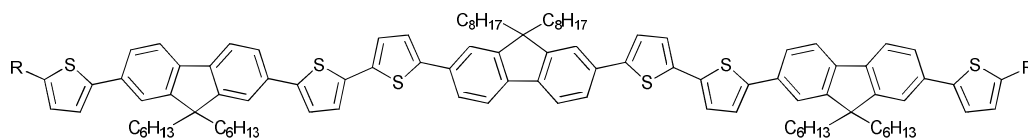


Compound <b>45</b>	IP	$E_g$	EA
Solution	5.43	2.55	2.87
Thin Film	5.43	2.42	3.00

The ionisation potential and electron affinities of compounds **27** and **45** are very similar, see Tables 4.14 and 4.17, respectively, as could be reasonably be expected taking into account that the only difference between these two compounds is the length of the alkyl substituents attached to the 9,9-dialkyl-2,7-disubstituted fluorenes unit, i.e., octyl chains in compound **27** and hexyl chains in compound **45**. The similarity in energy levels is shown by cyclic voltammetry and UV-vis absorption spectra of the two compounds determined in thin films, Figures 4.25 and 4.26. It is not surprising to see very similar HOMO and LUMO energy levels and optical band gap for the compounds **27** and **45** as the fluorene chromophore in each compound is almost identical.

The mesomorphic behaviour and liquid crystalline temperatures of the 2,7-disubstituted-9,9-(dioctyl)fluorenes **32** and **SMK**, differing in the nature of the terminal aromatic groups R, are collated in table 4.18.

**Table 4.18** The mesomorphic behaviour and liquid crystalline transition temperatures (°C) of the compounds **32** and **SMK**.



Compound	R	Tg	Cr	N	I
<b>32</b>		• 50	• 210	• 295	•
<b>SMK</b> <sup>18</sup>		• 46	• 55	• 235	•

Analysis by a combination of optical microscopy and DSC of the mesomorphic behaviour of the 2,7-disubstituted-9,9-(dioctyl)fluorene **32** shows that it exhibits the nematic mesophase with a high glass transition temperature, melting point and clearing point (50 °C, 210 °C and 295 °C, respectively) in spite of the presence of six relatively long alkyl chains in lateral positions. The presence of the two terminal methoxy groups attached to the 2,5-disubstituted thiophene rings at the periphery of aromatic core in compound **32** most probably produces a high length-to-breadth ratio, which would lead to strongly anisotropic intermolecular forces of attraction, which in turn, would give rise to high liquid crystalline transition temperatures.

The glass transition temperature, melting point and the clearing point (50 °C, 210 °C and 295 °C, respectively) of the fluorene **32** shown in Table 4.18 are significantly higher than those (46 °C, 55 °C and 235 °C, respectively) of the corresponding fluorene **SMK** with the same aromatic core, but longer alkyl substituents attached to the periphery of the fluorenes and incorporating two extra thiophene rings. The lower transition temperatures of fluorene **SMK** are probably attributable to differences in steric effects. The two octyl groups attached at the both ends of fluorene in **SMK** will project further from the plane of the conjugated molecular core than the two methoxy-groups in compound **32**, which may well lead to a greater intermolecular separation for

the compound **SMK**. This will in turn reduce the strength of the van der Waals forces of attraction between the aromatic core of adjacent molecules and, consequently, lower transition temperatures.

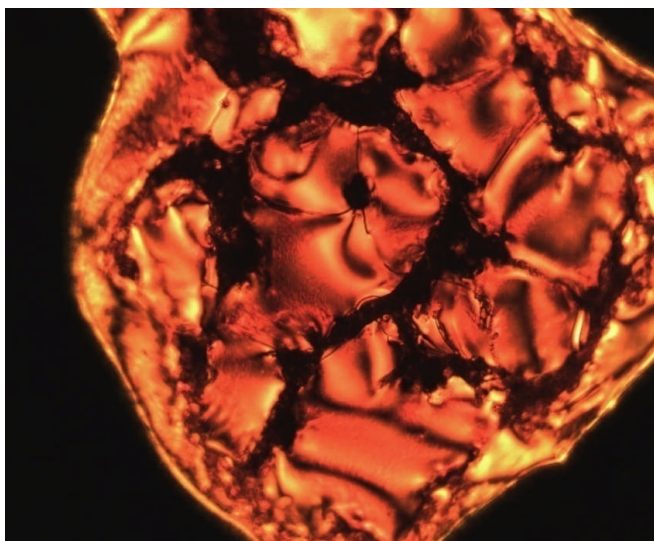


**Figure 4.27** Schlieren texture of the nematic phase observed below the clearing point of compound **32** formed on cooling from the isotropic liquid.

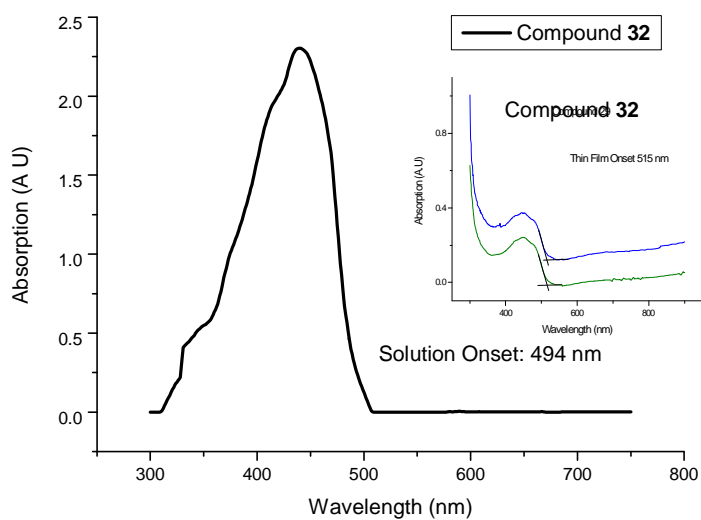
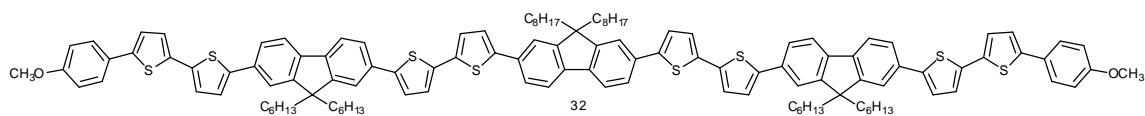


**Figure 4.28** UV-vis absorption spectra of compound **32**.

**Table 4.19** Band gap ( $E_g$ ), ionisation potential (IP) and electron affinity (EA) in eV of compound **32**.



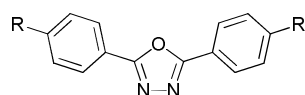
Compound <b>32</b>	IP	$E_g$	EA
Solution	5.52	2.51	3.00
Thin Film	5.52	2.41	3.10

The values determined for the ionisation potential and electron affinities of compounds **32** in both solution and thin film are quite similar as shown in Table 4.19. The presence of three 9,9-dihexyl, 2,7-disubstituted fluorene rings in compound with thiophene spacers does not seem to be influence the energy levels of the molecule **32**. It is surprising to see that the ionisation potential and electron affinities of simple central fluorene compound and long chain fluorene compounds (altering fluorene with bithiophene spacer i.e.,**32**) are very similar. This indicates that central fluorene ring is the dominant factor in determining the energy levels of this kind of compound.

## 4.4 Oxadiazoles

The mesomorphic behaviour and liquid crystalline temperatures of the 2,5-disubstituted-1,3,4-oxadiazoles **JHW**, **51**, **53**, **55**, **57** and **94** differing only in the nature of the moiety R in a terminal position, are collated in table 4.20.

**Table 4.20** The mesomorphic behaviour and liquid crystalline transition temperatures (°C) of the 2,5-di-(4-substituted-phenyl)-oxadiazoles **JHW**, **49**, **51**, **53**, **56** and **93**.



Compound	R	T <sub>g</sub>	Cr	SmA	N	I				
<b>JHW</b> <sup>9</sup>	C <sub>5</sub> H <sub>11</sub> -	•	-	•	127	•	-	•	-	•
<b>53</b>		•	-	•	225	•	247	•	-	•
<b>55</b>		•	-	•	175	•	-	•	199	•
<b>51</b>		•	-	•	204	•	-	•	-	•
<b>57</b>		•	80	•	171	•	-	•	-	•
<b>94</b>		•	177	•	181	•	-	•	-	•

Compound **51** melts with a crystal to isotropic transition at 204 °C and shows no liquid crystalline phases or a glass transition despite substantial supercooling below the melting point. Compound **57** with two carbazole groups exhibits a much lower melting point (171 °C) than that of compound **51**. On cooling compound **57** in the isotropic phase, above the melting point, recrystallisation is not observed and a glassy state is formed at 80 °C and, despite the greater length-to-breadth ratio of compound **57**, due to the presence of two additional thiophene rings compared to compound **51**, no liquid crystalline phases could be observed. This might be attributed to the bulky nature of the carbazole end groups. A comparison between the mesomorphic behaviour and liquid crystal transition temperatures of compounds **53** and **JHW** shows that the presence of an additional 1,4-disubstituted phenyl ring in compound **53** has a large effect on the

temperature range of the smectic mesophase. A SmA mesophase is observed for compound **53** due to the high melting point, which is much higher than that of the compound **JHW**. The presence of an alkyl chain with a 1,4-disubstituted phenyl group in the compound **JHW** results in the elimination of mesomorphic behaviour. Hence, extension of  $\pi$ -conjugation of aromatic ring results in the mesophase formation.

Compounds **53** and **55** have shown in Table 4.20 exhibits a smectic A phase and a nematic phase, respectively, Figures 4.29 and 4.30. A glass transition could not be observed despite substantial cooling below the melting point. The biphenyl oxadiazole **53** exhibits a higher melting and clearing point as well as a change in the mesophase compared to those of the analogous thiophene-containing oxadiazole **55**. This may be due to the fact that compound **53** has a higher length-to-breadth ratio than that of compound **55**, Figures 4.31 and 4.32.

A comparison between the oxadiazole **53** and the oxadiazole **55** shows that replacing the thiophene in place of a phenyl ring has a large effect on the temperature range of the mesophase, Table 4.20. The melting and clearing point (225 °C and 247 °C, respectively) of the oxadiazole **53** are higher than those (175 °C and 199 °C, respectively) of the corresponding oxadiazole **55**.

These differences in the transition temperatures can be explained by taking to account the non co-axial and non co-linear nature of the 2,5-disubstituted thiophene bonds, whereas in 1,4-disubstituted phenyl ring the bonds are parallel and co-linear, Figure 4.33 and 4.34. Therefore, the compound **53** has a higher length-to-breadth ratio than that of the compound **55**, MMFF94 optimised geometry of compounds **53** and **55**, Figures 4.31 and 4.32. A combination of these factors would lead to much lower liquid crystalline transition temperatures for the compound **55** compared to those of the related compound **53**.

A comparison between the oxadiazole **57** and the oxadiazole **94** shows that replacing the phenyl carbazole in place of a thiophene carbazole ring has a slight effect on the temperature range of the mesophase, see table 4.20. The melting and clearing point (181 °C) of the oxadiazole **94** are higher than those (171 °C) of the corresponding oxadiazole **57**. This may be due to the fact that compound **94** has a higher length-to-breadth ratio than that of compound **57**. A glass transition could be observed for both compounds below the melting point.

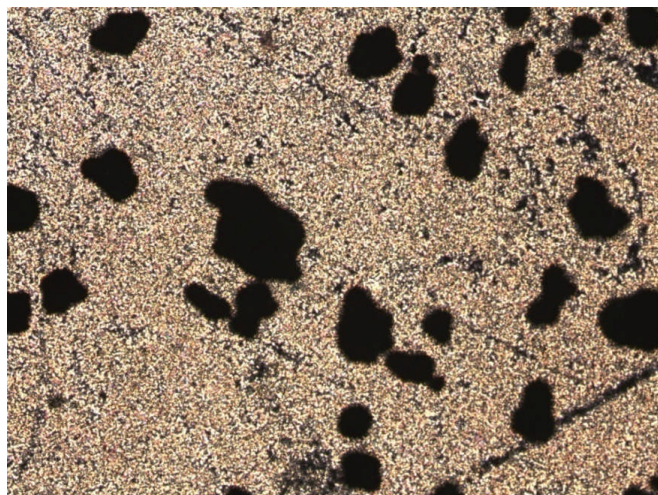


**Figure 4.29** SmA phase observed below the clearing point of compound **53** formed from cooling of the isotropic liquid.

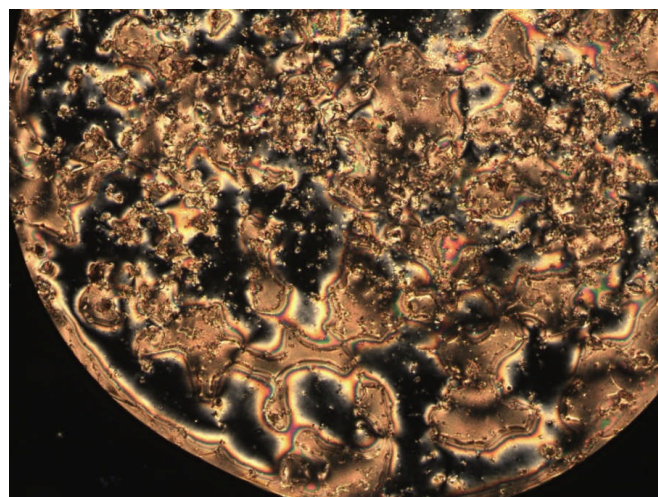


**Figure 4.30** Nematic phase observed below the clearing point of compound **55** formed from cooling of the isotropic liquid.

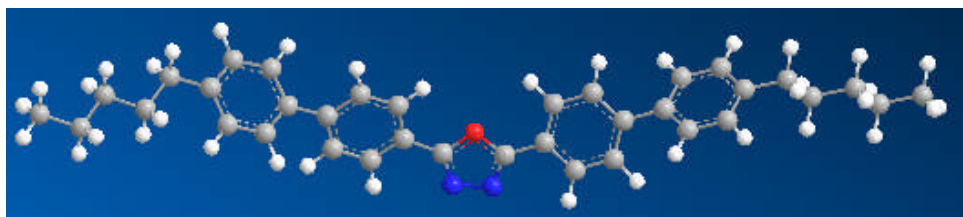


**Figure 4.31** MMFF94 optimised geometry of compound **53**.

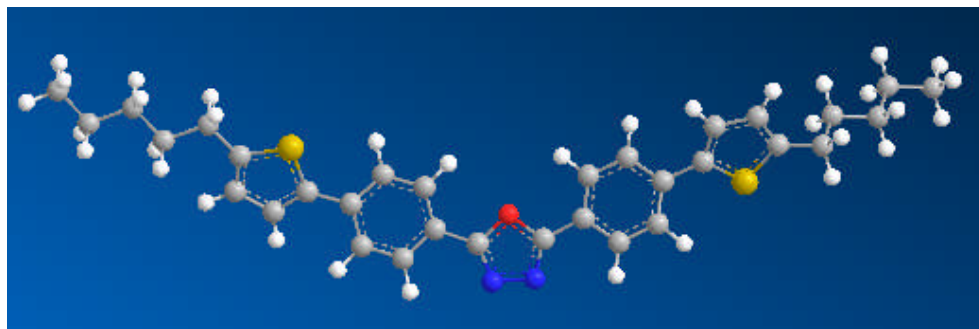


**Figure 4.32** MMFF94 optimised geometry of compound **55**.

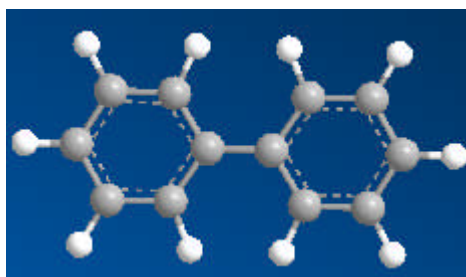


**Figure 4.33** Linear structure of the biphenyl with co-axial and co-linear bonds in the 4,4'-disubstituted biphenyl moiety.

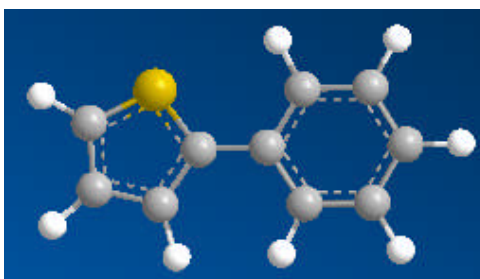


**Figure 4.34** non co-linear or co-axial nature of the 1-substituted-4-(thiophen-2-yl) phenyl moiety.

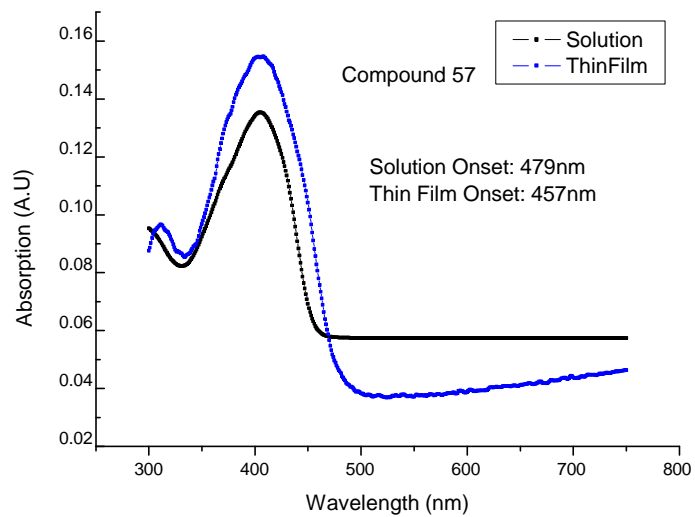


**Figure 4.35** UV-vis absorption spectra of compound **57**.

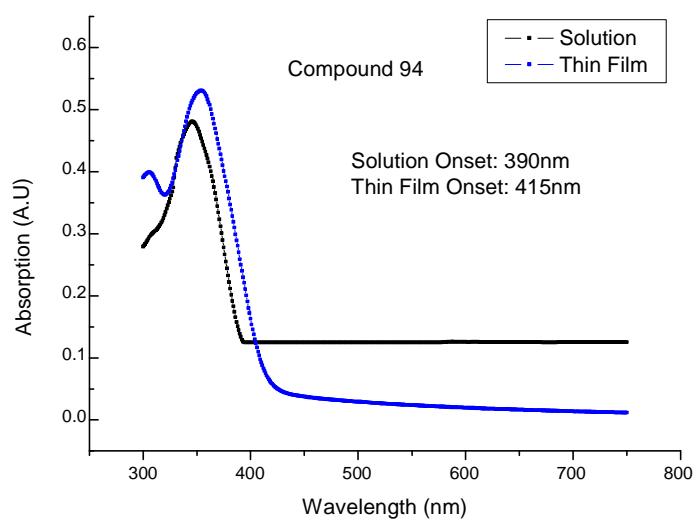


**Figure 4.36** UV-vis absorption spectra of compound **94**.

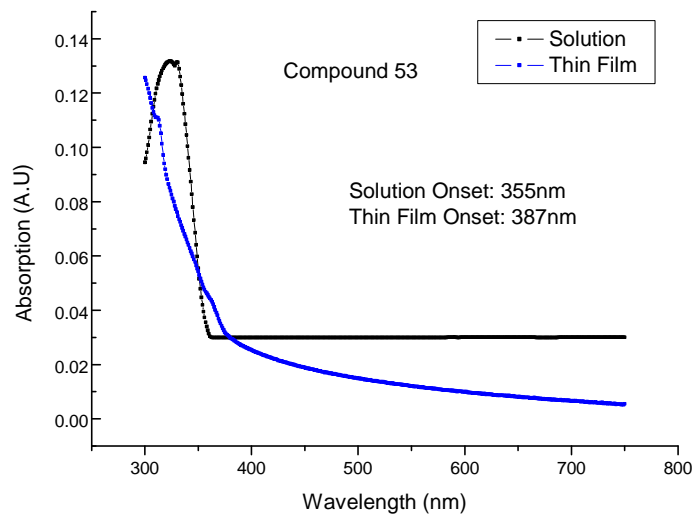


**Figure 4.37** UV-vis absorption spectra of compound **53**.

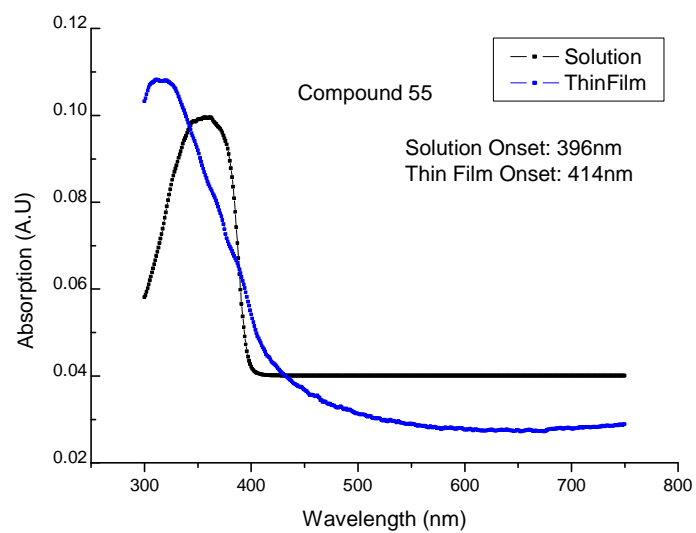
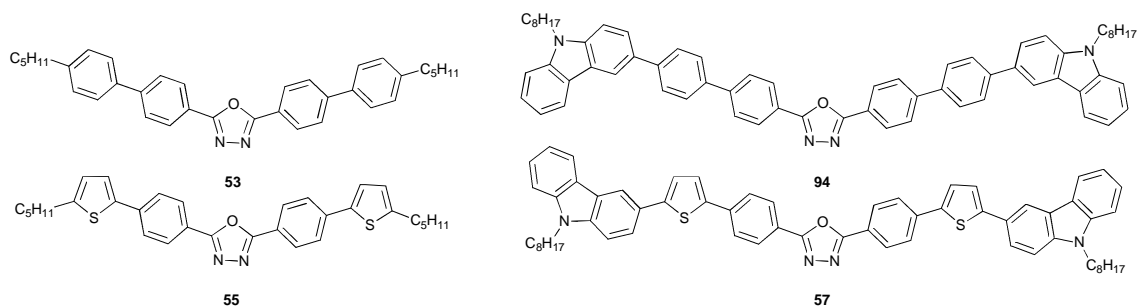


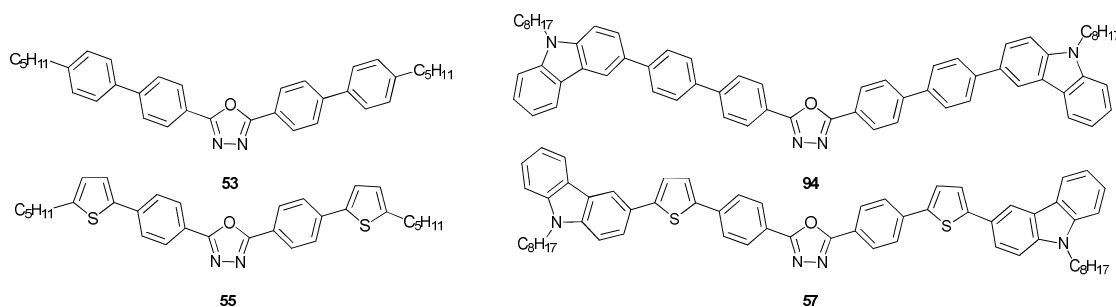
**Figure 4.38** UV-vis absorption spectra of compound **55**.

**Table 4.21** Band gap ( $E_g$ ), ionisation potential (IP) and electron affinity (EA) in eV of the 2,5-di-(4-substituted-phenyl)-oxadiazoles **53**, **55**, **57** and **94** determined in solution.



Compound (Solution)	IP	$E_g$	EA
<b>53</b>	6.30	3.50	2.80
<b>55</b>	6.06	3.13	2.92
<b>57</b>	5.51	2.71	2.79
<b>94</b>	5.71	3.18	2.52

**Table 4.22** Band gap ( $E_g$ ), ionisation potential (IP) and electron affinity (EA) in eV of the 2,5-di-(4-substituted-phenyl)-oxadiazoles **53**, **55**, **57** and **94** determined in a thin film.



Compound (Thin Film)	IP	E <sub>g</sub>	EA
<b>53</b>	6.30	3.20	3.10
<b>55</b>	6.06	3.00	3.03
<b>57</b>	5.51	2.59	2.91
<b>94</b>	5.71	2.99	2.72

Tables 4.21 and 4.22 show the band gap (E<sub>g</sub>), ionisation potential (IP) and electron affinity (EA) in eV for 2,5-di-(4-substituted-phenyl)-oxadiazoles **53**, **55**, **57** and **94** in solution and as a thin film, respectively.

The ionisation potential (IP) and optical band gap (E<sub>g</sub>) of compound **53** are significantly higher than those values of compound **55**, in which 1,4-disubstituted phenyl ring in compound **53** is replaced with a 2,5-disubstituted thiophene ring. The electron affinity of compound **53**, differing only in the presence of a 1,4-disubstituted phenyl ring compared to a 2,5-disubstituted thiophene ring in compound **55**, is lower, as expected.

Similar trends are seen for compounds **57** and **94**, also only differing in the presence of a 2,5-disubstituted thiophene ring in compound **57** compared to a 1,4-disubstituted phenyl ring in compound **94**. The ionisation potential (IP) and optical band gap (E<sub>g</sub>) of compound **94** are higher than that of compound **57**, in which the phenyl-carbazole moiety in compound **94** replaces the thiophene-carbazole moiety in compound **57**, as shown by the UV-vis absorption spectra shown in Table 4.35 and 4.36 for compounds **57** and **94**, respectively. It is not very surprising that the incorporation of a 2,5-disubstituted thiophene ring in place of a 1,4-disubstituted phenyl ring results in significant change in HOMO and band gap, which is lower by 0.2 eV for the compound **57**.

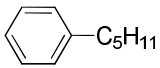
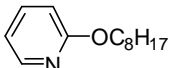
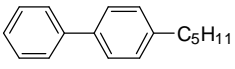
These results illustrate again the fact that the electron-rich 2,5-disubstituted thiophene ring is a very significant factor in controlling the band gap of a extended  $\pi$ -conjugated system.

## 4.5 Dithienopyrroles

The mesomorphic behaviour and liquid crystalline temperatures of the 2,6-disubstituted-dithieno[3,2[-b:2'3'-d]pyrroles **62**, **64** and **79**, differing only in the nature of the moiety R in a terminal position, are collated in Table 4.23.

**Table 4.23** The mesomorphic behaviour and liquid crystalline transition temperatures (°C) of the compounds **62**, **64** and **79**.



Compound	R	Cr	N	I
<b>62</b>		• 98	• -	•
<b>64</b>		• 81	• -	•
<b>79</b>		• 200	• 299	•

The presence of pyridine ring in compound **64** leads to a lower melting point than that of compound with phenyl ring **62**. However, no liquid crystal transition or a glassy state could be observed in both compounds. Compound **62** and **64** exhibit melting transitions at 98 °C and 81 °C, respectively. The transitions from solid to liquid and from liquid to solid occurred with no evidence of liquid crystalline behaviour.

Molecular modelling using MMFF94 geometry optimisation of compound **62** and **64** shows that when each molecule is viewed from above, down the molecular axis with the molecule perpendicular to the page subtle differences in the structure can be seen, Figures 4.39 and 4.40. The presence of the pyridine ring in compound **64** leads to a more planar molecular structure due to intra-molecular interactions between the nitrogen atoms and the neighbouring hydrogen on the adjacent aromatic ring. It is not clear how this leads to a lower melting point for compound **64** than that of compound **62**. However, this planar structure may lead to a greater degree of intermolecular  $\pi$ - $\pi$  stacking and may lead to a high electron transport.<sup>10-11</sup>

A direct comparison of the liquid crystalline transition temperatures of compound **62** and compound **79** shown in Table 4.23 shows that the presence of two 1,4-disubstituted phenylene rings, instead of one 1,4-disubstituted phenyl ring, has a large effect on the transition temperatures and the temperature range of the nematic mesophase. The DSC thermogram and optical microscopy of compound **62** shows only a melting point (98 °C), whereas compound **79** exhibits a nematic phase, Figures 4.41. Compound **79** exhibits a higher melting point (200 °C) and a much higher nematic clearing point (299 °C) as well as a broader nematic phase.

Compound **62** does not exhibit any liquid crystalline phases or glass transitions. This is probably due to the aspect ratio, which is too low to induce mesophase formation. The presence of an additional 1,4-disubstituted phenyl ring in compound **79**, successfully induce a nematic mesophase and high melting point, probably due to the much higher length-to-breadth ratio and, consequently, a greater anisotropy in the intermolecular forces of attraction. Polarised optical microscopy provided confirmation that compound **79** possess a nematic phase. Nematic droplets were observed on cooling from the isotropic liquid to a temperature just below the nematic clearing point, Figure 4.41. The droplets then coalesced after further cooling to form a characteristic schlieren texture Figure. 4.42.

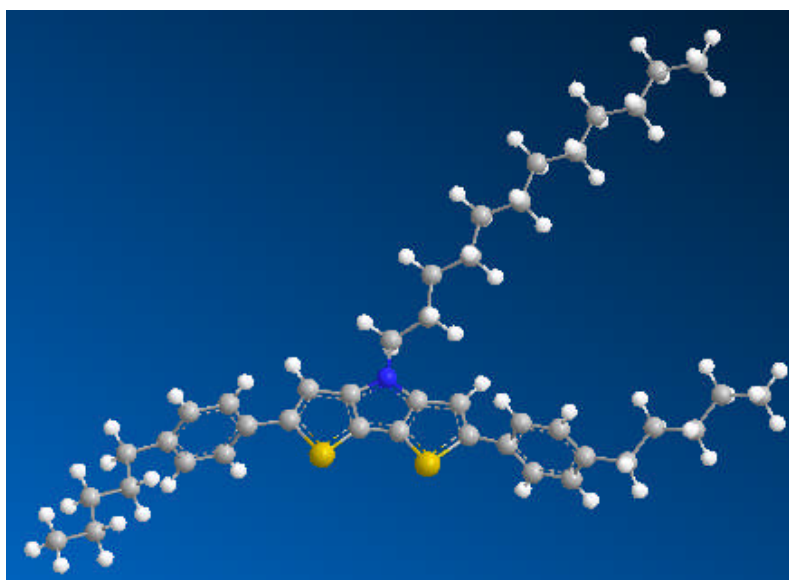


**Figure 4.39** MMFF94 optimised geometry of compound **62**.

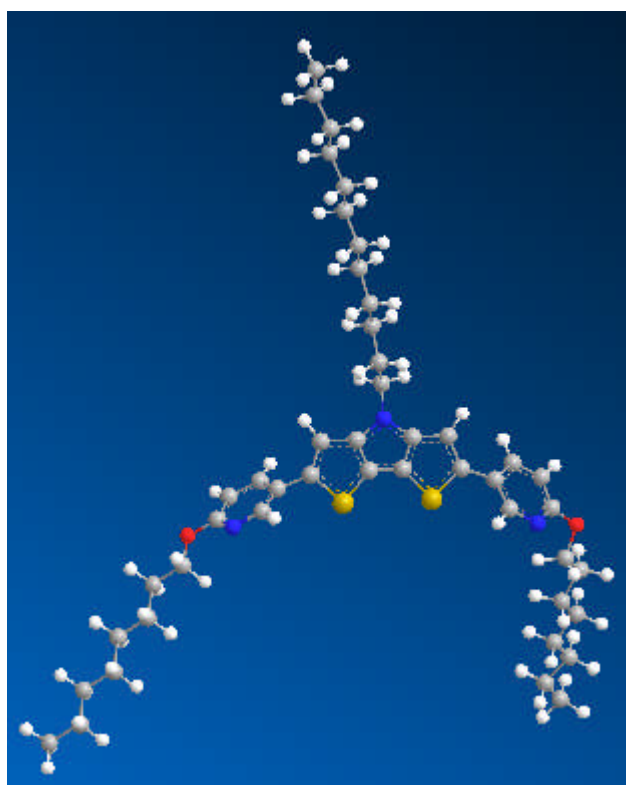


**Figure 4.40** MMFF94 optimised geometry of compound **64**.

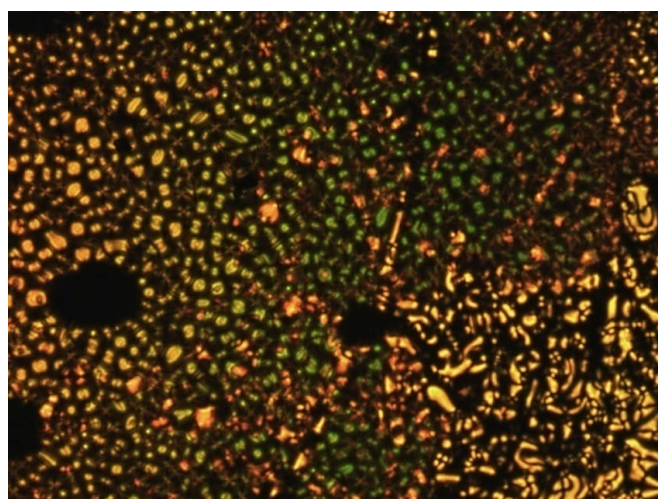


**Figure 4.41** Nematic droplets of compound **79** formed on cooling from the isotropic liquid.

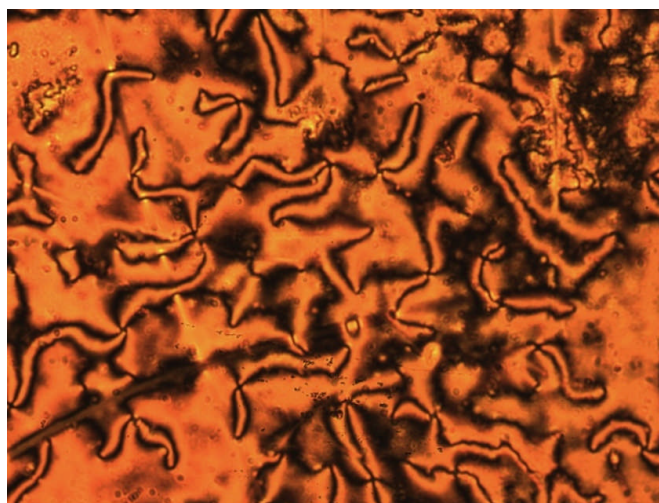


**Figure 4.42** Schlieren texture of nematic phase of compound **79**.

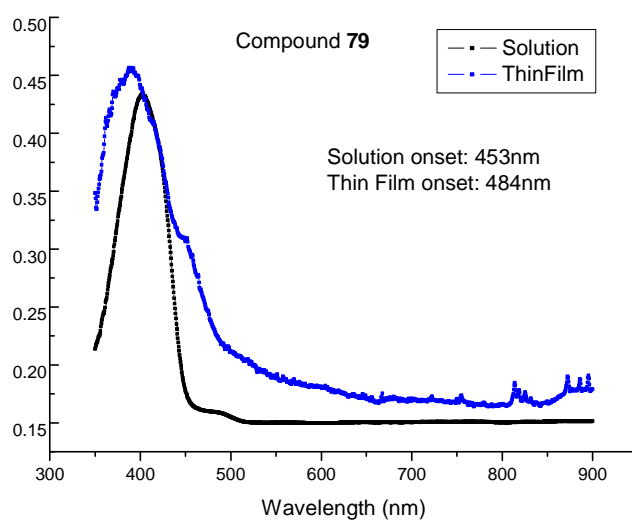


**Figure 4.43** UV-vis absorption spectra of compound **79**.

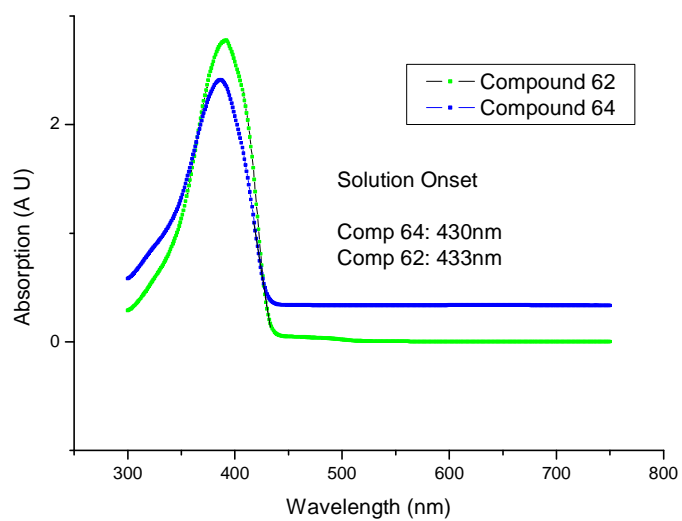


**Figure 4.44** UV-vis absorption spectra of compounds **62** and **64** in solution.

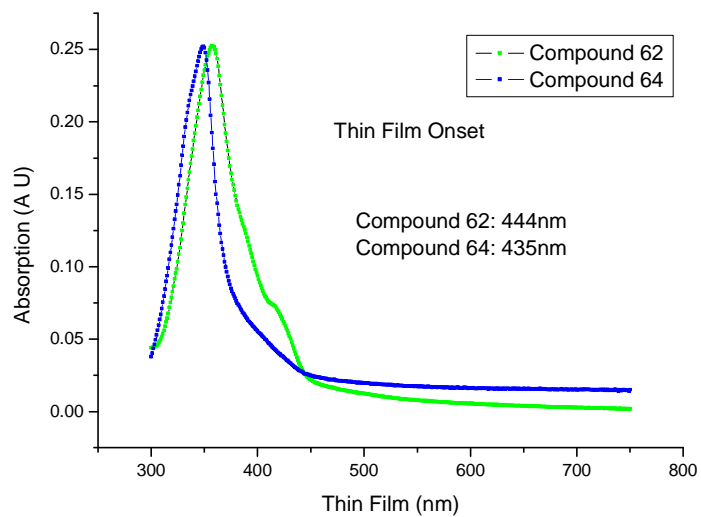
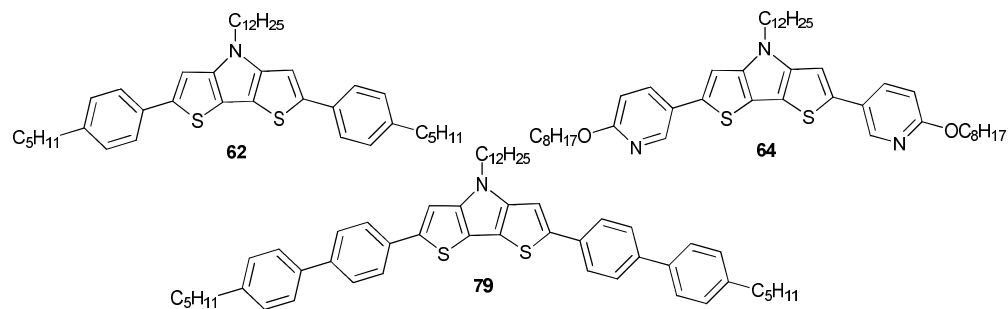


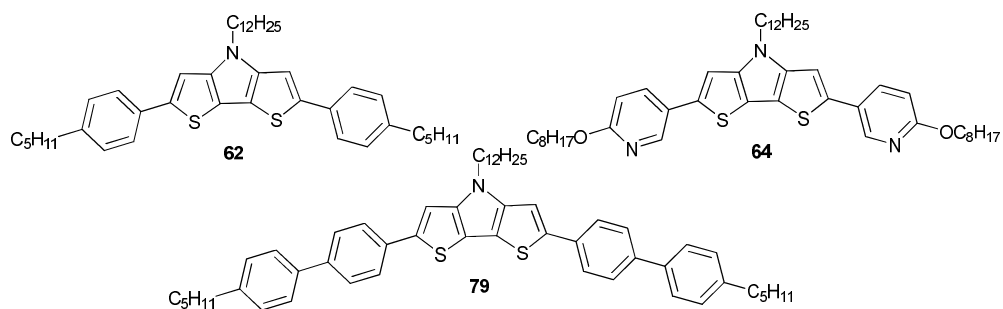
**Figure 4.45** UV-vis absorption spectra of compounds **62** and **64** in a thin film.

**Table 4.24** Band gap ( $E_g$ ), ionisation potential (IP) and electron affinity (EA) in eV of compounds **62**, **64** and **79** determined in solution.



Compound (Solution)	IP	$E_g$	EA
<b>62</b>	5.26	2.86	2.39
<b>64</b>	5.26	2.88	2.37
<b>79</b>	5.25	2.74	2.51

**Table 4.25** Band gap ( $E_g$ ), ionisation potential (IP) and electron affinity (EA) in eV of compounds **62**, **64** and **79** determined in a thin film.



Compound (Thin Film)	IP	$E_g$	EA
<b>62</b>	5.26	2.79	2.46
<b>64</b>	5.26	2.85	2.40
<b>79</b>	5.25	2.56	2.68

The ionisation potential, optical band-gap and electron-affinities of compounds **62** and **64** are very similar, Table 4.24 and 4.25, as the dithienopyrrole chromophore in each compound is identical. The similarity in behaviour is confirmed by comparison of the UV-vis absorption spectra of the two compounds in both solution and as a thin film, Figures 4.44 and 4.45. There is no noticeable difference in absorption spectra of the solutions, where-as there is a slight difference in absorption spectra of thin film. The slight difference in the band gap is due to small differences in the van der Waal forces of attraction between the slightly different aromatic cores of the compounds **61** and **63**, which are attributable to the presence of either the 2,5-disubstitued pyridine or the 1,4-disubstitued benzene rings. The optical band-gap of compound **79** is significantly lower than that of compounds **62** and **64**. Cyclic voltammetry results are very similar for all these compounds.

## 4.6 Fused Phenylenes

The mesomorphic behaviour and liquid crystalline temperatures of the oligothiophenes **38** and **WB52** and the naphthalene and anthracene derivatives **71** and **74**, differing in the nature of the moiety R in the central part of the aromatic core, are collated in Table 4.26.

**Table 4.26** Transition temperatures (°C) of the compounds **38**, **WB52**, **71**, and **74**.

Compound	R	T <sub>g</sub>	Cr	N	I
<b>WB52</b>	-	• 162	• -	• -	• -
<b>38</b>		• 119	• 170	• 215	•
<b>71</b>		• 62	• 121	• -	•
<b>74</b>		• -	• 245	• -	•

Compound **38**, with R = 2,5-disubstituted thiophene, has a higher length-to-breadth ratio than that of the other compounds **WB52**, **71**, and **74** shown in Table 4.26 and this fact is probably responsible for the observation of liquid crystalline mesophases at high temperatures for compound **38**. The anisotropy of the intermolecular forces of attraction will be greater for compound **38** compared to that of the compounds **WB52**, **71** and **74**. Compound **74**, with an anthracene ring in the centre of the molecular core, exhibits a very much higher melting point (245 °C) than that (121 °C) of compound **71**, with a naphthalene ring in a similar position. Analysis by DSC shows that the compounds **71** and **74** exhibit a melting peak and no mesophases are observed either on heating or cooling. A glass transition could be observed on the first heating cycle for compound **71** at (62 °C). No glass transition is exhibited for compound **74** despite the substantial super-cooling to below the melting point. This could be due to the large bulky nature of the naphthalene and anthracene rings and the fact that these fused rings are not in the

same plane to adjacent thiophene rings due to inter-annular rotation, Figures 4.46 and 4.47. This will lower the effective length-to-breadth ratio and could well lead to elimination of any potential liquid crystalline phases.

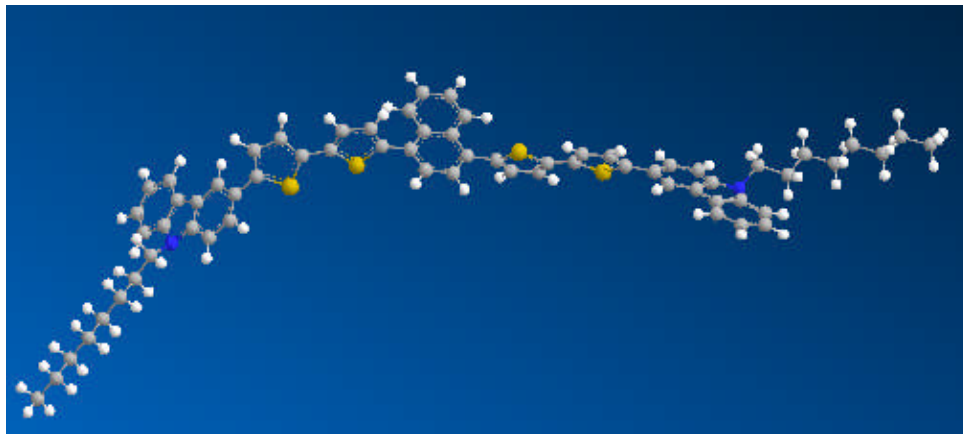


**Figure 4.46** MMFF94 optimised geometry of compound **71**.

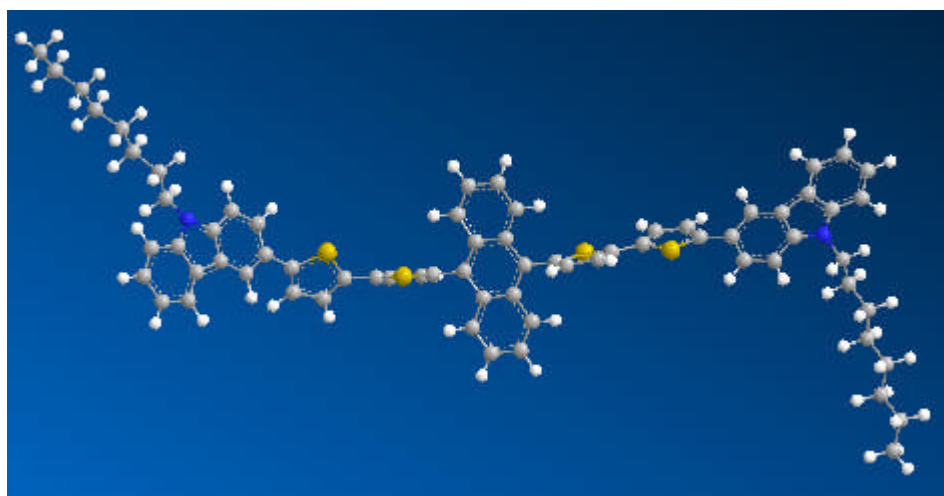


**Figure 4.47** MMFF94 optimised geometry of compound **74**.

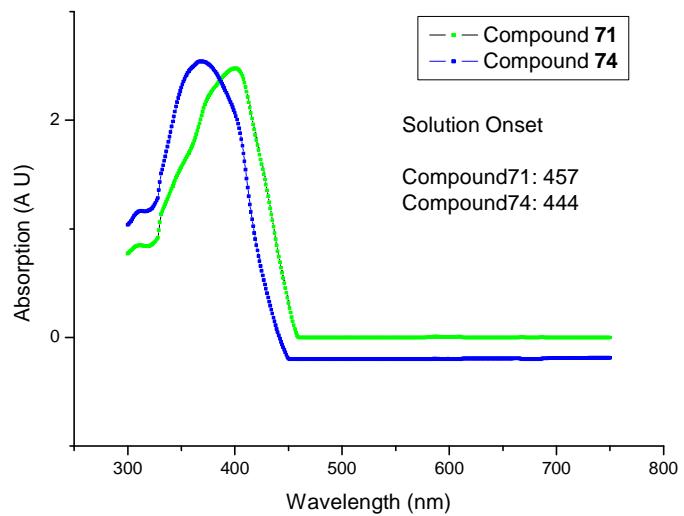


**Figure 4.48** UV-vis absorption spectra of compounds **71** and **74** in solution.

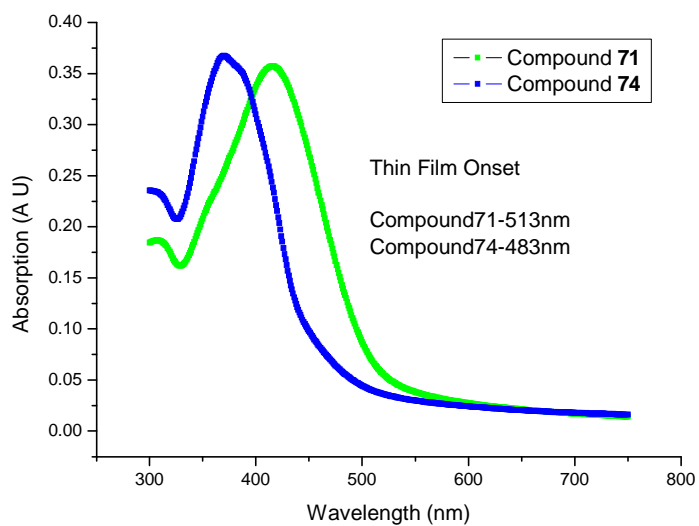
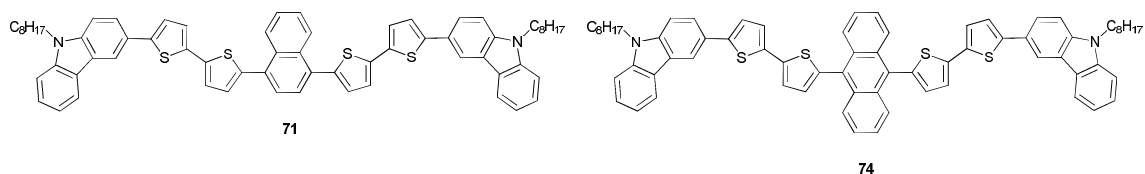


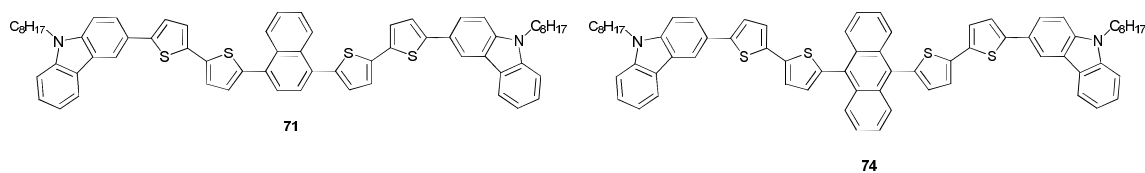
**Figure 4.49** UV-vis absorption spectra of compounds **71** and **74** in a thin film.

**Table 4.27** Band gap ( $E_g$ ), ionisation potential (IP) and electron affinity (EA) in eV of compounds **71** and **74**.



Compound (Solution)	IP	$E_g$	EA
<b>71</b>	5.44	2.71	2.68
<b>74</b>	5.44	2.79	2.64

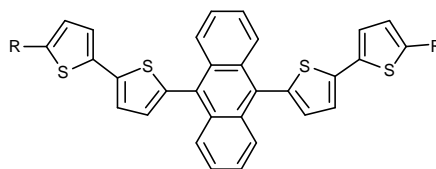
**Table 4.28** Band gap ( $E_g$ ), ionisation potential (IP) and electron affinity (EA) in eV of compounds **71** and **74**.

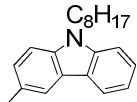


Compound (Thin Film)	IP	$E_g$	EA
<b>71</b>	5.44	2.41	2.98
<b>74</b>	5.44	2.56	2.87

The ionisation potential, optical band-gap and electron-affinities of compounds **71** and **74** are very similar, Table 4.27 and 4.28. The similarity in behaviour is confirmed by comparison of the UV-vis absorption spectra of the two compounds in solution, Figures 4.48 and 4.49. There is no noticeable difference in absorption spectra of solution, where as there is a slight difference in absorption spectra of thin film. So, there is no significant energy difference between both the compounds in which anthracene was replaced with naphthalene.

**Table 4.29** Melting temperatures (°C) of the compounds **74** and **76**.



Compound	R	Cr	I	
<b>74</b>		•	245	•
<b>76</b>	C <sub>10</sub> H <sub>21</sub> O-	•	222	•

The melting points of the anthracene derivatives **74** and **76**, differing in the nature of the moiety R in a terminal position, are shown in table 4.29. A comparison between the compound **74** and the compound **76** shows that replacing the carbazole end chain by the decyloxy chain has a small effect on the melting point, see Table 4.29. Both the compounds do not exhibit any observable mesophase behaviour. The melting point (245 °C) of the compound **74** is slightly higher than that (222 °C) of the compound **76**. This phenomenon cannot be explained by differences in steric hindrance, which is much lower for the compound **76**, where the anthracene ring and the terminal alkoxy chains appear to lie in the same plane as that of the aromatic core of the molecule, Figure 4.50. The two bulky *N*-octyl carbazole end chains attached to compound **74** lie out of the plane of the aromatic core, Figure 4.47.

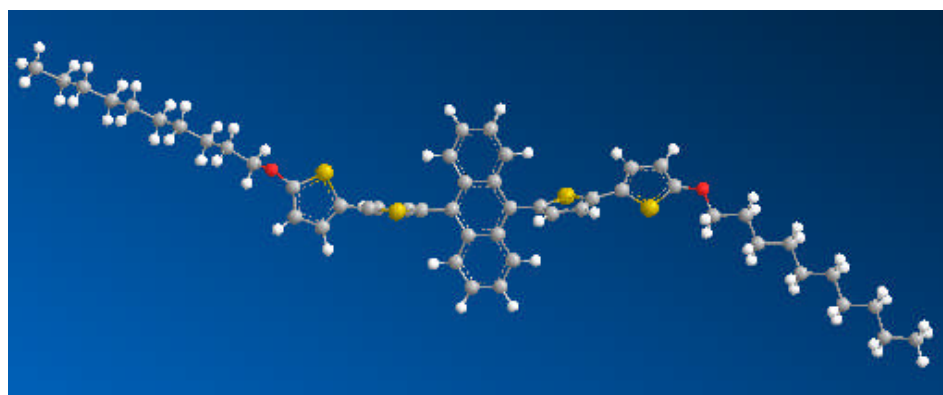


**Figure 4.50** MMFF94 optimised geometry of compound **76**.

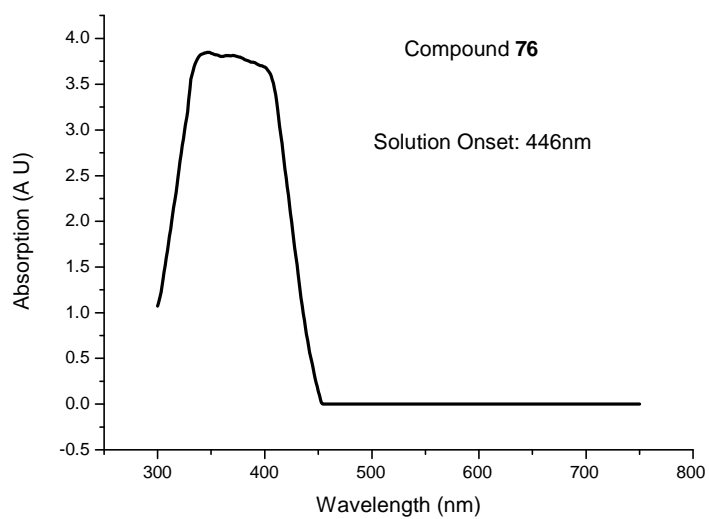
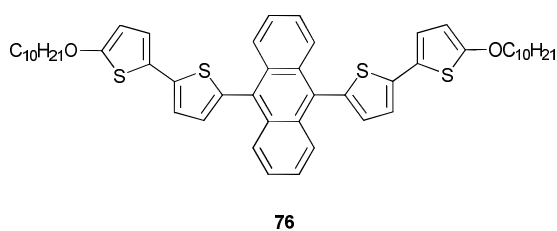


**Figure 4.51** UV-vis absorption spectra of compound **76**.

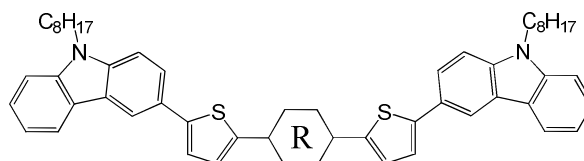
**Table 4.30** Band gap ( $E_g$ ), ionisation potential (IP) and electron affinity (EA) in eV of compound **76**.



Compound (Solution)	IP	$E_g$	EA
<b>76</b>	5.54	2.78	2.75

The melting points of the compound **13** and compound **67** derivatives, differing in the nature of the moiety R in a central position, are shown in table 4.31.

**Table 4.31** Melting temperatures (°C) of the compounds **13** and **67**.



Compound	R	Cr		I
<b>13</b>		•	166	•
<b>67</b>		•	215	•

Both compounds **13** and **67** shown in Table 4.31 do not exhibit any mesomorphic behaviour and a glass transition could also not be observed despite substantial cooling below the melting point of either compound. A typical DSC trace of compound **67** shows that a crystal-crystal transition is observed in two heating cycles (215 °C) and there is only one crystallisation peak in the cooling cycle. A comparison between compound **67** and the compound **13** shows that replacing the 2,5-disubstituted-thiophene ring in compound **13** by a 1,4-disubstituted-phenyl ring to form compound **67** results in a significant increase in the melting point (+49 °C). This difference may be attributed to differences in the linear and co-linear nature of these compounds as has already been discussed in the oxadiazole section 4.4, i.e., compound **67** has a higher length-to-breadth ratio than that of compound **13**.

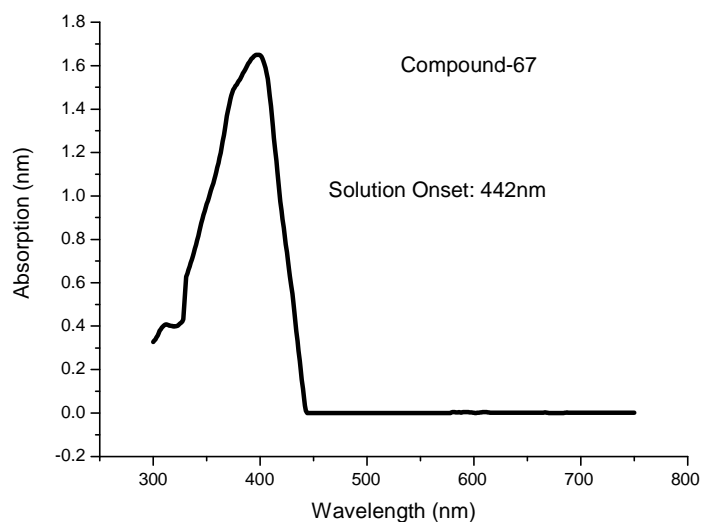
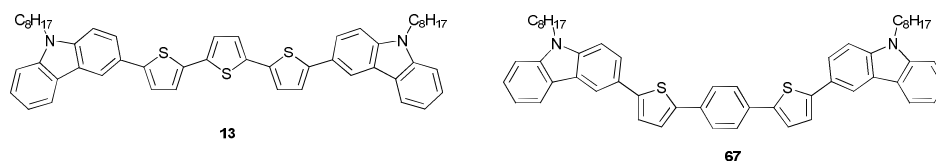


**Figure 4.52** UV-vis absorption spectra of compound **67**.

**Table 4.32** Band gap ( $E_g$ ), ionisation potential (IP) and electron affinity (EA) in eV of compounds **13** and **67**.



Compound (Thin Film)	IP	$E_g$	EA
<b>13</b>	5.28	2.51	2.77
<b>67</b>	5.35	2.80	2.54

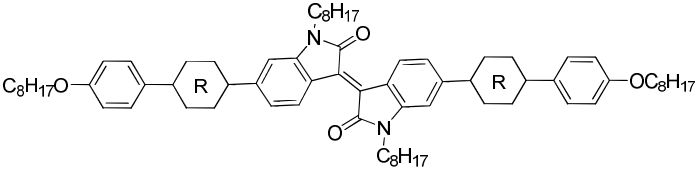
A comparison between the compound **74** and the compound **76** shows that replacing the terminal alkyl chain in place of a terminal carbazole ring has a slight effect on energy levels. The ionisation potential (IP) and optical band gap ( $E_g$ ) of compound **74** are slightly lower than that of compound **76**. This indicates the terminal carbazole ring being the dominant force to determine ionisation potential of the compound.

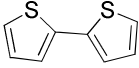
The ionisation potential (IP) and optical band gap ( $E_g$ ) of compound **67** are significantly higher than that of compound **13**, in which central phenyl ring in compound **67** was replaced with thiophene. Tables 4.32 show the physical data for compounds **13** and **67** respectively. This phenomenon attributes to nature of the thiophene ring which has already been discussed oxadiazole section 4.0.

## 4.7 Isoindigo

The mesomorphic behaviour and liquid crystalline temperatures of the 5,5-disubstituted isoindigo compounds **87** and **90**, differing in the nature of the moiety R in a terminal position of the aromatic core, are collated in table 4.33.

**Table 4.33** Transition temperatures (°C) of the compounds **87** and **90**.



Compound	R	T <sub>g</sub>	Cr	N	I			
<b>87</b>		•	-	•	195	•	-	•
<b>90</b>		•	96	•	238	•	281	•

A direct comparison of the liquid crystalline transition temperatures of compound **87** and compound **90** are shown in Table 4.33. This shows that the presence of two 1,4-disubstituted thiophene rings, instead of one 1,4-disubstituted thiophene ring, has a considerable effect on the transition temperatures and the temperature range of the nematic mesophase. Compound **87** only possesses a melting point (195 °C), whereas compound **90** exhibits a nematic phase, Figure 4.66. Compound **90** exhibits a higher melting point (238 °C) and a much higher nematic clearing point (281 °C) as well as a broader nematic phase.

Compound **87** does not exhibit any liquid crystalline phases or glass transitions. This is probably due to the aspect ratio, which is too low to induce mesophase formation. The presence of an additional 1,4-disubstituted thiophene ring in compound **90**, successfully induces a nematic mesophase and results in a high melting point, probably due to the much higher length-to-breadth ratio and, consequently, a greater anisotropy in the intermolecular forces of attraction. Polarised optical microscopy provided confirmation that compound **90** possess a nematic phase. A glass transition could be observed on the first heating cycle for the compound **90** at (96 °C). No glass transition is exhibited for compound **87** despite the substantial supercooling below the melting.

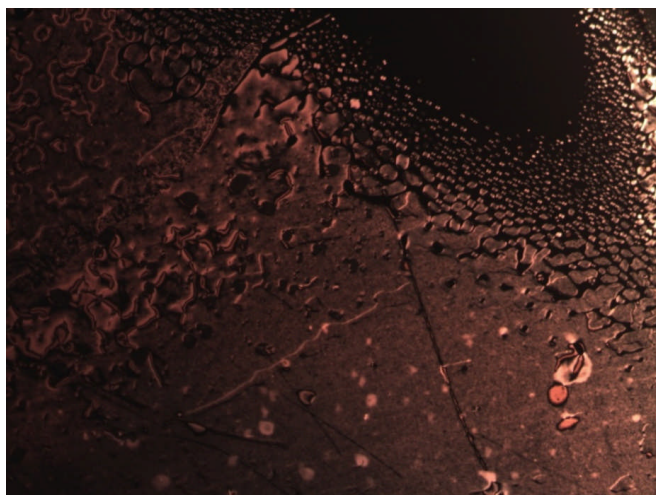


**Figure 4.53** Nematic droplets of compound **90** formed on cooling from the isotropic liquid.

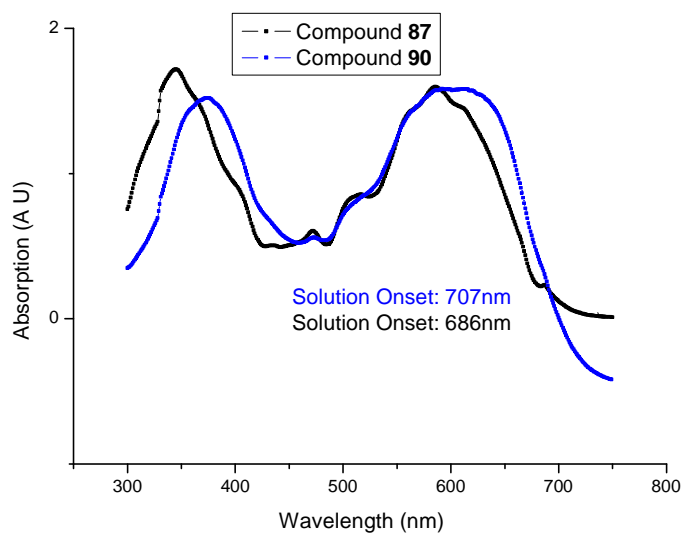


**Figure 4.54** UV-vis absorption spectra of compounds **87** and **90** in solution.

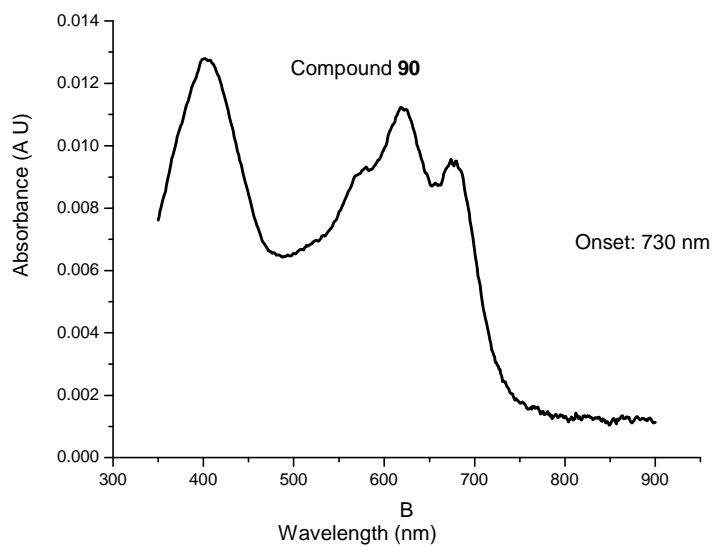
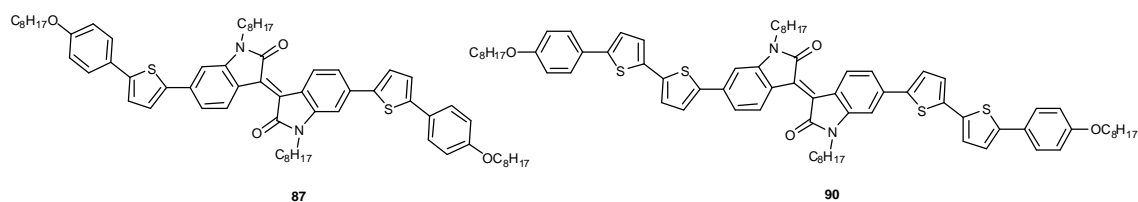


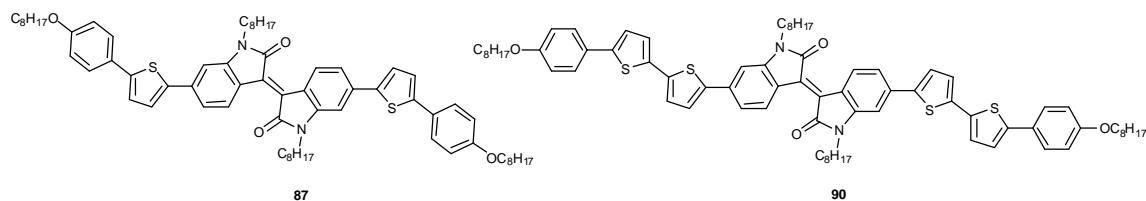
**Figure 4.55** UV-vis absorption spectra of compound **90** in a thin film.

**Table 4.34** Band gap ( $E_g$ ), ionisation potential (IP) and electron affinity (EA) in eV of compounds **87** and **90**.



Compound (Solution)	IP	$E_g$	EA
<b>87</b>	5.59	1.80	3.78
<b>90</b>	5.59	1.75	3.83

**Table 4.35** Band gap ( $E_g$ ), ionisation potential (IP) and electron affinity (EA) in eV of compounds **87** and **90**.



Compound (Thin Film)	IP	$E_g$	EA
<b>87</b>	5.59	1.70	3.89
<b>90</b>	5.59	1.70	3.89

Isoindigo has strong electron-withdrawing character due to its lactam rings. Although, many Donor-Acceptors-Donor (D-A-D) materials have been synthesised in the past few years, it is only recently that D-A-D compounds incorporating isoindigo as a central acceptor block have been described.<sup>12</sup>

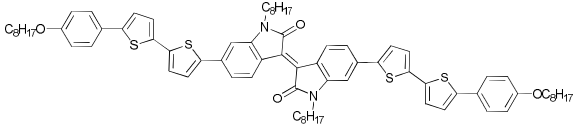
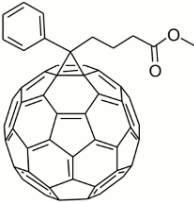
Isoindigo based liquid crystalline semiconductors have not yet been reported. So it was decided to synthesize the isoindigo compounds with a liquid crystal mesophase. The optical band gap of newly synthesised isoindigo is below 1.8 eV. This low optical band gap is one of the most important criteria for efficient organic solar cells. Many isoindigo based materials exhibit an intense and broad absorption, which is beneficial for achieving high power conversion efficiency (PCE).<sup>13</sup>

UV-vis absorption spectra of the compounds **87** and **90** both in chloroform solution were measured. Both compounds broadly absorb at wavelength up to 686 nm and 707 nm respectively in solution. Thin film absorption is almost same for both the compounds, which is at 730 nm.

The ionisation potential, optical band-gap and electron-affinities of compounds **87** and **90** are exactly same, Table 4.34 and 4.35 as the central core isoindigo in each compound are identical. The similarity in behaviour is confirmed by comparison of the UV-vis absorption spectra of the two compounds in solution, Figure 4.54. So, with the central indigo core is the dominant force in deciding the band gap of the compound. The

compound featured a low band gap (1.7 eV) and a low lying HOMO energy level (5.59 eV), both of which were ideal for photovoltaic application.

A solar cell device was created using compound **90** as the donor material and **PCBM** as the acceptor material. PEDOT-PSS was spin coated at 5000rpm for 30s. A thin film of compound **90** was spin-coated onto PEDOT-PSS layer from chlorobenzene, followed by the deposition of lithium fluoride and then aluminium as a combined cathode. The device was then tested to find the characteristics, current density, photo current and EQE were measured and the power conversion efficiencies were also calculated. Unfortunately device made with compound **90** shows a very low power conversion efficiency of  $\eta = <0.01\%$ . This is due to the low charge separation between the donor and acceptor, poor thin film quality and poor absorption. Figure 4.56.

	<p>IP EA E<sub>g</sub>, (eV)</p> <p>5.59, 3.89, 1.70</p> <p><b>Compound 90</b></p>
	<p>IP EA E<sub>g</sub>, (eV)</p> <p>6.1 , 3.7 , 2.4</p> <p><b>PCBM</b></p>

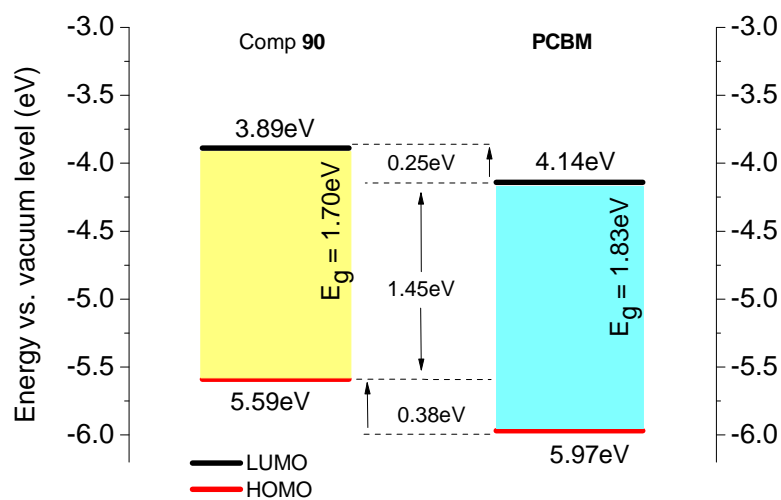


**Figure 4.56** Energy level diagram of Compounds **90** and PCBM.

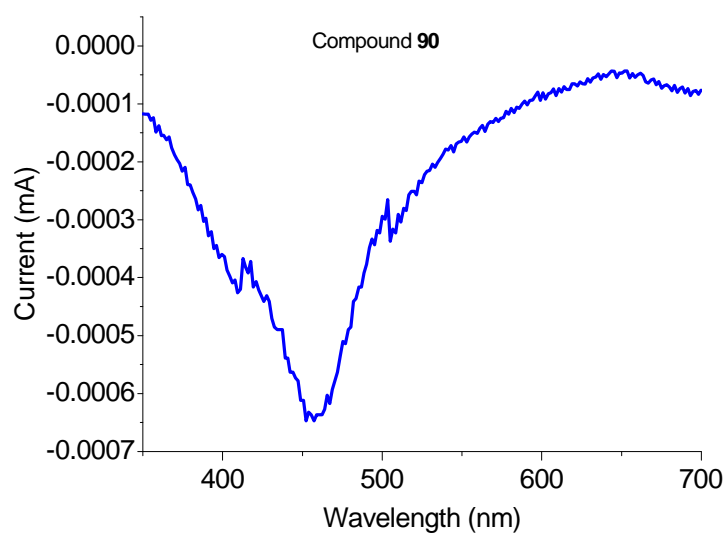


**Figure 4.57** Photocurrent produced by the compound **90**.

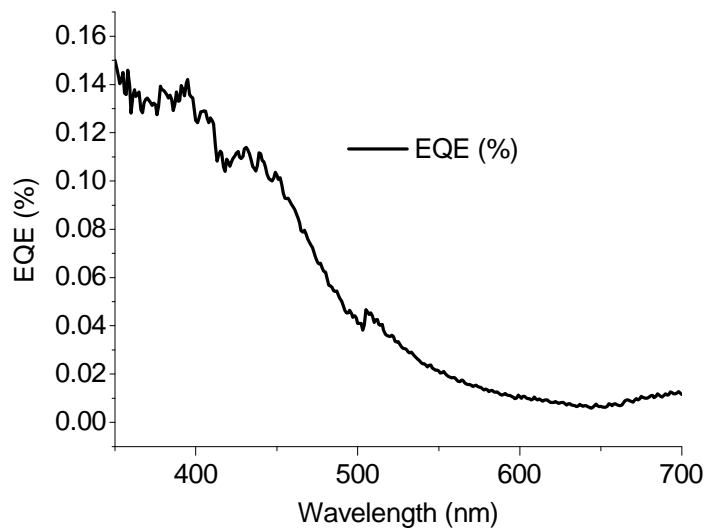


**Figure 4.58** EQE spectra of compound **90**.

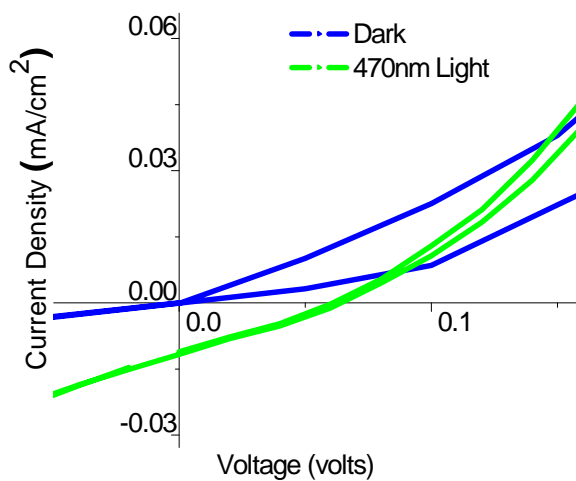


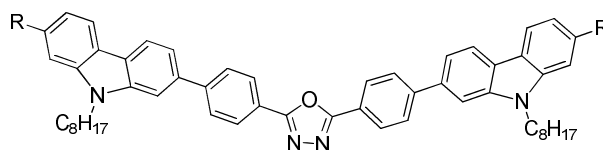
**Figure 4.59** Electrical current per unit of cross section for compound **90**.

## 4.8 Derivatives incorporating 2-substituted carbazole rings

### 4.8.1 Oxadiazole/carbazoles

The melting temperatures of 2,5-disubstituted-1,3,4-oxadiazoles **101**, **108** and **115**, differing only in the nature of the moiety R in a terminal position, are collated in Table 4.36.

**Table 4.36** The melting temperatures (°C) of the compounds **101**, **108** and **115**.



Compound	R	Cr	Cr	Cr	I	
<b>101</b>	H	•	-	•	205	•
<b>108</b>	CH <sub>3</sub> O-	•	118	•	178	•
<b>115</b>	C <sub>8</sub> H <sub>17</sub> O-	•	138	•	148	•

The melting point (178 °C) of the methoxy substituted oxadiazole **108** shown in Table 4.36 is significantly higher than that (148 °C, respectively) of the corresponding octyloxy-substituted oxadiazole **115** with the same aromatic core, but longer alkyl substituents attached to the terminal carbazoles. The lower transition temperatures are also probably due to steric effects. The two octyloxy groups attached at the terminal position on the oxadiazole in **115** will project further from the plane of the conjugated molecular core than the two methoxy chains in **108**. This will lead to a greater intermolecular separation for the compound **115**. This will in turn lead to weaker van der Waals forces of attraction between the aromatic core of adjacent molecules and lower transition temperatures.

This difference may be due to the steric nature of these compounds as has already been discussed. Compound **108** has a greater intermolecular separation than that of compound **101**.

Both the compounds (**108** and **115**) do not exhibit any observable mesomorphic behaviour despite incorporating longer alkyl chains. Analysis by a combination of optical microscopy and DSC thermography of the mesomorphic behaviour of these compounds reveals a highly ordered crystal to crystal transition and typical thread like behaviour when cooled from the isotropic liquid Figure 4.60. However X-ray diffraction studies suggest that there is no morphological change during heating/cooling.

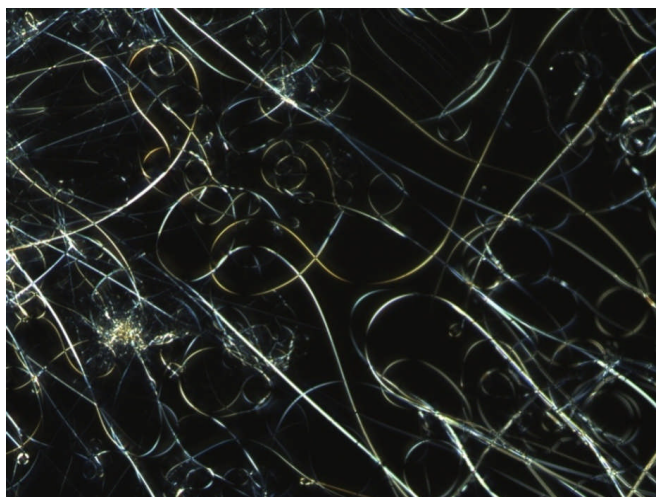


**Figure 4.60** Typical ordered crystalline phase of compound **108**.

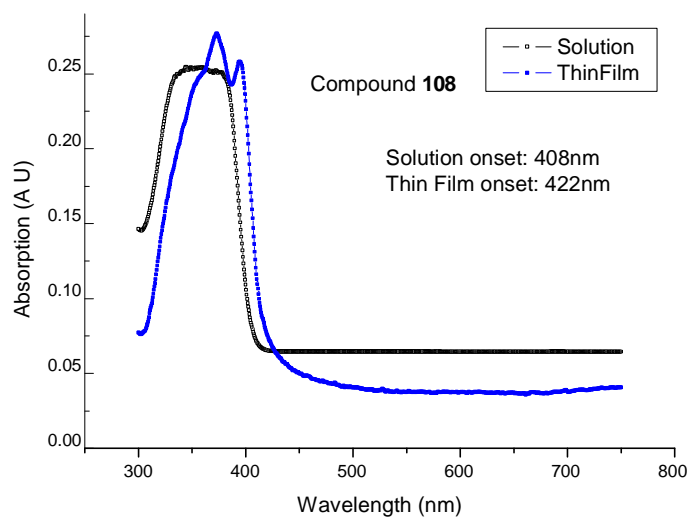


**Figure 4.61** UV-vis absorption spectra of compound **108**.

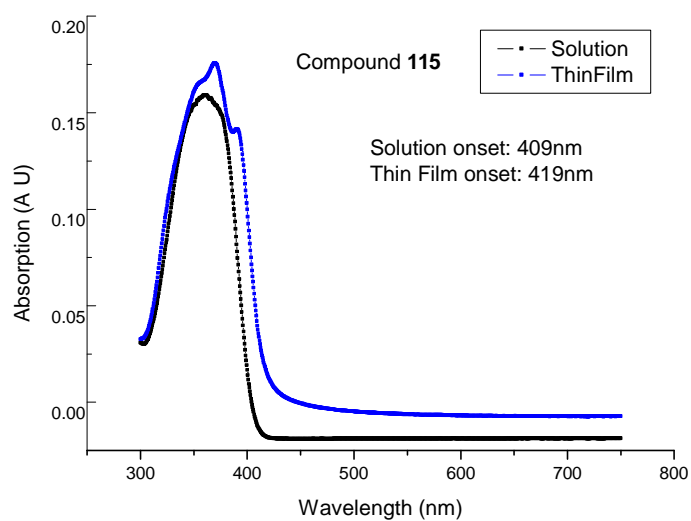
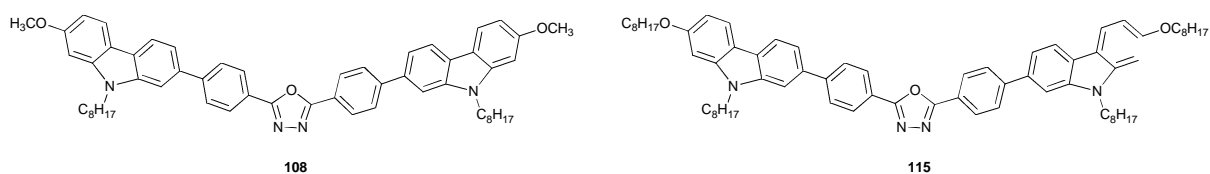


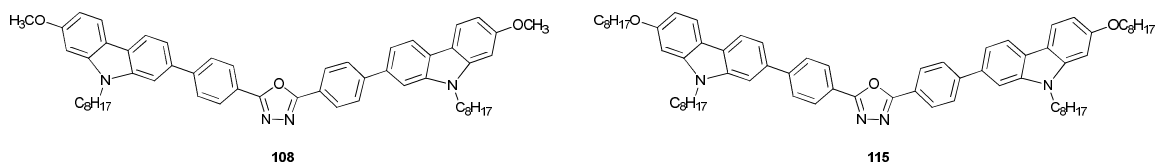
**Figure 4.62** UV-vis absorption spectra of compound **115**.

**Table 4.37** Band gap ( $E_g$ ), ionisation potential (IP) and electron affinity (EA) in eV of compounds **108** and **115** in solution.



Compound (Solution)	IP	$E_g$	EA
<b>108</b>	5.64	3.04	2.60
<b>115</b>	5.63	3.00	2.63

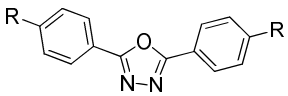
**Table 4.38** Band gap ( $E_g$ ), ionisation potential (IP) and electron affinity (EA) in eV of compounds **108** and **115** in a thin film.

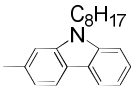
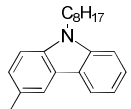


Compound (Thin Film)	IP	$E_g$	EA
<b>108</b>	5.64	2.94	2.69
<b>115</b>	5.63	2.96	2.66

The ionisation potentials, optical band-gaps and electron-affinities of compounds **108** and **115** are very similar, Tables 4.37 and 4.38, as the central core oxadiazole and terminal alkyl carbazole in each compound are identical. The similarity in behaviour is confirmed by comparison of the UV-vis absorption spectra of the two compounds in both solution and thin film, Figures 4.61 and 4.62.

**Table 4.39** The melting temperatures ( $^{\circ}\text{C}$ ) of the compounds **51** and **101**.



Compound	R	Cr	Cr	I		
<b>101</b>		•	-	•	205	•
<b>51</b>		•	195	•	204	•

Compounds **101** and compound **51** both exhibit the same melting point ( $205\text{ }^{\circ}\text{C}$ ) without any observable glass transition, despite significant super-cooling below the melting point from the isotropic liquid.

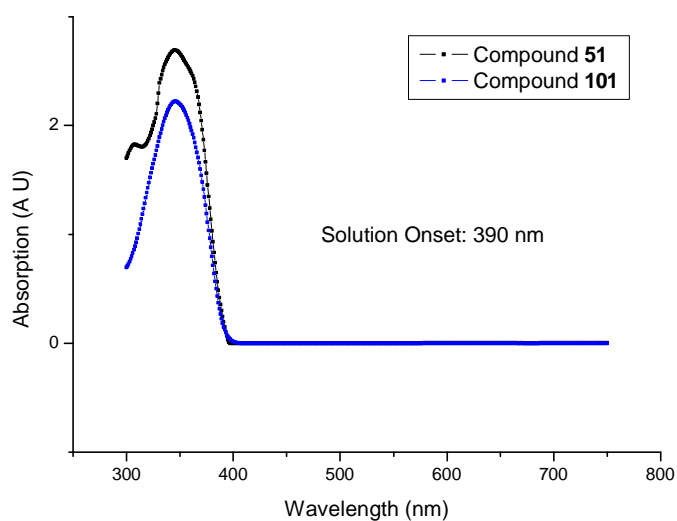


**Figure 4.63** Absorption spectra of compounds **51** and **101** in solution.

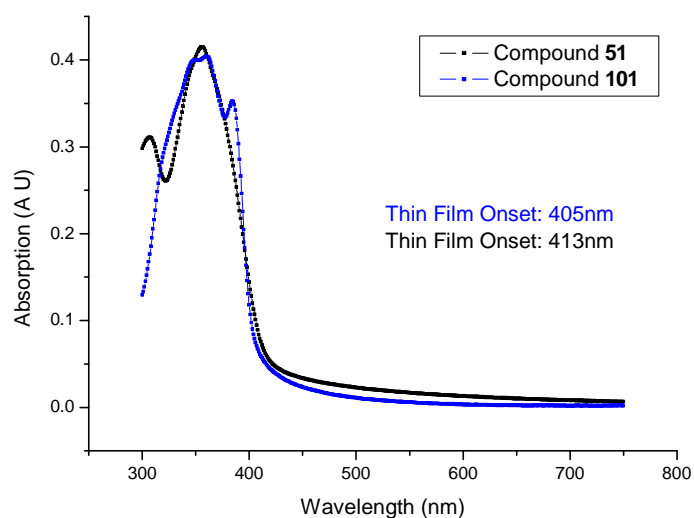
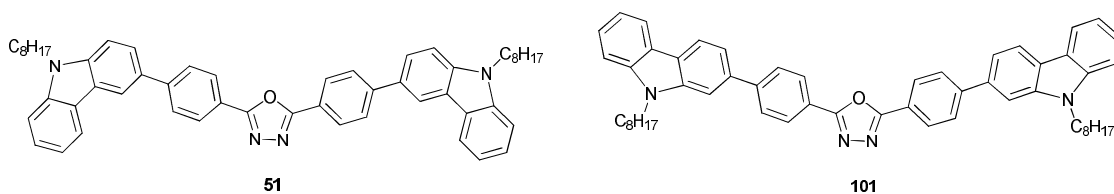


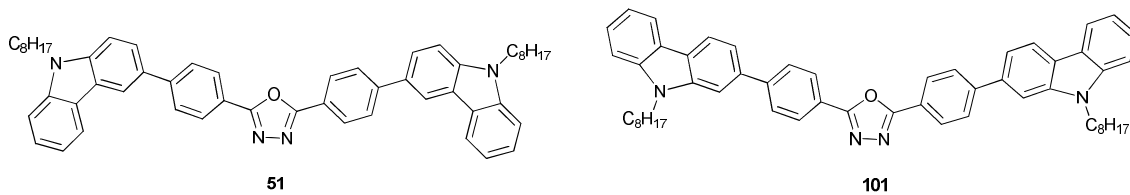
**Figure 4.64** Absorption spectra of compounds **51** and **101** in a thin film.

**Table 4.40** Band gap ( $E_g$ ), ionisation potential (IP) and electron affinity (EA) in eV of compounds **51** and **101** in solution.



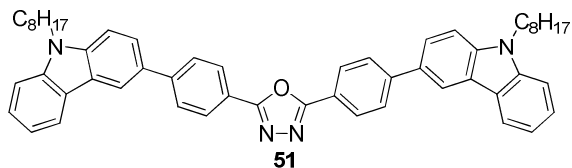
Compound (Solution)	IP	$E_g$	EA
<b>51</b>	5.51	3.18	2.32
<b>101</b>	5.49	3.18	2.31

**Table 4.41** Band gap ( $E_g$ ), ionisation potential (IP) and electron affinity (EA) in eV of compounds **51** and **101** in thin films.



Compound (Thin Film)	IP	$E_g$	EA
<b>51</b>	5.51	3.00	2.50
<b>101</b>	5.49	3.06	2.42

## Characteristics of an OLED incorporating compound **51**.



Compound **51** was intended to be a phosphorescent host in an OLED. Two different types of phosphorescent dopants were used, i.e., a green dopant [Ir(ppy)<sub>3</sub>] and a red dopant [Ir(piq)<sub>3</sub>], Figure 4.65. First, an OLED was fabricated with compound **51** designed to be a host for the green dopant as the emissive layer. The results shown in Figure 4.68 that the spectra was blue, mean that compound **51** was not acting as a host for the dopant, but was emitting the light itself as a fluorescent material. So a device was made without the dopant in the emissive layer, showing that the compound **51** on its own had a higher efficiency than the device with the Ir(ppy)<sub>3</sub> present meaning the dopant was simply acting as an impurity in the device shown in Figure 4.71.

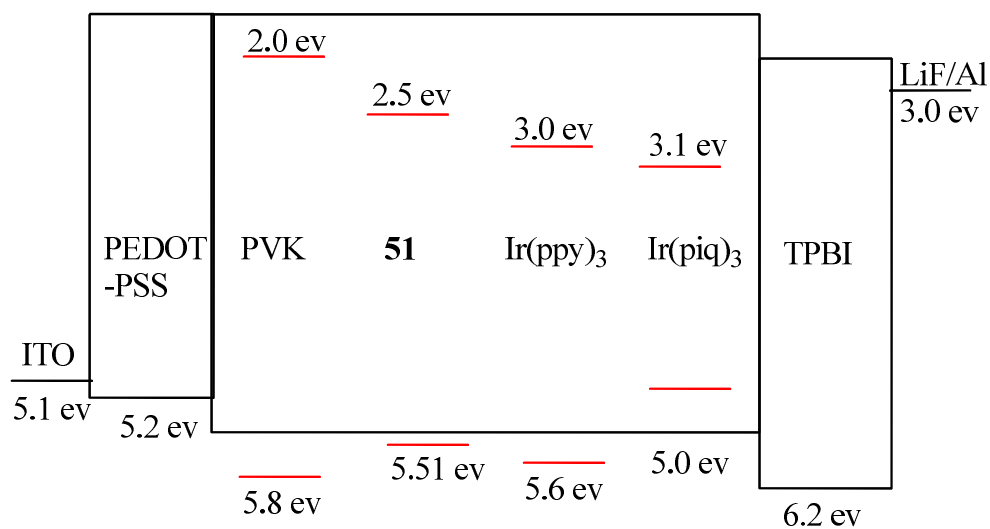


**Figure 4.65** Schematic energy level diagram of a phosphorescent OLED device: LiF/Al as a combined electron-injection layer/cathode; TPBI as an electron-transport layer; Ir(ppy)<sub>3</sub> as a green phosphorescent light-emitting dopant; Ir(piq)<sub>3</sub> as a red phosphorescent light-emitting dopant; PVK as a phosphorescent host; ITO/PEDOT-PSS as a combined anode/hole injection layer.

## Compound 51 & green phosphorescent dopant [Ir(ppy)<sub>3</sub>]

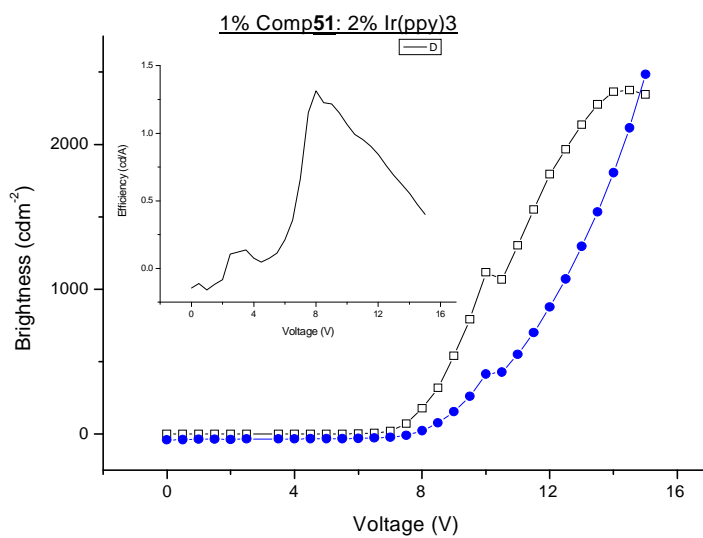


**Figure 4.66** PhOLED device made using PEDOT:PSS, 1% Compound **51**: 2% Ir(ppy)<sub>3</sub> in PVK, TPBI, LiF-doped Al.

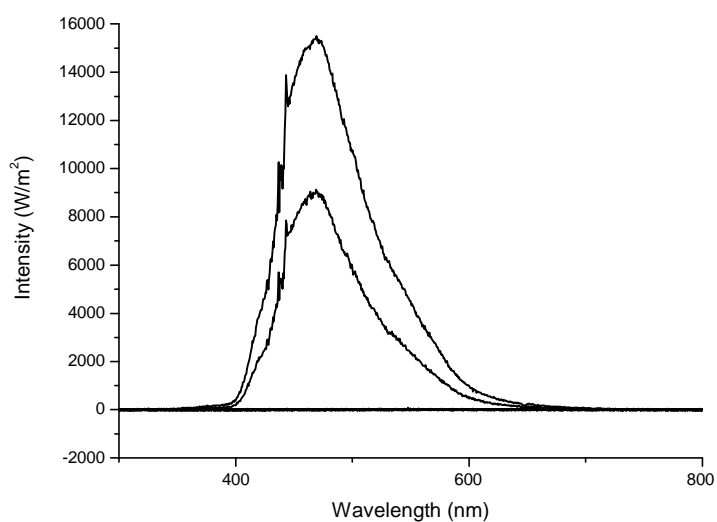


**Figure 4.67** PhOLED device (PEDOT:PSS, Compound **51** (1%): Ir(ppy)<sub>3</sub> (2%), TPBI, LiF and Al) shows constant spectral output with increasing voltage.

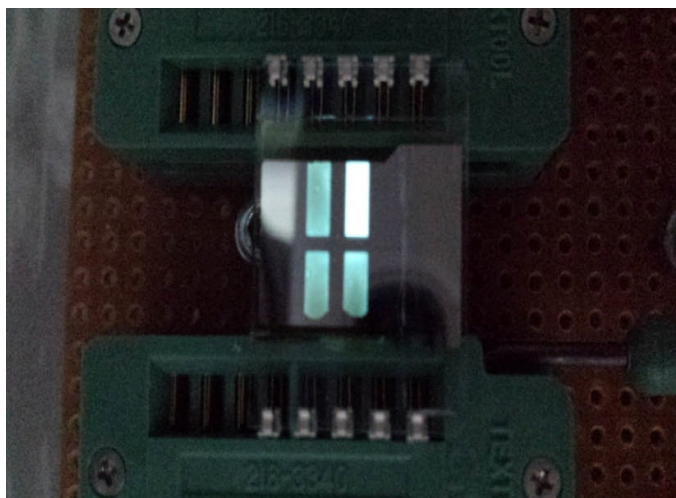


**Figure 4.68** Blue phosphorescent OLED.

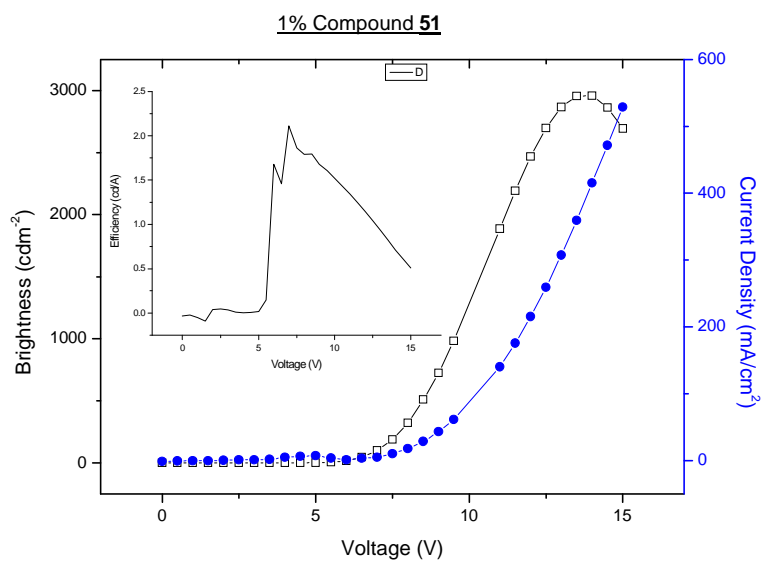


**Figure 4.69** PhOLED device made using; PEDOT:PSS, 1% Compound **51**, TPBI, LiF and Al.

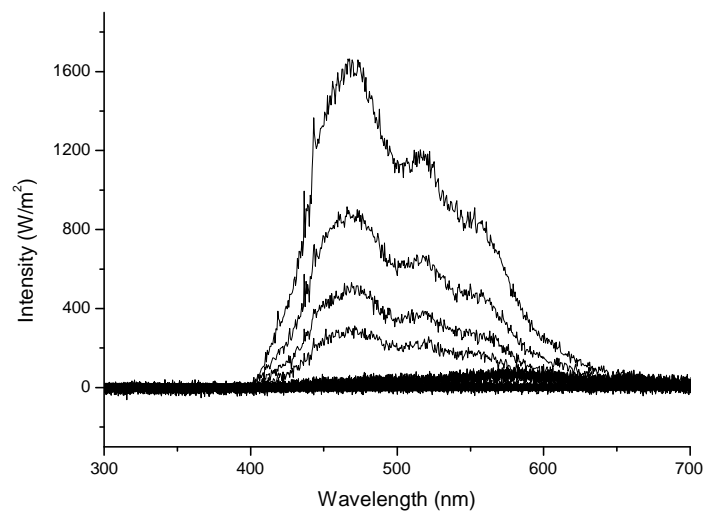


**Figure 4.70** PhOLED device (PEDOT:PSS, 1% Compound **51**, TPBI, LiF and Al) shows constant spectral output with increasing voltage.

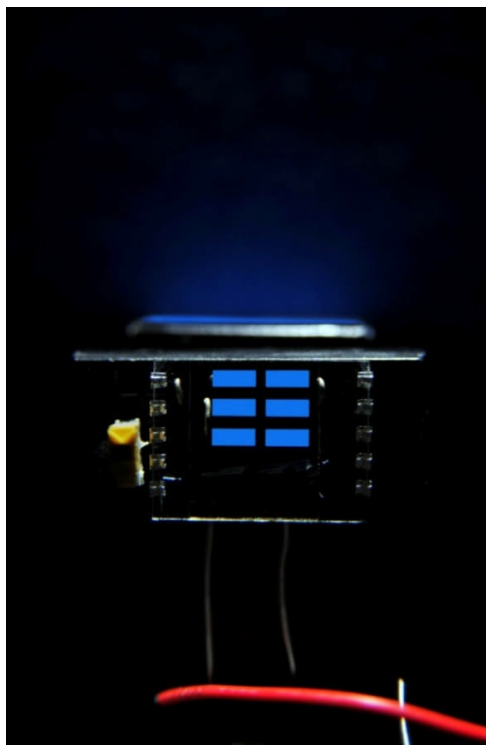


**Figure 4.71** Blue fluorescent OLED.

The electro-optic performance of two OLEDs is shown in Figure 4.72. One OLED uses PVK as the host and Ir(ppy)<sub>3</sub> as a green phosphorescent dopant. The second device uses a mixture of compound **51** and PVK as the host with Ir(ppy)<sub>3</sub> as the emissive dopant. The concentration of compound **51** in the combined transport layer with PVK was varied from 14%, 24% to 34%. Reference to figure 4.72 shows that the presence of compound **51** in the composite emissive layer increases the efficiency of the OLED compared to that of the reference OLED using PVK alone as the dopant host. Compound **51** probably increases the hole-transporting characteristics of the transport layer and so creates a more balanced OLED in terms of charge transport of both holes and electrons. As shown in figure 4.72, a concentration of 24% results in an optimum efficiency.

The addition of a PEDOT-PSS layer lowers the hole injection energy barrier, so a maximum current efficiency of 20.0 cd A<sup>-1</sup> is achieved in a green-emitting PhOLED.

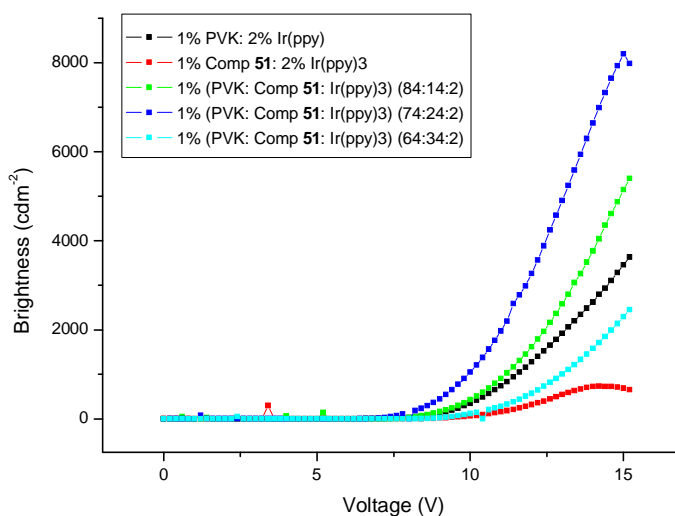


**Figure 4.72** Brightness (cd m<sup>-2</sup>) as a function of voltage (V) for the PhOLEDs shown.

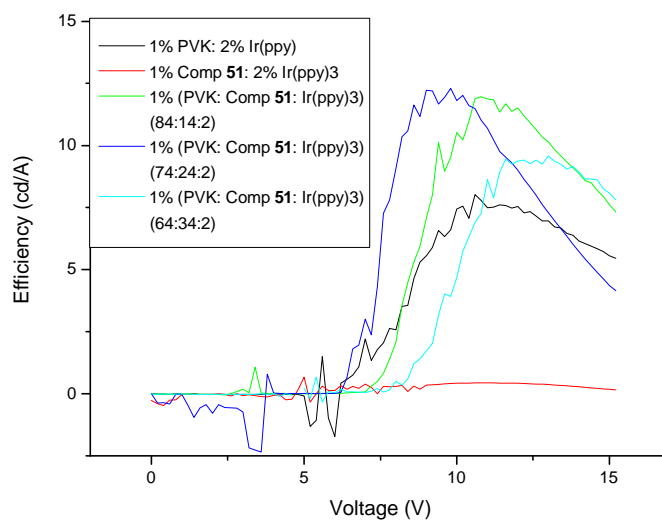


**Figure 4.73** Efficiency ( $\text{cd A}^{-1}$ ) as a function of voltage for the PhOLEDs shown.

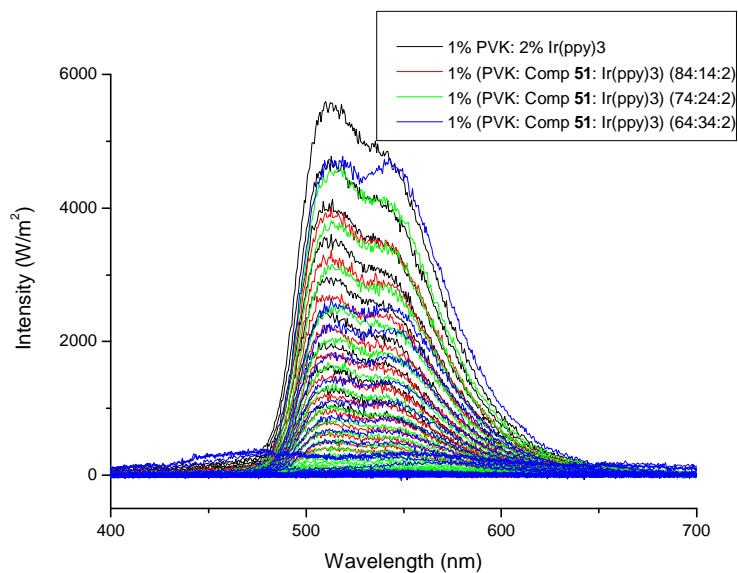


**Figure 4.74** A PhOLED device (PEDOT:PSS, 1% Compound **51**, Ir (ppy)<sub>3</sub>, TPBI, LiF-doped Al) shows a constant spectral output with increasing voltage.

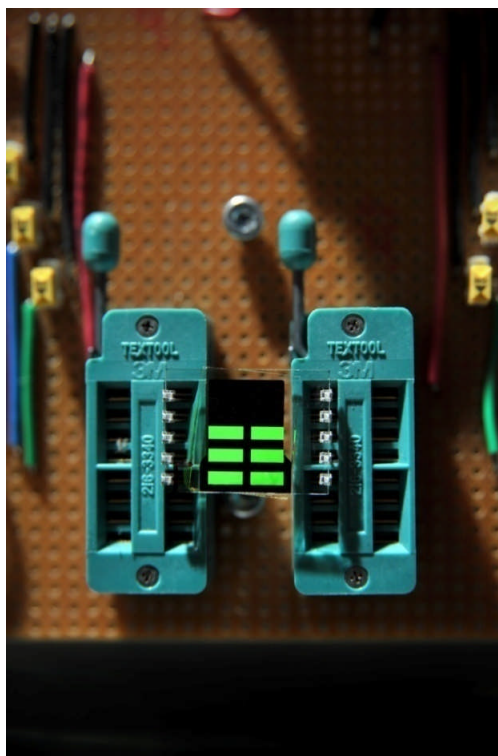


**Figure 4.75** A PhOLED device (PEDOT:PSS, 1% Compound **51**, Ir (ppy)<sub>3</sub>, TPBI, LiF-doped Al) shows a uniform bright green emission.

#### **Compound 51 with red phosphorescent dopant [Ir(piq)<sub>3</sub>]**

Next, the compound **51** was added with the red dopant to see if it would act as a host material. As shown in Figure 4.79 the spectra shows that the light given out was a blue/white colour so again the compound **51** was not acting as a host for the dopant. Again, a standard device was made using PVK as the host with the Ir(piq)<sub>3</sub> as the emissive dopant and then making devices with compound **51** also included with the PVK and Ir(piq)<sub>3</sub> in the emissive layer. The concentration of compound **51** was altered: 14% - 84% with 10% increments. It was found that compound **51** helped increase the efficiency of emission compared to that of the standard PVK device and that increasing the concentration of compound **51** also increases the efficiency further upto a maximum value of 44%, after which the efficiency starts to decrease. After 44% there is a charge imbalance with too many holes in the emissive layer due to the increasing amount of compound **51**. A maximum current efficiency of 6 cd A<sup>-1</sup> is achieved for a red-emitting phosphorescent OLED.

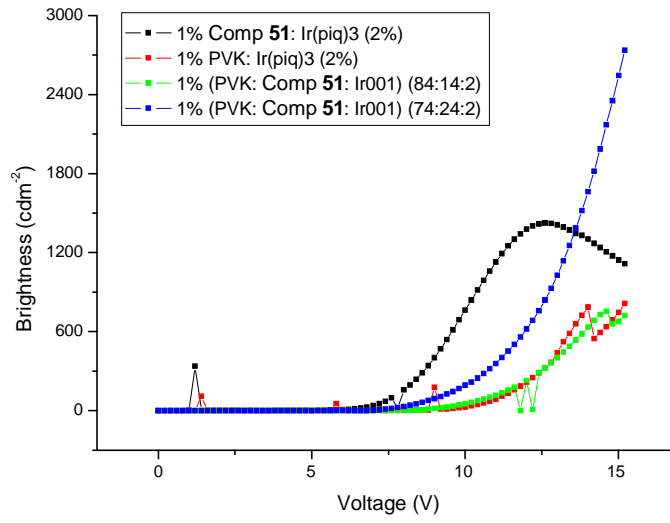


**Figure 4.76** Brightness as a function of voltage for devices.

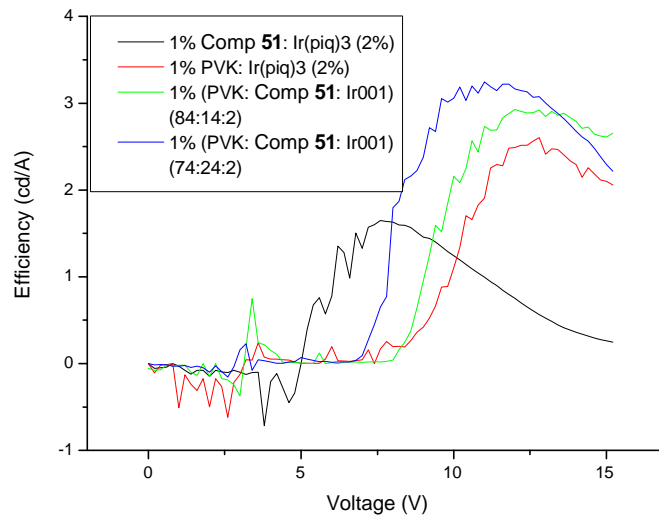


**Figure 4.77** Efficiency as a function of voltage for devices.

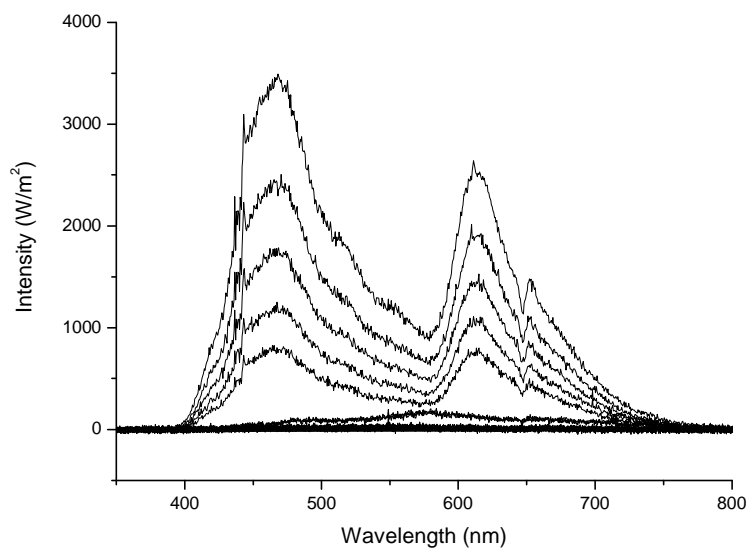


**Figure 4.78** PhOLED device (PEDOT:PSS, 1% Compound **51**: 2% Ir(piq)<sub>3</sub> in PVK, TPBI, LiF-doped Al) shows a similar spectral output with increasing voltage.

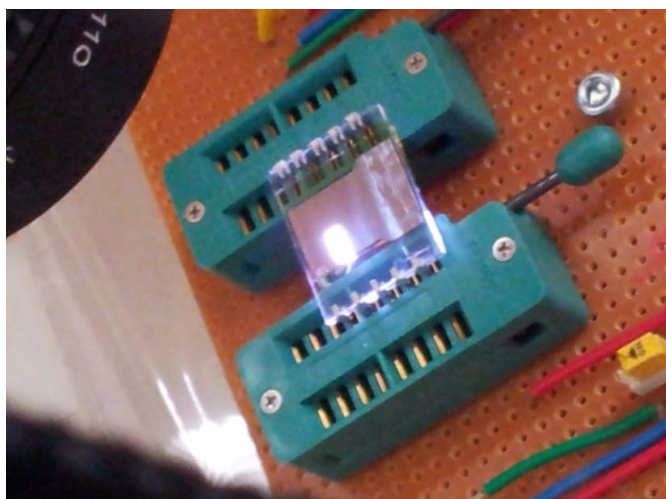


**Figure 4.79** Purple/blue/white light.

### Compound 51 & red phosphorescent dopant [Ir(piq)<sub>3</sub>] and PVK.

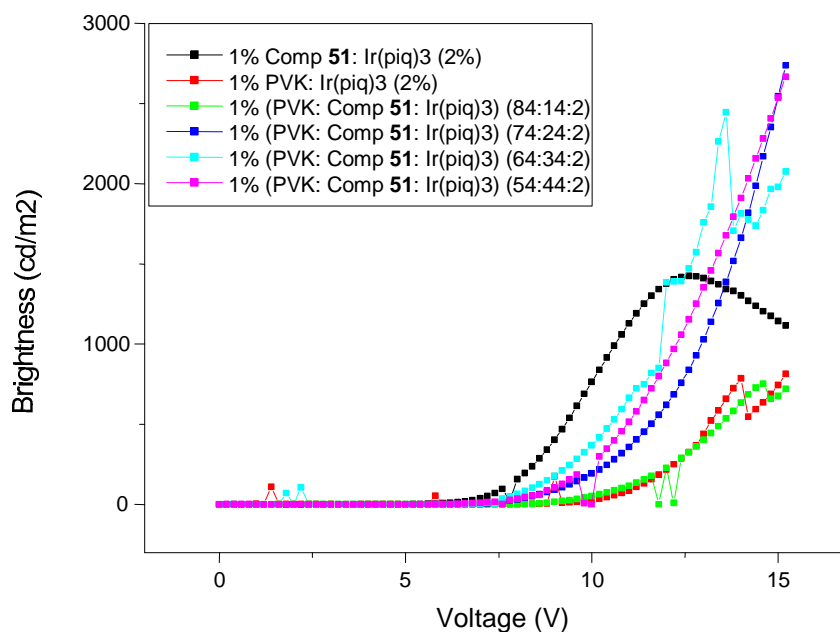


Figure 4.80 Brightness as a function of voltage for devices.

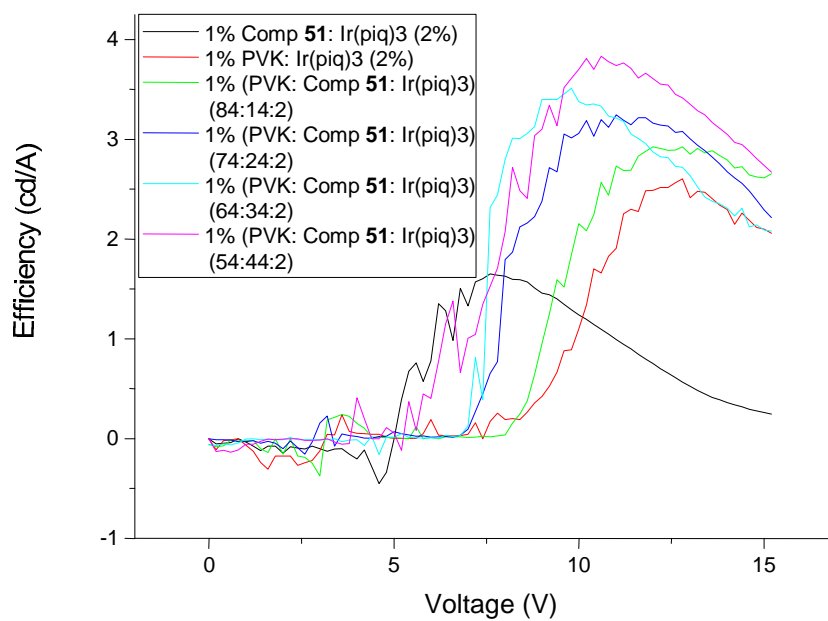
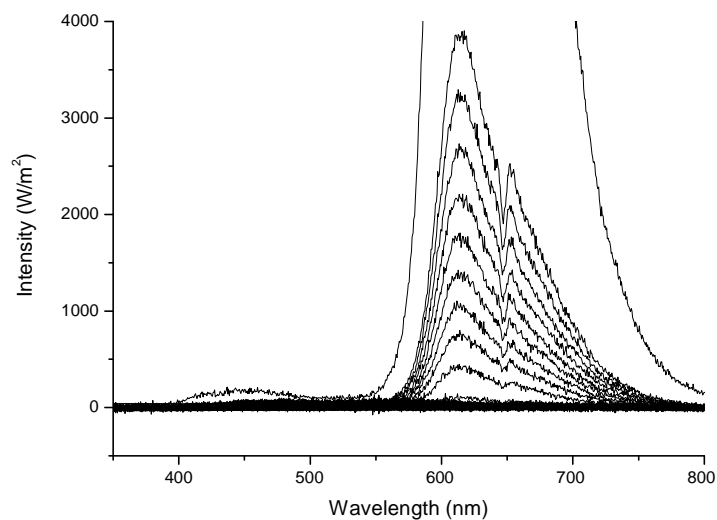
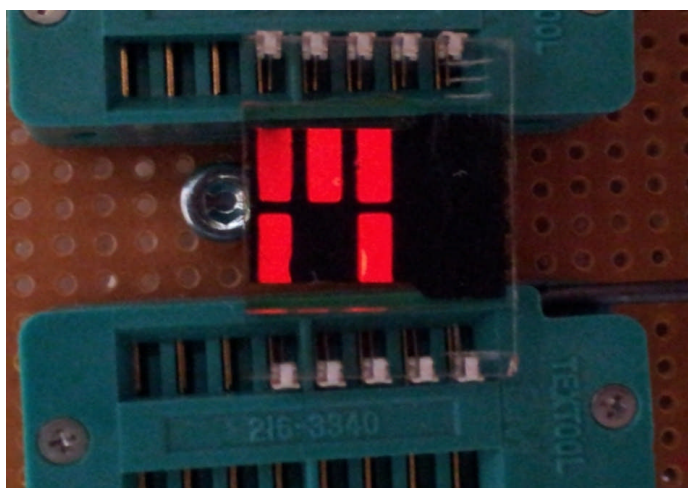


Figure 4.81 Efficiency as a function of voltage for devices.



**Figure 4.82** PhOLED device (PEDOT:PSS, 1% (PVK: Compound **51**: Ir(piq)<sub>3</sub>) (54:44:2), TPBI, LiF and Al) shows constant spectral output with increasing voltage.



**Figure 4.83** Red phosphorescent OLED

Figure 4.83: The presence of compound **51** in the emissive layer of PVK and Ir(piq)<sub>3</sub> increases the brightness, Figure 4.80, and efficiency, Figure 4.81, compared to that of just having PVK and Ir(piq)<sub>3</sub> as the emission layer & increasing the amount of compound **51** in the emissive layer improves the efficiency.

### Comparison of compounds 51, 94 and 101 in an OLED device.

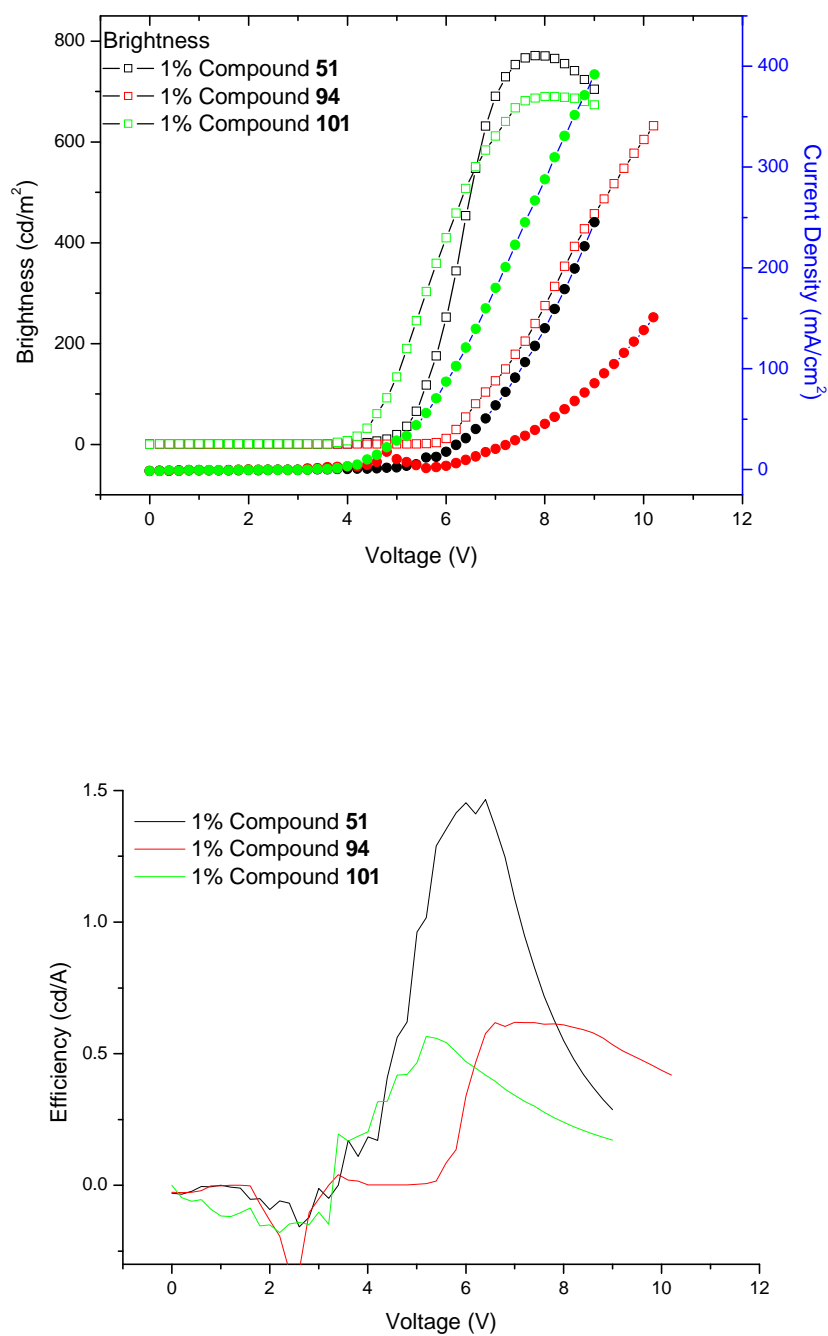


**Figure 4.84:** Characteristics of a) Brightness and current density-voltage and b) Efficiency-voltage for devices using Compound 51, 94 and 101 as the varying emissive layers.

The ionisation potential, optical band-gap and electron-affinities of compounds **51** and **101** are very similar, Table 4.40 and 4.41. The similarity in behaviour is confirmed by comparison of the UV-vis absorption spectra of the two compounds in both solution and thin film, Figures 4.63 and 4.64. It is not surprising to see very similar energy levels as the 2-carbazole end groups in compound **101** was replaced by 3-carbazole end groups in compound **51**.

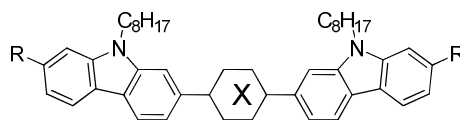
A comparison between the graphs for the compound **51** and **101**, Figure 4.84, shows that the compound **51** in the emissive layer increases the brightness and efficiency of the device compared to that of compound **101** in the emission layer. Conjugation of 2,7-carbazole is spread entirely over the  $sp^2$ -bonded carbon atoms of the main monomer backbone. In this case, the nitrogen atom is at the *meta*-position in the conjugated framework. In contrast, the nitrogen atom of 3,6-carbazole is at the *para*-position in the conjugated framework and significantly influence the properties. The electron-donating strength of the 3,6-carbazole to an electron-deficient unit is stronger than that of the 2,7-carbazole because the nitrogen atom is at the *para*-position with respect to the backbone in the 3,6-carbazoles. Stronger intra-molecular charge transfer and more planar conjugated backbone is expected to facilitate the chain-chain interactions among the compounds and improve the hole mobility.<sup>6,14-15</sup> So compound **51** has better charge transport to the electron deficient unit than compound **101**.

A comparison between the graphs for the compound **94** and **51**, Figure 4.84, shows that that the compound **51** in the emissive layer increases the brightness and efficiency of the device compared to that of compound **94** in the emission layer. Incorporation of phenyl ring into compound **51** does not seem to influence device performance. The brightness and efficiency of compound **94** in emissive layer is poor when compared to the compound **51** and **101**. This might be due to the poor guest-host interaction.

## 4.8.2 Thiophene/carbazoles

The mesomorphic behaviour and liquid crystalline temperatures of the biphenyl **116** and **GH 36**, differing in the nature of the moiety X in a central position and R in a terminal position of the aromatic core, are collated in Table 4.42.

**Table 4.42** The mesomorphic behaviour and liquid crystalline transition temperatures (°C) of the compounds **116** and **GH 36**.



Compound	X	R	Cr	N	I		
<b>GH 36</b> <sup>d</sup>		CH <sub>3</sub> O-	•	265	•	266	•
<b>116</b>		C <sub>8</sub> H <sub>17</sub> O-	•	165	•	198	•

Notes for table<sup>d</sup>: Data collected by Guang Hu of the University of Hull.

Both compounds shown to exhibit nematic mesophases, Figure 4.85. No glass transition could be observed despite significant super cooling below the melting point. The melting and clearing point (265, 266 °C) of the phenyl thiophene **GH 36** is significantly much higher than that (165, 198 °C) of the terthiophene **116** with longer alkyl chains attached to the terminal carbazole, see table 4.42. This may be attributable to steric effects. The octyl groups attached at the terminal position on the carbazole in compound **116** will project further from the plane of the conjugated molecular core and lead to a greater intermolecular separation. This will in turn lead to weaker van der Waals forces of attraction between the aromatic cores of adjacent molecules.

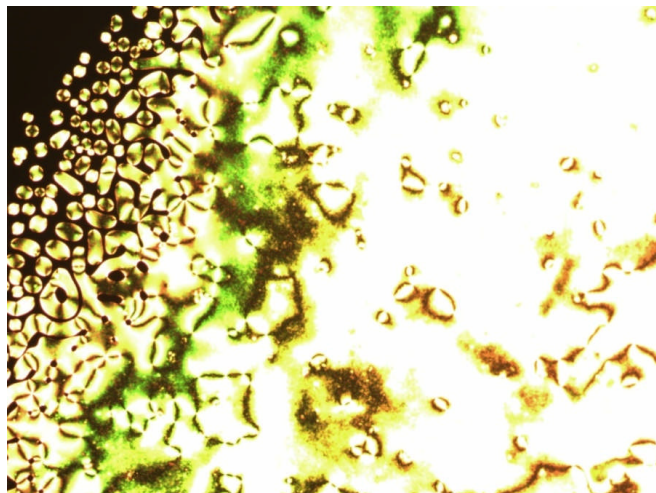


**Figure 4.85** Nematic droplets observed for compound **116** when cooled to just below the clearing point from the isotropic liquid.

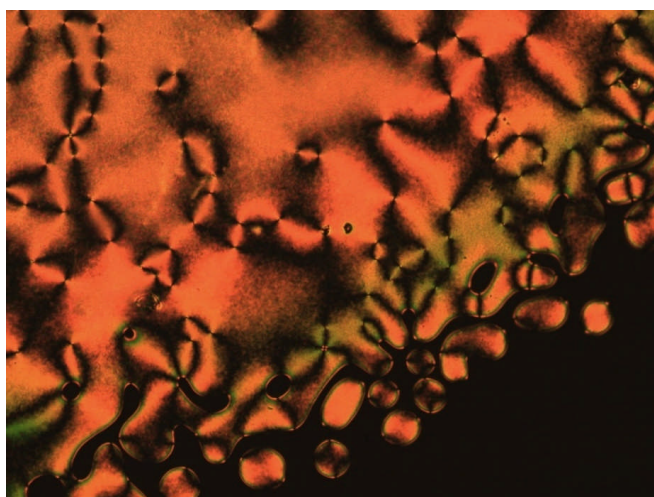


**Figure 4.86** Schlieren texture of the nematic phase observed below the clearing point of compound **116**.

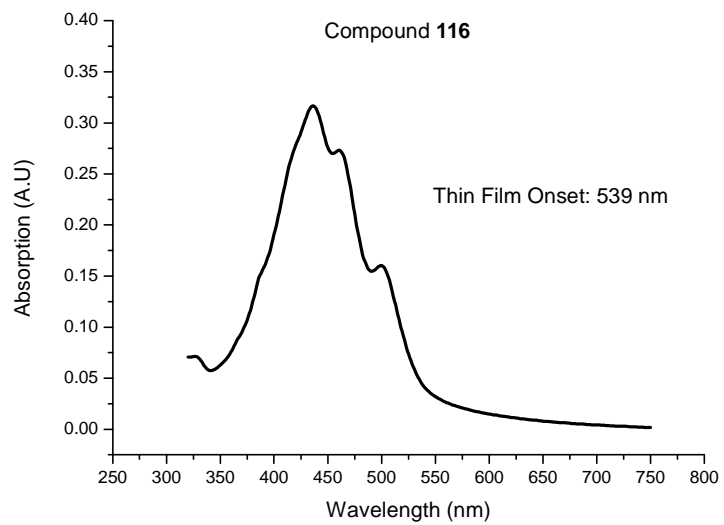


**Figure 4.87** UV-vis absorption spectra of compound **116** in a thin film.

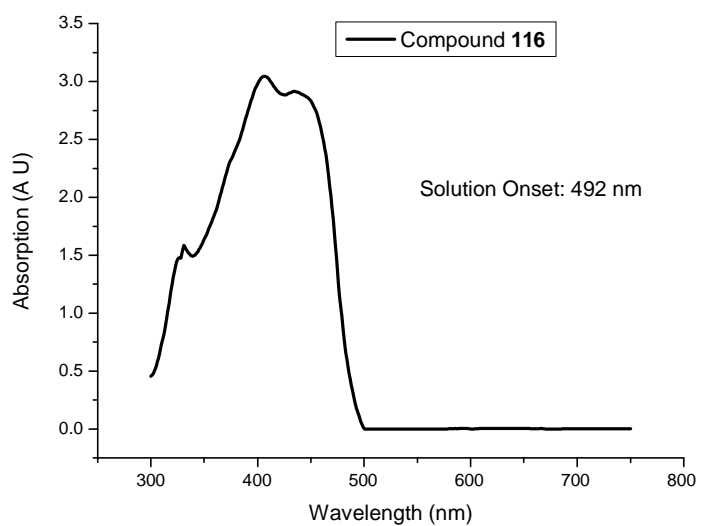
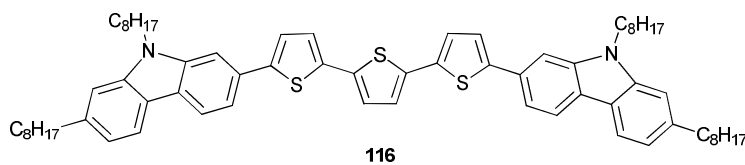


**Figure 4.88** UV-vis absorption spectra of compound **116** in solution.

**Table 4.43** Band gap ( $E_g$ ), ionisation potential (IP) and electron affinity (EA) in eV of compound **116**.



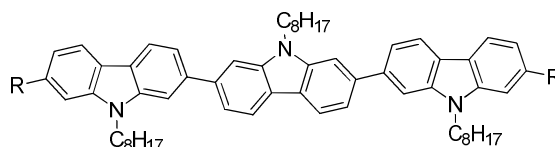
Compound <b>116</b>	IP	$E_g$	EA
Solution	5.30	2.52	2.77
Thin Film	5.30	2.30	3.00

The ionisation potential, optical band-gap and electron-affinities of compounds **116** are collated, Table 4.43. When compared to biphenyl/carbazole compound **121** (Table 4.50) the ionisation potential and electron affinities are lower for thiophene/carbazole compound **116** (Table 4.43), as shown by the UV-vis absorption spectra of the compounds **116** in both solution and thin film, Figures 4.87 and 4.88, respectively.

### 4.8.3 Tercarbazoles

The mesomorphic behaviour and liquid crystalline temperatures of the biphenyl **117** and **CCC**, differing in the nature of the moiety R in a terminal position of the aromatic core, are collated in Table 4.44.

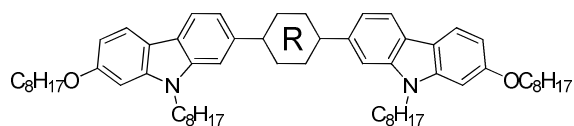
**Table 4.44** The mesomorphic behaviour and liquid crystalline transition temperatures (°C) of the compounds **117** and **CCC**.



Compound	R	T <sub>g</sub>	Cr	N	I			
<b>CCC</b> <sup>14</sup>	H	•	20	•	-	•		
<b>117</b>	C <sub>8</sub> H <sub>17</sub> O-	•	72	•	90	•	109	•

Direct comparison between the data in Table 4.44 for the compounds **117** and **CCC** shows that incorporating a longer alkyl chain at terminal carbazole moiety has a large effect on the transition temperatures, which has also induced mesophase formation for compound **117**.

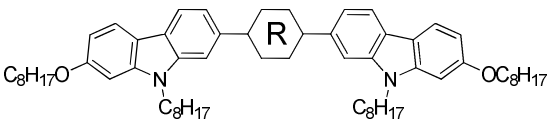
The melting point and the clearing point (90 °C and 109 °C, respectively) of the octyl carbazole **117** shown in Table 4.44 are significantly higher than those (T<sub>g</sub>~20°C) of the corresponding carbazole. The lower transition temperatures are also probably due to steric effect, which has already been discussed in the section **4.3**.

**Table 4.45** Transition temperatures (°C) of the compounds **124** and **117**.

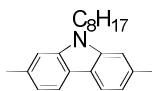
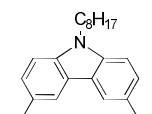
Compound	R	T <sub>g</sub>	Cr	N	I			
<b>124</b>		•	-	•	52	•	60	•
<b>117</b>		•	72	•	90	•	109	•

A comparison between the data in table 4.45 for the fluorene **124** and the carbazole **117** shows that replacing the 2,7-disubstituted-9,9-dipropylfluorene unit with a 2,7-disubstituted-9-octyl-carbazole unit has a large effect on the temperature range of the compounds, although both of these compounds exhibit a nematic mesophase. The melting and clearing point (90 °C and 109 °C, respectively) of the carbazole **117** are much higher than those (52 °C and 60 °C, respectively) of the corresponding 9,9-diopropyl-substituted fluorene **124**. This phenomenon is clearly attributable to steric effects, which has already been discussed in the section **4.2**. In addition to which, the carbazole **117** also exhibits a glass transition above room temperature (72 °C).

**Table 4.46** Transition temperatures (°C) of the compounds **117** and **120**.



The structure shows two carbazole units connected at their 3 and 6 positions to a central hexagonal ring labeled 'R'. Each carbazole unit has an octyl chain (C<sub>8</sub>H<sub>17</sub>) attached to its 2-position. The left carbazole also has an octyl chain (C<sub>8</sub>H<sub>17</sub>O) attached to its 7-position, and the right carbazole has an octyl chain (OC<sub>8</sub>H<sub>17</sub>) attached to its 7-position.

Compound	R	T <sub>g</sub>	Cr	N	I
<b>117</b>		• 72	• 90	• 109	•
<b>120</b>		• -	• 57	• -	•

Direct comparison between the data in Table 4.46 for the compounds **117** and **120** shows that incorporating terminal carbazole groups to central carbazole at 3 and 6 position has large effect on transition temperature. The melting point of 3,6 carbazole is much lower than that of 2,7 carbazole due to the bulky nature and close packing which also disrupt the planarity of the compound **120** leads to eliminate the mesophase formation.

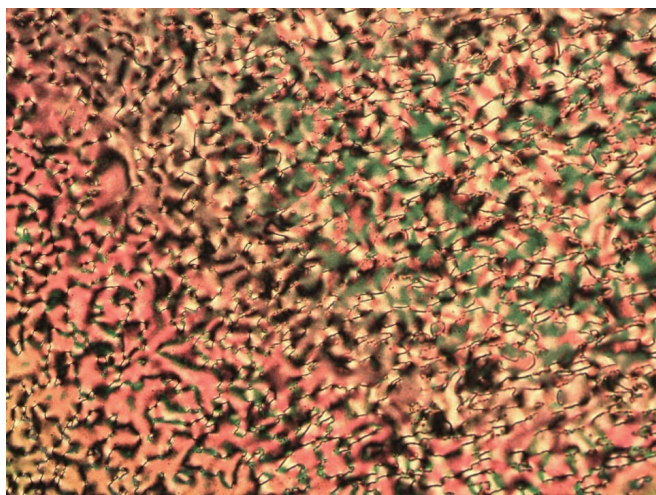


**Figure 4.89** Schlieren texture of nematic phase of compound **117**.

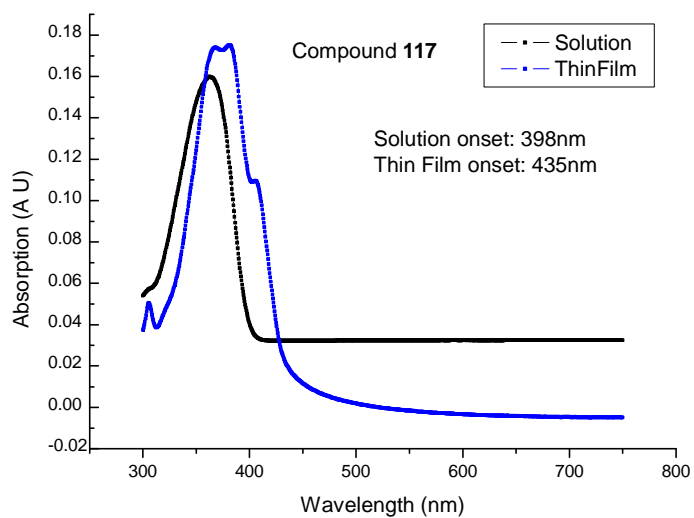


**Figure 4.90** UV-vis absorption spectra of compound **117**.

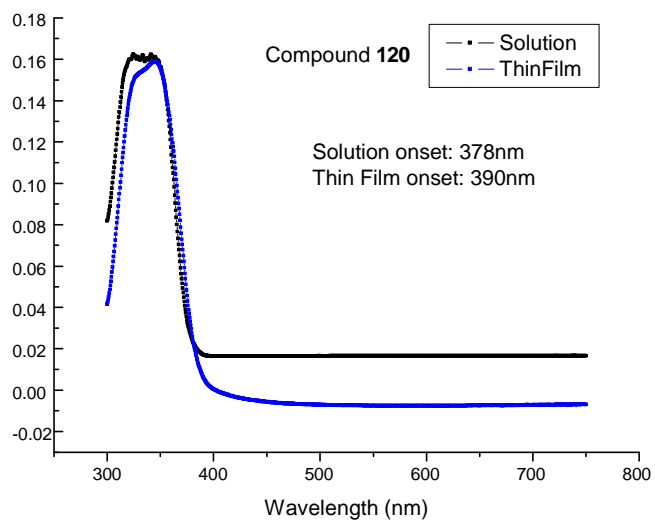
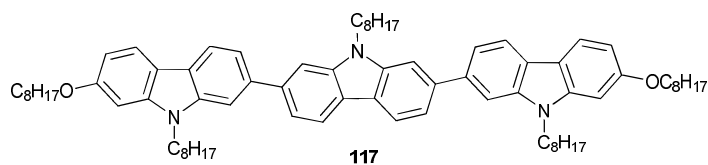


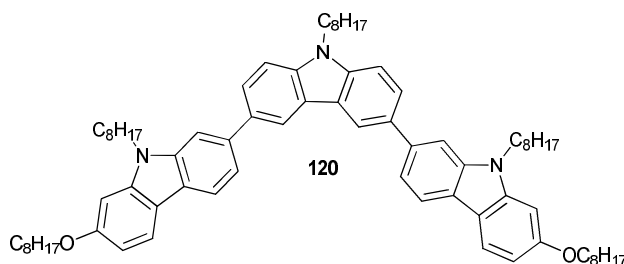
**Figure 4.91** UV-vis absorption spectra of compound **120**.

**Table 4.47** Band gap ( $E_g$ ), ionisation potential (IP) and electron affinity (EA) in eV of compound **117**.



Compound <b>117</b>	IP	$E_g$	EA
Solution	5.50	3.11	2.39
Thin Film	5.50	2.85	2.65

**Table 4.48** Band gap ( $E_g$ ), ionisation potential (IP) and electron affinity (EA) in eV of compound **120** in solution and also as a thin film.



Compound <b>120</b>	IP	$E_g$	EA
Solution	5.48	3.28	2.20
Thin Film	5.48	2.18	2.30

The ionisation potential, optical band-gap and electron-affinities of compounds **117** and **120** are very similar, Tables 4.47 and 4.48, as the carbazole chromophore in each compound is identical. The similarity in behaviour is confirmed by comparison of the UV-vis absorption spectra of the two compounds in both solution and as a thin film, Figures 4.90 and 4.91. There is no significant energy difference in absorption spectra of the thin films, where-as there is a slight difference in absorption spectra of the solutions.

The electron affinity of compound **117** is slightly higher than that of compound **120**. This could be due to close packing of the compound **117**. 3 and 6 positions of carbazole are the most reactive sites and are responsible for producing low band gap. By changing the position from 2 and 7 to 3 and 6 carbazole had a very small effect on energy levels. The electron-donating strength of the 3,6-carbazole to an electron-deficient unit is stronger than that of the 2,7-carbazole.

#### Compound 117 Conductivity Measurements:

Conductivity: P1 =  $3.17 \times 10^{-5}$  S/cm to P3 =  $1.98 \times 10^{-5}$  S/cm.

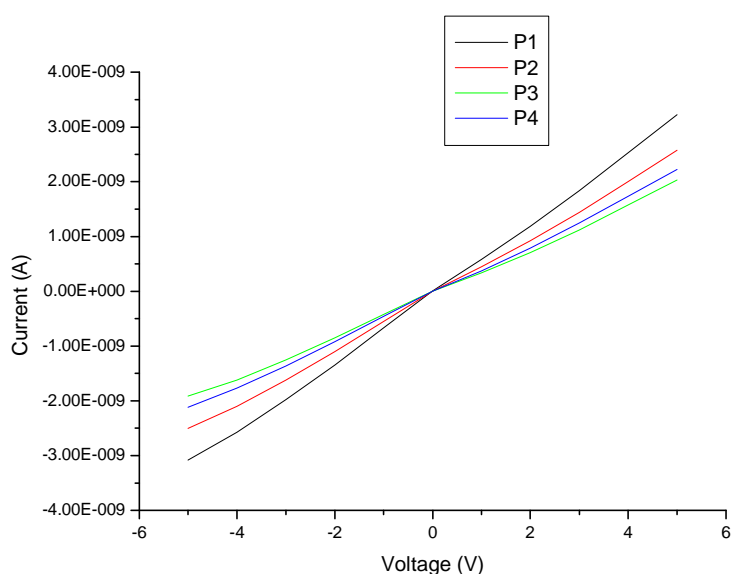


**Figure 4.92** Conductivity of compound **117**.

*N,N,N',N'*-Tetrakis(4-methoxyphenyl)benzidine (MeO-TPD) is a popular hole transport material for organic semiconducting devices which has excellent conductivity. It is often doped to improve mobility and performance.

Conductivity of commercial MeO-TPD was measured as  $1.2 \times 10^{-4}$  S/cm to  $8.15 \times 10^{-5}$  S/cm.<sup>16</sup> Conductivity of compound 116 is very much comparable to MeO-TPD at P1 =  $3.17 \times 10^{-5}$  S/cm to P3 =  $1.98 \times 10^{-5}$  S/cm. Figure 4.92.

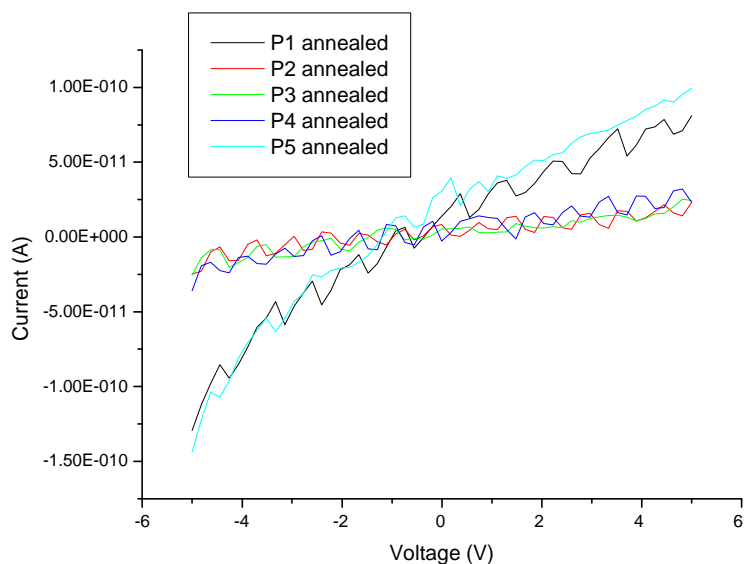


**Figure 4.93** Conductivity of compound **117** at annealed temperature.

Conductivity: P4 =  $1.85 \times 10^{-5}$  S/cm to P3 =  $1.74 \times 10^{-7}$  S/cm.

Compound **117** was annealed at liquid crystalline temperature to see if this improves the conductivity. Unfortunately conductivity of annealed data shows poor conductivity than not annealed data. Comparing the best annealed data against the not annealed data show a factor a 10 difference with the not annealed data having better conductivity.

The graph in the Figure 4.93 shows that molecular aggregation during annealing which could cause poor conductivity.

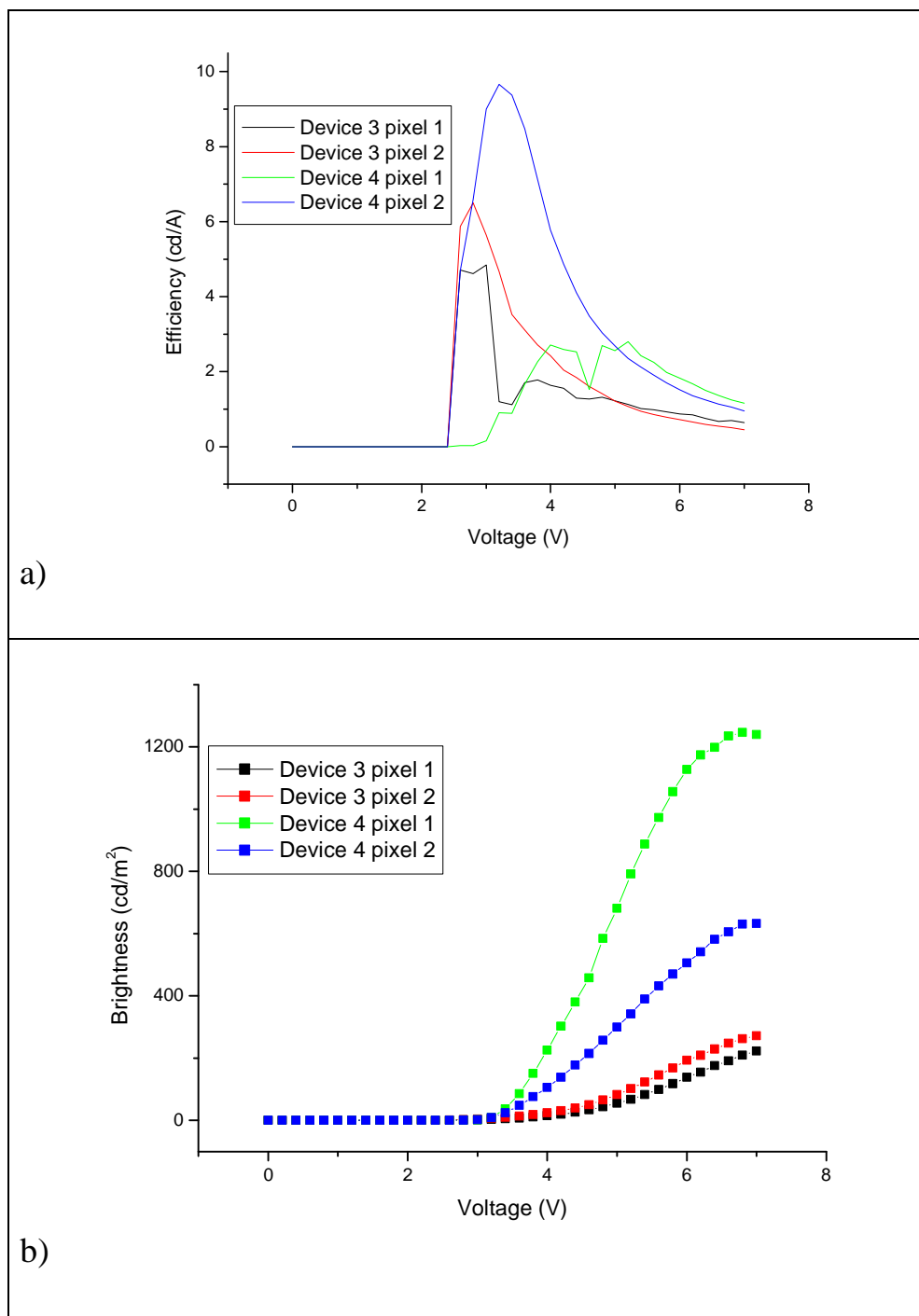


**Figure 4.94** Characteristics of a) Efficiency-voltage and b) Brightness-voltage for device 3 with compound **117** as the host in the emissive, and device 4 with the HT material PBD also included in the emissive layer.

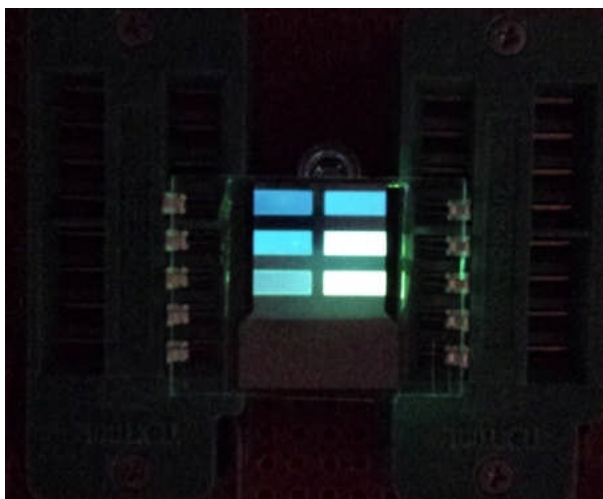


**Figure 4.95** Picture of device 3, showing a mixture of blue/green pixels due to poor guest-host interaction.

#### **Compound 120 Conductivity Measurements:**

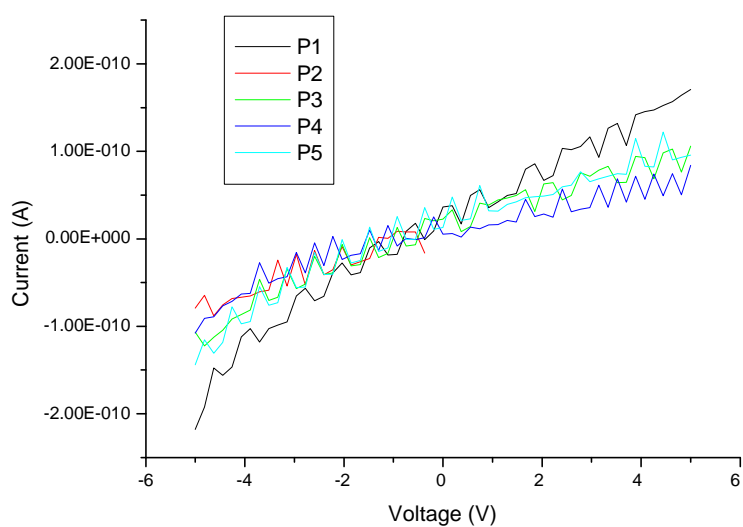


**Figure 4.96** Conductivity of compound 120.

Conductivity: P1 =  $1.66 \times 10^{-6}$  S/cm to P4 =  $7.25 \times 10^{-7}$  S/cm.

Compared to the compound **117**, conductivity of compound **120** is poor figure 4.96. This could be due to the molecular aggregation and close packing of compound **120**.

A OLEDs device was created using compound **117** as the host material in the emissive layer. The OLED was fabricated on a glass substrate, covered with an ITO transparent anode and a PEDOT-PSS was spin coated at 5000rpm for 30s, then baked at 150 °C for 10 minutes. The PVK and a thin film of compound **117** was doped with the Ir(mppy)<sub>3</sub> as well as the PBD (2-(4-biphenyl)-5-(4-tert-butylphenyl)-1,3,4-oxadiazole) was added (using chlorobenzene as solvent) and was spun at 2000 rpm for 30s and then baked at 60°C for 30 minutes. A thin film of compound **117** was spin-coated onto PEDOT-PSS layer from chlorobenzene solution. A hole-blocking layer TPBI was deposited on top of compound **117**, followed by the deposition of lithium fluoride and then aluminium as a combined cathode. The device was then tested to find the characteristics, spectral response and brightness were measured and the efficiencies were also calculated. 2-(4-biphenyl)-5-(4-tert-butylphenyl)-1,3,4-oxadiazole (PBD) was used as an electron transport material.

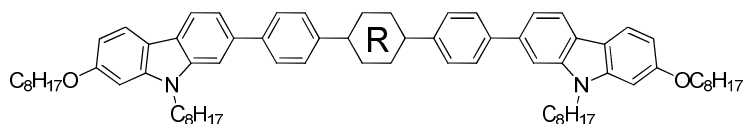
Device 3 shows that Compound **117** (Figure 4.94) is not a good host, as the pixels were blue Figure 4.95, so there was little interaction between the guest and host, some pixels also appeared to have green-blue tint.

A similar result was also seen on device 4. Both devices produced low efficiencies < 10 cd A<sup>-1</sup>. So compound **117** appears to be a poor host with poor hole-transport properties.

#### 4.8.4 Biphenyl/carbazoles

The mesomorphic behaviour and liquid crystalline temperatures of the biphenyls **115** and **121**, differing in the nature of the moiety R in a central position of the aromatic core, are collated in Table 4.49.

**Table 4.49** The mesomorphic behaviour and liquid crystalline transition temperatures (°C) of the compounds **115** and **121**.



Compound	R	Cr	N	I		
<b>121</b>	-	•	141	•	222	•
<b>115</b>		•	148	•	-	•

A direct comparison of the liquid crystalline transition temperatures of compound **121** and compound **115** shown in Table 4.49 shows that the incorporation of oxadiazole ring into two phenylene rings of compound **121** has a large effect on these transition temperatures and the temperature range of the nematic mesophase. The phenyl-carbazole **121** forms a nematic mesophase (141 °C) below a high clearing point (222 °C), Figures 4.97 and 4.98, whereas the oxadiazole-carbazole **115** do not exhibits any mesophase. The oxadiazole-carbazole **115** exhibits a slightly higher melting point (148 °C) compared the values observed for the phenyl-carbazole **121** with same terminal chains. These differences are difficult to explain taking to account and non co-linear nature of the 2,5-disubstituted oxadiazole bonds which may disrupt the planarity of the compound and subsequently eliminates the liquid crystallinity. Therefore, the phenyl-carbazole **121** has a longer length-to-breadth ratio than the oxadiazole-carbazole **115**.

The DSC thermograph shows that compound **121** exhibits a broader nematic range (141-222 °C) and no indication of a glass transition despite supercooling below room

temperature, the DSC thermograph of compound **115** shows no peaks indicative of a mesophase either on heating or cooling.

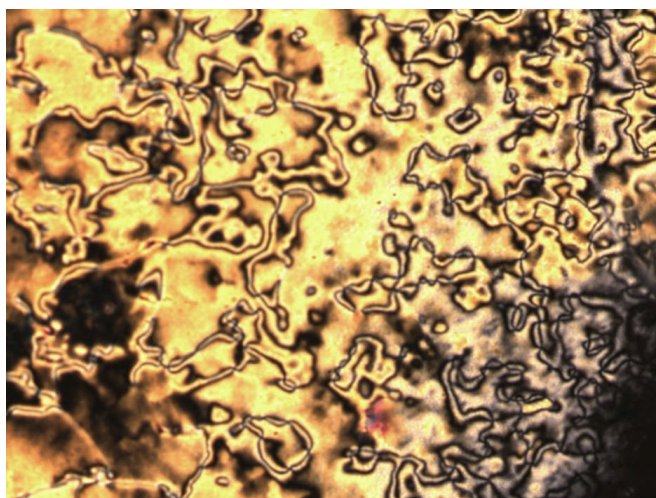


**Figure 4.97** Schlieren texture of nematic phase of compound **121**.

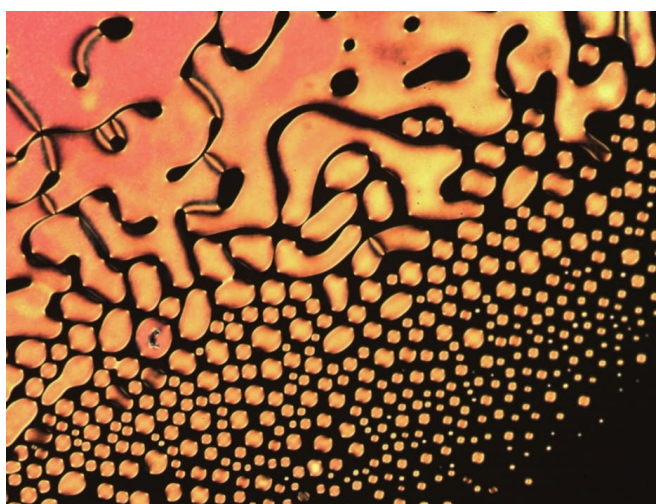


**Figure 4.98** Nematic droplets of compound **121**.

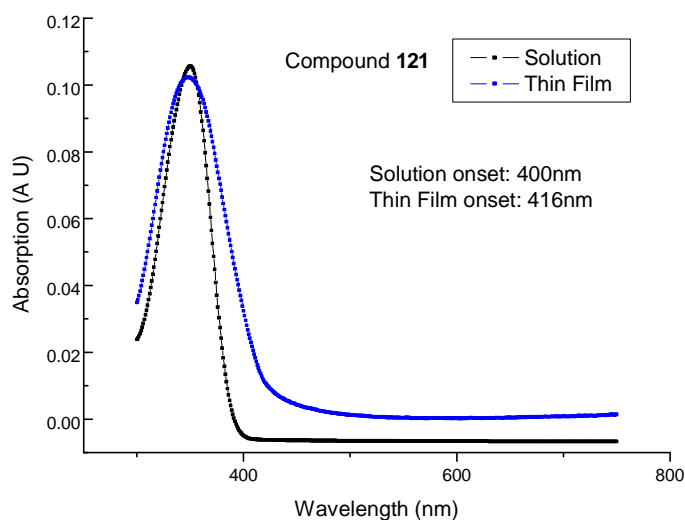
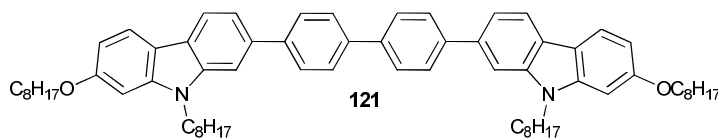


**Figure 4.99** UV-vis absorption spectra of compound **121**.

**Table 4.50** Band gap ( $E_g$ ), ionisation potential (IP) and electron affinity (EA) in eV of compound **121**.



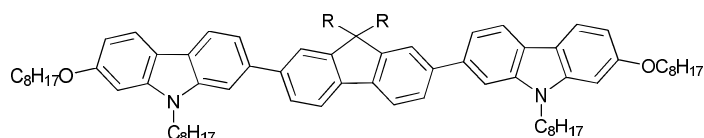
Compound <b>121</b>	IP	$E_g$	EA
Solution	5.60	3.10	2.50
Thin Film	5.60	2.98	2.61

The ionisation potential, optical band-gap and electron-affinities of compounds **115** and **121** are very similar, Table 4.37 and 4.50. It is very surprising that incorporation of oxadiazole ring into the biphenyl does not seem to influence the energy levels significantly. The similarity in behaviour is confirmed by comparison of the UV-vis absorption spectra of the two compounds in both solution and thin film, Figures 4.62 and 4.99. Hence, the terminal carbazole group is one of the major driving forces that controls the ionisation potential and band gap of the extended  $\pi$ -conjugated system. This might be due to the electron deficient nature of oxadiazole and electron rich nature of the terminal carbazole end groups.

#### 4.8.5 Fluorene/carbazoles

The mesomorphic behaviour and liquid crystalline temperatures of the fluorene **124** and **125**, differing in the nature of the moiety R in a central position of the aromatic core, are collated in Table 4.51.

**Table 4.51** The mesomorphic behaviour and liquid crystalline transition temperatures (°C) of the compounds **124** and **125**.



Compound	R	Cr	N	I		
<b>124</b>	C <sub>3</sub> H <sub>7</sub> -	•	52	•	60	•
<b>125</b>	H	•	127	•	198	•

Both of the compounds **124** and **125** are shown to exhibit an enantiotropic nematic mesophase, Figures 5.00 and 5.01. No glass transition could be observed despite a significant degree of super-cooling below the melting point. The DSC thermograph of **125** shows a melting transition at 127 °C, Figure 5.03. The clearing point (198 °C) of the 9,9-fluorene **125** is significantly higher (60 °C) than that of the 9,9-dipropyl-substituted fluorene **124**, Table 4.51. This may be attributable to steric effects. The two propyl groups attached at the 9-position on the fluorene moiety in the centre of compound **124** project further from the plane of the conjugated molecular core and lead to a greater intermolecular separation, which will, in turn, lead to weaker van der Waals forces of attraction between the aromatic cores of adjacent molecules and so to a lower clearing point. This phenomenon also explains the much lower melting point (52 °C) of compound **124** compared to that (127 °C) of compound **125**.

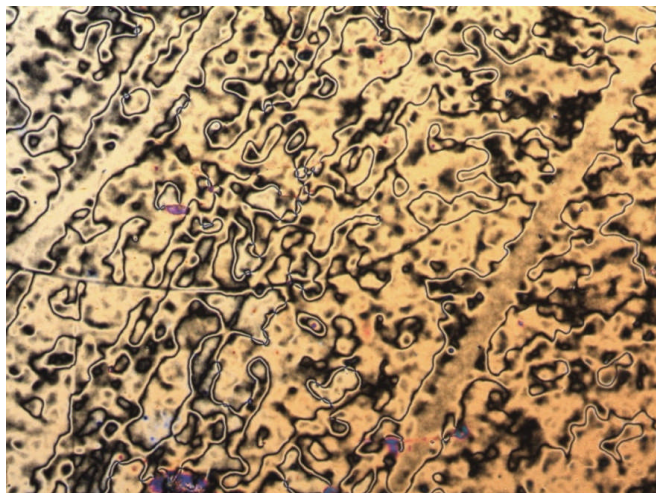


**Figure 5.00** Schlieren texture of nematic phase of compound **125**.

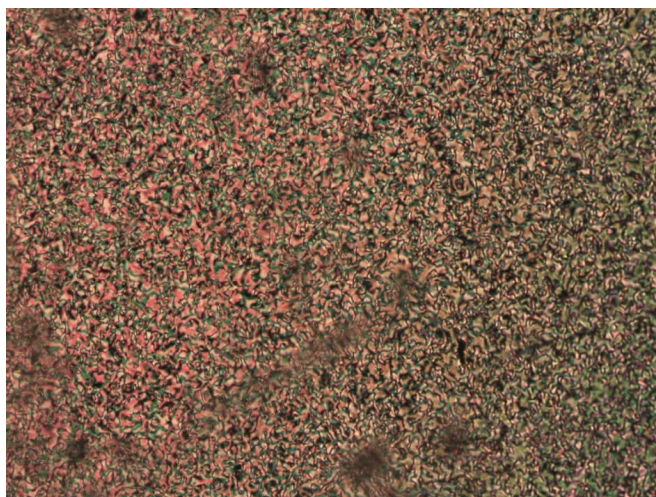


**Figure 5.01** Schlieren texture of nematic phase of compound **124**.

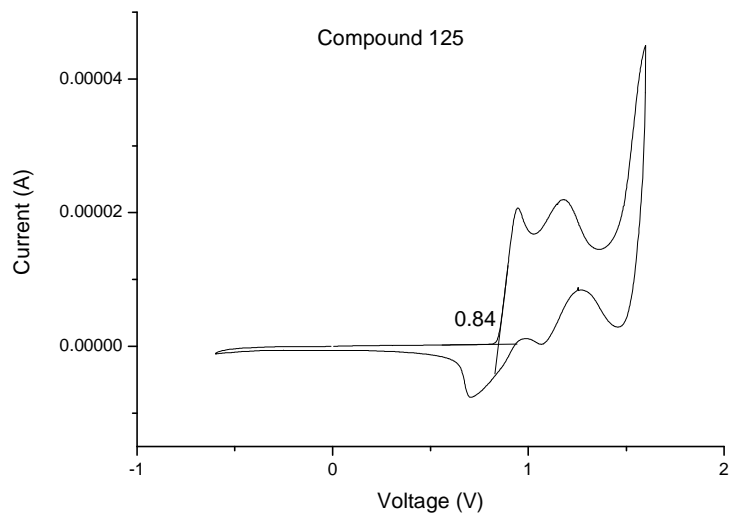


**Figure 5.02** Cyclic voltammogram of compound **125**.

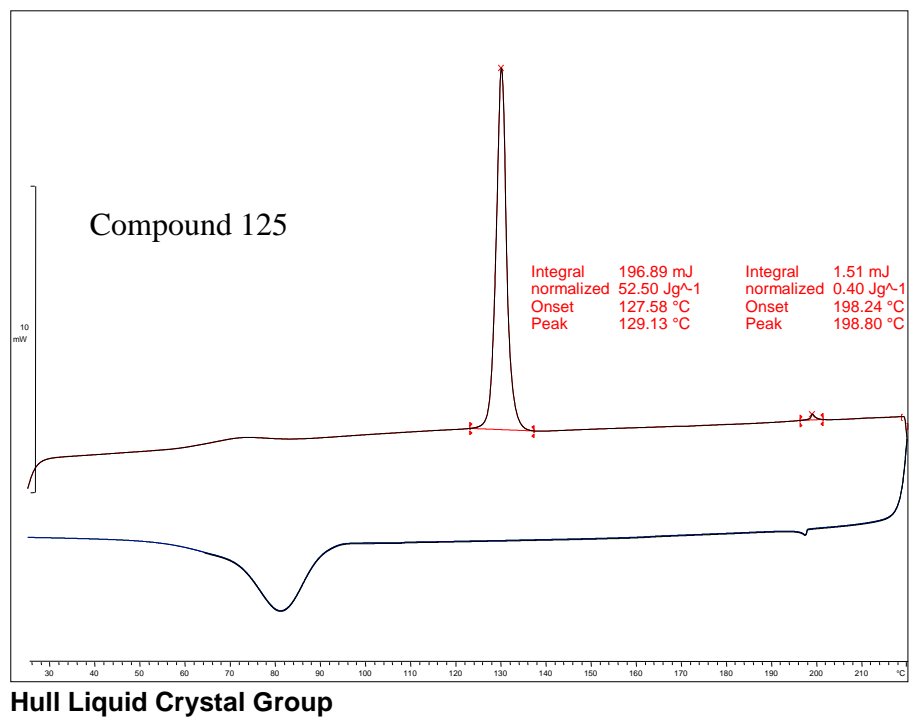


**Figure 5.03** DSC thermograph of compound **125**.

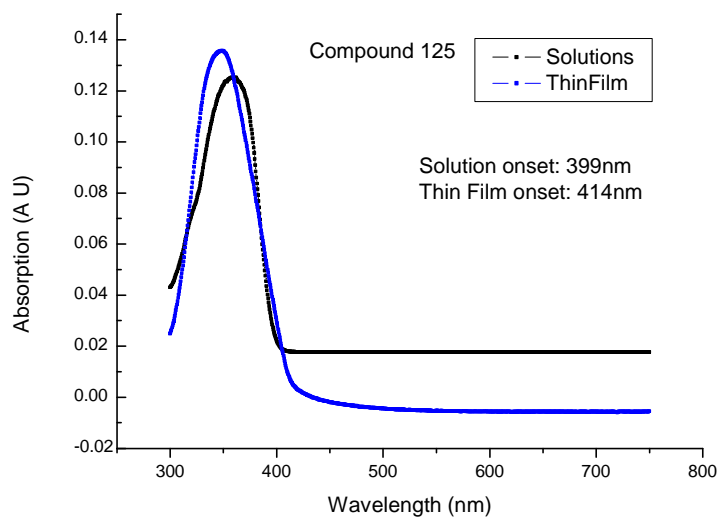


**Figure 5.04** UV-vis absorption spectra of compound **125**.

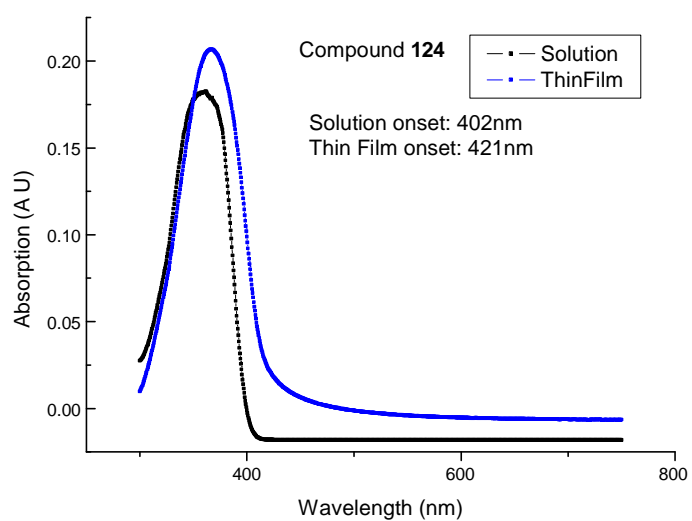
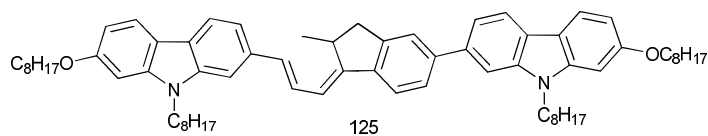


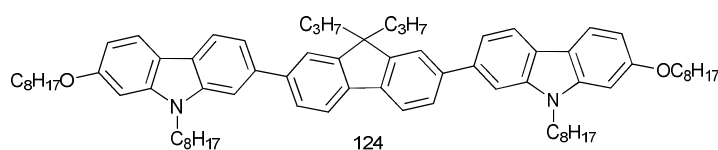
**Figure 5.05** UV-vis absorption spectra of compound **124**.

**Table 4.52** Band gap ( $E_g$ ), ionisation potential (IP) and electron affinity (EA) in eV of compounds **125**.



Compound <b>125</b>	IP	$E_g$	EA
Solution	5.52	3.11	2.41
Thin Film	5.52	2.99	2.52

**Table 4.53** Band gap ( $E_g$ ), ionisation potential (IP) and electron affinity (EA) in eV of compounds **124**.



Compound <b>124</b>	IP	$E_g$	EA
Solution	5.58	3.08	2.50
Thin Film	5.58	2.94	2.63

### Compound 125 Conductivity Measurements:

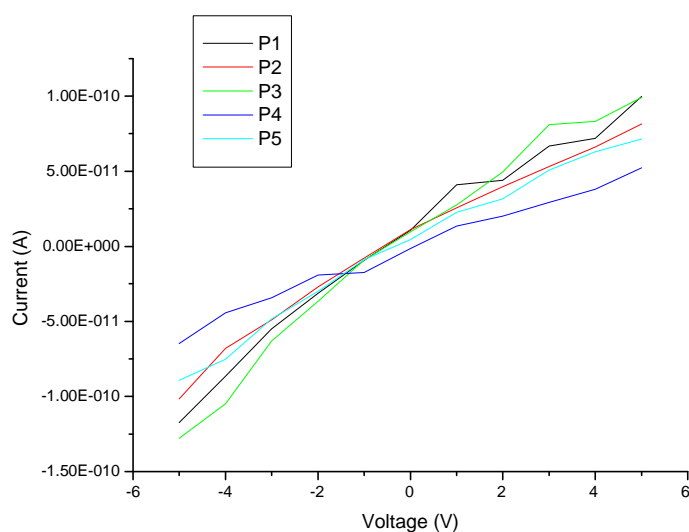


**Figure 5.06** Conductivity of compound **125**.

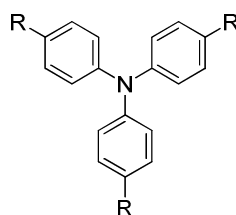
Conductivity of compound **125** shown in Figure 5.06 and was measured as P1 =  $1.04 \times 10^{-6}$  S/cm to P4 =  $5.5 \times 10^{-7}$  S/cm. Compared to the conductivity of standard MeO-TPD data against the compound **125** data show a factor 10 difference with poor conductivity.

The ionisation potentials, optical band-gaps and electron-affinities of compounds **124** and **125** are very similar, Tables 4.52 and 4.53 as the central core fluorene and terminal alkyl carbazole in each compound are identical. The similarity in behaviour is confirmed by comparison of the UV-vis absorption spectra of the two compounds in both solution and thin film, Figures 5.04 and 5.05. There is no significant energy difference between these two compounds in solution and thin film as well.

#### 4.8.6 Triphenylamine/carbazoles

The melting temperatures of the triphenylamine **127** and **POL 514**, differing in the nature of the moiety R in a terminal position of the aromatic core, are collated in Table 4.54.

**Table 4.54** Melting temperatures (°C) of the compounds **127** and **POL 514**.



Compound	R	Cr	I	
<b>127</b>		•	111	•
<b>POL 514<sup>c</sup></b>		•	115	•

Notes for table<sup>c</sup>: Data obtained by Dr. Stuart P. Kitney of the University of Hull.

A comparison between the compound **127** and the compound **POL 514** shows that replacing the carbazole end chain by the phenyl octyloxy chain has a small effect on the melting point, Table 4.54. Both the compounds do not exhibit any observable mesomorphic behaviour. The melting point (111 °C) of the compound **127** is slightly lower than that (115 °C) of the compound **POL 514**. This phenomenon cannot be explained by differences in steric hindrance, which is much higher for the compound **127**. This difference may be attributed to the number of alkyl chains attached to these compounds. Compound **POL 514** has only one alkyl chain attached to the terminal phenyl group, whereas, compound **127** has two alkyl chains attached to the carbazole end groups, which leads to lowering of the melting point despite the bulky nature of the carbazole **127**.

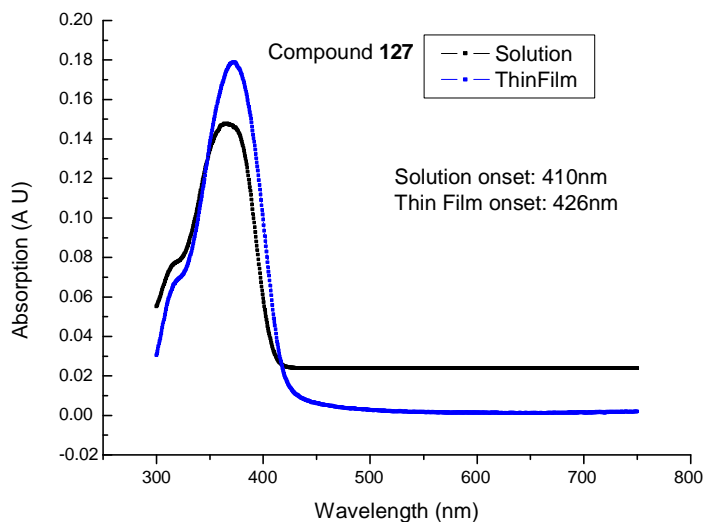
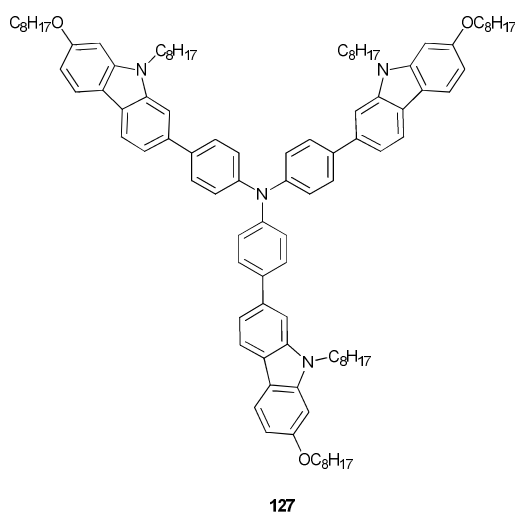


**Figure 5.07** UV-Vis absorption spectra of compound **127**.

**Table 4.55** Band gap ( $E_g$ ), ionisation potential (IP) and electron affinity (EA) in eV of compound **127**.



Compound <b>127</b>	IP	$E_g$	EA
Solution	5.20	3.02	2.17
Thin Film	5.20	2.92	2.28

### Compound 127 Conductivity Measurements:

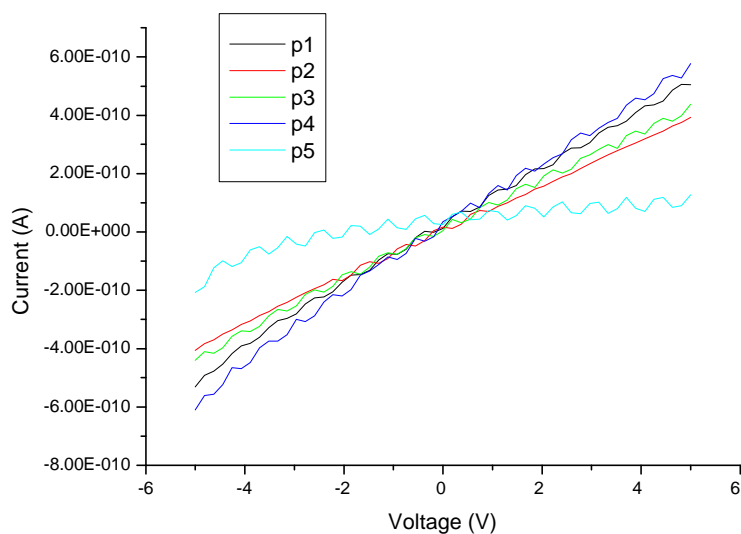


**Figure 5.08** Conductivity of compound **127**.

Conductivity: P4 =  $5.7 \times 10^{-6}$  S/cm to P5 =  $1.17 \times 10^{-6}$  S/cm.

Triphenyl amine and its derivatives are very useful materials in phosphorescent OLEDs as they are an excellent hole transport materials. The triphenylamine derivatives have very good hole-mobilities, good solubility and relatively low ionisation potential.<sup>17</sup>

To improve the thermal and morphological stabilities of triphenyl amines it was decided to synthesise a larger molecular weight compound with greater steric bulk, so as to minimise the chance of crystallisation.

The ionisation potential, optical band-gap and electron-affinities of compounds **127** are collated in Table 4.55. Incorporation of bulky carbazole end groups onto the triphenyl amine core moiety leads to a relatively low ionisation potential and band gap. This was confirmed by the Uv-vis absorption spectrum of compound **127**, Figure 5.07.

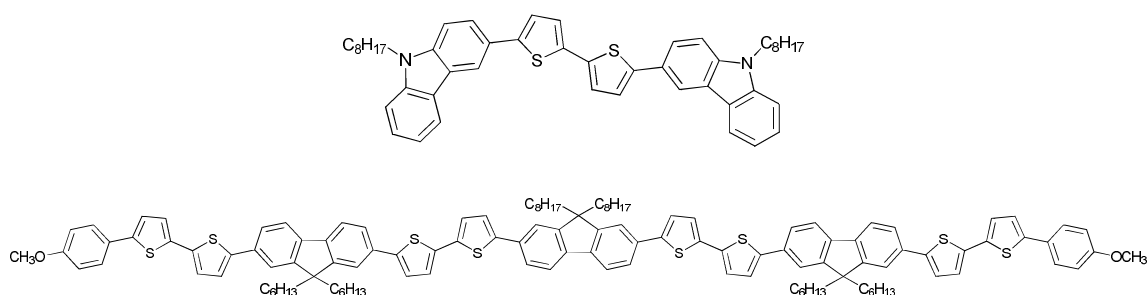
The conductivity of compound **127** was measured, Figure 5.08, and exhibits good conductivity as compared to MeO-TPD. It can act as good hole-transport material in OLEDs with high-lying HOMO levels.

## 4.9 References

1. M. S. Dixon, PhD Thesis, Hull University, 2009.
2. S. M. Kelly “*Flat panel displays: Advanced organic materials*” RSC, 2000.
3. S. P. Kitney, PhD Thesis, Hull University, 2008.
4. A. C. Grimsdale and K. Mullen, *Macromol. Rapid Commun.*, 2007, **28**, 1676.
5. T. T. Steckler, P. Henriksson, S. Mollinger, A. Lundin, A. Salleo and M. R. Anderson, *J. Am. Chem. Soc.*, 2014, **136**, 1190.
6. G. P. Chang and K. H. Hsieh, *Thin Solid Films.*, 2013, **527**, 291.
7. A. C. Grimsdale and K. Mullen, *Macromol. Rapid Commun.*, 2007, **28**, 1676.
8. S. I. Kato, S. Shimizu and H. Taguchi, *J. Org. Chem.*, 2012, **77**, 3222.
9. J. H. Wild, K. Bartle, N. T. Kirkman, S. M. Kelly, M. O'Neill, T. Stirner and R. P. Tuffin, *Chem. Mater.*, 2005, **17**, 6354.
10. P. Imin, M. Imit and A. Adronov, *Macromol.*, 2011, **44**, 9138.
11. H. Mo, K. R. Radke, K. Ogawa, L. H. Christopher, B. T. Erpelding and S. C. Rasmussen, *Phys. Chem. Chem. Phys.*, 2010, **12**, 14585.
12. J. Mei, K. R. Graham, R. Stalder and J. R. Reynolds, *Org. Lett.*, 2010, **12**, 660.
13. K. Mahmood, Z.P. Liu, C. Li, Z. Lu, T. Fang, X. Liu, J. Zhou, T. Lei, J. Peib and Z. Bo, *Polym. Chem.*, 2013, **4**, 3563.
14. M. Belletête, M. Bédard, J. Bouchard, M. Leclerc and G. Durocher, *Can. J. Chem.*, 2004, **82**, 1280.
15. S. Koyuncu, I. Kaya and F. B. Koyuncu, *Synth. Metals.*, 2009, **159**, 1034.
16. M. L. Tietze, L. Burtone, M. Riede, B. Lussem and K. Leo, *Phys. Review.*, 2012, **86**, 0353.
17. P. Cias, C. Slugovc and G. Gescheidt, *J. Phys. Chem.*, 2011, **115**, 14519.
18. M. O'Neill and S. M. Kelly, *Adv. Mater.*, 2011, **23**, 566.
19. T. A. Halgren, *J. Comp. Chem.*, 1996, **17**, 490.

## 5. Conclusions

A direct arylation method has been developed to synthesis a wide range of highly conjugated organic electronic materials more efficiently. This direct arylation method is a straightforward approach that generates little waste and no toxic by-products, in contrast to traditional coupling methods such as Suzuki coupling and Stille coupling. It should facilitate the scaling up of the laboratory synthesis of promising lead compounds synthesized as part of this thesis, e.g., thiophene-based organic semiconductors, which have been successfully synthesised in high yields by employing this palladium-catalyzed direct arylation reaction.

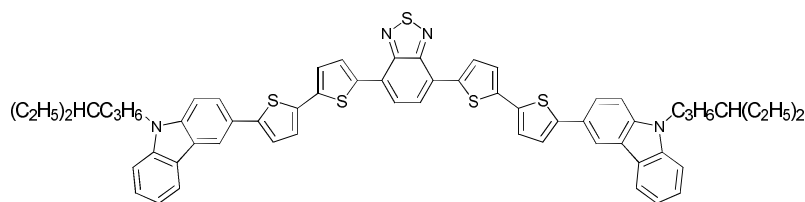


A series of novel compounds with *N*-octyl-3-carbazole end groups to be used as charge-transporting, light-emitting fluorophores, hosts for organo-metallic phosphorescent emitters and/or electron-donors and/or electron-acceptors for use in OLEDs, PhOLEDs, OPVs and OFETS has been synthesised and the relationships between molecular structure, especially the nature of the carbazole end-group, and the mesomorphic behaviour and liquid crystalline transition temperatures were established.

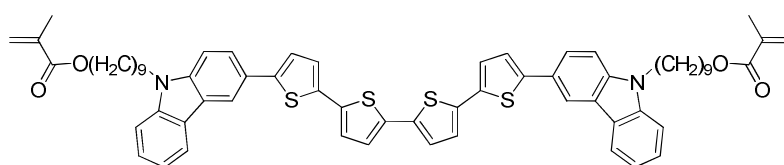
Some of the compounds exhibit liquid crystalline mesophases over significant temperature ranges. Unfortunately many of these compounds were found not to exhibit any liquid crystalline properties due to the bulky nature of the extended *N*-alkyl carbazole group and the small length-to-breadth ratio of the overall molecular core. However, these compounds could still be useful in plastic electronic applications as molecular glasses with suitable properties as, such appropriate energy levels and good charge transport properties.

A series of novel donor-acceptor conjugated compounds based on the benzothiadiazole acceptor moiety has been synthesized for use as efficient donor materials in OPVs. A

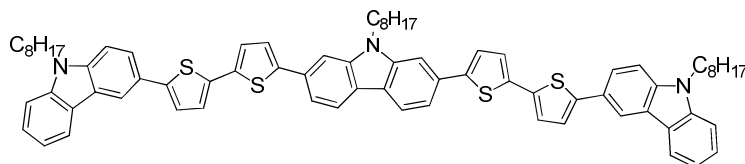
solar cell made with one of these compounds exhibits a maximum power conversion efficiency of  $\eta = 1.6\%$ .



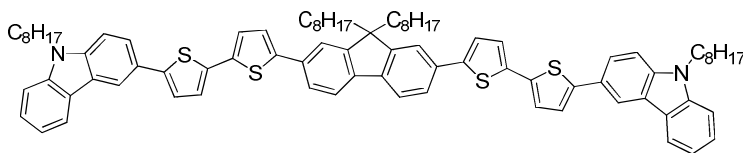
A 2,2':5',2'':5'',2'''-quaterthiophene with a 3-substituted carbazole attached to each end of the molecule was prepared with a methacrylate polymerisable groups at the end of each of the two flexible aliphatic groups attached to the carbazole moiety. The processing conditions of this new reactive mesogen to form polymer networks as thin solid films are being investigated.



A number of *N*-alkyl-carbazoles with additional 3-substituted carbazoles attached to the ends of the molecular core have been synthesised for the first time. Branching of the aliphatic chain attached to the nitrogen atom in the carbazole ring leads to a significantly broader smectic temperature range compared to that of a straight-chain analogue. Carbazoles generally give rise to higher liquid crystalline transition temperatures than the 9,9-dialkyl fluorenes because the *N*-alkyl group lies in the plane of the molecule in the carbazoles in contrast to the out-of-plane orientation of the two alkyl chains in the corresponding 9,9-dialkyl fluorenes. Molecular modelling suggests that the *N*-alkyl chain lies primarily in the plane of the aromatic core of the molecule.

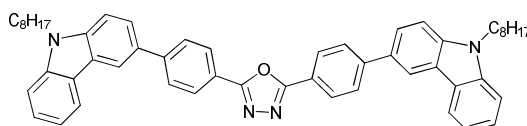


A small number of liquid crystalline 2,7-disubstituted-9,9-dioctyl-fluorenes with a 3-substituted carbazole at each end of the molecular core has been synthesised. A correlation between the size and shape of the alkyl chain attached the nitrogen atom of the carbazole and the transition temperatures of the nematic and smectic phases observed for them has been established and explained using steric arguments.

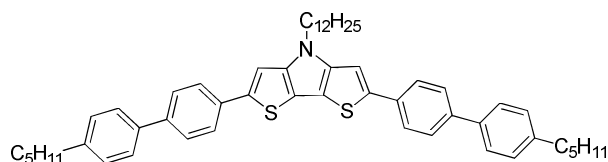


Compounds with an 2,5-disubstituted-1,3,4-oxadiazole ring in the centre of the molecular core with 3-substituted carbazole, 5-alkylthiophene or 4-alkylphenyl rings on both ends of the aromatic core were synthesised. Some of these compounds exhibit either an ordered smectic phase or a nematic phase and are promising as electron-transporting or hole-blocking materials in OLEDs. Molecular design allows similar structures to be prepared either with a smectic or a nematic phase as required.

A phosphorescent host incorporating an electron-rich *N*-octyl-3-carbazole moiety and an electron-deficient 2,5-disubstituted-1,3,4-oxadiazole ring was used in highly efficient small-molecule-based OLEDs and PhOLEDs. A current efficiency of 20 cd A<sup>-1</sup> for a green-emitting PhOLED and 6 cd A<sup>-1</sup> for a red-emitting PhOLED were achieved.

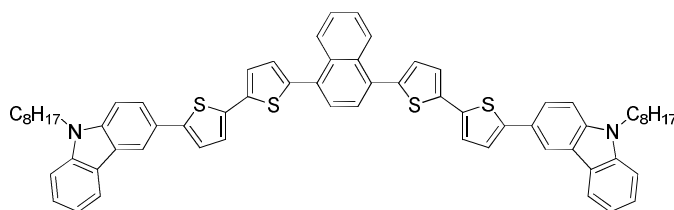


Three dithienopyrrole-based oligomers were synthesised as electron donors for use in OLEDs, OPVs and OFETs. One of these compounds exhibits a nematic phase. Cyclic voltammetry (CV) and UV-vis analyses of these compounds reveal that the rigid, planar and fused dithienopyrrole moiety is a very useful building block for producing compounds with a low band gap. Furthermore, the presence of the alkyl chain attached to the central nitrogen atom of the dithienopyrrole renders such compounds readily soluble in common organic solvents used in the deposition of thin, uniform layers of organic semiconductors from solution onto device substrates.

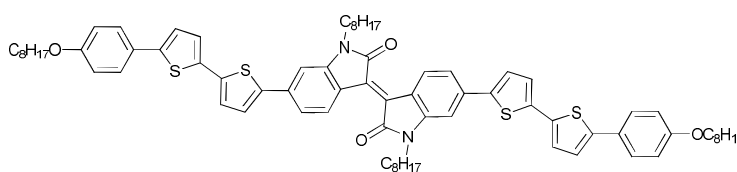


A novel series of compounds containing the 3-*N*-octyl-carbazole or 4-*n*-alkoxyphenyl end groups connected *via* 2,5-disubstitutedthiophene rings to a naphthalene or anthracene central moiety were synthesised. Unfortunately most of these compounds do not exhibit any observable liquid crystalline behaviour due to the bulky nature of extended carbazole group and the fact that the central fused rings lie out of the plane of

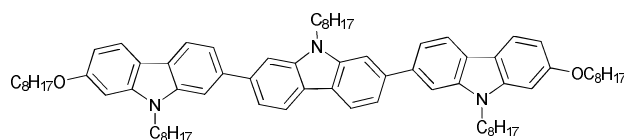
the molecule. However, these compounds may still be useful in plastic electronic applications as functional molecular glasses.



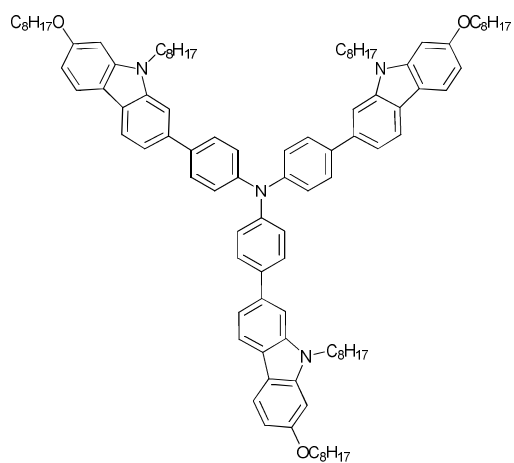
Isoindigo based liquid crystalline organic semiconductors have been synthesised for the first time to the author's knowledge. Compounds incorporating isoindigo as an electron-acceptor component and thiophene as an electron-donor component of the aromatic molecular core for use in organic solar cells absorb across almost all the visible spectrum and also exhibit appropriate energy levels for OPV applications. Unfortunately, a bulk hetero-junction solar cell fabricated using one of these compounds exhibits a maximum power conversion efficiency ( $\eta$ ) of less than 0.1%.



A series of compounds with 2-carbazole end groups and different central aromatic cores have been synthesised as charge transport and host materials for organo-metallic phosphorescent emitters in PhOLEDs. A green-emitting PhOLED fabricated using one of these compounds incorporating a *ter*-carbazole moiety as the host layer for an organo-metallic emitter exhibits a current efficiency of 10 cd A<sup>-1</sup>. The *ter*-carbazole compound has been shown to have high conductivity values, which are very similar to those of the widely used commercial hole-transport materials MeO-TPD.



Some novel compounds incorporating the triphenyl amine moiety as hole-transport/electron-blocking materials have been synthesised and are very useful in phosphorescent OLEDs with good hole mobilities and high-lying HOMO levels. Moreover, one of these compounds has shown to have good conductivity value, which means that it could be very useful in PhOLEDs.



The new compounds synthesised in this thesis have optimised energy levels due to informed “band gap engineering” and some of them have been used to fabricate efficient blue, green, red and white light PhOLEDs. The stability and life-time of the new materials as highly-crosslinked polymer networks in OLEDs will also be tested in prototype PhOLEDs.

## Appendix

### Publications

W. Bao, M. R. Billa, K. Kassireddy, M. Haro, M. J. Kelly, S. P. Kitney, M. S. Al Kalifah, P. Wei, D. Dong, M. O'Neill & S. M. Kelly, *Liq. Cryst.*, 2010, **37**, 1289-1303.

M. R. Billa, K. Kassireddy, M. Haro, M. S. Al-Kalifah, S. M. Kelly, S. P. Kitney & M. O'Neill, *Liq. Cryst.*, 2011, **38**, 813-829.